THE UNIVERSITY
of EDINBURGH

Response to Environmental Perturbations in Microbial Nutrient-Cycling Ecosystems

Timothy Bush

Doctor of Philosophy
The University of Edinburgh
October 2015

Lay Summary

Micro-organisms are everywhere, and carry out many important chemical reactions that control the chemistry of our planet. For example, micro-organisms produce more carbon dioxide every year than human beings do. Because of the environmental importance of micro-organisms we want to try to predict how they might be affected by changes like global warming, or the runoff of pollution into the ocean. However, this a very difficult problem because microbial communities are so hard to understand. This is partly because microbial communities contain so many different species (often tens of thousands), and partly because the relationships between different types of micro-organism are not understood, even at a very simple level.

We use a combination of mathematical modelling and experimental work in our research. In the first project, we use mathematical models to look at how microbial communities respond to environmental changes that affect nutrient availability. We find that gradual environmental changes can cause very dramatic, sharp changes in the microbial community. We then make predictions about where you might find this behaviour in the environment.

In the second project, we use experiments to look at how a real microbial ecosystem responds to changes in nutrient availability. Our experiments consist of plastic tubes containing pond mud and water, which develop into an interesting, layered microbial ecosystem over time. We find that different groups of micro-organisms respond in very different ways to changes in nutrient availability.

In the third project, we attempt to reproduce some of our experimental data in a mathematical model which includes more realistic chemical reactions that are not carried out by micro-organisms. We find that these chemical reactions can also cause microbial ecosystems to undergo sharp changes.

Abstract

The habitability of Earth is dependent upon the global recycling of elements essential for life, such as nitrogen, sulfur and carbon. Nutrient-cycling by microorganisms is vital to these biogeochemical cycles because many key steps are mediated primarily, or exclusively, by microbial life. The dynamics of these cycles are highly complex, and environmental perturbations (such as changes in the oceanic oxygen concentration) can have unexpected or catastrophic effects; often causing abrupt switches between chemical states. Despite the importance of these environmental perturbations however, few theoretical models have addressed how they affect the dynamical behaviour of nutrient-cycling microbial ecosystems.

In this work, we investigate the effect of environmental perturbations on microbially-mediated nutrient cycles and assess the likelihood of "sudden transitions" between chemical states of the ecosystem occurring in a variety of ecological contexts. To do this, we first use computational modelling of microbial nutrient-cycling, using a "box model" approach. We then move on to an experimental study using the microbial sulfur cycle as a model ecosystem, with freshwater pond sediment/water microcosms. These microcosms have the advantage of retaining many of the features of the real ecosystem (such as microbial diversity, spatial structure, and abiotic interactions) while allowing the controlled manipulation of environmental perturbations. We study these microcosms using a combination of chemical measurements and high-throughput sequencing of the microbial community. Finally, we return to the computational side, and attempt to reproduce chemical data from our experiments in a mathematical model containing realistic abiotic chemical interactions.

Declaration

I declare that this thesis was composed by myself, that the work contained herein is my own except where explicitly stated otherwise in the text, and that this work has not been submitted for any other degree or professional qualification except as specified.

Parts of this work have been published in [1].

(*Timothy Bush, October 2015*)

Acknowledgements

This thesis sits at an intersection between many scientific disciplines, and would not have been possible without discussions with a diverse group of physicists, biologists, geologists, chemists, mathematicians and astrobiologists. There were many people who were very kind in response to my basic questions, and I have many people to thank.

First, and most importantly, I would like to thank my supervisor Rosalind Allen, for her patient support and encouragement, and for showing me what it means to actually understand something. Having such a good teacher has been more important at this stage, than at any other stage of my education.

I would like to thank Andrew Free for introducing me to the world of biology, for providing such clear explanations and for showing me how to do labwork. From the lab, I would also like to thank Fiona Strathdee and Helen Williamson. I would like to thank Ian Butler for teaching me a new, complicated technique, and for his advice.

I would like to thank Charles Cockell and everybody associated with the Astrobiology group, for their enthusiastic commitment to having an unusual perspective on "the big questions", and for the mud from Disko Island.

Obviously, I would also like to thank all of the people associated with "The Cottage" for being so much fun. With regards to this thesis, a few of these people deserve a special mention. Toby and Elliot for discussions and programming help. Justin for so many moments of assistance, and for being my desk/crossword/tea/youtube buddy for four years.

I would also like to extend a general word of thanks to the whole ICMCS group. It has been a great privilege to spend time with so many interesting and clever people, and I have learnt so much from all of the journal clubs, theory clubs and seminars. Also, I am grateful to the EPSRC for financial support.

Thanks to my family, for getting me here in the first place.

Thanks to Casey, for endless discussions.

Contents

List of Figures

List of Tables

Chapter 1

Introduction

1.1 The Importance of Microbial Life for the Global Cycling of Chemical Elements

All of life depends on the continual recycling of essential chemical elements, such as carbon, nitrogen and phosphorus between different chemical forms. Many of the chemical transformations involved in this recycling are abiotic, such as the supply of sulfur to the atmosphere by volcanoes [2], or the weathering of limestone, which removes billions of tons of carbon dioxide from the atmosphere annually [3]. Chemical cycles that involve only such abiotic reactions are known as "geochemical cycles" because they are mediated by geological effects.

However, many important chemical transformations in the Earth-system are mediated primarily or exclusively by micro-organisms [4–6]. These microbially-mediated global element cycles are referred to as "biogeochemical cycles", because they are mediated by both biological and geological effects.

Without these microbially-mediated biogeochemical cycles our planet would be completely unable to support any higher order life. For example, for most of the

Earth's history (before the invention of the Haber process) micro-organisms were almost solely responsible for converting atmospheric gaseous nitrogen (N_2), which is inert, into biologically available forms, i.e. forms that can be used by plants and animals, in a process known as microbial nitrogen fixation. Indeed, the apparent ability of many plants, such as legumes, to perform nitrogen fixation, is actually the result of symbiotic bacteria associated with their roots [7]. Even today, micro-organisms have a huge effect on global chemical cycles. For example, the microbial decomposition of soil carbon exceeds the anthropogenic contribution of carbon dioxide to the atmosphere by an order of magnitude [8].

An important factor in explaining why micro-organisms are so important on a global scale is their ubiquity. Micro-organisms are adapted to live in extremes of temperature, pH, pressure, salinity and radiation [9]. This extreme adaptability means microbial life inhabits a wide range of environments, including hundreds of metres below the surface of the Earth [10], below the Antarctic ice sheet [11] and deep sea hydrothermal vents [12]. This led the microbiologist Lourens Baas Becking to remark that "everything is everywhere: but the environment selects", meaning that all microbial taxa, or species, are found in all habitable environments but local environmental conditions select which taxa thrive [13]. To cope with such a diversity of environmental conditions, micro-organisms have evolved a diverse array of metabolic strategies. They are able to "breathe", or extract energy from the environment, using many different chemicals, to name a few: sulfate, iron, carbon, nitrogen [6], uranium [14] and mercury [15] compounds. This metabolic and functional diversity is compounded by further diversity *within* functional groups of microbes with the same fundamental metabolism. For example, many different sulfate reducing taxa can co-exist in the same environment [16].

Despite their importance, key questions related to the composition and dynamics of microbial ecosystems remain unanswered. For example, how does the incredible diversity of microbial ecosystems affect their overall composition, and furthermore what is the cause of this diversity? Do microbial communities in a given

environment converge to a single specific composition over time, or are there many different community compositions that can give rise to similar overall environmental processes? In this thesis, we focus on a question that is particularly important in the light of current global environmental change: can we use simple mathematical models, together with simple laboratory experiments to predict how microbial communities will respond to an environmental change?

1.2 The Response of Biogeochemical Cycles to Environmental Change

Understanding biogeochemical cycles is an extremely challenging problem because of the complex feedbacks between Earth system processes and microbial life. Geological processes drive the evolution of different microbial metabolic strategies. For example, a massive increase in the availability of inorganic carbon in the ocean 250 million years ago may have led to the evolution of a new metabolic pathway; the microbial production of methane, known as methanogenesis [17]. At the same time, microbes themselves influence large scale global processes, and have shaped the history and development of our planet. For example, without microbes our atmosphere would not be oxygenated [18], and it has even been suggested that microbial life is responsible for the formation of continents as well as plate tectonics [19].

The existence of these feedbacks between the Earth's geology and microbial population dynamics can create non-linearities in the dynamics of biogeochemical cycles, such that a perturbation to a biogeochemical cycle can have drastic and unpredictable environmental consequences. For example, the previously mentioned perturbation to the global carbon cycle 250 million years ago led to the runaway production of sulfide by micro-organisms, resulting in the poisoning of the oceans and the subsequent extinction of as much as 90% of the marine

biodiversity on Earth [17, 20].

Moreover, a change in one biogeochemical cycle can have a knock-on effect on another one. For example, the oxygenation of the atmosphere (between 2.3 and 2.0 billion years ago) significantly altered the chemistry of the oceans and permanently changed the global iron, carbon and sulfur cycles (among many others) [21].

Also of great current interest is the effect of anthropogenic perturbations on biogeochemical cycles. In particular, a major concern is the increase in mean global temperature due to human CO_2 emissions. This global temperature rise is likely to have diverse effects on biogeochemical cycles, for example, changing the solubility of oceanic oxygen [22] and changing the rate of the microbial decomposition of carbon [23]. Consequently, predicting the response of biogeochemical cycles to environmental changes, including climate change, is a central current challenge in Earth system science [24].

Mathematical modelling is essential in tackling this challenge. However, mathematical models for global biogeochemical cycles often represent microbially-mediated transformations as crude "black boxes". For example, microbial decomposition in soil is often represented as a first-order decay process [25, 26]. Indeed, many of the models cited in the most recent Intergovernmental Panel on Climate Change (IPCC) report use linear representations of microbially-mediated processes [24]. Improving the representation of microbial population dynamics in biogeochemical models will be a key focus of this thesis.

The simplified mathematical representation of microbial population dynamics that is often used in current models contrasts strongly with the wealth of data on microbial community diversity and functional complexity which is being generated by recent advances in high-throughput sequencing technology [27]. This diversity, and its response to environmental perturbations, provides the second key focus of this thesis. The connection between the diversity of a microbial ecosystem and its response to perturbations has been a topic of debate in the literature. Some theoretical [28] and experimental work [29]

predicts that more diverse microbial communities should be more stable in response to environmental changes, because they contain many "functionally equivalent" species capable of restoring the overall ecosystem state if the population of another species collapses. However, other work suggests that in some circumstances, more diverse microbial ecosystems might be more prone to collapse, because of increased antagonistic interactions [30]. In this thesis, using experiments with microbial microcosms, we attempt to understand how diversity affects the response of microbial ecosystems to perturbations.

1.3 Objectives and Thesis Outline

In this thesis we use a combination of mathematical modelling and experiments to attempt to understand how microbially-mediated biogeochemical cycles respond to environmental perturbations. First, in chapters 2 and 3, we provide some background. Chapter 2 focuses on the mathematical modelling of microbial growth and biogeochemical cycles. In chapters 4 and 5, we show how we can use generic mathematical models for biogeochemical cycles to make predictions about how they respond to environmental perturbations.
Chapter 3 focuses on experimental techniques from the biological and geological sciences that are commonly used to study microbial ecosystems. Broadly, the experimental techniques we discuss can be categorised into two main groups:

1. Techniques for identifying which micro-organisms are present (sequencing).
2. Chemical techniques for analysing chemistry of the environment that micro-organisms inhabit (such as voltammetry).

In chapter 6, we present experimental work on a microbial ecosystem; examining the impact that an environmental perturbation has on the composition of the microbial community.

In chapter 7, we attempt to reproduce some of these experimental results in a model that incorporates more detailed geochemical processes. In chapter 8 we draw conclusions.

Chapter 2

Background: Models of Biogeochemical Cycles

2.1 Introduction

In this chapter we introduce previous work relevant to the modelling of biogeochemical cycles, focusing especially on the role of microbial population dynamics. First, we review previous biogeochemical models of various chemical cycles (such as the carbon cycle), many of which adopt a "box model" approach. We then note that many of these models neglect the details of microbial population dynamics and instead, often include highly simplified linear representations of microbially-mediated processes. Next, we review methods for modelling microbial population dynamics and discuss how these can be incorporated into biogeochemical models.

2.2 Biogeochemical Models

Many attempts have been made to unravel the processes that regulate global chemistry, and how these have changed over geological time, using simple mathematical models with small numbers of components or processes. For example, Goldbatt et al. showed that the delay between the evolution of oxygenic photosynthesis and the transition to an oxic atmosphere (the Great Oxidation Event) could have been the result of a bistable global redox state [31]. Using a similar approach, Kump et al. developed a simple model that showed that, potentially, at multiple times in Earth history, high concentrations of hydrogen sulfide in the deep ocean leaked out and generated toxic concentrations of sulfide in the atmosphere, destroying the ozone shield, and delaying the evolutionary development of life on land [32].

In a contrasting approach, other researchers have constructed very detailed models with many components, processes and feedbacks. Examples include the COPSE (Carbon-Oxygen-Phosphorus-Sulfur-Evolution) model [33] and the GEOCARB model [34], which have been used to reproduce atmospheric carbon dioxide concentrations over the past 500 million years.

Detailed models of this type are also used to make important projections about how biogeochemical cycles might affect the climate in the future, particularly in response to anthropogenic environmental perturbations. For example, complex models have been used to predict the effect of greenhouse gas emissions on global temperature [35] or how nitrogen pollution will affect reactive nitrogen availability over the next 100 years [36].

Complex and simple models have relative advantages and disadvantages. Complex models can be used to make specific quantitative predictions but may not give much insight into underlying mechanisms. On the other hand, the predictions made by simple models can often be understood intuitively but these predictions typically do not give quantitative information about a specific system or problem.

In this thesis we will focus on simple models, as our goal is to understand the underlying mechanisms that govern microbially-mediated biogeochemical cycles.

2.2.1 Box Models

Many of the models we have already mentioned contain some representation of spatial structure. Clearly spatial structure can have an impact on biogeochemical cycles. For example, it is known that subsurface microbial communities are typically separated into vertical spatial "zones" with different functional groups of microbes predominating in each zone [37]. However, including detailed spatial structure in a model can be complicated and make models much more difficult to solve.

A very common simplification in modelling biogeochemical cycles involves the use of a "box model". This involves separating the system into separate homogeneous boxes with flow rates for chemicals, microbial populations etc. defining the coupling between the boxes. Parameters such as temperature or pH can be defined independently in each box. Furthermore, each box can contain different processes. For example, boxes representing oxygenated environments such as the shallow ocean may only contain aerobic processes, such as microbial iron oxidation. This simplifies the model because the effect of each process does not have to be calculated in every box.

In geochemical models of the Earth, different boxes are often used to represent generic environments such as the deep ocean, the shallow ocean, the ocean sediment and the atmosphere. For example, many models of ocean dynamics use only two boxes, representing the deep ocean and the shallow ocean. An example of such a model is shown in Fig. 2.1; a generic model of nutrient cycling in the ocean. Chemical concentrations (such as phosphate) are defined separately in each box, and chemicals move between the boxes at some constant rate. There is also a biological export term that defines the loss of each nutrient from the

shallow ocean to the deep ocean due to the sinking of dead biomass. Many other biogeochemical models in the literature also use a similar, coupled box approach, often including other generic regions such as the atmosphere [32] or intermediate ocean zones [38].

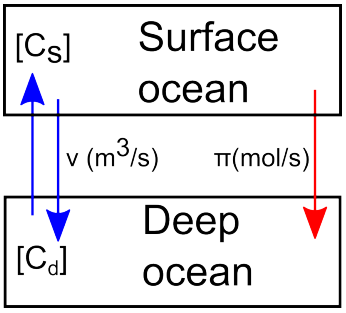

Figure 2.1 A generic two-box model of biogeochemical cycling in the ocean. v is a vertical exchange rate and π defines the "biological pump" (the nutrient loss due to sinking organic matter). $[C_s]$ and $[C_d]$ refer to the concentration of chemical C in the shallow and deep ocean boxes respectively. Taken from [39].

Instead of using different boxes to represent generic parts of the Earth-system (e.g. deep and shallow ocean), other models use boxes to represent specific geographical regions. For example, the PANDORA model of the global carbon cycle developed by Broecker and Peng contains 11 "reservoirs" or boxes representing regions in the modern global ocean, such as the Indo-Pacific ocean (INDO-PAC), the Atlantic and the Antarctic. The volume of each reservoir and the couplings between them are based on the known properties of each ocean. For example, the deep Pacific Ocean box is much larger than the deep Atlantic Ocean box [40].

2.2.2 The Lack of Microbial Population Dynamics in Current Biogeochemical Models

Chemical transformations mediated by microbes play a crucial role in the biogeochemical cycling of elements. For example, microbial nitrogen fixation

contributes an estimated 100-200 Tg of nitrogen to the world's oceans annually [41]. Furthermore, many reactions are *exclusively* carried out by microbial populations, such as methanogenesis [6].

Because of their importance in global chemical cycling, microbial populations cannot be ignored, and many biogeochemical models (including those already discussed) do include terms for the production or consumption of substrates by different microbial populations. However, most of these models include microbial processes very crudely as linear chemical production or decay terms, or a simple rate parameter independent of the dynamics of microbial growth, despite the fact that microbial growth is non-linear, and their respiration rates are a function of their population dynamics [42].

For example, a recent model which predicted the existence of vast methane reservoirs beneath Antarctica (1000s of Pg) assumed that the production of methane by microbes scales linearly with nutrient availability, neglecting the fact that this rate is proportional to the size of the relevant microbial population [11]. To give another example, a global marine ecosystem model simply included the rate of microbial processes such as nitrification (the biological oxidation of ammonia) as a fixed parameter, rather than including any dynamics or even a simple mathematical function [43]. The inclusion of microbial population dynamics in models of biogeochemical cycles will be a key aim of this thesis. To illustrate the importance of this goal for biogeochemical models we now discuss a specific example in more detail.

Specific example: The microbial decomposition of soil carbon

The microbial decomposition of soil organic carbon contributes ten times more carbon dioxide to the atmosphere annually than total human emissions [25]. There is believed to be four times more carbon stored in soil than in the global pool of plant biomass. Many models have tried to predict how the rate of

microbial decomposition of this vast carbon pool will change in response to anthropogenic global warming, since it is known that global warming is likely to increase the decomposition rate [44–46]. In these models the microbially-mediated process of soil carbon decomposition is generally represented by an equation in the form of Eq. 2.1, where C is the size of the global soil organic carbon pool, k is a constant, and f is a function of environmental variables such as temperature or moisture [47].

$$\frac{\mathrm{d}C}{\mathrm{dt}} = -kCf(\mathrm{Temp}, \mathrm{Moisture}, ...) \tag{2.1}$$

Eq. 2.1 neglects entirely the population dynamics of soil micro-organisms, representing their metabolism as linear in the size of the organic carbon pool C. However, the need to include the population dynamics of microbial soil decomposers in more detail has recently become more widely recognised, and some models have attempted to include decomposer dynamics [48, 49] i.e. to replace Eq. 2.1 by two coupled equations, one representing the population dynamics of the decomposers and the other representing the dynamics of the soil carbon pool. Fig. 2.2 illustrates the drastic impact of including microbial population dynamics in a model of soil carbon decomposition. This figure shows the predicated response of the soil carbon pool to an organic carbon influx (from increased litterfall) for two models containing conventional first order decomposition kinetics (similar to Eq. 2.1), compared with a model containing realistic microbial population dynamics (similar to the dynamics we describe later in section 2.3). The conventional models both predict that the increased litterfall results in a large gradual increase in size of the soil carbon pool. The microbial model however, predicts that the size of the soil carbon pool will remain constant in response to the same perturbation. The reason for this is that the microbial population responds to an increase in nutrient availability (in this case, brought about by an increase in litterfall) by increasing its population size, and thus increasing

the total decomposition rate and consuming the additional carbon. Models that assume a linear decomposition rate entirely miss this effect, because they ignore the fact that microbial populations can grow (or shrink) in response to changes in the environmental conditions.

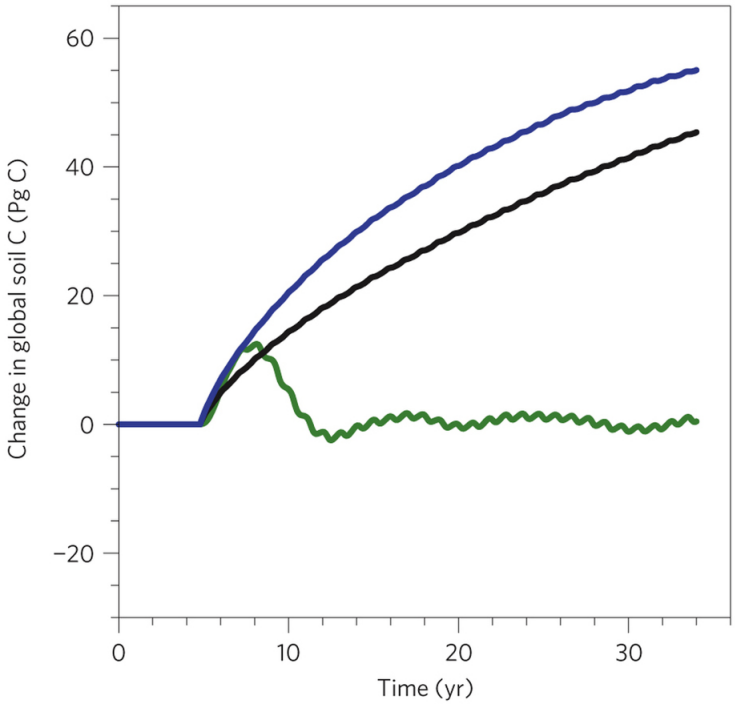

Figure 2.2 Response of steady-state soil carbon pools for conventional soil biogeochemistry models (CLM4cn, black; DAYCENT, blue) and a model that includes growth of the decomposer microbial population in response to changes in available nutrients (green) to a 20% global increase in litterfall beginning in year five. Reproduced from [48] with permission from Nature Publishing Group.

This example highlights the importance of including microbial populations in biogeochemical models. Recently, microbial populations have also begun to be considered in more detail in models of oceanic primary productivity (the synthesis of organics by the fixation of carbon dioxide, mainly through photosynthesis) [50] and global microbial nitrous oxide production [51].

However, despite these advances, the integration of microbial dynamics into biogeochemical models remains rare. There is thus an urgent need to re-evaluate the role of microbial population dynamics in biogeochemical models [23, 25]. The

construction of models which include microbial population dynamics needs, of course, to be informed by an experimental understanding of microbial ecosystems and geochemical processes.

2.3 Modelling Microbial Growth

In order to be able to incorporate microbial population dynamics into biogeochemical models it is first important to understand how to model microbial populations. In this section, we review how the dynamics of microbial populations can be represented mathematically.

2.3.1 The Definition of Microbial Growth

The rate of change over time of the density of a microbial population n (cells/litre) can be defined according to Eq. 2.2. This defines net growth as the difference between a growth term, parameterised by a growth rate r (hr^{-1}) and a loss term, parameterised by a loss rate d (hr^{-1}) which represents loss due to washout or death due to, for example, viral predation [52].

$$\frac{\mathrm{d}n}{\mathrm{d}t} = n(r - d) \tag{2.2}$$

The specific growth rate r (growth rate per unit population density) is a function of nutrient concentration and can be defined in multiple ways. We now discuss the most widely used functional form for r, Monod kinetics.

2.3.2 Monod Kinetics

In 1949 Jacques Monod published a famous paper proposing an empirical law for the growth rate of a microbial population as a function of the concentration of its nutrient source. This law (termed the "Monod equation", after its proposer) remains the most popular approach to modelling the kinetics of microbial growth to this day. The function is defined in terms of nutrient concentration S (μM) in Eq. 2.3, and is plotted in Fig. 2.3.

$$r = \frac{vS}{K_{\mathrm{S}} + S} \tag{2.3}$$

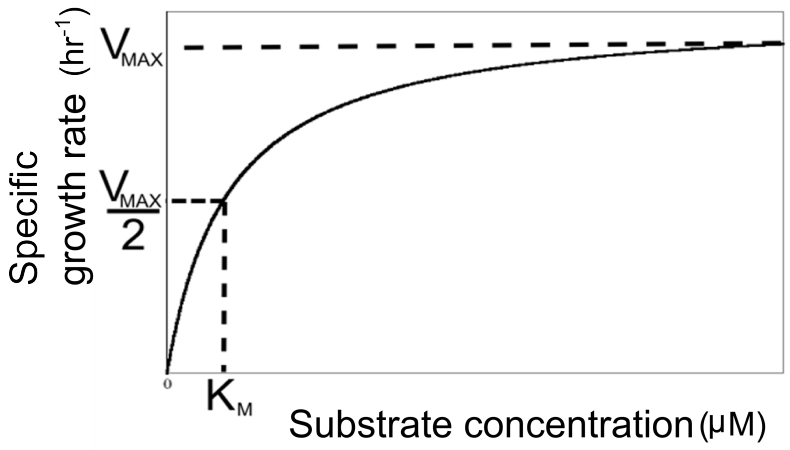

Figure 2.3 The Monod growth function defined in Eq. 2.3. The specific growth rate saturates at high nutrient concentration.

In Eq. 2.3 v (hr^{-1}) defines the maximal growth rate and K_{S} (μM) defines the substrate concentration at which the growth rate is half the maximal growth rate, i.e. if $S = K_{\mathrm{S}}$ then $r = v/2$ [42]. The specific growth rate r as defined by Eq. 2.3 is linear in S at low nutrient concentrations but saturates at higher concentrations. This means that once the specific growth rate reaches its maximum value v, no further increase in the availability of this nutrient can possibly push the growth

rate of the population any higher, although the population density will continue to increase exponentially with rate v.

Combining Eq. 2.3 with Eq. 2.2 gives an equation for the rate of change of the population density n (cells/litre) over time.

$$\frac{\mathrm{d}n}{\mathrm{d}t} = \frac{vSn}{K_\mathrm{S} + S} - dn \tag{2.4}$$

The rate of change of the nutrient concentration is then given by Eq. 2.5, where γ (μmol substrate/cell) defines a growth yield.

$$\frac{\mathrm{d}S}{\mathrm{d}t} = -\gamma \frac{vSn}{K_\mathrm{S} + S} \tag{2.5}$$

Several alternatives to the Monod equation (Eq. 2.3) have been proposed. For example, the "Contois equation" incorporates the fact that microbial populations can have a limiting density, as well as a limiting growth rate [53]. However, none of these alternatives have become as widely used as Monod kinetics.

2.3.3 Limitation by Additional Nutrients

The Monod equation (Eq. 2.3) assumes that the microbial growth rate depends on the concentration of only one chemical nutrient. However, in reality microbes require many different nutrients [5, 54]. In the environment, microbial growth can be limited by the availability of multiple nutrients, for example, nitrogen and phosphorus are often limiting for ocean communities [55]. Here, we discuss how to model a microbial population limited by multiple nutrients.

Some debate exists about how best to model growth on multiple nutrients or substrates. A commonly used approach is to use a very simple generalisation of the Monod function in which two Monod functions are multiplied together.

The specific growth rate of the population as a function of two nutrients S_1 and S_2 (which, for instance, could be nitrogen and phosphorus) is then given by Eq. 2.6. This approach was first proposed by MeGee et al. in 1972 [56] where the subscript notation on the half saturation constant K denotes association with either nutrient.

$$r = v\left(\frac{S_1}{K_1 + S_1}\right)\left(\frac{S_2}{K_2 + S_2}\right) \tag{2.6}$$

This form has been used in many studies, from large-scale global ocean models [43], to simpler models of methanogenesis or sulfate reduction in sediments [57]. However, the multiplicative Monod approach (Eq. 2.6) has been criticized because it contradicts "Liebig's law of the minimum"; a principle from agricultural science which states that the most limiting nutrient is the one that actually limits growth, with the concentration of the less limiting nutrient becoming essentially irrelevant. Liebig's law of the minimum can be implemented into a microbial growth function by using a relation like Eq. 2.7.

$$r = v\min\left(S_1K_1 + S_1, S_2K_2 + S_2\right) \tag{2.7}$$

Some experimental studies on phytoplankton have found that Eq. 2.7 fits experimental data better than Eq. 2.6 [58, 59], and it has been implemented in some models [60]. Despite this, the multiplicative approach of Eq. 2.6 remains by far the most popular method.

Further complications arise if we consider the fact that the abundance of one nutrient may affect the uptake rate of another. As an example, one nutrient might be necessary for the production of an enzyme which facilitates the uptake of the other nutrient [61].

It is also important to note that the representations shown in Eqs. 2.6-2.7 are for microbial growth limited by two nutrients, but can easily be extended to model

growth limitation by any number of nutrients.

2.3.4 Including Population Density Limitation

The growth functions presented so far describe explicit limitation of microbial growth rate by the availability of chemical substrates. However, it can also be useful to write functions in which growth rate is not limited by substrate availability explicitly but instead is dependent on some external factor that is included implicitly via nonlinear terms in the population density. This could be a way to implicitly include dependence on a substrate that is not explicitly modelled, or it could describe limitation by some other factor (e.g. space)[62].
To account for this, a logistic population density limitation term can be used, as shown in Eq. 2.8. This causes the growth rate to decrease to zero as the population approaches some maximal density $n_{\max}$.

$$\frac{dn}{dt} = \frac{vSn}{K_{\mathrm{S}} + S}\left(1 - \frac{n}{n_{\max}}\right) - Dn \tag{2.8}$$

This type of logistic population density limitation is a convenient and commonly-used way to encapsulate growth-limitation by factors not explicitly included in the model. It has been used in a range of high profile microbial models, including models of the intestinal microbiota of rats and mice [63], models of biodiversity in temperate lake microbial ecosystems [64] and generic models of microbial inter-species interactions [65]. It has the advantage of being extremely simple, and also allows the maximal population density $n_{\max}$ to be a controllable parameter, allowing easy scalability of the system size (for example, scaling up from a microcosm to an ocean).

2.3.5 Including Thermodynamics in Microbial Growth Kinetics

Monod kinetics alone would predict that a microbe will continue to metabolize substrate until none remains, but in reality microbes can only grow if there is enough energy available in the environment for them to respire [66, 67]. In this section we introduce a term that explicitly accounts for the thermodynamics of the metabolic reaction being performed.

The Biology of Microbial Respiration

Respiration is the process by which microbes use chemical reactions to obtain the energy to grow and divide. In respiration, microbes extract energy from a chemical redox reaction and convert it into the form of the adenosine triphosphate (ATP) molecule, the universal energy currency of life. ATP is synthesized from adenosine diphosphate (ADP) and phosphate. The ATP molecule releases a lot of energy ($\sim$ 50kJ/mol) when it undergoes hydrolysis, and this is what makes it an effective energy storage molecule for life. For example the hydrolysis of stored ATP can be used to drive biosynthetic reactions (making biomass) that would be thermodynamically unfavourable in the absence of ATP [68].

Fig. 2.4 shows schematically how the coupling between a respiratory redox reaction and ATP synthesis works. In the respiratory redox reaction, electrons are transferred from an electron donor D, which is often some kind of organic compound such as glucose or acetate. This electron is then transferred, via a series of membrane proteins, to an electron acceptor A. For obvious reasons, the molecule used as an electron acceptor must be electronegative (have a tendency to accept electrons) and consequently oxygen is the most commonly used electron acceptor because it is highly electronegative. Correspondingly, the molecule used as an electron donor must have a tendency to lose electrons. The respiratory redox

reaction can be written in the general form of Eq. 2.9, where D^+ and A^- are the oxidized and reduced forms of the electron donor and acceptor respectively.

$$D + A \rightarrow D^+ + A^- \tag{2.9}$$

The movement of an electron from donor to acceptor along the series of membrane proteins (known as the electron transport chain) releases free energy. This free energy is used by the proteins of the electron transport chain to pump protons from the inside to the outside of the cell, creating a difference in both pH and electrical potential across the cell membrane. As the pumped protons flow back across the membrane they drive a "motor" enzyme complex called ATP-synthase which synthesizes ATP from ADP and phosphate (PO_4^{3-}) [68].
Incorporating the fact that the redox reaction given in Eq. 2.9 is coupled to the synthesis of ATP gives the generic microbial respiratory reaction defined in Eq. 2.10, where m is the number of ATP molecules synthesized per reaction.

$$D + A + m\text{ADP} + mPO_4^{3-} \rightarrow D^+ + A^- + m\text{ATP} \tag{2.10}$$

Deriving a Thermodynamic Limitation Term for Microbial Growth

Since micro-organisms exploit a free energy difference to synthesize ATP it is therefore reasonable to assume that their growth rate is controlled by the availability of this free energy. If there were not enough free energy available to synthesize ATP, then the microbial population should not be able to grow. Qusheng Jin and Craig M Bethke used this fact to derive a thermodynamic expression for the limitation of microbial growth [67]. We reproduce part of this derivation here.
The free energy change ΔG associated with the redox reaction defining microbial

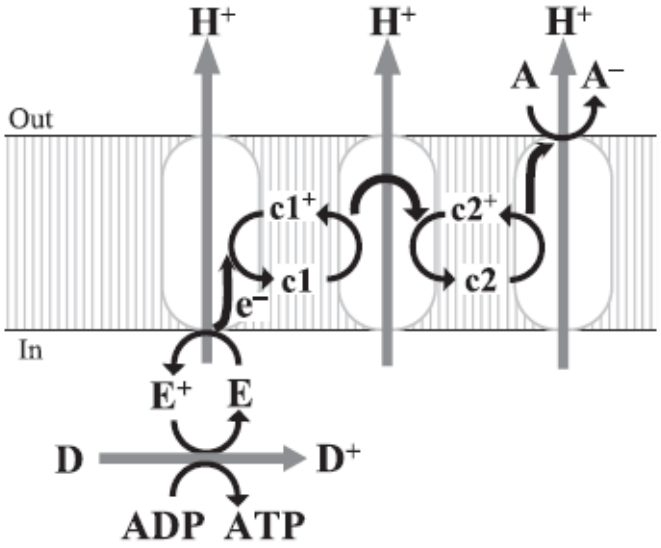

Figure 2.4 Schematic diagram of microbial respiration [66]. An electron is removed from some electron donor D and cycled through intermediate compounds c1 and c2 to some electron acceptor A. This is known as the electron transport chain. The free energy difference this generates is used to pump protons across the membrane, this in turn results in the synthesis of ATP, the energy current molecule of life.

respiration given in Eq. 2.9 (not including the synthesis of ATP) is given by Eq. 2.11, where R is the ideal gas constant and T is the absolute temperature [6].

$$\Delta G = \Delta G^0 + \mathrm{R}T \ln\left(\frac{[\mathrm{D}^+][\mathrm{A}^-]}{[\mathrm{D}][\mathrm{A}]}\right) \tag{2.11}$$

This is determined by the standard Gibbs free energy change of the reaction ΔG^0 and the concentrations of the chemical substrates in the redox reaction [D],[A],[D^+],[A^-]. Thus, if the concentration of the end products of the reaction D^+ and A^- becomes too high then the reaction will become thermodynamically unfeasible. This incorporates the fact that microbial growth can become inhibited by a build-up of its waste products, a fact not included in Monod kinetics.

For ΔG, a negative value describes a reaction that favours the forwards direction (towards D^+ and A^-), and a positive value describes a reaction that favours the

reverse direction (towards D and A).

Eq. 2.11 describes the free energy change associated with any redox reaction and must be adapted to describe microbial respiration to incorporate the fact that microbes store some free energy by synthesizing the ATP molecule. $\Delta G_p \approx 50$ kJ mol^{-1} defines the energy required to carry out the reaction ADP + $P_i \rightleftharpoons$ ATP [67]. In other words, ΔG_p is the amount of free energy stored in the synthesis of the ATP molecule.

Including the free energy needed to synthesize ATP allows a "thermodynamic driving force" f for the full reaction describing microbial respiration (Eq. 2.10) to be defined (where, as before, m is the number of ATP molecules synthesized per reaction).

$$f = -\Delta G - m\Delta G_p \tag{2.12}$$

Since ΔG_p is positive, the synthesis of ATP decreases the thermodynamic driving force f. The forward rate for the respiratory reaction exceeds the reverse rate when the net driving force f is positive, and the overall reaction proceeds forwards. Conversely, when the net driving force is negative the population does not grow.

The net reaction rate V of a micro-organism's respiratory reaction can be assumed to be the difference in the forwards and backwards reaction rates, defined as v^+ and v^- respectively. This gives Eq. 2.13.

$$V = v^+ - v^- \tag{2.13}$$

Pulling out a factor of v^+ gives:

$$V = v^+ \left(1 - \frac{v^-}{v^+}\right) \tag{2.14}$$

For a generalised reaction of the form $A + B \rightleftharpoons C + D$ the reaction rates are then given by the product of the chemical concentrations and the associated rate coefficients, so $v^+ = k^+[A][B]$ and $v^- = k^-[C][D]$, where square brackets denote concentration. Substituting these into Eq. 2.14 gives:

$$V = v^+ \left(1 - \frac{k^-[C][D]}{k^+[A][B]}\right) \tag{2.15}$$

However, to connect the thermodynamic driving force f to the rate of reaction we need to know v^+ and v^-. Here, Jin and Bethke invoke a result from the field of nonlinear nonequilibrium thermodynamics [69]. The thermodynamic driving force f for the generalised reaction $(A + B \rightleftharpoons C + D)$ is given by Eq. 2.16

$$f = RT \ln \left(\frac{k^+[A][B]}{k^-[C][D]}\right) \tag{2.16}$$

This can be re-arranged to give:

$$\frac{k^+[A][B]}{k^-[C][D]} = \exp\left(\frac{f}{RT}\right) \tag{2.17}$$

Eq. 2.17 can then be substituted into Eq. 2.15 to give:

$$v = v^+ \left(1 - \frac{k^-[C][D]}{k^+[A][B]}\right) = v^+ \left(1 - \exp\left(\frac{-f}{RT}\right)\right) \tag{2.18}$$

Rewriting Eq. 2.18 and assuming that the microbes do not grow if their respiratory reaction does not produce enough free energy to make ATP (i.e. if $f < 0$), we arrive at the relations Eq. 2.19 and Eq. 2.18 where a thermodynamic limitation function F_T is also defined.

$$v = v^+ F_{\mathrm{T}} \tag{2.19}$$

$$F_{\mathrm{T}} = \begin{cases} 1 - \exp\left(\dfrac{\Delta G + m\Delta G_{\mathrm{ATP}}}{RT}\right), & \text{if } \Delta G + m\Delta G_{\mathrm{P}} \leq 0 \quad (2.20a) \\ 0, & \text{if } \Delta G + m\Delta G_{\mathrm{P}} \geq 0 \quad (2.20b) \end{cases}$$

Finally, the structure of the microbial electron transport chain itself can also be taken into account. χ represents the number of protons translocated across the cellular membrane per substrate molecule consumed. This value is known from the structure of the respiratory chain of the specific metabolism. For example, for sulfate reduction, 5 protons are translocated across the membrane for every electron that is transferred through the electron transport chain and so $\chi = 5$ [37]. For the microbial respiration example shown in Fig. 2.4, 3 protons are translocated across the membrane for every electron transported through the chain. Mathematically, this means that microbial respiration is thermodynamically less limited for a higher χ. Physically, this means that if more protons are translocated per electron, then the proton motive force available for the synthesis of ATP is greater and so microbial respiration will become thermodynamically limited less easily. Including this χ factor gives Eq. 2.19.

$$F_{\mathrm{T}} = \begin{cases} 1 - \exp\left(\dfrac{\Delta G + m\Delta G_{\mathrm{ATP}}}{\chi RT}\right), & \text{if } \Delta G + m\Delta G_{\mathrm{P}} \leq 0 \quad (2.21a) \\ 0, & \text{if } \Delta G + m\Delta G_{\mathrm{P}} \geq 0 \quad (2.21b) \end{cases}$$

Incorporating the limitation of microbial growth by the free energy available in their respiratory reaction (as described by Eq. 2.19) into an equation for the rate of change of the microbial population density n over time, would then give Eq. 2.22.

$$\frac{\mathrm{d}n}{\mathrm{d}t} = \frac{vSn}{K_{\mathrm{S}} + S} F_{\mathrm{T}} - Dn \qquad (2.22)$$

2.4 Numerical Solution of Differential Equations

The microbial and geochemical models that we have discussed so far generally consist of sets of coupled ordinary differential equations of the form given in Eq. 2.23, where $y(t)$ is a variable of interest and t is time.

$$\frac{\mathrm{d}y(t)}{\mathrm{d}t} = f(t, y(t)) \tag{2.23}$$

These models are often not analytically solvable, and in these cases integration by a numerical method is required. In this brief section, we describe two such numerical methods.

2.4.1 The Euler Method

The simplest method for solving Eq. 2.23 is the Euler method. Here, Δt defines the size of a timestep where $t_n = t_0 + n\Delta t$ and n represents the number of timesteps. One step of the Euler method from t_n to $t_{\mathrm{n}+1} = t_n + n\Delta t$ is given by Eq. 2.24 [70, 71].

$$y_{\mathrm{n}+1} = y_\mathrm{n} + f(t_\mathrm{n}, y_\mathrm{n})\Delta t \tag{2.24}$$

The idea of the Euler method is to compute the slope of tangent lines at a series of points along the function. The Euler method has the advantage of being extremely simple (it is the most basic method for numerically solving differential equations). However, the Euler method can be very inaccurate; every step of the Euler method has an associated error $O(\Delta t^2)$. Furthermore the Euler method can be very unstable, i.e. for some equations the numerical solution computed by the Euler method can diverge wildly from the true solution.

2.4.2 The Fourth Order Runge-Kutta Method

A more sophisticated extension of the Euler method gives the Runge-Kutta method, described by Eqs. 2.25-2.29.

$$k_1 = f(y_\mathrm{n})\Delta t \tag{2.25}$$

$$k_2 = f\left(y_\mathrm{n} + \frac{k_1}{2}\right)\Delta t \tag{2.26}$$

$$k_3 = f\left(y_\mathrm{n} + \frac{k_2}{2}\right)\Delta t \tag{2.27}$$

$$k_4 = f(y_\mathrm{n} + k_3)\Delta t \tag{2.28}$$

$$y_{\mathrm{n}+1} = y_\mathrm{n} + \frac{1}{6}\left(k_1 + 2k_2 + 2k_3 + k_4\right) \tag{2.29}$$

This method essentially combines the information from several Euler-steps. It is more stable than the simple Euler method and importantly, is also more accurate, because the error for each step is $O(\Delta t^5)$. In chapters 4 and 5 of this thesis, the Euler method is used to solve very simple models, and the fourth-order Runge-Kutta method is used to solve more detailed models; the exact method used is specified in each case.

2.5 Discussion and Conclusions

In this chapter we introduced the concept of a geochemical box model, and discussed how such models can be used to make predictions about how a microbially-mediated biogeochemical cycle might respond to an environmental perturbation, in particular, an anthropogenic one. Using the example of the microbial decomposition of soil carbon, we then showed that current models of global biogeochemistry often represent microbially-mediated processes using simplified linear kinetics or constants, completely neglecting the actual dynamics of microbial growth and the fact that microbial population density changes in response to changes in nutrient availability.

With the ultimate goal of including microbial population dynamics in a substrate-cycling biogeochemical model, we then discussed how to model microbial populations; introducing the Monod growth function, and also discussed different ways that microbial population growth can be limited. In chapters 4 and 5 we will apply this knowledge to develop a generic model of microbial nutrient cycling, and show how the dynamics of microbial population growth itself can have a dramatic impact on the chemical state of a ecosystem. In chapter 7 we apply the same techniques to develop a more chemically complex model of a specific system, the microbial sulfur cycle.

Chapter 3

Experimental Techniques for Studying Microbial Ecosystems

3.1 Introduction

In this thesis we have combined theoretical model development with experiments on model systems consisting of nutrient-cycling microbial microcosms. In this chapter we outline experimental techniques relevant to the study of microbial ecosystems. We focus on techniques that will be relevant to our own experiments on microbial sediment/water ecosystems, that we present in chapter 6.

We first explain how the micro-organisms in an environment can be identified using "next generation sequencing". The development of next generation sequencing (also called high-throughput sequencing) techniques has caused a revolution over the past 20 years in the study of microbial communities by allowing DNA from many different organisms to be sequenced in parallel without needing to first extract, isolate and culture the organisms [72]. This has revealed an incredible diversity of micro-organisms in many environmental systems. For example, high throughput sequencing studies on the diversity of bacteria in soil

have revealed the presence of thousands of microbial species in a typical 1 gram sample [73].

Our experimental work is unusual in the field as it combines high throughput DNA sequence analysis with spatially-resolved chemical measurements of the ecosystem state. In this chapter, we therefore also explain how spatially-resolved chemical measurements can be made using a technique called voltammetry. We use this technique in chapter 6 to measure sulfide gradients in our experimental microcosms.

3.2 Sequencing Microbial Communities

3.2.1 Taxonomy in Microbial Ecology

All of life is classified in a system based on shared characteristics, and the classification of an organism within these groups is referred to as its "taxonomy". In this section, we briefly discuss the classification of organisms into taxonomic groups.

Life is divided into three "domains": Eucarya (eukaryotes), Bacteria and Archaea (prokaryotes). The domain Eucarya comprises all forms of multicellular life, including all plants, animals and fungi. Bacteria and Archaea are both single celled micro-organisms lacking a cell nucleus. However, Bacteria and Archaea differ in cell composition and organization enough to be classified into separate domains [74]. Life can then be classified at higher levels of taxonomy into phylum, class, order, family, genus, and finally species. "Sequencing" a microbial community refers to experimentally classifying the taxonomy of the micro-organisms in a sample.

3.2.2 DNA Extraction and the Structure of DNA

Before describing the details of how to sequence a sample of micro-organisms we first briefly describe the structure of DNA and the process of DNA extraction. DNA consists of the nucleobases Adenine (A), Guanine (G), Cytosine (C) and Thymine (T). These bases form hydrogen-bonded pairs connecting the two strands of the DNA double helix, A binds to T and G binds to C, creating a sugar-phosphate backbone. The two strands of DNA therefore contain complementary information.

Before the micro-organisms in a sample can be sequenced, the DNA must first be extracted and purified. The specific details of DNA extraction are described in detail in the methods of chapter 6, but we briefly outline the general process here. The first step of a DNA extraction generally involves "lysing" (breaking open) the cells in the sample with chemical or physical procedures such as grinding, freezing-thawing, bead-beating or heating. Further chemical steps remove cellular components other than DNA, such as proteins, lipids, carbohydrates and cell debris. The DNA can then be purified, extracted by centrifugation, and stored in sterile buffer solution [75].

3.2.3 Sequencing Using the 16S rRNA Gene

Modern high-throughput sequencing methods do not sequence the entire genome at once (the entire genome of a bacterium can be as long as several million base-pairs [76]). Instead, many short fragments of DNA (approximately hundreds of base-pairs in length) are sequenced very rapidly, and these fragments are then analysed [77].

There are two distinct approaches to using next generation sequencing to identify the microbial community in a given environment. Perhaps the most obvious is to

attempt to sequence all of the DNA in a sample, and then try to piece together which micro-organisms the DNA fragments correspond to. This method, known as "shotgun metagenomics", is widely used in microbial ecology. For example, a high profile study used shotgun metagenomics to examine the microbial community of the Sargasso sea, and found 1.2 million previously unknown genes from as many as 1800 genomic species of micro-organism [78]. However, shotgun metagenomics has several disadvantages. First, the cost of sequencing such large quantities of DNA can be prohibitively high, particularly for large numbers of samples. Second, assembling DNA fragments into functional genes or whole genomes can be very computationally intensive and is likely to miss rarer genomes. A method known as "amplicon sequencing" provides a cheaper and computationally less demanding alternative. This method relies on sequencing a specific gene, present in all micro-organisms of interest, that allows taxonomic assignment because it differs in sequence between different species of micro-organism. By far the most widely used gene for this purpose in microbial ecology is called the 16S ribosomal RNA (or 16S rRNA) gene [79, 80], a technique pioneered by Carl Woese in 1977 [81, 82]. The 16S rRNA gene encodes the core of a small subunit of the ribosome (the cell's protein-making machinery) and is found in all bacteria. Some sections of this gene (or "regions") change only very slowly over evolutionary time, and are therefore effectively "conserved" across all micro-organisms. Other regions of the gene sequence are highly variable between different micro-organisms. These variable regions can be used to distinguish between different microbial taxa.

3.2.4 The Polymerase Chain Reaction (PCR)

The "Polymerase Chain Reaction" (PCR) is used to selectively obtain fragments of the 16S rRNA gene from our extracted DNA samples. PCR is an experimental technique developed by Kary Mullis [83] that allows a specific DNA sequence to

amplified (copied many times) from any complex mixture of DNA molecules; for example, from the mixture of DNA extracted from an environmental sample. It is an extremely widely used method in all areas of molecular biology. Fig. 3.1 illustrates the PCR process schematically.

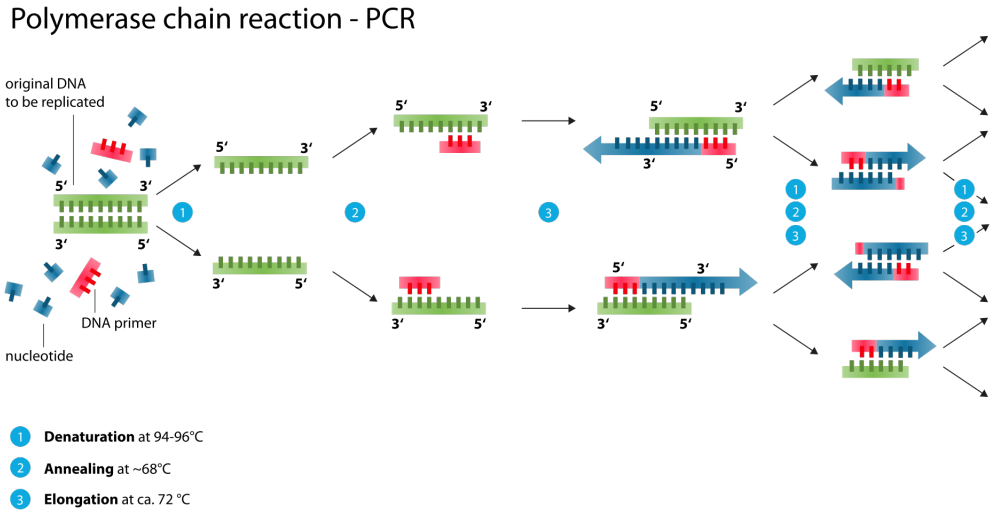

Figure 3.1 Schematic picture of the cycle of the polymerase chain reaction (PCR). The labels $3^{'}$ and $5^{'}$ refer to directionality of the sugar-phosphate backbone (the -OH end and the PO_4^- end respectively) Taken from [84].

The PCR process relies on thermal cycling to generate millions of copies of a particular fragment of DNA. DNA extracted from the sample, containing a diverse mixture of sequences, is mixed with a solution containing the raw material for making new DNA, consisting of deoxynucleotide triphosphates (or "dNTPs"), molecules which themselves consist of the nucleotides A,C,T and G bound to phosphate. A solution containing a thermostable enzyme called *Taq* DNA polymerase (from a thermophilic hot spring bacterium, *Thermus aquaticus*), and another solution containing a "primer" are then added. The primer consists of a sequence that is designed to bind to the ends of the specific fragment of DNA sequence that we aim to amplify (for example, a region of the 16S rRNA gene). Furthermore, each primer can have an additional set of bases which act as a "barcode". Primers with different unique barcode sequences are then added to

each sample. This allows all samples to be sequenced together, and the sample that each sequence was initially associated with can be reconstructed later by analysing the barcode sequences.
The steps of the thermal cycling then proceed as follows:

1. **Denaturation**: A very high temperature ($94 - 96°C$) is applied, causing DNA strands to separate.

2. **Annealing**: The temperature is lowered ($50 - 65°C$) to allow the primers to bind to the now separated DNA strands.

3. **Elongation**: The temperature is raised to the optimum temperature of the thermostable polymerase enzyme ($72-80°C$). This enzyme then synthesizes a new DNA strand complementary to the template strand out of the dNTPs (deoxynucleotide triphosphates) which are present in solution. The primers dictate directionally which sequences are to be copied (indicated by the arrows in Fig. 3.1).

This cycle is then repeated many times (potentially 20 to 30 times), causing the number of DNA sequences corresponding to the targeted sequence to increase exponentially.
We note here that the PCR process does generate errors. One important error that can occur in the PCR process is known as a "chimera". Chimeras are created when a partially amplified sequence representing a DNA fragment (for example, the 16S rRNA gene) from one organism acts as a primer for the amplification of a different sequence from a different organism, causing DNA fragments from different organisms to become fused together [85]. However, chimeric sequences can be removed and identified when the data is analysed (this is briefly discussed in a subsequent section).

Sequencing Technology

Having undergone the PCR process the samples can now be sequenced. The samples are "run" on a sequencing machine, which identifies all of the sequences of nucleobases present in the sample (this normally involves sending the samples to a sequencing centre). We do not discuss this stage of the process here. However, we note that many different sequencing machines exist, each of which has its own associated benefits and disadvantages. In this thesis, we will focus on sequencing using a 454 Titanium (Roche) machine [77].

3.2.5 Processing Sequence Data Using QIIME

The raw data that comes off the sequencer consists of large set of sequences (e.g. ATCGGTCCTG....) associated with each sample. For 454 Titanium technology there are 1 million "reads" per plate (where a read refers to a sequenced copy of a gene) and the maximum read-length is 750 base pairs. Typically, we would obtain 2000 to 10000 reads per sample once errors are removed. Each of these reads should correspond to a copy of the 16S rRNA gene from one of the micro-organisms that was in the sample. This dataset now has to be processed and the sequences that we have obtained from the sample have to be compared to a database of the 16S rRNA genes of known microbial taxa.

QIIME (pronounced "chime") stands for Quantitative Insights Into Microbial Ecology and is the standard pipeline for processing and analysing 16S rRNA sequence data. [86]. It consists of a large set of scripts written in python that are used to process the raw sequence data that comes off the sequencing machine (a .fasta file and a .qual quality file in the case of 454 Titanium sequencing), into a table of taxa and associated abundances across samples. Fig. 3.2 illustrates the standard procedure for analysing 454 data using QIIME. In the rest of this section we discuss the stages of QIIME analysis.

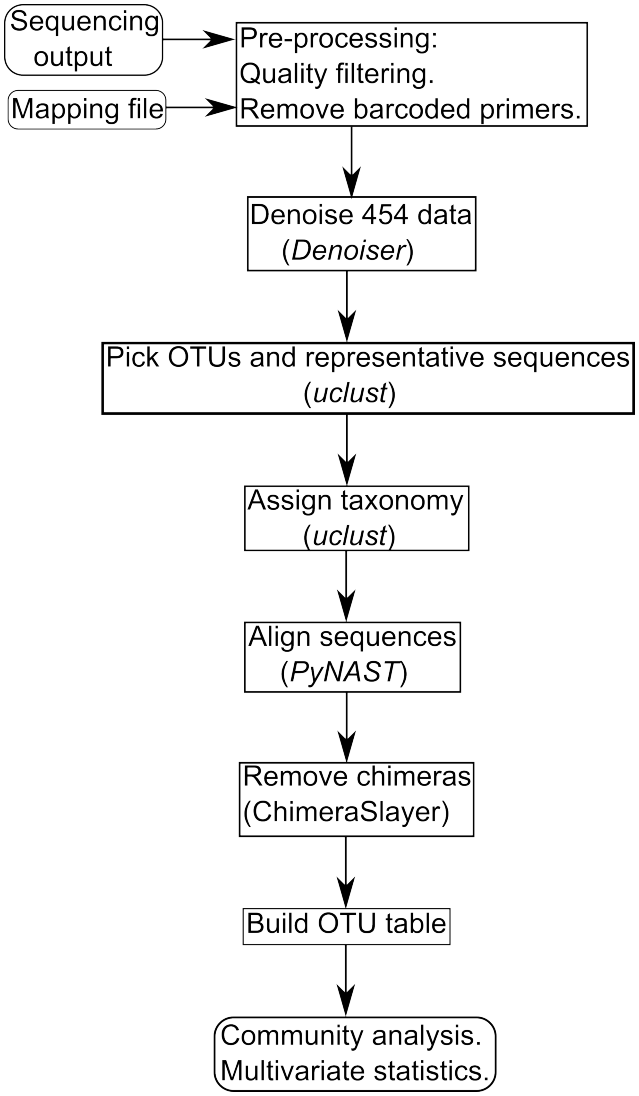

Figure 3.2 Workflow of the QIIME pipeline when analysing 454 sequence data. Italics indicate the package within QIIME that is used to perform the associated function. Rounded boxes indicate inputs and outputs that are not strictly part of the QIIME workflow. Adapted from [87].

Pre-processing and Denoising

First, the dataset is pre-processed. The sequencing platform has previously assigned each base with a quality score, which denotes the probability that base is actually an error. Each sequencing method has its own associated errors, for example, 454 sequencing often incorrectly identifies bases if the same base appears

several times in a row (e.g. AAAA...); so-called "homopolymer errors" [88]. Some quality threshold is defined and QIIME truncates the read at the first base below this quality threshold.

The next step in pre-processing is the removal of the barcoded primers. A mapping file defines which barcode is associated with which sample. Each sequence can then be associated with a sample-ID according to its barcode, and the bases corresponding to the primers are removed. All of these pre-processing steps are performed by one script within QIIME.

Next, a denoising algorithm identifies and removes errors inherent in the 454 sequencing procedure (the misidentification of bases) that cannot be included in the quality score, and so were not removed in pre-processing. This denoising algorithm is specific to the errors associated with identifying bases using 454 Titanium sequencing [89], such as the homopolymer errors that we previously discussed.

Assigning Taxonomy

At this stage we have a collection of several thousand short DNA sequences per sample. The next stage is to determine which micro-organism each sequence corresponds to; this is called assigning taxonomy. In microbial ecology an "Operational Taxonomic Unit" (OTU) is used as an operational definition of a species. In this thesis we will use the terms "OTU" and "species" interchangeably. Assigning sequences to OTUs relies on grouping them according to similarity. Sequences above some threshold level of similarity (usually 97 %) are grouped into an OTU. A representative sequence from each OTU is then picked; usually the most abundant sequence within a given OTU. This representative sequence is then compared to representative sequences that are more than 90% similar to a 16S rRNA gene sequence in the database. For example from this procedure we might find out that a particular 16S rRNA gene sequence belongs to the sulfate

reducing genus *Desulfovibrio* .

Next, the taxonomy is checked using sequence alignment, which compares sequences against one another. This is a final error-checking step which is used to remove sequences which are highly divergent from other sequences within that OTU. Sequences which failed to align are removed from the data table.

Finally, chimeric sequences that occurred in the original PCR process are identified and removed [90].

3.3 Statistical Comparison of Different Microbial Communities

The preceding sections described how to use next-generation sequencing and the QIIME package to identify which micro-organisms are present in a particular sample. However, to go further than a basic abundance distribution of microbial taxa, and actually understand the microbial community in some way, we need to apply some further analysis. We now explain some of the different statistical techniques that are used to make comparisons between the microbial communities that are found in different samples.

3.3.1 Transforming Sequence Data

Typically in sequence data we get different numbers of sequences per sample and this does not necessarily reflect actual total DNA abundance in the sample. We therefore normalise the total number of sequences across samples in one of two ways:

1. **Proportion**: The number of sequences associated with an OTU is divided by the total number of sequences in that sample.

2. **Rarefaction:** A maximum number of sequences is chosen (usually the total number of sequences in the sample containing the *lowest* total number of sequences). Sequences from each sample are then randomly sub-sampled until this maximum number is reached [91].

In chapter 6 of this thesis we use either of these methods, depending on what the situation requires. Other, more complex data transformation methods do exist, but we do not discuss them here [91].

3.3.2 Measuring Ecological Diversity

Ecological studies often focus on the diversity of the organisms present in a given ecosystem. However, the study of diversity is particularly important in microbial ecology, because the diversity of microbial ecosystems has been found to be very high in comparison to that of macro-organisms [73]. Several approaches exist for defining and quantifying diversity [92]. Here we outline the key principles.

α-diversity

α-diversity simply refers to the local diversity of species within an ecosystem or sample. There are two main important concepts relevant to the measurement of α-diversity:

1. **Species richness**: This measure is simply defined as the the number of different species present in a given ecosystem [93]. For example, if environment A contains 100 different species and environment B contains 200 different species then by this measure environment B would be considered more diverse.

2. **Species evenness**: This is a measure of how numerically similar the species abundance distributions of different samples are. For example, if

two environments each comprising 100 individuals and four species had the abundance distributions A = {25,25,25,25} and B = {97,1,1,1} then environment A would be considered to have high evenness and environment B would be considered to have low evenness [94]. Species evenness is important in microbial ecology because microbial communities have very low evenness. Microbial ecosystems are typically described by a long-tail distribution, where a very small number of species comprise most of the biomass in an environment, and a very large number of species (perhaps tens of thousands) are in extremely low abundance [92].

For microbial communities an α-diversity measure accounting for both species richness and species evenness is generally used. One such measure is the Shannon index $H^{'}$, defined by Eq. 3.1 [95].

$$H^{'} = -\sum_{i=1}^{N} p_i \ln(p_i) \tag{3.1}$$

N defines the number of different species i in an environment, and p_i defines the proportion of the total community that species i comprises. For microbial sequence data, i would refer to an OTU and p_i would be defined in terms of the total number of sequences in that sample. The Shannon index considers both richness and evenness because it is a function of both the total number of species in a sample *and* the proportion of the total community that a particular species comprises.

Many studies have used the Shannon index to measures diversity. For example, a study of microbial diversity in an anoxic zone of the tropical South-Pacific ocean [96], and a study of the microbial diversity in a glacial outflow in Antarctica [97].

β-diversity

Where α-diversity reflects the species diversity within a sample, β-diversity reflects the change in species composition *between* different samples.

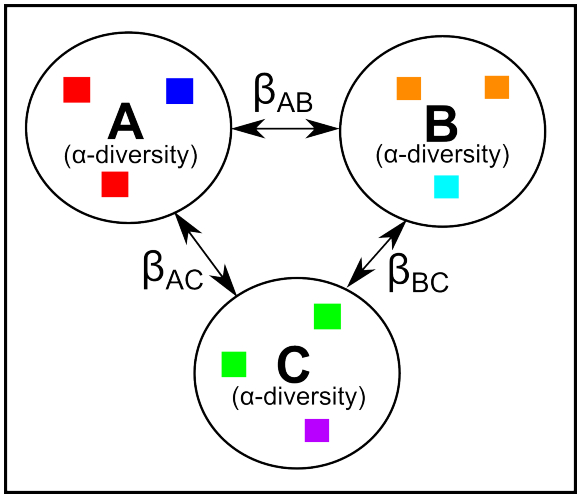

Figure 3.3 Schematic illustrating the difference between α-diversity and β-diversity. Each coloured square illustrates a different species. The three circles indicate three different environments/samples A,B and C. [94].

Fig. 3.3 illustrates the difference between α and β-diversity. The three samples pictured have exactly the same α-diversity (species number and evenness). However, they contain completely dissimilar species. β-diversity defines the similarity of the species composition between these environments, where $\beta_{i,j}$ defines the β-diversity between samples i and j.

Many different statistical approaches can be used for comparing communities (i.e. calculating β-diversity). One of these is the Bray-Curtis coefficient [98]. The Bray-Curtis coefficient between two samples j and k is defined as S'_{jk} by Eq. 3.2.

$$S'_{jk} = 100\left[1 - \frac{\sum_{i=1}^{p} y_{ij} - y_{ik}}{\sum_{i=1}^{p}(y_{ij} + y_{ik})}\right] \tag{3.2}$$

Here, y_{ij} defines the the abundance of the ith species in the jth sample, and y_{ik} defines the abundance of the ith species in the kth sample. "Abundance" here refers to the number of sequences associated with a particular OTU. p is the number of distinct species (OTUs) and n is the number of samples, so $i = 1, 2, ..., p$ and $j = 1, 2, ..., n$. A Bray-Curtis index of 100 between 2 samples indicates identical species compositions whereas an index of 0 indicates total dissimilarity [94].

Using a coefficient such as Bray-Curtis allows us to construct a matrix defining the similarity between all possible pairings of samples, Eq. 3.3.

$$S' = \begin{pmatrix} S'_{1,1} & S'_{1,2} & \cdots & S'_{1,n} \\ S'_{2,1} & S'_{2,2} & \cdots & S'_{2,n} \\ \vdots & \vdots & \ddots & \vdots \\ S'_{n,1} & S'_{n,2} & \cdots & S'_{n,n} \end{pmatrix} \tag{3.3}$$

Multidimensional Scaling: NMDS Plots

Multdimensional scaling is a method of visualising the similarity matrix defined by Eq. 3.3. A so-called "NMDS plot" (NMDS stands for "Non-metric multidimensional scaling") is a 2D projection of the multidimensional Bray-Curtis matrix in which, as far as possible, the distance between 2 points maps onto the similarity between the species composition of those 2 samples.

The NMDS plot is in practice computed by an iterative procedure, using a package such as the PRIMER statistical package [94]. This also produces a measure called stress which defines how well the plot represents the real dissimilarities.

3.3.3 Multivariate Statistics

Fig. 3.4 shows an example NMDS plot. There are clear differences between the microbial community from environment A (red squares) and environment B (blue squares). On this plot, the two environments are clearly grouped separately, the datapoints representing the microbial community of each environment are clustered together. However, to go beyond making broad qualitative statements like these, we need to use multivariate statistics.

The PRIMER statistical package allows us to perform a multivariate statistical test called a "PERMANOVA test". This test can be used to determine whether the difference between the means of two datasets is due to random variation or not (i.e. is "statistically significant"). In microbial ecology, this could be used to distinguish whether differences in the Bray-Curtis Coefficient (Eq.3.2) is due to random variation or not; for example, whether the difference in microbial community composition from replicate samples of two different environments is statistically significant.

In Fig. 3.4 it appears likely that there is a true difference in the microbial community comprising environments A and B. Fig. 3.4 also illustrates the basic principle behind a PERMANOVA test. A PERMANOVA test uses a version of the F-statistic (called a Pseudo-F), which compares the variability within groups to the variability among different groups. A larger F-statistic thus indicates that there is a statistically significant difference between the means of two datasets. A PERMANOVA test calculates a version of an F-statistic by calculate the sum of the squared distances to the mean centroid (centre point) of each group. If the sum of the squared distances to the overall centroid is much large than the sum of the squared distances to the mean centroid of each group, then the PERMNANOVA test would produce a large Pseudo-F score, and a p-value indicating statistical significance [99].

Another useful test within PRIMER is the PERMDISP test. This can be used to establish inter-replicate variability. A PERMANOVA test also detects this

dispersion difference but is unable to separate it from a difference in the means of each group. For this reason, most analyses conduct both a PERMDISP *and* a PERMANOVA test to determine whether the apparent difference between two groups is entirely due to dispersive effects or not.

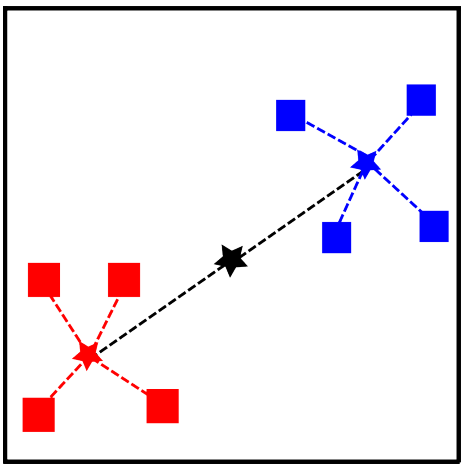

Figure 3.4 Example NMDS plot that also illustrates the basic principle behind a PERMNANOVA test. Axes represent arbitrary distances. Stars indicate the centroids of each group of points, and the overall centroid. Red and blue squares represent replicate samples from generic environments A and B respectively. The example data presented here would be statistically significant for a PERMANOVA test [94]. The axes are arbitrary units.

3.4 Chemical Measurements

In the experimental work presented in this thesis we will be measuring chemical composition as well as looking at the microbial community composition. In this section, we introduce and discuss the main method we use for measuring the chemical composition of a microbial ecosystem in chapter 6; voltammetry. Voltammetry is an electrode-based technique used to measure chemical concentrations in solution. It can be applied to measuring the chemical state of microbial ecosystems, for example, it has been used to measure bacterial sulfide oxidation rates [100] and to determine the chemistry of deep sea hydrothermal vents [101]. In this section we explain the principles behind making chemical measurements

using voltammetric electrodes, how these electrodes are calibrated, and how they can be used to measure dissolved chemical concentrations.

3.4.1 Voltammetry

Introduction to Voltammetry

Voltammetry is a type of microelectrode technique used to determine dissolved chemical concentrations. Microelectrodes have been an important tool for understanding microbial processes in the natural environment. For example, microelectrodes have been used to determine rates of phototrophic sulfide oxidation in an inland estuary [100] and to study the chemistry of microbial mats surrounding deep sea hydrothermal vents [102].

The use of microelectrode techniques such as voltammetry for chemical analysis has two main advantages. First, such electrodes are typically very versatile, and are able to simultaneously measure the concentrations of many different dissolved chemicals, such as iron, manganese, or sulfide [103]. Second, microelectrodes are able to measure the spatial profiles of chemicals to millimetre degrees of spatial resolution, and as such have been widely used to measure chemical depth profiles in, for example, ocean sediments [104].

The principle behind voltammetry is based on different ionic species (dissolved chemicals) dynamically reacting with the surface of an electrode in response to a change in voltage. When the ion reacts with the electrode it produces a change in measured current which corresponds to its concentration. This produces a so-called "voltammagram", a graph of voltage against current with peaks at different specific voltages. These current peaks can be matched up to different dissolved chemicals, because each chemical ion reacts with the electrode at a different specific voltage

Different voltammetric methods differ in the shape of the voltage pulse over time.

In linear sweep voltammetry the voltage is gradually increased over time, and a current measurement is made at each voltage. In square wave voltammetry the voltage is stepped-up in a square pulse over time, and current measurements can be made at the peak and trough of each square. The difference between square wave and linear sweep voltammetry is further illustrated by Fig. 3.5.

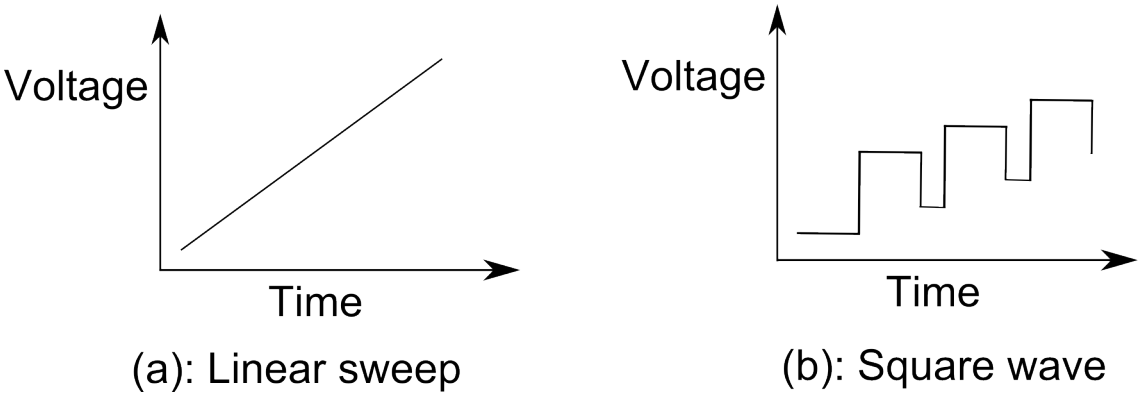

Figure 3.5 Schematic illustration of the difference between (a) linear sweep voltammetry and (b) square wave voltammetry.

In chapter 6 of this thesis voltammetric chemical measurements are made using square-wave voltammetry with a three electrode array consisting of a gold-amalgam (mercury) working electrode, a platinum counter electrode and a silver/silver chloride (Ag/AgCl) reference electrode. The reference electrode applies a voltage against the working electrode. A range of voltages is scanned through, and different dissolved chemicals react with the mercury surface of the working electrode at specific, known voltages.

The counter electrode passes current to keep the effective potential between the reference electrode and the working electrode stable. The reference electrode is designed to have a known, stable electrode potential against which the potential at the working electrode can be judged. The amount of current that the counter electrode had to pass in order to keep the voltage stable corresponds to the concentration of the chemical. Fig. 3.6 shows an example voltammagram with a dissolved sulfide peak at -0.8V.

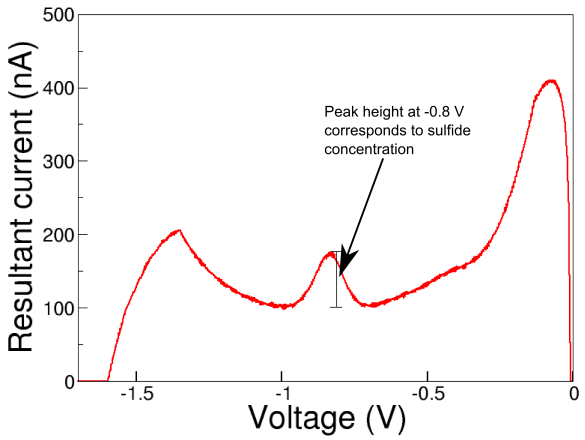

Figure 3.6 Typical voltammagram. A peak at approximately -0.8 V indicates the presence of dissolved sulfide. The height of this peak in current corresponds to the sulfide concentration; the conversion between sulfide concentration and peak height in current is determined by the calibration curve shown in Fig. 3.8.

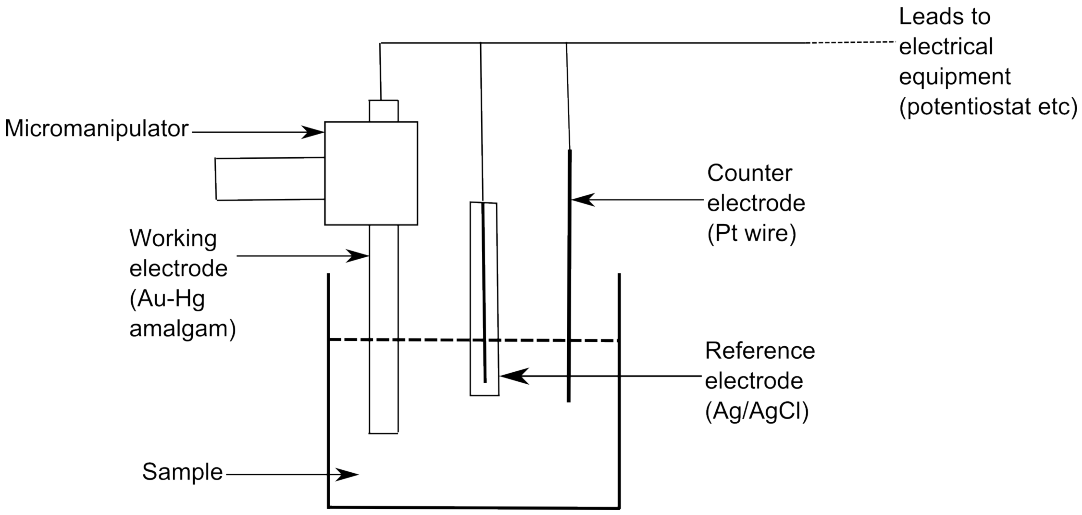

Figure 3.7 Schematic diagram of a typical setup when making voltammetric measurements.

Fig. 3.7 shows a diagram of a typical voltammetric setup. To obtain chemical depth profiles the working electrode can be attached to a micromanipulator. The counter and reference electrodes do not need to be repositioned for every measurement and so only the working electrode needs to be raised and lowered by the micromanipulator. The system then measures chemical concentrations at

the surface of the working electrode. The working electrode can the be gradually lowered through the system and a voltammetric measurement can be made at each depth. This allows chemical depth profiles to be obtained to millimetre spatial resolution. We constructed electrodes in house using the methods described by Luther et al. [105]. We outline this construction process in Appendix A. The advantage of constructing electrodes in house is that, if the electrodes break, they can be cheaply and quickly repaired.

Measuring Hydrogen Sulfide

Voltammetric electrodes must be calibrated with respect to each chemical that the experimenter wishes to measure. In chapter 6 of this thesis we use voltammetric electrodes to measure sulfide concentrations, and so in this section we discuss how our system of voltammetric electrodes was calibrated for measuring dissolved sulfide concentrations.

The voltammetric peak for sulfide is the sum of the H_2S, HS^-, and any polysulfide species and is defined as total S(-II) [105, 106]. Dissolved sulfide undergoes the following reaction (Eq. 3.4) with mercury at approximately -0.8 V (see Fig. 3.6).

$$HS + Hg \rightarrow HgS + H^+ + 2e \tag{3.4}$$

The specificity of the potential at which this reaction happens makes voltammetric measurements of sulfide highly accurate. Furthermore, the reliability of voltammetric chemical measurements has been demonstrated by comparison with chemical measurements obtained by other methods (for example, by comparison with chemical measurements obtained spectrophotometrically [106]). The possibility of other species reacting at -0.8 V is limited by the following:

1. Only those chemical species that react *with mercury* can be measured.

2. The number of possible reactive species present in natural solution at a measurable concentration is limited.

3. The range of pH and concentration values that exist within natural systems is narrow, meaning that the potential at which this reaction occurs is unlikely to vary much (although it does vary slightly).

Calibration was made using standard solutions of sodium sulfide nonahydrate in 0.1M potassium chloride (KCl) electrolyte. Data were acquired using an Analytical Instrument Systems DLK-60 potentiostat. Calibrations were performed for both square wave and linear voltammetry sweeping from 0V to -1.7V, with a scanning rate of 500 mV/s with a conditioning step of -0.8V. Each data point is an average over 3 replicate voltammagrams. Fig. 3.8 shows the calibration curve for the square wave mode. As square wave voltammetry is more accurate this is the only method we use in this thesis, and linear sweep voltammetry is not discussed further.

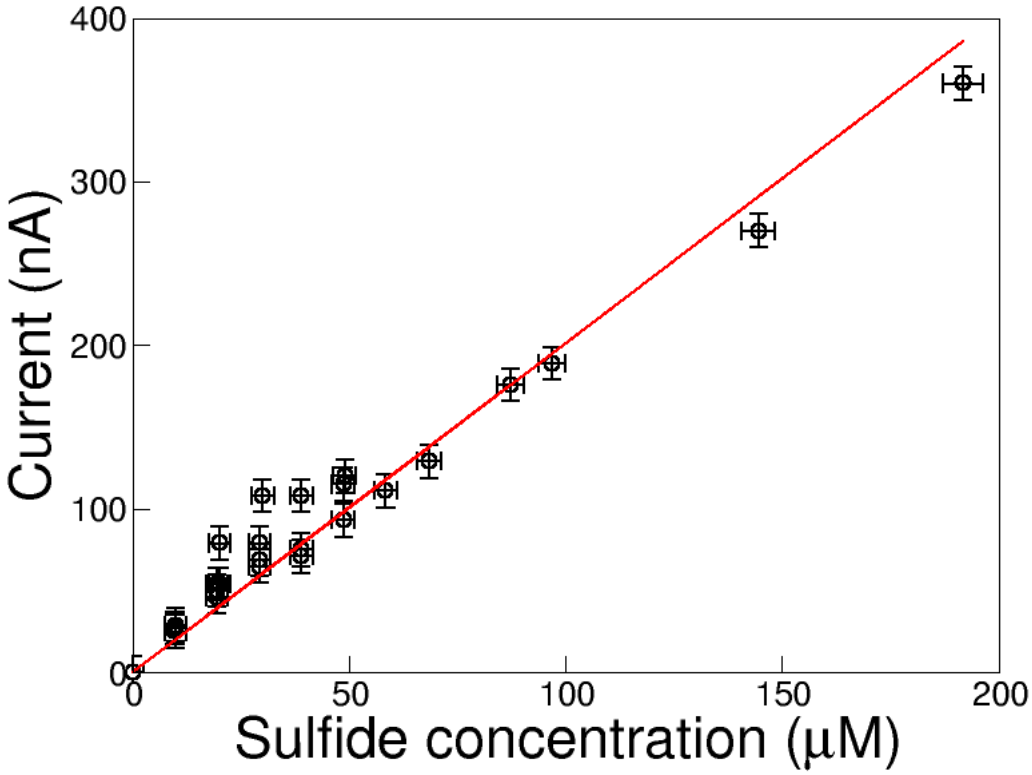

Figure 3.8 Calibration curve for Square-Wave measurements with the voltammetry system.

3.5 Discussion and Conclusions

We have explained how high-throughput sequencing techniques allow the members of a microbial ecosystem to be identified taxonomically. We then discussed how multivariate statistical techniques can be used to be make statistical comparisons between microbial communities present in different environments. Finally, we explained how an electrode technique called voltammetry can be used to measure dissolved chemical concentrations. In chapter 6, we apply both these experimental techniques to study how the chemical and microbial composition of a freshwater environment changes in response to an environmental perturbation.

Chapter 4

Theoretical Predictions of Redox Regime Shifts in Microbially-Mediated Biogeochemical Cycles

4.1 Introduction

In this chapter and the following chapter we use simple mathematical models to show that microbial population dynamics can have important qualitative effects on the response of microbially-mediated biogeochemical cycles to environmental change. Specifically, limitations on microbial population size can lead to regime shifts - abrupt changes in redox state in response to a gradual change in an environmental parameter. We term this a "redox regime shift" i.e. a nonlinear transition in the predominant redox state of a biogeochemical cycle in response to a gradual change in an environmental stimulus. We note that in some other

studies, the term "regime shift" has been associated with bistability. Here, we use the term simply to describe a sharp response, without any implied bistability. In the next chapter (chapter 5) we go on to show that redox regime shifts are preserved in more detailed models containing a variety of environmentally realistic modifications. We then discuss under what environmental conditions these models predict such regime shifts would occur, and use this to suggest some likely candidate ecosystems for observing this behaviour.

Regime shifts are known to occur in diverse ecosystems in response to diverse stimuli; examples range from aquatic ecosystems in the leaves of carniverous pitcher plants [107] to large-scale shifts in terrestrial vegetation cover [108]. These regime shifts are usually caused by specific features of the ecosystem topology such as feedback mechanisms [109]. The simple mathematical models outlined in this chapter and the next suggest that for microbially-mediated biogeochemical cycles, non-linear effects arising from microbial population dynamics can lead to regime shifts between oxidized and reduced ecosystem states, even for ecosystems with simple topologies.

4.2 Constructing Simple Models for Microbially-Mediated Biogeochemical Cycles

In this section, we briefly review the concept of a microbially-mediated biogeochemical cycle and discuss how they are all based on a core "redox topology". We then introduce a set of simple mathematical models for these cycles.

4.2.1 Microbial Redox-Cycling Systems

In a microbially-mediated biogeochemical cycle or a nutrient-cycling microbial ecosystem, a chemical element is shuttled between its oxidized and reduced forms

in a series of steps that may be biotically or abiotically mediated [6]. Fig. 4.1 illustrates schematically the topologies of the iron, sulfur, carbon and nitrogen cycles (panels a-d) [4, 6, 110, 111].

A redox reaction in a microbially-mediated biogeochemical cycle couples the oxidation/reduction of the element being cycled to the reduction/oxidation of another chemical species. For example, in the sulfur cycle, the microbial reduction of sulfate can be coupled to the oxidation of acetate [6], while in the nitrogen cycle, the oxidation of ammonia can be coupled to the reduction of molecular oxygen [6]. In order to avoid confusion, we refer to the latter chemical species (in these examples acetate or oxygen) as the "electron donor/acceptor". The electron donor/acceptor may be supplied from some external source (e.g. oxygen from the atmosphere) or may be generated by another biogeochemical process (e.g. microbial decomposition producing acetate). Many different chemical species can act as electron donors or acceptors; for example acetate or hydrogen can function as the electron donor for reductive reactions while nitrate or oxygen can function as the electron acceptor for oxidative reactions [6]. The redox-shifting behaviour which arises in our models is generic, independent of which chemical species performs the role of electron donor/acceptor.

Crucially, if the electron acceptor/donor is in short supply then its availability can control the rate of the redox reaction, and hence the flux of the biogeochemical cycle. Moreover, in natural environments, the availability of electron acceptors and donors is strongly dependent on the environmental conditions. For example, in aquatic ecosystems, the supply of oxygen depends on its solubility, which is temperature-dependent [22], and on the rate of photosynthesis [112], while the supply of acetate depends on the rate of the microbial decomposition of organic matter, which can be drastically affected by factors like sewage effluent or phosphorus inflow from agricultural runoff [113].

The aim of our model is to predict the response of microbially-mediated biogeochemical cycles and nutrient-cycling microbial ecosystems to changes in the availability of electron acceptors (such as oxygen) and electron donors (such

as acetate). To encapsulate the basic topology of these cycles, we begin by considering a simplified two-state model (Fig. 4.1e), in which an oxidized form of a chemical element (here denoted s_{o}) is converted via microbial metabolism to a reduced form (s_{r}), which is recycled back to the oxidized form either by a second microbial metabolism or by an abiotic reaction. The reduction step $s_{\mathrm{o}} \rightarrow s_{\mathrm{r}}$ (blue right-to-left arrow in Fig. 4.1e) is assumed to be biotic, i.e. mediated by microbial metabolism. This step requires acetate as an electron donor. The oxidation step $s_{\mathrm{r}} \rightarrow s_{\mathrm{o}}$ may occur biotically or abiotically (indicated by the blue and red left-to-right arrows in Fig. 4.1e), and requires oxygen as an electron acceptor. The possibility of an abiotic reduction reaction is not included in the model because these are minor reactions at ambient temperatures in the natural environment (with the notable exception of the reaction of Fe(III) with sulfide [114]).

Although this model is topologically very simple, it reveals an important and non-trivial regime shifting behaviour. In the next chapter, we show that this behaviour is preserved in more realistic models that include features such as spatial heterogeneity, multiple redox states and explicit coupling to the environment.

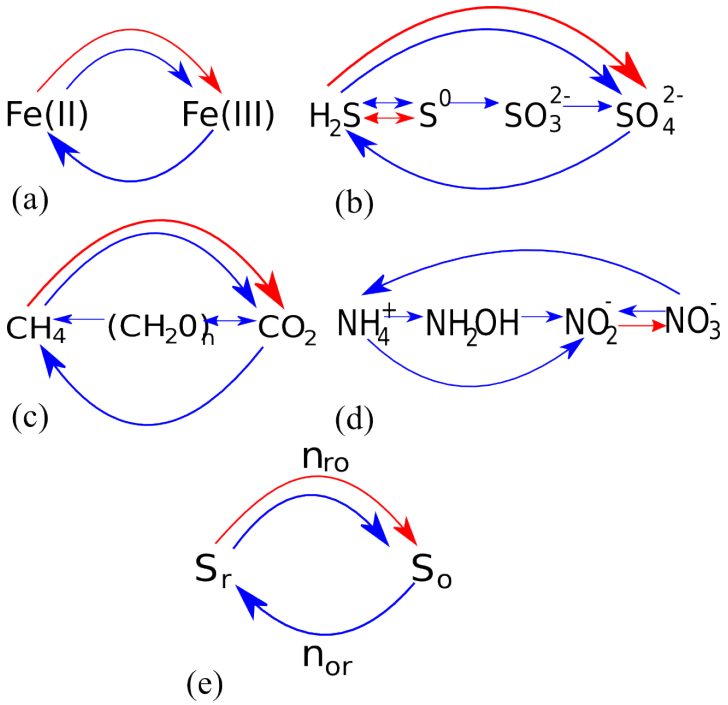

Figure 4.1 Schematic view of the biogeochemical redox cycles involving iron, sulfur, carbon and nitrogen (a-d) [4, 6, 110, 111], together with the simple model investigated in this chapter (e). In all panels, oxidation reactions proceed to the right, and reduction reactions proceed to the left. Biologically catalysed (metabolic) reactions are shown in blue, and abiotic reactions are shown in red. Abiotic reduction reactions are not shown, as these are minor reactions in the natural environment (but can be included see section 4.5). Many important chemical states are not shown (but inclusion of extra states does not affect modelling results; this is one of the modifications to the model that we discuss in section 4.6.2). In panel e, s_r and s_o represent the reduced and oxidized forms of the chemical element being cycled.

4.2.2 Modelling Fully Biotic Redox Cycles

If both the oxidative and reductive steps in the redox cycle are mediated by micro-organisms, the dynamics of the two-state model can be represented by the following set of differential equations (in which the dot represents a time rate of

change):

$$\dot{n}_{\mathrm{or}} = n_{\mathrm{or}} G_{\mathrm{or}}(s_{\mathrm{o}}, n_{\mathrm{or}}) - d n_{\mathrm{or}} \tag{4.1}$$

$$\dot{n}_{\mathrm{ro}} = n_{\mathrm{ro}} G_{\mathrm{ro}}(s_{\mathrm{r}}, n_{\mathrm{ro}}) - d n_{\mathrm{ro}} \tag{4.2}$$

$$\dot{s}_{\mathrm{r}} = \gamma \left[n_{\mathrm{or}} G_{\mathrm{or}} - n_{\mathrm{ro}} G_{\mathrm{ro}} \right] = -\dot{s}_{\mathrm{o}}. \tag{4.3}$$

The variables in this dynamical system are n_{ro} and n_{or}, the population densities of the oxidizing and reducing microbial populations respectively, and the concentrations s_{o} and s_{r} of the oxidized and reduced chemical species. Eqs. 4.1 and 4.2 describe the microbial population dynamics; the reducing and oxidizing populations have growth rates $G_{\mathrm{or}}(s_{\mathrm{o}}, n_{\mathrm{or}})$ and $G_{\mathrm{ro}}(s_{\mathrm{r}}, n_{\mathrm{ro}})$ respectively, which depend explicitly on s_{o} and s_{r}, but also depend implicitly on the concentrations of acetate and oxygen respectively. Both populations are assumed to die at a constant rate d (e.g. due to viral predation). Eq. 4.3 describes changes in the substrate dynamics due to microbial consumption and production; here γ is a yield coefficient, which is assumed for simplicity to be the same for both reactions. In this simple model, there is no inflow or washout of substrate, and as such the total quantity of substrate within the system ($s_{\mathrm{tot}} = s_{\mathrm{o}} + s_{\mathrm{r}}$) is completely conserved.

The microbial growth rate functions G_{or} and G_{ro} play a crucial role in the model. As outlined in chapter 2, the microbial growth rate on a limiting nutrient is often described by a Monod function $vs/(K+s)$ where s is the nutrient concentration, v is the maximal growth rate and K is the nutrient concentration at which growth rate is half-maximal [54]. This encapsulates the key fact that the growth rate is nutrient-dependent at low nutrient concentration but saturates at high nutrient concentration. Importantly, however, this growth rate function assumes that growth is limited by a single nutrient, while, in the natural environment, the rate of microbial growth may be limited by other factors such as the availability of carbon or micronutrients, toxin or waste product formation at high densities, or simply competition for space [62]. To account for this in a generic way, the

Monod term is multiplied by a population density-limitation factor $(1 - n/n_{\max})$, where the parameter $n_{\max}$ sets a maximal population density. Again, as outlined in chapter 2 this type of logistic population size limitation is a convenient and commonly-used way to encapsulate growth-limitation by factors not explicitly included in the model [63–65].

These considerations lead to the following simple forms for the microbial growth rates:

$$G_{\mathrm{or}} = \left[\frac{v_{\mathrm{or}} s_{\mathrm{o}}}{K_{\mathrm{or}} + s_{\mathrm{o}}}\right] \times \left[1 - \frac{n_{\mathrm{or}}}{n_{\mathrm{or,max}}}\right] \tag{4.4}$$

$$G_{\mathrm{ro}} = \left[\frac{v_{\mathrm{ro}} s_{\mathrm{r}}}{K_{\mathrm{ro}} + s_{\mathrm{r}}}\right] \times \left[1 - \frac{n_{\mathrm{ro}}}{n_{\mathrm{ro,max}}}\right] \tag{4.5}$$

in which the parameters are v_{or} and v_{ro}, the maximal growth rates for the reducing and oxidizing microbial populations respectively, K_{or} and K_{ro}, the concentrations of the chemical species $\mathrm{s_o}$ or $\mathrm{s_r}$ at which the growth rate is half-maximal, and $n_{\mathrm{or,max}}$ and $n_{\mathrm{ro,max}}$, the maximal densities of the two populations. Importantly, the concentrations of acetate and oxygen are implicit in the maximal growth rate parameters v_{or} and v_{ro}: v_{or} is expected to increase with the availability of acetate, while v_{ro} is expected to increase with the availability of oxygen.

4.2.3 Modelling Biotic-Abiotic Redox Cycles

If the oxidation step in the redox cycle is instead abiotic, the model has only 3 variables: the population density of the reducing microbial population n_{or}, and the concentrations of the oxidized and reduced chemical species, s_{o} and s_{r}. In this case, the dynamics of the microbial population n_{or} is still described by Eq. 4.1, but the chemical dynamics obey

$$\dot{s_{\mathrm{r}}} = -F(s_{\mathrm{r}}) + \gamma n_{\mathrm{or}} G_{\mathrm{or}} = -\dot{s_{\mathrm{o}}}. \tag{4.6}$$

Here, the abiotic oxidation rate is described by the function $F(s_\mathrm{r})$. Abiotic oxidation reactions can occur spontaneously (e.g. the atmospheric oxidation of hydrogen sulfide [115]), or they can be catalyzed (e.g. some electron transfer processes on mineral surfaces [116]) or limited by transport processes [117]. To account for these factors in a generic way, we assume a Michaelis-Menten form for $F(s_\mathrm{r})$ [118]:

$$F = \frac{v_\mathrm{a} s_\mathrm{r}}{K_\mathrm{a} + s_\mathrm{r}} \tag{4.7}$$

where v_a is the maximal abiotic rate constant (which may implicitly depend on a catalyst concentration) and K_a is the concentration s_r at which the abiotic reaction rate is half-maximal. If K_a is large such that $K_\mathrm{a} \gg s_\mathrm{r}$, the reaction rate becomes linear in s_r.

4.3 Analytical Solutions to the Simple Redox-Cycling Models

The simple nutrient cycling models shown in Eqs. 4.1-4.6 can be solved analytically. In this chapter we derive and discuss these solutions, which are presented in the following subsections.

4.3.1 Analytical Solution for the Fully Biotic Redox Cycling Model

Setting $\dot{n_\mathrm{or}}$ and $\dot{n_\mathrm{ro}}$ in Eqs. 4.1-4.2 to zero, Eq. 4.8 can be obtained:

$$d = \left(\frac{v_\mathrm{or} s_\mathrm{o}}{s_\mathrm{o} + K_\mathrm{or}}\right)\left(1 - \frac{n_\mathrm{or}}{n_\mathrm{or,max}}\right) = \left(\frac{v_\mathrm{ro} s_\mathrm{r}}{s_\mathrm{r} + K_\mathrm{ro}}\right)\left(1 - \frac{n_\mathrm{ro}}{n_\mathrm{ro,max}}\right), \tag{4.8}$$

which, upon substitution into Eq. 4.3, implies that in the steady state $n_\mathrm{or} = n_\mathrm{ro}$,

i.e. the two population densities are equal.

By rearranging Eq. 4.8 the following relations for the densities of the reducing and oxidizing microbial populations can be obtained:

$$n_{\mathrm{or}} = n_{\mathrm{or,max}} \left[1 - \frac{d[K_{\mathrm{or}} + s_{\mathrm{o}}]}{v_{\mathrm{or}} s_{\mathrm{o}}} \right] \tag{4.9}$$

and

$$n_{\mathrm{ro}} = n_{\mathrm{ro,max}} \left[1 - \frac{d[K_{\mathrm{ro}} + s_{\mathrm{r}}]}{v_{\mathrm{ro}} s_{\mathrm{r}}} \right]. \tag{4.10}$$

Defining $s_{\mathrm{tot}} = s_{\mathrm{o}} + s_{\mathrm{r}}$ and using the fact that $n_{\mathrm{or}} = n_{\mathrm{ro}}$ gives

$$n_{\mathrm{ro,max}} \left[1 - \frac{d[K_{\mathrm{ro}} + s_{\mathrm{tot}} - s_{\mathrm{o}}]}{v_{\mathrm{ro}}(s_{\mathrm{tot}} - s_{\mathrm{o}})} \right] = n_{\mathrm{or,max}} \left[1 - \frac{d[K_{\mathrm{or}} + s_{\mathrm{o}}]}{v_{\mathrm{or}} s_{\mathrm{o}}} \right]. \tag{4.11}$$

A parameter $\xi = n_{\mathrm{ro,max}}/n_{\mathrm{or,max}}$ can be defined, which measures the ratio of the maximal population densities, allowing Eq. 4.11 to be re-written:

$$\xi \left[1 - \frac{d[K_{\mathrm{ro}} + s_{\mathrm{tot}} - s_{\mathrm{o}}]}{v_{\mathrm{ro}}(s_{\mathrm{tot}} - s_{\mathrm{o}})} \right] = \left[1 - \frac{d[K_{\mathrm{or}} + s_{\mathrm{o}}]}{v_{\mathrm{or}} s_{\mathrm{o}}} \right], \tag{4.12}$$

which, upon rearranging, gives a quadratic equation for s_{o}:

$$\begin{aligned} & s_{\mathrm{o}}^2[\xi v_{\mathrm{or}} v_{\mathrm{ro}} - d\xi v_{\mathrm{or}} - v_{\mathrm{or}} v_{\mathrm{ro}} + d v_{\mathrm{ro}}] \\ & + s_{\mathrm{o}}[-\xi v_{\mathrm{ro}} s_{\mathrm{tot}} v_{\mathrm{or}} + d\xi v_{\mathrm{or}}(K_{\mathrm{ro}} + s_{\mathrm{tot}}) + v_{\mathrm{or}} v_{\mathrm{ro}} s_{\mathrm{tot}} + d K_{\mathrm{or}} v_{\mathrm{ro}} - d v_{\mathrm{ro}} s_{\mathrm{tot}}] \\ & - d K_{\mathrm{or}} v_{\mathrm{ro}} s_{\mathrm{tot}} = 0. \end{aligned} \tag{4.13}$$

Defining the new parameter combinations $\alpha = v_{\mathrm{ro}}/v_{\mathrm{or}}$ and $\omega = (\xi - 1)v_{\mathrm{ro}}$, Eq.

4.13 can be re-written as

$$s_{\mathrm{o}}^2[\omega+d(\alpha-\xi)]+s_{\mathrm{o}}[d\xi(K_{\mathrm{ro}}+s_{\mathrm{tot}})+d\alpha(K_{\mathrm{or}}-s_{\mathrm{tot}})-\omega s_{\mathrm{tot}}]-dK_{\mathrm{or}}s_{\mathrm{tot}}\alpha=0. \quad (4.14)$$

This equation has the steady-state solution

$$s_{\mathrm{o}}=\frac{-B+\sqrt{B^2+4dK_{\mathrm{or}}s_{\mathrm{tot}}\alpha[\omega+d(\alpha-\xi)]}}{2[\omega+d(\alpha-\xi)]} \quad (4.15)$$

where

$$B=d\xi(K_{\mathrm{ro}}+s_{\mathrm{tot}})+d\alpha(K_{\mathrm{or}}-s_{\mathrm{tot}})-\omega s_{\mathrm{tot}}. \quad (4.16)$$

An expression for the steady-state concentration of the reduced chemical species s_{r} can be obtained from Eq. 4.15 using $s_{\mathrm{r}}=s_{\mathrm{tot}}-s_{\mathrm{o}}$. Expressions for the steady-state population densities n_{or} and n_{or} can be calculated by substitution into Eqs. 4.9 and 4.10. The positive solution to the square root in Eq. 4.15 is the relevant solution, as the other root gives a solution where $s_{\mathrm{o}}>s_{\mathrm{tot}}$ which is not physically realistic. (i.e. it leads to solution where the concentration of s_{o} is larger than the total amount of substrate in the system, and the concentration of s_{r} is negative).

The solution Eq. 4.15 is not well-defined right at the threshold between oxidized and reduced states, since both its numerator and denominator go to zero at this point (when $\omega+d(\alpha-\xi)=0$). Here, we can use L'Hopital's rule to show that Eq. 4.15 approaches $s_{\mathrm{tot}}/2$ at this point (i.e. evaluating $\frac{f'(\alpha)}{g'(\alpha)}$ as $\alpha\to 1$ where $f(\alpha)$ and $g(\alpha)$ are the numerator and denominator of Eq. 4.15 respectively, gives a solution $s_{\mathrm{tot}}/2$.) Furthermore, common sense suggests that at the exact threshold point $s_{\mathrm{r}}=s_{\mathrm{o}}=s_{\mathrm{tot}}/2$.

4.3.2 Analytical Solution for the Abiotic-Biotic Redox Cycling Model

We now repeat the calculation for the abiotic-biotic case Setting $\dot{n_{\mathrm{or}}} = 0$ in Eq. 4.1 gives, as for the fully biotic cycle

$$d = \left(\frac{v_{\mathrm{or}} s_{\mathrm{o}}}{s_{\mathrm{o}} + K_{\mathrm{or}}}\right)\left(1 - \frac{n_{\mathrm{or}}}{n_{\mathrm{or,max}}}\right). \tag{4.17}$$

Setting $\dot{s_{\mathrm{o}}} = 0$ in Eq. 4.6 gives

$$\frac{v_{\mathrm{a}} s_{\mathrm{r}}}{K_{\mathrm{a}} + s_{\mathrm{r}}} = \frac{\gamma v_{\mathrm{or}} n_{\mathrm{or}} s_{\mathrm{o}}}{K_{\mathrm{or}} + s_{\mathrm{o}}}\left[1 - \frac{n_{\mathrm{or}}}{n_{\mathrm{or,max}}}\right]. \tag{4.18}$$

Combining Eqs. 4.17 and 4.18 gives

$$\frac{v_{\mathrm{a}} s_{\mathrm{r}}}{K_{\mathrm{a}} + s_{\mathrm{r}}} = \gamma n_{\mathrm{or}} d = \gamma d n_{\mathrm{or,max}}\left[1 - \frac{d[K_{\mathrm{or}} + s_{\mathrm{o}}]}{v_{\mathrm{or}} s_{\mathrm{o}}}\right]. \tag{4.19}$$

Using the fact that $s_{\mathrm{r}} = s_{\mathrm{tot}} - s_{\mathrm{o}}$, and defining a new parameter combination $\phi = \gamma d n_{\mathrm{or,max}}$, allows Eqs. 4.20 to be obtained

$$\frac{v_{\mathrm{a}}(s_{\mathrm{tot}} - s_{\mathrm{o}})}{K_{\mathrm{a}} + (s_{\mathrm{tot}} - s_{\mathrm{o}})} = \phi - \frac{\phi d[K_{\mathrm{or}} + s_{\mathrm{o}}]}{v_{\mathrm{or}} s_{\mathrm{o}}}. \tag{4.20}$$

Rearranging Eq. 4.20 produces a quadratic equation for s_{o}:

$$s_{\mathrm{o}}^2\left[\phi v_{\mathrm{or}} - \phi d - v_{\mathrm{or}} v_{\mathrm{a}}\right] + s_{\mathrm{o}}\left[\phi d(K_{\mathrm{a}} + s_{\mathrm{tot}}) - \phi v_{\mathrm{or}}(K_{\mathrm{a}} + s_{\mathrm{tot}}) - v_{\mathrm{or}} v_{\mathrm{a}} s_{\mathrm{tot}} - \phi d K_{\mathrm{or}}\right] \tag{4.21}$$

$$+ \phi d K_{\mathrm{or}} K_{\mathrm{a}} + \phi d K_{\mathrm{or}} s_{\mathrm{tot}} = 0$$

the solution of which is

$$s_{\mathrm{o}} = \frac{-B' + \sqrt{B'^2 - 4(\phi v_{\mathrm{or}} - \phi d - v_{\mathrm{or}} v_{\mathrm{a}})(K_{\mathrm{or}} d\phi(K_{\mathrm{a}} + s_{\mathrm{tot}}))}}{2(\phi v_{\mathrm{or}} - \phi d - v_{\mathrm{or}} v_{\mathrm{a}})} \tag{4.22}$$

where B' is

$$B' = \phi d(K_{\mathrm{a}} + s_{\mathrm{tot}}) - \phi v_{\mathrm{or}}(K_{\mathrm{a}} + s_{\mathrm{tot}}) - v_{\mathrm{or}} v_{\mathrm{a}} s_{\mathrm{tot}} - \phi d K_{\mathrm{or}}. \tag{4.23}$$

Again, the solution where the positive of the square root is taken is relevant, as taking the negative of the square root gives a solution where $s_{\mathrm{o}} > s_{\mathrm{tot}}$ which is not physically realistic (i.e. it leads to solution where the concentration of s_{o} is larger than the total amount of substrate in the system, and the concentration of s_{r} is negative). An expression for s_{r} can be calculated from Eq. 4.22 using $s_{\mathrm{r}} = s_{\mathrm{tot}} - s_{\mathrm{o}}$. An expression for the density n_{or} of the reducer population can be obtained by substituting Eq. 4.22 into Eq. 4.17.

4.4 The Effect of Environmental Perturbations in Simple Redox- Cycling Models

The analytical solutions to these simple models can be studied to investigate the ecosystem-level responses of the models to environmental change. In this section we discuss such ecosystem level responses. First, we show that environmental perturbations can drive an abrupt change in the global redox state of the ecosystem. We then discuss how the corresponding microbial populations are affected by this regime shift. We focus on environmental changes that affect the availability of oxygen or acetate, such as temperature-related changes in oxygen solubility [22], changes in photosynthesis rate, or changes in the abundance or rate of decomposition of organic matter [113]. For the fully biotic cycle, the parameters

v_{or} and v_{ro} are proxies for the availability of acetate and oxygen respectively. For the biotic-abiotic cycle, the equivalent parameters are v_{or} and v_{a}.

4.4.1 Regime Shifts in the Redox State

The response of the ecosystem to changes in acetate or oxygen abundance can be quantified via the steady-state fraction of oxidized species, $s_{\mathrm{o}}/s_{\mathrm{tot}}$, which acts as a proxy for the global redox state of the system.

The key result of this chapter is that for both the fully biotic and the biotic-abiotic models, the model can undergo regime shifts: sharp changes in ecosystem redox state as the availability of oxygen or acetate crosses a critical threshold (Fig. 4.2). These regime shifts happen under circumstances where the total concentration of the chemical element being cycled ($s_{\mathrm{tot}} = s_{\mathrm{o}} + s_{\mathrm{r}}$) is high, such that $s_{\mathrm{tot}} \gg K_{\mathrm{or}}, K_{\mathrm{ro}}, K_{\mathrm{a}}$, implying that the microbial population density is limited by factors other than the availability of $\mathrm{s_o}$ or $\mathrm{s_r}$. In contrast, for lower concentrations of the chemical element being cycled, $s_{\mathrm{tot}} < K_{\mathrm{or}}, K_{\mathrm{ro}}, K_{\mathrm{a}}$, the model predicts a more gradual change in ecosystem state as the availability of oxygen/acetate varies. For the biotic-biotic cycle, the model prediction is symmetric with respect to changes in v_{or} and v_{ro} (representing changes in acetate and oxygen; compare Fig. 4.2a and c). Consequently, it is the ratio of $v_{\mathrm{or}}/v_{\mathrm{ro}}$ (mimicking a change in the ratio of acetate/oxygen availability) that drives the behavior of the model. For the biotic-abiotic cycle, the model predicts regime shifts in response both increasing acetate (Fig. 4.2b) and increasing oxygen (Fig. 4.2d), but the shapes of these responses are different. This is because the biotic and abiotic reaction rates have different functional dependences on s.

The redox regime shifts which are observed in the model arise from the interplay between microbial population density limitation and nutrient cycling. In the model the global redox state is controlled by the balance between oxidative and

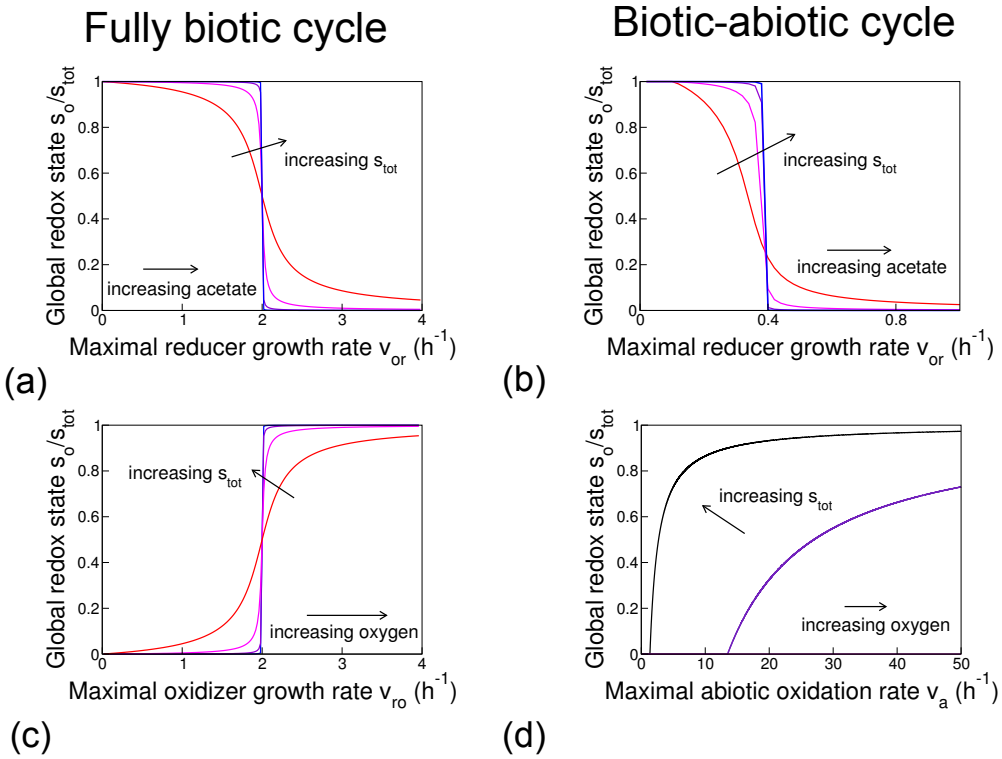

Figure 4.2 Redox regime shifts in model microbially-mediated redox cycles. The global redox state, as measured by the oxidized fraction s_o/s_{tot}, predicted by the analytic forms of the steady-state solution of the model equations for the fully biotic cycle (a and c, Eqs. 4.15-4.16) or the biotic-abiotic cycle (b and d, Eqs. 4.22 and 4.23) is plotted as a function of parameters that form proxies for the degree of reductive or oxidative driving. These parameters are: for reductive driving, the maximal growth rate of the reductive population, v_{or} (a and b, keeping v_{or} fixed at 2 h^{-1} or $v_a = 0.2\mu Mh^{-1}$), and, for oxidative driving, either the maximal growth rate of the oxidative population v_{ro} (c, keeping v_{ro} fixed at 2 h^{-1}) or the maximal abiotic oxidation rate v_a (d, also with $v_{ro} = 2$ h^{-1}). The results show a shift between oxidized and reduced ecosystem states as a threshold in reductive or oxidative driving is crossed; the sharpness of this transition increases with the concentration of the chemical species being cycled, s_{tot} (in panels a to c, red to blue lines; red: $s_{tot} = 20\mu M$, pink: $s_{tot} = 0.2$ mM, purple: $s_{tot} = 2$ mM blue: $s_{tot} = 20$ mM; in panel d, black line $s_{tot} = 2$ M: dark purple line: $s_{tot} = 200$ mM). The other parameters are $K_{or} = K_{ro} = K_a = 1\mu M$ [119], $n_{or,max} = n_{or,max} = 9 \times 10^7$ cells per l, $d = 0.1$ h^{-1} and $\gamma = 3 \times 10^{-8}\mu$mol per cell [120].

reductive chemical fluxes. An increase in the availability of oxygen stimulates the oxidation reaction, resulting in an increase in concentration of the oxidized chemical species, s_o. If there were no limitation on microbial population density, this increase in s_o would stimulate the growth of the reducing microbial population, which consumes s_o; thus the global ecosystem state would respond only gradually to changes in oxygen availability (and likewise for changes in the availability of acetate), as shown in Fig. 4.2 for small values of s_{tot} (red lines). However, the situation is different if the microbial population density is limited by other factors. In this case an increase in the availability of oxygen increases s_o, but the reducer population cannot respond to this increase in s_o because it is already close to its maximal population density. Once the oxygen supply crosses a critical threshold, the production rate of s_o exceeds the maximal consumption capacity of the reducer population and the system undergoes a regime shift to an oxidized state, as in Fig. 4.2 for large values of s_{tot} (blue lines). The same scenario holds in reverse for changes in the availability of acetate; here, as acetate availability increases, a redox regime shift from an oxidized to a reduced system state occurs.

4.4.2 How Does an Environmental Perturbation Affect the Microbial Population Density?

Fig. 4.2 shows how the global redox state of the model, s_o/s_{tot}, changes with the degree of reductive or oxidative driving. This data reveals sharp transitions (redox regime shifts), the sharpness of which increases with s_{tot}. In this section, we discuss how the microbial population densities vary during these transitions. Fig. 4.3 shows the density of the reducing microbial population, n_{or} (which for the fully biotic cycle is equal to n_{ro}) as a function of the parameters which form proxies for reductive or oxidative driving (v_{or}, v_{ro} and v_a). In all cases, the microbial population density responds gradually to changes in reductive or

oxidative driving, even when the global ecosystem redox state responds sharply (compare to Fig. 4.2). As the driving increases, the population responds by increasing in size, until it approaches its maximum density $n_{\max}$ which in this case is equal to 9×10^7 cells/l. For the fully biotic cycle, and for the biotic-abiotic cycle under reductive driving, the steady state population size is only weakly dependent on the total concentration of the element being cycled (s_{tot}).

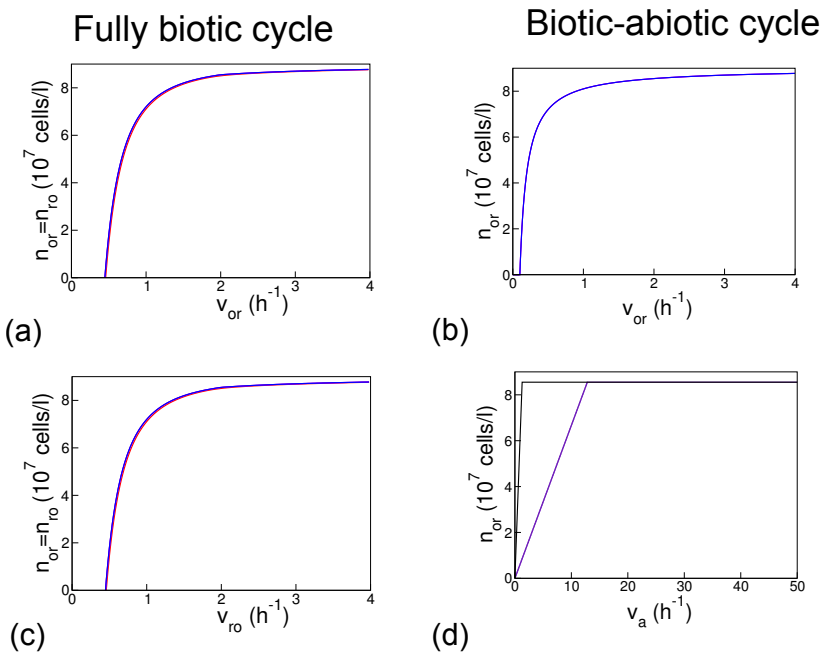

Figure 4.3 Changes in the microbial population density as the model undergoes a redox regime shift. For the fully biotic cycle (left panels), the oxidizing and reducing populations have equal population densities, $n_{\text{or}} = n_{\text{ro}}$. For the biotic-abiotic cycle (right panels), the population density of the reducing population, n_{or}, is plotted. The top panels show the response to increase in reductive driving (mimicking increase in acetate) while the bottom panels show the response to an increase in oxidative driving (mimicking increase in oxygen). The parameters are as in Fig. 4.2 $K_{\text{or}} = K_{\text{ro}} = K_{\text{a}} = 1\mu$M, $n_{\text{or,max}} = n_{\text{ro,max}} = 9 \times 10^7$ cells/l, $d = 0.1$ h^{-1} and $\gamma = 3 \times 10^{-8}\mu$ mol/cell. In a, v_{ro} is fixed at 2 h^{-1}, in b and d v_{or} is fixed at 2 h^{-1} and in c, $v_{\text{a}} = 0.2\mu$Mh^{-1}. Different colors represent different values of s_{tot}, as in Fig. 4.2; however, in most cases different values of s_{tot} produce such similar population densities that the lines are indistinguishable when plotted. Where the analytical solution of the model equations predicts a negative population density, we set $n_{\text{or}} = n_{\text{ro}} = 0$.

4.5 The Role of the Maximal Population Density Parameter

In the model, the fact that the microbial population density is ultimately limited by factors other than the chemical being cycled (s) is represented by introducing a "logistic" term $(1 - n/n_{\max})$ in the equation for the microbial growth kinetics. In this section we discuss the parameter $n_{\max}$ in more detail. We first explore the effect of varying the parameters $n_{\mathrm{or,max}}$ and $n_{\mathrm{ro,max}}$ corresponding to the reducer and oxidizer populations, and find that the qualitative steady-state behaviour of the model is unaffected by these parameters, although the time-scale for reaching the steady state is affected. We then show that redox regime shifts are still obtained in a model where this logistic term is replaced by equations that represent explicit growth-limitation by an additional nutrient source.

4.5.1 The Maximal Population Density in the fully biotic model

In the fully biotic model, the steady state solution (Eqs. 4.15-4.16) depends only on the ratio of the maximal population densities of the reducer and oxidizer populations, $\xi = n_{\mathrm{or,max}}/n_{\mathrm{ro,max}}$, and not on the absolute values of $n_{\mathrm{or,max}}$ and $n_{\mathrm{ro,max}}$. However, the timescale at which the steady state is reached does depend on the absolute maximal population densities; as these increase the system responds more slowly (Fig. 4.4a). Considering only the steady-state solution, changing the ratio of maximal population densities ξ alters the tipping point at which the redox regime shift is predicted to occur in the model (Fig. 4.4b) but does not change the qualitative behaviour of the model.

4.5.2 The Maximal Population Density in the Biotic-abiotic model

For the biotic-abiotic model, the steady-state solution (Eqs.4.22-4.23) does depend on the maximal population density of the reducer population, $n_{\mathrm{or,max}}$. Upon varying this parameter (Fig. 4.4c) we find that the tipping point at which the redox regime shift happens changes; for a smaller value of $n_{\mathrm{or,max}}$, we require a greater value of the maximal reducer growth rate v_{or} to trigger the regime shift. In fact, in this model, regime shifting is lost altogether if the maximal microbial population density is too small. To observe regime shifts, we require that $v_{\mathrm{a}} < \gamma d n_{\mathrm{or,max}}$. This is because, at steady state, the maximal microbial "conversion rate" of $\mathrm{s_o}$ to $\mathrm{s_r}$ is given by $\gamma d n_{\mathrm{or,max}}$ while the maximal abiotic conversion rate of $\mathrm{s_r}$ to $\mathrm{s_o}$ is set by v_{a}. For regime shifting to occur, the biotic conversion rate must be able to exceed the abiotic conversion rate.

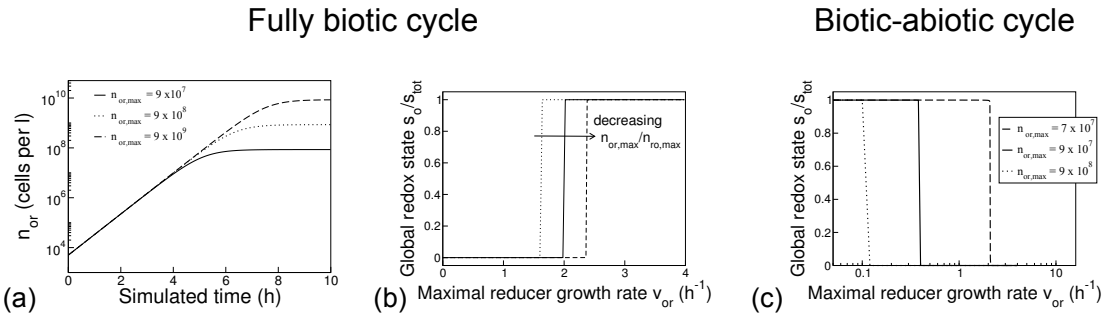

Figure 4.4 The role of the maximal population density parameter. Panel (a) shows that the time to reach the steady state increases as $n_{\mathrm{or,max}}$ increases, for the fully biotic cycle. Panel (b), also for the fully biotic cycle, shows that changing the ratio of maximal population sizes shifts the tipping point at which the redox regime shift happens but does not alter the qualitative behaviour of the model. Panel (c), for the biotic-abiotic cycle, shows that changing the maximal microbial population density $n_{\mathrm{or,max}}$ again shifts the tipping point, but redox regime shifts are still present. For this case, if $n_{\mathrm{or,max}}$ becomes too small the regime shift is lost (the system remains oxic for all values of v_{or}). The parameters are as in Fig. 2 of the main text: $K_{\mathrm{or}} = K_{\mathrm{ro}} = K_{\mathrm{a}} = 1\mu\mathrm{M}$, $d = 0.1\ \mathrm{h}^{-1}$, $\gamma = 3 \times 10^{-8}\mu$mol/cell and $s_{\mathrm{tot}} = 0.2$ M. In panel c, $v_{\mathrm{a}} = 0.2\mu\mathrm{Mh}^{-1}$.

4.5.3 Modelling Explicit Growth Limitation

In this subsection the population density limitation term $g(n(t), n_{\max}) = (1 - n(t)/n_{\max})$ is replaced with an explicit model for growth limitation by an external nutrient source. This is important because the logistic term used previously is density-dependent (depends directly on $n(t)$), and while it is possible that in many ecosystems the microbial populations are limited in a density-dependent way, it may not *always* be the case. Thus, it is important to demonstrate that the redox switching behaviour is preserved if the microbial populations are instead limited by the availability of an additional nutrient (in a non-density-dependent way). This model still reproduces the regime shifting phenomenon as the availability of acetate (or an alternative electron donor) is varied. To represent limitation by an external nutrient we introduce additional differential equations for the concentration $x(t)$ of this nutrient into the model for the fully biotic cycle. We suppose that the nutrient is supplied at a fixed rate b and is consumed by both the oxidizer and reducer populations as they grow. Both microbial growth rates are assumed to depend on $x(t)$ via multiplicative Monod growth terms (with half-saturation constant K_{x}). This results in the following set of equations:

$$\frac{dx(t)}{dt} = b - \gamma \left(\frac{x}{K_{\mathrm{x}} + x} \right) \left[\left(\frac{n_{\mathrm{ro}} v_{\mathrm{ro}} s_{\mathrm{r}}}{K_{\mathrm{ro}} + s_{\mathrm{r}}} \right) + \left(\frac{n_{\mathrm{or}} v_{\mathrm{or}} s_o}{K_{\mathrm{or}} + s_o} \right) \right] \tag{4.24}$$

$$\frac{dn_{\mathrm{ro}}(t)}{dt} = \frac{v_{\mathrm{ro}} n_{\mathrm{ro}}(t) s_{\mathrm{r}}(t)}{K_{\mathrm{ro}} + s_{\mathrm{r}}(t)} \left(\frac{x}{K_{\mathrm{x}} + x} \right) - d n_{\mathrm{ro}}(t) \tag{4.25}$$

$$\frac{dn_{\mathrm{or}}(t)}{dt} = \frac{v_{\mathrm{or}} n_{\mathrm{or}}(t) s_{\mathrm{o}}(t)}{K_{\mathrm{or}} + s_{\mathrm{o}}(t)} \left(\frac{x}{K_{\mathrm{x}} + x} \right) - d n_{\mathrm{or}}(t) \tag{4.26}$$

$$\frac{ds_{\mathrm{r}}(t)}{dt} = -\frac{\gamma v_{\mathrm{ro}} n_{\mathrm{ro}}(t) s_{\mathrm{r}}(t)}{K_{\mathrm{ro}} + s_{\mathrm{r}}(t)} \left(\frac{x}{K_{\mathrm{x}} + x} \right) + \frac{\gamma v_{\mathrm{or}} n_{\mathrm{or}}(t) s_{\mathrm{o}}(t)}{K_{\mathrm{or}} + s_{\mathrm{o}}(t)} \left(\frac{x}{K_{\mathrm{x}} + x} \right) \tag{4.27}$$

$$\frac{ds_{\mathrm{o}}(t)}{dt} = -\frac{ds_{\mathrm{r}}(t)}{dt} \tag{4.28}$$

These equations were integrated numerically using the Euler method (as outlined in chapter 2) to compute the steady state, for the parameter set $v_{\mathrm{ro}} = 2\ \mathrm{h}^{-1}$, $\gamma = 3 \times 10^{-8} \mu\mathrm{mol/cell}$, $K_{\mathrm{ro}} = K_{\mathrm{or}} = K_{\mathrm{x}} = 1 \mu\mathrm{M}$, $s_{\mathrm{tot}} = 1\ \mathrm{M}$, $d = 0.1\ \mathrm{h}^{-1}$ and $b = 0.001\ \mathrm{Mh}^{-1}$. Fig. 4.5 shows the resulting prediction for the redox state of the ecosystem ($s_{\mathrm{o}}/s_{\mathrm{tot}}$) as a function of the maximal growth rate of the reducer population (v_{or}, which serves as a proxy for the availability of acetate). Comparing with Fig. 4.2, it is clear that indeed this extended model does produce a redox regime shift which is qualitatively similar to that of the model with a logistic population size limitation term.

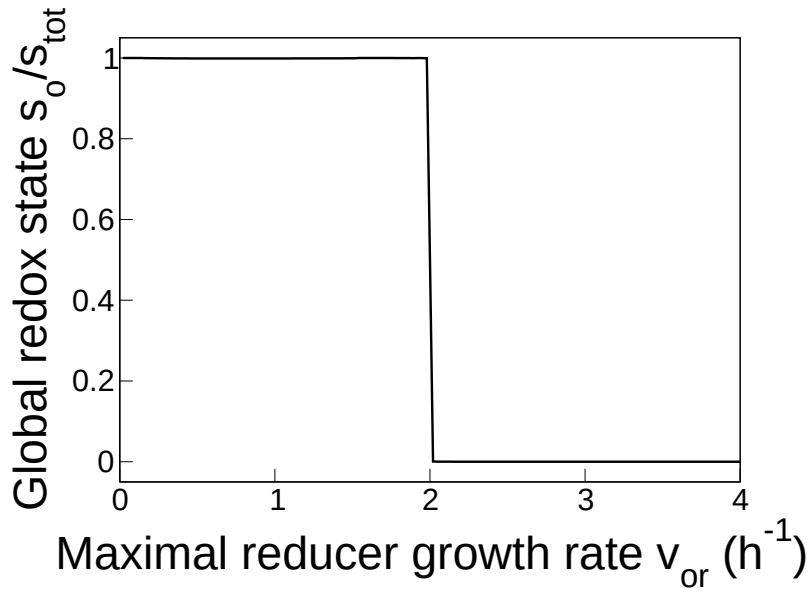

Figure 4.5 Redox regime shifts are still observed in a model where the term $(1 - n(t)/n_{\max})$ is replaced by explicit growth limitation by a supply of an external nutrient. The results show the redox state of the ecosystem (s_o/s_{tot}) as a function of the maximal growth rate of the reducer population (v_{or}). The data was obtained by numerical solution to steady state of Eqs. 4.24-4.28, for the parameter set $v_{ro} = 2$ h^{-1}, $\gamma = 3 \times 10^{-8}\mu$mol/cell, $K_{ro} = K_{or} = K_x = 1\mu$M, $s_{tot} = 1$ M, $d = 0.1$ h^{-1} and $b = 0.001$ Mh^{-1}.

4.6 The Mathematical Similarity of the Nutrient-Cycling Model to Phosphorylation-Dephosphorylation Cycles

An interesting mathematical analogy exists between the microbial nutrient-cycling models introduced in this work and classic results obtained by Goldbeter and Koshland for a phenomenon on a completely different scale, relating to the biochemical networks that control the response of a single biological cell to an external stimulus. Cells often mediate metabolic responses to stimuli

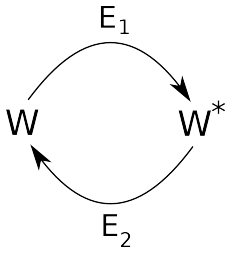

Figure 4.6 The model of Goldbeter and Koshland for an enzymatic phosphorylation-dephosphorylation cycle. Here E_1 represents a kinase enzyme, E_2 represents a phosphatase enzyme, W represents the unphosphorylated form of a protein and W^* represents its phosphorylated form [121].

such as changes in temperature or nutrient concentration, using phosphorylation-dephosphorylation cycles [122, 123]. In these cycles, a target protein is activated by addition of a phosphate group, and deactivated by removal of the phosphate group; the kinase and phosphatase enzymes mediating these reactions act in opposition to each other, the kinase being stimulated by the extracellular signal (Fig. 5.2). Activation of the target enzyme leads ultimately to the cell's response. In this model, the "input signal" is mediated via a change in the relative activities of the kinase and phosphatase enzymes, while the "output response" is manifest as a change in the relative proportions of the target protein W which are in the phosphorylated and dephosphorylated forms.

Assuming Michaelis-Menten kinetics for the phosphorylation and dephosphorylation steps, Goldbeter and Koshland derived steady-state solutions for the concentration of protein substrate W in the dephosphorylated form ($[W]$). These results revealed a phenomenon which Goldbeter and Koshland termed "zero order ultrasensitivity": when the total substrate concentration W_{tot} is high, the system responds extremely sharply to a small change in the relative activities of the kinase and phosphatase enzymes [121, 123].

Goldbeter and Koshland's steady state solution is given by

$$[W] = \frac{-B - \sqrt{B^2 - 4[W_{\rm tot}][E_2]K_{\rm M}\alpha([E_1]\alpha - [E_2])}}{2(\alpha[E_1] - [E_2])} \tag{4.29}$$

where

$$B = [W_{\rm tot}]([E_2] - \alpha[E_1]) + K_{\rm M}([E_2] + \alpha[E_1]). \tag{4.30}$$

Here, $[E_1]$ and $[E_2]$ represent the concentrations of the kinase and phosphatase enzymes, $K_{\rm M}$ is the half-saturation constant for the enzymatic reactions (assumed to be the same for kinase and phosphatase) and α is the ratio of the maximal reaction rates for the kinase and phosphatase.

The two-population, fully biotic, nutrient cycle models studied in this chapter bear a striking topological similarity to the Goldbeter-Koshland model (compare Fig. 4.1 with Fig. 5.2). In this analogy, the role of the kinase and phosphatase enzymes is played by the reducing and oxidizing microbial populations while the role of the protein target molecule is played by the chemical species being cycled. This analogy extends to the mathematical solutions of the two models. Assuming that both microbial populations have identical half-saturation constants ($K_{\rm ro} = K_{\rm or} = K$) and maximal population densities ($n_{\rm ro,max} = n_{\rm or,max} = n_{\rm max}$), then $\xi = 1$ and $\omega = (\xi - 1)v_{\rm ro} = 0$.

The following solution for the concentration of the oxidized chemical species can then be obtained (from Eqs. 4.15-4.16):

$$s_{\rm o} = \frac{-B - \sqrt{B^2 - 4s_{\rm tot}K\alpha(\alpha - 1)}}{2(\alpha - 1)} \tag{4.31}$$

where

$$B = s_{\rm tot}(1 - \alpha) + K(1 + \alpha) \tag{4.32}$$

and $\alpha = v_{\rm ro}/v_{\rm or}$. Comparing Eq. 4.31 with Eq. 4.29 one can see that the two models are mathematically equivalent, as long as the enzyme concentrations in the Goldbeter-Koshland model are set equal ($[E_1] = [E_2]$). Note that the

maximal population density $n_{\max}$ does not play an analogous role to the enzyme concentration, however. When the two maximal population densities are set to be different, the more complex steady state solution shown in Eq. 4.15 can be obtained.
It is important to note that this mathematical analogy does not extend to the biotic-abiotic cycle model, which has a more complex steady state solution, Eq. 4.23, although with a similar functional form.

In a cycle with 2 abiotic steps, the model is exactly the same as Goldbeter-Koshland kinetics, and therefore obviously produces redox regime shifts.

4.7 Conclusions

In this chapter, we have shown that a simple, generic mathematical model of redox cycling microbial ecosystems can undergo abrupt regime shifts between redox states, as the respective growth rates of the oxidizing and reducing populations are varied. This behaviour is analogous to the well-studied behaviour of zero-order ultrasensitivity in enzyme kinetics. In the next chapter, we extend this model further.

Chapter 5

Redox Regime Shifts in a More Detailed Ecosystem Model

5.1 Introduction

To determine the relevance for the natural environment of the microbially-mediated redox regime shifts predicted in the previous chapter, we here discuss more detailed models. We first discuss an extension of the biotic-biotic model presented in chapter 4, where the oxidation and reduction steps are now also spatially separated into two boxes, following the "box-modelling" approaches to modelling biogeochemical cycles that we introduced in chapter 2. This mimics the fact that they are generally spatially separated in microbial nutrient cycles in the environment [6]. The superscript notations u and d refer to the up and down boxes respectively, so for example, $s_o^u(t)$ refers to the concentration of oxidized substrate in the top box. Substrate moves between the boxes at a constant rate, also following the approach of the box models discussed in chapter 2. Using this two-box model we show that spatial separation actually accentuates redox regime shifts. Full details and dynamical equations for this model are presented in the

subsection 5.1.1 (the following subsection).

Next, we extend the two-box model even further, and introduce a more detailed "complete ecosystem model"; this more detailed model still produces regime shifts between redox states in response to environmental perturbations. This model explicitly includes the population dynamics of microbial decomposers and photosynthesizers as well as the reducers and oxidizers. It also accounts for the concentrations of acetate and oxygen as well as the oxidized and reduced forms s_{r} and s_{o} of the chemical species being cycled (Fig. 5.3a). Here, oxygen is explicitly generated by microbial photosynthesis (driven by light) and acetate is generated by microbial decomposition of organic matter. In the model, oxidative and reductive processes occur in different spatial zones, coupled by chemical transport. The growth rate of the oxidizing microbial population is assumed to depend on the concentrations of s_{r} and oxygen via a multiplicative Monod term, with explicit population density limitation, and the equivalent scenario holds for the reducer population. As outlined in chapter 2, multiplicative Monod kinetics are a common way of modelling microbial growth as a function of more than one nutrient [120]. The growth rates of the photosynthesizer and decomposer populations are assumed to depend (via Monod kinetics) on environmental inputs, here taken to be the light intensity and organic matter concentration, respectively. The effects of environmental change are mimicked by varying these inputs. The model also includes generic competition for oxygen and acetate by other biotic or abiotic processes. Full details and dynamical equations for this model are presented in the subsection 5.1.2.

5.1.1 Spatial Heterogeneity Accentuates Redox Regime Shifts

In chapter 4, we showed analytically that redox regime shifts can occur in response to changes in oxygen or acetate availability, for a "well-mixed" model with two

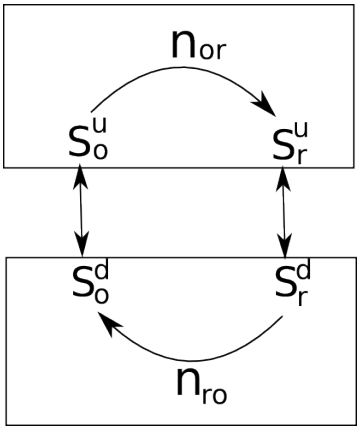

Figure 5.1 The "two population, two box" model. The oxidizing and reducing microbial populations are shown by n_{ro} and n_{or}, while the oxidized and reduced forms of chemical species s are denoted s_{o} and s_{r}. The superscripts u and d refer to the upper and lower boxes respectively. The double-headed arrows denote chemical diffusion.

microbial populations (reducers and oxidizers). In reality, however, microbial reduction and oxidation processes are usually spatially separated. In this section, we show that redox regime shifting is in fact enhanced for a simple model which captures this spatial separation.

We extend the basic "two-population" model of chapter 4, for the fully biotic cycle, by introducing two spatial boxes, coupled by chemical diffusion. We assume that the reducer population is located in the lower box while the oxidizer population is located in the upper box. The reduced and oxidized chemical species s_{r} and s_{o} can be located in either box and are transferred between boxes by diffusion, as shown in Fig. 5.1. This "two population, two box model" is described by the following dynamical equations:

$$\frac{dn_{\mathrm{or}}(t)}{dt} = \frac{v_{\mathrm{or}} n_{\mathrm{or}}(t) s_{\mathrm{o}}^{\mathrm{u}}(t)}{K_{\mathrm{or}} + s_{\mathrm{o}}^{\mathrm{u}}(t)} \left(1 - \frac{n_{\mathrm{or}}(t)}{n_{\mathrm{or,max}}}\right) - d n_{\mathrm{or}}(t) \tag{5.1}$$

$$\frac{dn_{\mathrm{ro}}(t)}{dt} = \frac{v_{\mathrm{ro}} n_{\mathrm{ro}}(t) s_{\mathrm{r}}^{\mathrm{d}}(t)}{K_{\mathrm{ro}} + s_{\mathrm{r}}^{\mathrm{d}}(t)} \left(1 - \frac{n_{\mathrm{ro}}(t)}{n_{\mathrm{ro,max}}}\right) - d n_{\mathrm{ro}}(t) \tag{5.2}$$

$$\frac{ds_{\mathrm{o}}^{\mathrm{u}}(t)}{dt} = -\frac{\gamma v_{\mathrm{or}} n_{\mathrm{or}}(t) s_{\mathrm{o}}^{\mathrm{u}}(t)}{K_{\mathrm{or}} + s_{\mathrm{o}}^{\mathrm{u}}(t)} \left(1 - \frac{n_{\mathrm{or}}(t)}{n_{\mathrm{or,max}}}\right) - k s_{\mathrm{o}}^{\mathrm{u}}(t) + k s_{\mathrm{o}}^{\mathrm{d}}(t) \tag{5.3}$$

$$\frac{ds_{\mathrm{o}}^{\mathrm{d}}(t)}{dt} = \frac{\gamma v_{\mathrm{ro}} n_{\mathrm{ro}}(t) s_{\mathrm{r}}^{\mathrm{d}}(t)}{K_{\mathrm{ro}} + s_{\mathrm{r}}^{\mathrm{d}}(t)} \left(1 - \frac{n_{\mathrm{ro}}(t)}{n_{\mathrm{ro,max}}}\right) - k s_{\mathrm{o}}^{\mathrm{d}}(t) + k s_{\mathrm{o}}^{\mathrm{u}}(t) \tag{5.4}$$

$$\frac{ds_{\mathrm{r}}^{\mathrm{u}}(t)}{dt} = \frac{\gamma v_{\mathrm{or}} n_{\mathrm{or}}(t) s_{\mathrm{o}}^{\mathrm{u}}(t)}{K_{\mathrm{or}} + s_{\mathrm{o}}^{\mathrm{u}}(t)} \left(1 - \frac{n_{\mathrm{or}}(t)}{n_{\mathrm{or,max}}}\right) - k s_{\mathrm{r}}^{\mathrm{u}}(t) + k s_{\mathrm{r}}^{\mathrm{d}}(t) \tag{5.5}$$

$$\frac{ds_{\mathrm{r}}^{\mathrm{d}}(t)}{dt} = -\frac{\gamma v_{\mathrm{or}} n_{\mathrm{or}}(t) s_{\mathrm{o}}^{\mathrm{u}}(t)}{K_{\mathrm{or}} + s_{\mathrm{o}}^{\mathrm{u}}(t)} \left(1 - \frac{n_{\mathrm{or}}(t)}{n_{\mathrm{or,max}}}\right) - k s_{\mathrm{r}}^{\mathrm{d}}(t) + k s_{\mathrm{r}}^{\mathrm{u}}(t) \tag{5.6}$$

Here, as before, K_{or} and K_{ro} are the half-saturation constants for the microbial reducers and oxidizers respectively, v_{or} and v_{ro} are their maximal growth rates, $n_{\mathrm{or,max}}$ and $n_{\mathrm{ro,max}}$ are their maximal population sizes, γ is the yield parameter (amount of chemical substrate needed to create one bacterium) and d is the microbial death rate. Compared to the model presented in chapter 4, we now have a new parameter k which represents the rate of diffusive chemical transport between the two spatial boxes.

To investigate the behaviour of the two-population, two-box model, we integrated Eqs. 5.1-5.6 numerically to steady state. Fig. 5.2 shows that indeed we obtain redox regime shifting behaviour as we vary the parameters v_{or} or v_{ro}, which serve as proxies for the acetate and oxygen availabilities. Comparing Fig. 5.2a and 5.2b we see that the redox regime shift occurs over a broader range of parameter values as the rate of chemical diffusion (k) increases.

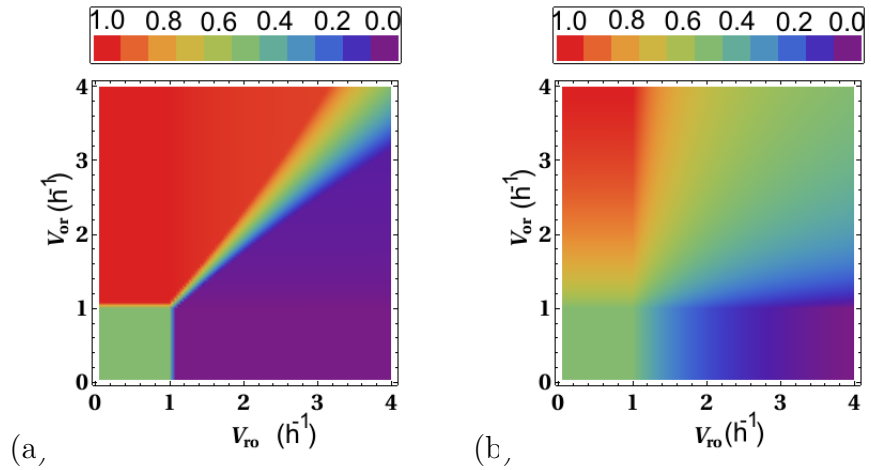

Figure 5.2 Steady state of the fully biotic spatial heterogeneous model (a) and (b) are phase plots where the colour key refers to the steady state value of s_o/s_{tot} with parameters $d = 1.0h^{-1}$, $\gamma = 3 \times 10^{-8}\mu$moles/cell, $n_{max} = 9 \times 10^7$cells/litre, and $K_{ro} = K_{or} = K_M = 1\mu$M. $s_{tot} = 40$mM (a): Slow diffusion $k = 0.001h^{-1}$. (b): Fast diffusion, $k = 100h^{-1}$.

5.1.2 Defining the More Detailed Model

We now extend the two-box model to include additional microbial populations. The equations corresponding to the model shown in Fig. 5.3a are listed below (Eqs. 5.7-5.16), with a brief description of the meaning of each one. We note that all of the microbial populations included in this model require many essential nutrients such as carbon, nitrogen, phosphorus and sulfur [5, 54]; we only explicitly model growth dependence on those nutrients that the relevant microbial populations gain energy from, for example, for the oxidizing population we only explicitly model growth dependence as a function of oxygen and reduced substrate. We consider growth limitation by other essential nutrients to be represented by the logistic growth limitation term (this point is discussed in more detail in section 5.2.2).

$$\frac{dn_{\mathrm{P}}(t)}{dt} = \frac{v_{\mathrm{P}} n_{\mathrm{P}}(t) L}{K_{\mathrm{L}} + L} \left(1 - \frac{n_{\mathrm{P}}(t)}{n_{\mathrm{P,max}}}\right) - d n_{\mathrm{P}}(t) \tag{5.7}$$

Eq. 5.7 describes growth of the photosynthesizer population, with density n_{P}. Photosynthesizers are located in the upper box. They grow in response to light intensity L (which is a constant parameter in our model), with maximal growth rate v_{P} and half-saturation constant K_{L}. A population density limitation term with maximal population density $n_{\mathrm{P,max}}$ and a death rate d are imposed.

$$\frac{dn_{\mathrm{D}}(t)}{dt} = \frac{v_{\mathrm{D}} n_{\mathrm{D}}(t) C}{K_{\mathrm{C}} + C} \left(1 - \frac{n_{\mathrm{D}}(t)}{n_{\mathrm{D,max}}}\right) - d n_{\mathrm{D}}(t) \tag{5.8}$$

Eq. 5.8 describes growth of the decomposer population, with density n_{D}. Decomposers are located in the lower box. They grow in response to organic carbon concentration C (which is a constant parameter in our model), with maximal growth rate v_{D} and half-saturation constant K_{C}. A population density limitation term with maximal population density $n_{\mathrm{D,max}}$ and a death rate d are imposed.

$$\frac{dn_{\mathrm{or}}(t)}{dt} = v_{\mathrm{or}} n_{\mathrm{or}}(t) \left[\frac{s_{\mathrm{o}}^{\mathrm{d}}(t)}{K_{\mathrm{or}} + s_{\mathrm{o}}^{\mathrm{d}}(t)}\right] \left[\frac{a(t)}{a(t) + K_{\mathrm{ac}}}\right] \left(1 - \frac{n_{\mathrm{or}}(t)}{n_{\mathrm{or,max}}}\right) - d n_{\mathrm{or}}(t) \tag{5.9}$$

Eq. 5.9 describes growth of the microbial reducer population, with density n_{or}. Reducers are located in the lower box. Reducer growth requires both the oxidized form of the redox chemical species, $\mathrm{s_o}$, and acetate. This is described using multiplicative Monod terms, with maximal growth rate v_{or} and half-saturation constants K_{or} for $\mathrm{s_o}$ and K_{ac} for acetate. The concentration of acetate is denoted

as $a(t)$. The reducer population density is limited to $n_{\mathrm{or,max}}$ and we impose a death rate d.

$$\frac{dn_{\mathrm{ro}}(t)}{dt} = v_{\mathrm{ro}} n_{\mathrm{ro}}(t) \left[\frac{s_{\mathrm{r}}^{\mathrm{u}}(t)}{K_{\mathrm{ro}} + s_{\mathrm{r}}^{\mathrm{u}}(t)}\right] \left[\frac{o(t)}{o(t) + K_{\mathrm{ox}}}\right] \left(1 - \frac{n_{\mathrm{ro}}(t)}{n_{\mathrm{ro,max}}}\right) - d n_{\mathrm{ro}}(t) \quad (5.10)$$

Eq. 5.10 describes growth of the microbial oxidizer population, with density n_{ro}. Oxidizers are located in the upper box. Oxidizer growth requires both the reduced form of the redox chemical species, $\mathrm{s_r}$, and oxygen. Again, we describe this using multiplicative Monod terms, with maximal growth rate v_{ro} and half-saturation constants K_{ro} for $\mathrm{s_r}$ and K_{ox} for oxygen. The concentration of oxygen is denoted as $o(t)$. The oxidizer population density is limited to $n_{\mathrm{ro,max}}$ and we impose a death rate d.

$$\begin{aligned} \frac{do(t)}{dt} &= \gamma_{\mathrm{ox}} v_{\mathrm{P}} n_{\mathrm{P}}(t) \left[\frac{L}{K_{\mathrm{L}} + L}\right] \left(1 - \frac{n_{\mathrm{P}}(t)}{n_{\mathrm{P,max}}}\right) \\ &\quad - \gamma v_{\mathrm{ro}} n_{\mathrm{ro}}(t) \left[\frac{s_{\mathrm{r}}^{\mathrm{u}}(t)}{K_{\mathrm{ro}} + s_{\mathrm{r}}^{\mathrm{u}}(t)}\right] \left[\frac{o(t)}{o(t) + K_{\mathrm{ox}}}\right] \left(1 - \frac{n_{\mathrm{ro}}(t)}{n_{\mathrm{ro,max}}}\right) - \beta_{\mathrm{ox}} o(t) \end{aligned} \quad (5.11)$$

Eq. 5.11 describes the dynamics of the oxygen concentration. Oxygen is assumed to be located only in the upper box. Oxygen is produced upon growth of the photosynthesizers (first term in Eq. 5.11), with yield parameter γ_{ox} (number of micromoles of oxygen produced per bacterial division cycle). Oxygen is consumed upon growth of the oxidizer population (second term in Eq. 5.11), with yield parameter γ. A term describing consumption of oxygen by other processes is included (third term in Eq. 5.11), such as growth of aerobes or abiotic oxidation reactions. The parameter β_{ox} controls the strength of this "competition" term.

$$\frac{da(t)}{dt} = \gamma_{\mathrm{ac}} v_{\mathrm{D}} n_{\mathrm{D}}(t) \left[\frac{C}{K_{\mathrm{C}} + C}\right] \left(1 - \frac{n_{\mathrm{D}}(t)}{n_{\mathrm{D,max}}}\right) - \gamma v_{\mathrm{or}} n_{\mathrm{or}}(t) \left[\frac{s_{\mathrm{o}}^{\mathrm{d}}(t)}{K_{\mathrm{or}} + s_{\mathrm{o}}^{\mathrm{d}}(t)}\right] \left[\frac{a(t)}{a(t) + K_{\mathrm{ac}}}\right] \left(1 - \frac{n_{\mathrm{or}}(t)}{n_{\mathrm{or,max}}}\right) - \beta_{\mathrm{ac}} a(t) \tag{5.12}$$

Eq. 5.12 describes the dynamics of the acetate concentration. Acetate is assumed to be located only in the lower box. Acetate is produced upon growth of the decomposers (first term in Eq. 5.12), with yield parameter γ_{ac}. Acetate is consumed upon growth of the reducer population (second term in Eq. 5.12), with yield parameter γ (here assumed to be the same as that of the reducers). A "competition" term describing consumption of acetate by other processes (third term in Eq. 5.12), such as growth of methanogens, is also included here. The parameter β_{ac} controls the strength of this term.

$$\frac{ds_{\mathrm{o}}^{\mathrm{u}}(t)}{dt} = \gamma v_{\mathrm{ro}} n_{\mathrm{ro}}(t) \left[\frac{s_{\mathrm{r}}^{\mathrm{u}}(t)}{K_{\mathrm{ro}} + s_{\mathrm{r}}^{\mathrm{u}}(t)}\right] \left[\frac{o(t)}{o(t) + K_{\mathrm{ox}}}\right] \left(1 - \frac{n_{\mathrm{ro}}(t)}{n_{\mathrm{ro,max}}}\right) + k s_{\mathrm{o}}^{\mathrm{d}}(t) - k s_{\mathrm{o}}^{\mathrm{u}}(t) \tag{5.13}$$

$$\frac{ds_{\mathrm{o}}^{\mathrm{d}}(t)}{dt} = -\gamma v_{\mathrm{or}} n_{\mathrm{or}}(t) \left[\frac{s_{\mathrm{o}}^{\mathrm{d}}(t)}{K_{\mathrm{or}} + s_{\mathrm{o}}^{\mathrm{d}}(t)}\right] \left[\frac{a(t)}{a(t) + K_{\mathrm{ac}}}\right] \left(1 - \frac{n_{\mathrm{or}}(t)}{n_{\mathrm{or,max}}}\right) + k s_{\mathrm{o}}^{\mathrm{u}}(t) - k s_{\mathrm{o}}^{\mathrm{d}}(t) \tag{5.14}$$

$$\frac{ds_{\mathrm{r}}^{\mathrm{u}}(t)}{dt} = -\gamma v_{\mathrm{ro}} n_{\mathrm{ro}}(t) \left[\frac{s_{\mathrm{r}}^{\mathrm{u}}(t)}{K_{\mathrm{ro}} + s_{\mathrm{r}}^{\mathrm{u}}(t)}\right] \left[\frac{o(t)}{o(t) + K_{\mathrm{ox}}}\right] \left(1 - \frac{n_{\mathrm{ro}}(t)}{n_{\mathrm{ro,max}}}\right) + k s_{\mathrm{r}}^{\mathrm{d}}(t) - k s_{\mathrm{r}}^{\mathrm{u}}(t) \tag{5.15}$$

$$\frac{ds_{\mathrm{r}}^{\mathrm{d}}(t)}{dt} = \gamma v_{\mathrm{or}} n_{\mathrm{or}}(t) \left[\frac{s_{\mathrm{r}}^{\mathrm{d}}(t)}{K_{\mathrm{or}} + s_{\mathrm{r}}^{\mathrm{d}}(t)}\right] \left[\frac{a(t)}{a(t) + K_{\mathrm{ac}}}\right] \left(1 - \frac{n_{\mathrm{or}}(t)}{n_{\mathrm{or,max}}}\right) + k s_{\mathrm{r}}^{\mathrm{u}}(t) - k s_{\mathrm{r}}^{\mathrm{d}}(t) \tag{5.16}$$

Eqs. 5.13-5.16 describe the dynamics of the reduced and oxidized forms of the redox chemical species, s_{r} and s_{o}, in the upper and lower boxes. As in the two-population, two-box model, $\mathrm{s_r}$ and $\mathrm{s_o}$ can be transported between the upper and lower boxes by diffusion, described by the rate parameter k.

5.1.3 Redox Regime Shifts in the More Detailed Model

Simulations show that this model indeed undergoes redox regime shifts (Fig. 5.3b). These shifts occur in response to either changes in organic matter availability (which stimulates the degrader population and hence the reducer population), or changes in light intensity (which stimulates the photosynthesizers and hence the oxidizer population). As organic matter availability increases at fixed light intensity (vertical dashed line in Fig. 5.3b), the redox state of the ecosystem changes sharply from oxidized to reduced (red to purple) at a critical "tipping point". Likewise as the light intensity increases for fixed organic matter concentration (horizontal dashed line in Fig. 5.3b), the redox state also undergoes a regime shift, in this case from reduced (purple) to oxidized (red).

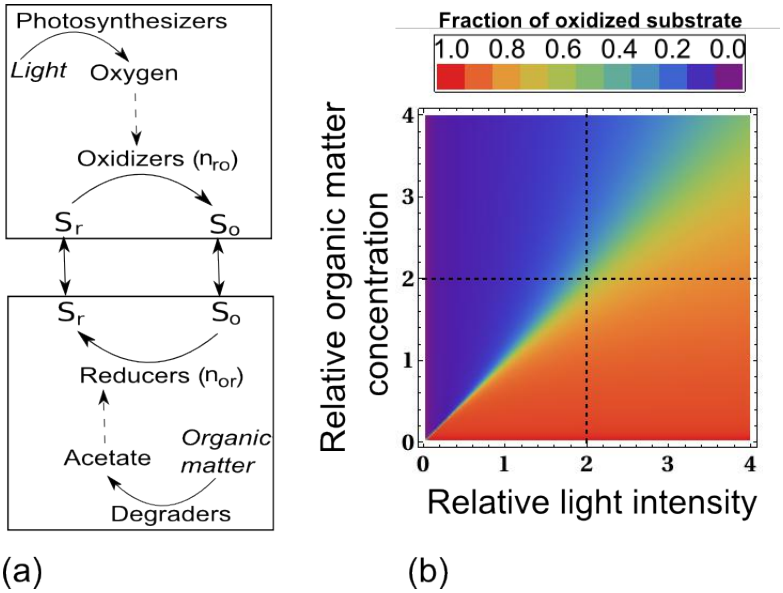

Figure 5.3 Redox regime shifts in a "complete ecosystem" model. (a) Illustration of the model. Oxidative and reductive processes take place in separate spatial zones, linked by chemical diffusion. The model explicitly represents the population dynamics of microbial photosynthesizers, decomposers, reducers and oxidizers, and the chemical dynamics of oxygen, s_o, s_r and acetate. Light intensity and organic matter availability are treated as control parameters. The dynamical equations corresponding to the model are Eqs. 5.1-5.10; these are integrated numerically to find the steady-state solution. Parameter values are also listed in Table 5.1. (b) Steady-state solution of the complete ecosystem model, obtained numerically using the Runge-Kutta method, plotted as a function of the control parameters, light intensity (relative to the typical value 10 μEinstein $s^{-1}m^{-2}$, where an Einstein is defined as a mole of photons [50]) and organic matter concentration (relative to the typical value 100 mg cm^{-3} [23]). The color represents the global redox state (see color key). The model shows redox regime shifts as the organic matter concentration is varied at fixed light intensity (vertical dashed line) or as the light intensity is varied at fixed organic matter concentration (horizontal dashed line).

Table 5.1 lists the parameter values used to generate the data shown in Fig. 5.3b. The calculations were run for different values of the light intensity L (with units of μEinstein s^{-1} cm^{-2}, where an Einstein is defined as a mole of photons, and the organic matter concentration (with units of mg cm^{-3}).

Table 5.1 Parameter values used in the model of Eqs. 5.1-5.10 to generate the data shown in Fig. 5.3b. These parameters are chosen to correspond approximately to the microbial freshwater sulfur cycle (with references where appropriate). Half saturation constants and maximal growth rates are given to an order of magnitude. Growth yields are calculated assuming a bacterial mass of 10^{-12} g. K_{ox} is set to 1μM as a conservative estimate, as previous work indicates it could be between 1μM [124] and 20μM [125]. K_{ac} is set to 1μM as a conservative estimate, to represent the fact that the electron donor could be either acetate ($K_{\mathrm{ac}} \sim 10\mu$M) or hydrogen ($K_{\mathrm{H}} \sim 1\mu$M), higher values of this parameter produce the same results. Growth rates are set to $v = 1$ h^{-1} for simplicity, but we acknowledge that this would represent quite a fast growth rate for the photosynthetic and degrading populations; lower values of v_{P} and v_{D} do not affect the result. Furthermore all yields have been set to $\gamma = 3 \times 10^{-8}$ μmol per cell for simplicity. Although in nature yield values may vary, this value is reasonable to an order of magnitude for all of the microbial populations discussed. Photosynthetic parameters are defined in terms of μ Einstein s^{-1} m^{-2} where an Einstein is defined as a mole of photons.

Parameter	Value	Unit
K_{L}	10	μ Einstein s^{-1} m^{-2} [50, 112]
K_{C}	100	mg cm^{-3} [23, 25]
K_{or}	1	μM [126]
K_{ro}	1	μM [111]
K_{ox}	1	μM [124, 125]
K_{ac}	1	μM [119, 127, 128]
v_{P}	1	h^{-1} [50, 129]
v_{D}	1	h^{-1} [130, 131]
v_{or}	1	h^{-1} [128]
v_{ro}	1	h^{-1} [111]
$n_{\mathrm{P,max}}$	1×10^9	cells per litre
$n_{\mathrm{D,max}}$	1×10^9	cells per litre
$n_{\mathrm{or,max}}$	1×10^9	cells per litre
$n_{\mathrm{ro,max}}$	1×10^9	cells per litre
γ	3×10^{-8}	μmoles per cell[120]
γ_{ox}	3×10^{-8}	μmoles per cell [132]
γ_{ac}	3×10^{-8}	μmoles per cell [133]
β_{ox}	0.5	h^{-1}
β_{ac}	0.5	h^{-1}
k	0.1	h^{-1}
d	0.1	h^{-1}

5.1.4 Inclusion of Abiotic Steps in the More Detailed Model

The equation set for an equivalent model, for a biotic-abiotic cycle (in which the reduction step is biotically-mediated but the oxidation step is abiotic), is

$$\frac{dn_{\mathrm{P}}(t)}{dt} = \frac{v_{\mathrm{P}} n_{\mathrm{P}}(t) L}{K_{\mathrm{L}} + L}\left(1 - \frac{n_{\mathrm{P}}(t)}{n_{\mathrm{P,max}}}\right) - d n_{\mathrm{P}}(t) \tag{5.17}$$

$$\frac{dn_{\mathrm{D}}(t)}{dt} = \frac{v_{\mathrm{D}} n_{\mathrm{D}}(t) C}{K_{\mathrm{C}} + C}\left(1 - \frac{n_{\mathrm{D}}(t)}{n_{\mathrm{D,max}}}\right) - d n_{\mathrm{D}}(t) \tag{5.18}$$

$$\frac{dn_{\mathrm{or}}(t)}{dt} = v_{\mathrm{or}} n_{\mathrm{or}}(t)\left[\frac{s_{\mathrm{o}}^{\mathrm{d}}(t)}{K_{\mathrm{or}} + s_{\mathrm{o}}^{\mathrm{d}}(t)}\right]\left[\frac{a(t)}{a(t) + K_{\mathrm{ac}}}\right]\left(1 - \frac{n_{\mathrm{or}}(t)}{n_{\mathrm{or,max}}}\right) - d n_{\mathrm{or}}(t) \tag{5.19}$$

$$\frac{do(t)}{dt} = \gamma_{\mathrm{ox}} v_{\mathrm{P}} n_{\mathrm{P}}(t)\left[\frac{L}{K_{\mathrm{L}} + L}\right]\left(1 - \frac{n_{\mathrm{P}}(t)}{n_{\mathrm{P,max}}}\right) - v_{\mathrm{a}}\left[\frac{s_{\mathrm{r}}^{\mathrm{u}}(t)}{K_{\mathrm{a}} + s_{\mathrm{r}}^{\mathrm{u}}(t)}\right]\left[\frac{o(t)}{o(t) + K_{\mathrm{a,ox}}}\right] - \beta_{\mathrm{ox}} o(t) \tag{5.20}$$

$$\begin{aligned}\frac{da(t)}{dt} &= \gamma_{\mathrm{ac}} v_{\mathrm{D}} n_{\mathrm{D}}(t)\left[\frac{C}{K_{\mathrm{C}} + C}\right]\left(1 - \frac{n_{\mathrm{D}}(t)}{n_{\mathrm{D,max}}}\right) \\ &\quad - \gamma v_{\mathrm{or}} n_{\mathrm{or}}(t)\left[\frac{s_{\mathrm{o}}^{\mathrm{d}}(t)}{K_{\mathrm{or}} + s_{\mathrm{o}}^{\mathrm{d}}(t)}\right]\left[\frac{a(t)}{a(t) + K_{\mathrm{ac}}}\right]\left(1 - \frac{n_{\mathrm{or}}(t)}{n_{\mathrm{or,max}}}\right) - \beta_{\mathrm{ac}} a(t)\end{aligned} \tag{5.21}$$

$$\frac{ds_{\mathrm{o}}^{\mathrm{u}}(t)}{dt} = v_{\mathrm{a}}\left[\frac{s_{\mathrm{r}}^{\mathrm{u}}(t)}{K_{\mathrm{a}} + s_{\mathrm{r}}^{\mathrm{u}}(t)}\right]\left[\frac{o(t)}{o(t) + K_{\mathrm{a,ox}}}\right] + k s_{\mathrm{o}}^{\mathrm{d}}(t) - k s_{\mathrm{o}}^{\mathrm{u}}(t) \tag{5.22}$$

$$\frac{ds_{\mathrm{o}}^{\mathrm{d}}(t)}{dt} = -\gamma v_{\mathrm{or}} n_{\mathrm{or}}(t) \left[\frac{s_{\mathrm{o}}^{\mathrm{d}}(t)}{K_{\mathrm{or}} + s_{\mathrm{o}}^{\mathrm{d}}(t)}\right] \left[\frac{a(t)}{a(t) + K_{\mathrm{ac}}}\right] \left(1 - \frac{n_{\mathrm{or}}(t)}{n_{\mathrm{or,max}}}\right) + k s_{\mathrm{o}}^{\mathrm{u}}(t) - k s_{\mathrm{o}}^{\mathrm{d}}(t) \tag{5.23}$$

$$\frac{ds_{\mathrm{r}}^{\mathrm{u}}(t)}{dt} = -v_{\mathrm{a}} \left[\frac{s_{\mathrm{r}}^{\mathrm{u}}(t)}{K_{\mathrm{a}} + s_{\mathrm{r}}^{\mathrm{u}}(t)}\right] \left[\frac{o(t)}{o(t) + K_{\mathrm{a,ox}}}\right] + k s_{\mathrm{r}}^{\mathrm{d}}(t) - k s_{\mathrm{r}}^{\mathrm{u}}(t) \tag{5.24}$$

$$\frac{ds_{\mathrm{r}}^{\mathrm{d}}(t)}{dt} = \gamma v_{\mathrm{or}} n_{\mathrm{or}}(t) \left[\frac{s_{\mathrm{r}}^{\mathrm{d}}(t)}{K_{\mathrm{or}} + s_{\mathrm{r}}^{\mathrm{d}}(t)}\right] \left[\frac{a(t)}{a(t) + K_{\mathrm{ac}}}\right] \left(1 - \frac{n_{\mathrm{or}}(t)}{n_{\mathrm{or,max}}}\right) + k s_{\mathrm{r}}^{\mathrm{u}}(t) - k s_{\mathrm{r}}^{\mathrm{d}}(t) \tag{5.25}$$

In Eqs. 5.20, 5.22 and 5.24, the parameter v_{a} is the maximal abiotic reaction rate, K_{a} denotes the half saturation constant with respect to $\mathrm{s_o}$ for the abiotic oxidation reaction, and $K_{\mathrm{a,ox}}$ is its half-saturation constant with respect to oxygen.

Fig. 5.4 shows that this biotic-abiotic cycle model can produce redox regime shifts. The steady-state global redox state of the system $((s_{\mathrm{o}}^{\mathrm{u}} + s_{\mathrm{o}}^{\mathrm{d}})/s_{\mathrm{tot}})$ is plotted as a function of the concentration C of organic carbon, for numerical solution of the steady-state of Eqs. 5.17-5.25. The parameter set used is as in Table 4.1, with $v_{\mathrm{a}} = 0.2$ μM h^{-1}, $K_{\mathrm{a}} = 1$ μM and $K_{\mathrm{a,ox}} = 1$ μM, $s_{\mathrm{tot}} = 4$ mM,$\beta_{\mathrm{ox}} = \beta_{\mathrm{ac}} = 0.5$

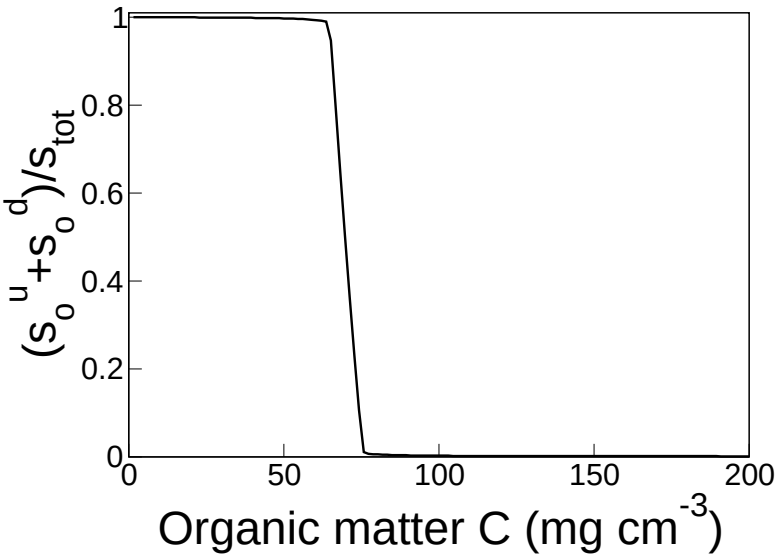

Figure 5.4 Redox regime shift in the biotic-abiotic model of Eqs. 5.17-5.25, obtained by numerical solution. The global redox state of the system $((s_{\mathrm{o}}^{\mathrm{u}} + s_{\mathrm{o}}^{\mathrm{d}})/s_{\mathrm{tot}})$ is plotted as a function of the concentration C of organic carbon. Light intensity L = 20 μEinstein s^{-1}m^{-2}, where an Einstein is defined as a mole of photons.

5.2 How Likely Are Redox Regime Shifts in the Natural Environment?

The analysis presented thus far provides a clear set of criteria that need to be satisfied for an ecosystem to be susceptible to redox regime shifts. In this section, we first briefly outline what these conditions are, before discussing them in more detail in individual subsections. We discuss which biogeochemical cycling ecosystems are likely to fulfil these conditions (and thus undergo redox regime shifts) by reviewing the microbial growth parameters and environmental concentrations of relevant nutrients associated with each ecosystem. Finally, we examine how likely are the environmental perturbations necessary for a redox regime shift to occur.

5.2.1 Under What Conditions Would Redox Regime Shifts Occur in the Natural Environment?

These conditions are as follows:

1. The density of the redox-cycling microbial populations must ultimately be limited by a factor other than the concentration of the chemical element being cycled. It is important to note, however, that the population density need not be small; large populations are also predicted to show regime shifts, albeit with longer response times.

2. The total concentration of the element being cycled must be high enough to saturate the growth rates of the microbial reducers and oxidizers (or the abiotic oxidation reaction): $s_{\mathrm{tot}} \gg K_{\mathrm{or}}$, K_{ro}, K_{a}. This ensures that the growth of the redox-cycling populations will become saturated with respect to s, causing a switch-like response to changes in oxygen or acetate.

3. The growth rates of the redox-cycling populations must be unsaturated with respect to the concentrations of oxygen and/or acetate, so that the system responds to changes in oxygen/acetate availability (or in the availability of an alternative electron acceptor/donor).

We now assess whether these conditions, required for redox regime shifts, are likely to be prevalent in the natural environment.

5.2.2 Condition 1: A Factor Exists That Ultimately Limits Population Density.

Without this condition the oxidizers and reducers would be able to continually adjust their population size, meaning that the system would naturally stabilise in response to an environmental perturbation instead of undergoing a regime shift. In the natural environment, many factors exist that limit microbial population density. Microbial growth requires sources not only of energy but also of carbon, nitrogen, phosphorus, sulfur and other, trace, biomass components [5, 54]. For redox cycling microbial populations, the redox reaction provides an energy source, but cannot satisfy all the requirements for formation of biomass. It is thus almost inevitable that growth is ultimately limited by the availability of biomass components rather than the redox species. Indeed, carbon limitation is common in microbial soil/sediment communities [134], while in ocean communities nitrogen or phosphorus is often growth-limiting [55].

5.2.3 Condition 2: High Concentration of the Chemical element Being Cycled.

This condition is necessary for the system to produce a switch-like response. As discussed in chapter 4, this is directly analogous zero-order ultra-sensitivity

in intracellular enzyme cycles, where a necessary condition to observe switch-like behaviour is that the total concentration of protein is high [121, 123]. To assess whether the condition $s_{\mathrm{tot}} \gg K_{\mathrm{or}}, K_{\mathrm{ro}}$ (growth saturation with respect to s_{r} or s_{o}) is fulfilled in the natural environment, we surveyed measured values of half-saturation constants K_{or} or K_{ro} for redox-cycling micro-organisms reported in the literature, and compared these values with typical concentrations of the chemical species being cycled, in various environmental settings. The results of this survey are shown in Table 5.2. For sulfur-cycling and nitrogen-cycling organisms, these data suggest that the concentration of the chemical species being cycled can exceed the half-saturation constant of the relevant microbial populations, $s_{\mathrm{tot}} \gg K_{\mathrm{or}}, K_{\mathrm{ro}}$. For example, sulfate reducers are generally not limited by sulfate, because sulfate is abundant (indeed it is the second most abundant anion in the oceans [115]). In contrast, this data survey suggests that redox regime shifts are unlikely to be associated with carbon cycles, because the typical half-saturation constant for methanogenesis is large relative to typical environmental concentrations of acetate.

For the iron cycle, this survey suggests that redox regime shifts are unlikely in modern-day environments, but may have occurred in the past. While modern oceanic concentrations of dissolved Fe^{2+} ions are generally low, the ancient oceans may have contained high concentrations of Fe^{2+} ($\approx$ 1mM), suggesting that redox regime shifts could have occurred in the Archean or Proterozoic iron cycles [135].

5.2.4 Condition 3: Low Concentration of Oxygen and/or Acetate.

Condition 3 states that, for biotic redox reactions, the concentrations of acetate and oxygen must be low enough that the growth rate of the microbial reducers and acceptors is unsaturated with respect to their availability. For biotic-abiotic cycles, the abiotic oxidation step must be unsaturated with respect to oxygen,

i.e. its rate must be controlled by the oxygen supply. This condition ensures that the system is responsive to environmental perturbations. We note here another analogy with zero-order ultra-sensitivity in enzymatic cycles (as discussed in chapter 4). Intracellular enzyme cycles are often connected into "cascades"; a change in the chemical state of an enzyme cycle further up the chain causing the next phosphorylation cycle to undergo a transition [136]. Clearly, in order for such a system to produce an overall response, the first enzyme in the chain has to be responsive. The microbial ecosystem models presented in this chapter are similar to such an enzymatic cascade, where the oxygen and acetate are analogous to enzymatic cycles further up an intracellular chain of phosphorylation cycles.

Biotic reduction processes often take place in the presence of strong competition for acetate (for example, sulfate-reducing micro-organisms typically compete with methanogens [137]). The concentration of acetate in freshwater sediments is typically about 1 μM [138]. This compares to approximate half-saturation constants for growth with respect to acetate of 70 μM for sulfate reduction and 12 μM for methanogenesis [119, 138], suggesting that indeed these reactions are very likely to be unsaturated.

For oxidative processes, the supply of oxygen is expected to be rate-limiting for growth in oxygen-poor environments (which are becoming widespread in the coastal oceans) [139]. The half saturation constant with respect to oxygen for bacterial sulfide oxidation is $1 - 20$ μM [124, 125], and while the concentration of oxygen in oxygen-saturated water is 0.3 mM [140] significant competition for oxygen means that the concentration is much lower in many environments [22]. It is interesting to note that oxygen concentrations were also low in the Proterozoic and Archean oceans [135]. Taken together, this analysis suggests that the redox regime shifts predicted by the model are likely to be relevant in the present-day natural environment, with respect to the sulfur and nitrogen cycles, and may also have played a role in iron cycling in the Proterozoic and Archean oceans.

Table 5.2 Typical values for the half saturation constants K_{or} or K_{ro} for microbial growth, for various nutrient-cycling microorganisms, compared to typical values for the concentrations of the relevant nutrients in marine environments. All values are given rounded to an order of magnitude.

Nutrient cycle	Reaction	Organism	K_{or} or K_{ro}	Concentration range
Sulfur	$H_2S \rightarrow SO_4^{2-}$	*Thiothrix* or *Thiobacillus*	1μM [111]	0.1μM$\leq$[H_2S]$\leq$100μM [115]
	$SO_4^{2-} \rightarrow H_2S$	*Desulfovibrio*	1μM [126]	0.1μM$\leq$[SO_4^{2-}]$\leq$10mM [115]
Iron	$Fe^{2+} \rightarrow Fe^{3+}$	*Thiobacillus ferrooxidans*	1mM [141]	1pM$\leq$[Fe^{2+}]$\leq$100μM [142, 143]
	Fe(III)-oxide $\rightarrow Fe^{2+}$	*Shewanella putrefaciens*	1mM [144]	0.1μM$\leq$[Fe(III)-oxide]$\leq$10mM [143, 145]
Carbon	$CH_4 \rightarrow CO_2$	*Methylocystis*	0.1μM [146]	1nM$\leq$[CH_4]$\leq$100μM [147]
	$CH_3CO_2^- \rightarrow CH_4$	*Methanosarcina*	1mM [148]	0.1μM$\leq$[$CH_3CO_2^-$]$\leq$100μM [149]
Nitrogen	$NH_4^+ \rightarrow NO_3^-$	*Nitrosomonas*	1μM [150]	0.01μM<[NH_4^+]$\leq$100μM [151, 152]
	$NO_3^- \rightarrow NO_2^-$	*Flavobacterium*	10μM [153]	0.01μM<[NO_3^-]$\leq$10μM [151, 152]

5.2.5 What Environmental Perturbations Might Cause Redox Regime Shifts?

How likely are the changes in oxygen and acetate availability (or the availability of equivalent electron acceptors or donors) that could trigger redox regime shifts? Oxygen concentrations in oceans or inland water bodies can be affected by temperature changes (for example, a 4.8 °C global temperature increase has been predicted to cause a 68% reduction in the mean oceanic oxygen concentration [22]) and by perturbations which affect the balance between photosynthesis and oxygenic respiration, such as eutrophication (which can lead to drastic increases of biomass, generating "oxygen minimum zones" [139]). Furthermore, over Phanerozoic time (the current geological aeon stretching back approximately 500 million years) pO_2 has varied between 15-37%, which represents a variation large enough to generate redox regime shifts [154].

The availability of acetate (or hydrogen) is expected to be altered by changes in the rate of organic matter degradation, which has been predicted to increase with temperature [113] (as described in chapter 2), and is also sensitive to changes in the abundance of organic matter due to sewage or phosphorus influx [25]. Changes in acetate (or hydrogen) availability could also arise due to competition effects, such as reductive degradation of pollutants [155], or perturbations in other biogeochemical cycles. This raises the interesting possibility that a redox regime shift in one geochemical cycle could trigger shifts in others, due to changes in the level of competition for acetate or hydrogen.

5.3 Environmentally Realistic Modifications to the Four-Species Model

In this section, we introduce a variety of environmentally realistic modifications to the model, and demonstrate that redox regime shifting behaviour is preserved. First, we show that the strength of the "competition" term for electron donors and acceptors is not important. Second, we show that the model results are robust to the inclusion of intermediate redox states.

5.3.1 Competition for Electron Donors and Acceptors

The four-population, two-box model includes terms representing the loss of oxygen and acetate from the system (controlled by the parameters β_{ox} and β_{ac}). These losses could be due to competition from other oxidizing or reducing microbial populations [156], abiotic processes, or diffusive loss.

Here, we show that the existence of redox regime shifts in our model is not very sensitive to the magnitudee of these loss terms. Fig. 5.5 shows predictions of the fully biotic, four-species model, Eqs. 5.7-5.16, for a range of values of $\beta_{\mathrm{ox}} = \beta_{\mathrm{ac}}$. Redox regime shifts are preserved in all cases; although the strength of the loss term affects the sharpness of the regime-shifting behaviour.

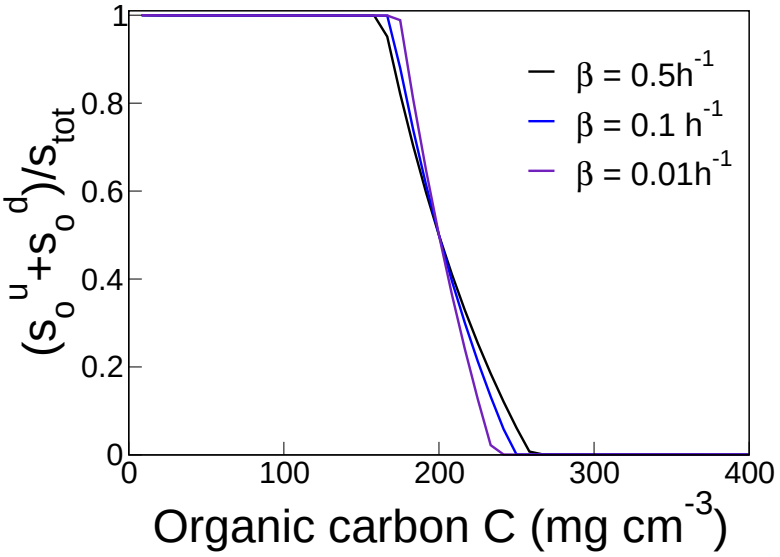

Figure 5.5 Redox regime shifts are not sensitive to the loss of oxygen and acetate from the system. These results were obtained by numerical solution using the Runge-Kutta method of Eqs. 5.7-5.16 for the steady state, for various values of the loss parameter $\beta_{ox} = \beta_{ac}$ (here denoted β). The global redox state of the system $((s_o^u + s_o^d)/s_{tot})$ is plotted as a function of the concentration C of organic carbon. Parameters as shown in Table 5.1, with L = 20 μEinstein s^{-1} m^{-2}, where an Einstein is defined as a mole of photons.

5.3.2 Intermediate Chemical States in Nutrient-Cycles

This chapter and the previous chapter have focused on models for biogeochemical cycles in which a chemical species is shuttled between two redox states. In reality, however, many biogeochemical cycles involve more than two redox states [5]; examples include the sulfur and nitrogen cycles as illustrated in Fig. 4.1. Here we show that our main result, the existence of redox regime shifts, still holds if additional, intermediate redox states are included.

To investigate the effect of intermediate redox species, the "4-species" model for the fully biotic cycle was extended to include a new chemical species, denoted s_i, whose redox state is intermediate between s_o and s_r. It is assumed that microbial

populations exist that can carry out all the possible oxidative and reductive transformations: the oxidative reactions $s_\mathrm{r} \to s_\mathrm{i}$, $s_\mathrm{i} \to s_\mathrm{o}$ and $s_\mathrm{r} \to s_\mathrm{o}$, all of which require oxygen, and the reductive transformations $s_\mathrm{o} \to s_\mathrm{i}$, $s_\mathrm{i} \to s_\mathrm{r}$ and $s_\mathrm{o} \to s_\mathrm{r}$, all of which require acetate. The population densities of these 6 populations are denoted n_ri, n_io, n_ro, n_oi, n_ir and n_or, respectively. It is assumed that oxidative transformations only happen in the top box and reductive transformations only happen in the lower box. The two boxes are coupled by chemical diffusion.
The equations corresponding to this model are:

$$\frac{dn_\mathrm{P}(t)}{dt} = \frac{v_\mathrm{P} n_\mathrm{P}(t) L}{K_\mathrm{L} + L}\left(1 - \frac{n_\mathrm{P}(t)}{n_\mathrm{P,max}}\right) - dn_\mathrm{P}(t) \tag{5.26}$$

$$\frac{dn_\mathrm{D}(t)}{dt} = \frac{v_\mathrm{D} n_\mathrm{D}(t) C}{K_\mathrm{C} + C}\left(1 - \frac{n_\mathrm{D}(t)}{n_\mathrm{D,max}}\right) - dn_\mathrm{D}(t) \tag{5.27}$$

$$\frac{dn_\mathrm{or}(t)}{dt} = v_\mathrm{or} n_\mathrm{or}(t)\left[\frac{s_\mathrm{o}^\mathrm{d}(t)}{K_\mathrm{or} + s_\mathrm{o}^\mathrm{d}(t)}\right]\left[\frac{a(t)}{a(t) + K_\mathrm{ac}}\right]\left(1 - \frac{n_\mathrm{or}(t)}{n_\mathrm{or,max}}\right) - dn_\mathrm{or}(t) \tag{5.28}$$

$$\frac{dn_\mathrm{ri}(t)}{dt} = v_\mathrm{ri} n_\mathrm{ri}(t)\left[\frac{s_\mathrm{r}^\mathrm{u}(t)}{K_\mathrm{ri} + s_\mathrm{r}^\mathrm{u}(t)}\right]\left[\frac{o(t)}{o(t) + K_\mathrm{ox}}\right]\left(1 - \frac{n_\mathrm{ri}(t)}{n_\mathrm{ri,max}}\right) - dn_\mathrm{ri}(t) \tag{5.29}$$

$$\frac{dn_\mathrm{io}(t)}{dt} = v_\mathrm{io} n_\mathrm{io}(t)\left[\frac{s_\mathrm{i}^\mathrm{u}(t)}{(K_\mathrm{io} + s_\mathrm{i}^\mathrm{u}(t))}\right]\left[\frac{o(t)}{o(t) + K_\mathrm{ox}}\right]\left(1 - \frac{n_\mathrm{io}(t)}{n_\mathrm{io,max}}\right) - dn_\mathrm{io}(t) \tag{5.30}$$

$$\frac{dn_{\mathrm{oi}}(t)}{dt} = v_{\mathrm{oi}} n_{\mathrm{oi}}(t) \left[\frac{s_{\mathrm{o}}^{\mathrm{d}}(t)}{(K_{\mathrm{oi}} + s_{\mathrm{o}}^{\mathrm{d}}(t))}\right] \left[\frac{a(t)}{a(t) + K_{\mathrm{ac}}}\right] \left(1 - \frac{n_{\mathrm{oi}}(t)}{n_{\mathrm{oi,max}}}\right) - d n_{\mathrm{oi}}(t) \quad (5.31)$$

$$\frac{dn_{\mathrm{ir}}(t)}{dt} = v_{\mathrm{ir}} n_{\mathrm{ir}}(t) \left[\frac{s_{\mathrm{i}}^{\mathrm{d}}(t)}{(K_{\mathrm{ir}} + s_{\mathrm{i}}^{\mathrm{d}}(t))}\right] \left[\frac{a(t)}{a(t) + K_{\mathrm{ac}}}\right] \left(1 - \frac{n_{\mathrm{ir}}(t)}{n_{\mathrm{ir,max}}}\right) - d n_{\mathrm{ir}}(t) \quad (5.32)$$

$$\frac{dn_{\mathrm{ro}}(t)}{dt} = v_{\mathrm{ro}} n_{\mathrm{ro}}(t) \left[\frac{s_{\mathrm{r}}^{\mathrm{u}}(t)}{K_{\mathrm{ro}} + s_{\mathrm{r}}^{\mathrm{u}}(t)}\right] \left[\frac{o(t)}{o(t) + K_{\mathrm{ox}}}\right] \left(1 - \frac{n_{\mathrm{ro}}(t)}{n_{\mathrm{ro,max}}}\right) - d n_{\mathrm{ro}}(t) \quad (5.33)$$

$$\begin{aligned}
\frac{do(t)}{dt} &= \gamma_{\mathrm{ox}} v_{\mathrm{P}} n_{\mathrm{P}}(t) \left[\frac{L}{K_{\mathrm{L}} + L}\right] \left(1 - \frac{n_{\mathrm{P}}(t)}{n_{\mathrm{P,max}}}\right) - \beta_{\mathrm{ox}} o(t) \\
&- \gamma v_{\mathrm{ro}} n_{\mathrm{ro}}(t) \left[\frac{s_{\mathrm{r}}^{\mathrm{u}}(t)}{K_{\mathrm{ro}} + s_{\mathrm{r}}^{\mathrm{u}}(t)}\right] \left[\frac{o(t)}{o(t) + K_{\mathrm{ox}}}\right] \left(1 - \frac{n_{\mathrm{ro}}(t)}{n_{\mathrm{ro,max}}}\right) \\
&- \gamma v_{\mathrm{ri}} n_{\mathrm{ri}}(t) \left[\frac{s_{\mathrm{r}}^{\mathrm{u}}(t)}{K_{\mathrm{ri}} + s_{\mathrm{r}}^{\mathrm{u}}(t)}\right] \left[\frac{o(t)}{o(t) + K_{\mathrm{ox}}}\right] \left(1 - \frac{n_{\mathrm{ri}}(t)}{n_{\mathrm{ri,max}}}\right) \\
&- \gamma v_{\mathrm{io}} n_{\mathrm{io}}(t) \left[\frac{s_{\mathrm{i}}^{\mathrm{u}}(t)}{K_{\mathrm{io}} + s_{\mathrm{i}}^{\mathrm{u}}(t)}\right] \left[\frac{o(t)}{o(t) + K_{\mathrm{ox}}}\right] \left(1 - \frac{n_{\mathrm{io}}(t)}{n_{\mathrm{io,max}}}\right)
\end{aligned} \quad (5.34)$$

$$\begin{aligned}
\frac{da(t)}{dt} &= \gamma_{\mathrm{ac}} v_{\mathrm{D}} n_{\mathrm{D}}(t) \left[\frac{C}{K_{\mathrm{C}} + C}\right] \left(1 - \frac{n_{\mathrm{D}}(t)}{n_{\mathrm{D,max}}}\right) - \beta_{\mathrm{ac}} a(t) \\
&- \gamma v_{\mathrm{or}} n_{\mathrm{or}}(t) \left[\frac{s_{\mathrm{o}}^{\mathrm{d}}(t)}{K_{\mathrm{or}} + s_{\mathrm{o}}^{\mathrm{d}}(t)}\right] \left[\frac{a(t)}{a(t) + K_{\mathrm{ac}}}\right] \left(1 - \frac{n_{\mathrm{or}}(t)}{n_{\mathrm{or,max}}}\right) \\
&- \gamma v_{\mathrm{oi}} n_{\mathrm{oi}}(t) \left[\frac{s_{\mathrm{o}}^{\mathrm{d}}(t)}{K_{\mathrm{oi}} + s_{\mathrm{o}}^{\mathrm{d}}(t)}\right] \left[\frac{a(t)}{a(t) + K_{\mathrm{ac}}}\right] \left(1 - \frac{n_{\mathrm{oi}}(t)}{n_{\mathrm{oi,max}}}\right) \\
&- \gamma v_{\mathrm{ir}} n_{\mathrm{ir}}(t) \left[\frac{s_{\mathrm{i}}^{\mathrm{d}}(t)}{K_{\mathrm{ir}} + s_{\mathrm{i}}^{\mathrm{d}}(t)}\right] \left[\frac{a(t)}{a(t) + K_{\mathrm{ac}}}\right] \left(1 - \frac{n_{\mathrm{ir}}(t)}{n_{\mathrm{ir,max}}}\right)
\end{aligned} \quad (5.35)$$

$$\begin{aligned}\frac{ds_{\mathrm{o}}^{\mathrm{u}}(t)}{dt} &= \gamma v_{\mathrm{ro}} n_{\mathrm{ro}}(t) \left[\frac{s_{\mathrm{r}}^{\mathrm{u}}(t)}{K_{\mathrm{ro}} + s_{\mathrm{r}}^{\mathrm{u}}(t)}\right] \left[\frac{o(t)}{o(t) + K_{\mathrm{ox}}}\right] \left(1 - \frac{n_{\mathrm{ro}}(t)}{n_{\mathrm{ro,max}}}\right) \\ &+ \gamma v_{\mathrm{io}} n_{\mathrm{io}}(t) \left[\frac{s_{\mathrm{i}}^{\mathrm{u}}(t)}{K_{\mathrm{io}} + s_{\mathrm{i}}^{\mathrm{u}}(t)}\right] \left[\frac{o(t)}{o(t) + K_{\mathrm{ox}}}\right] \left(1 - \frac{n_{\mathrm{io}}(t)}{n_{\mathrm{io,max}}}\right) \\ &+ k s_{\mathrm{o}}^{\mathrm{d}}(t) - k s_{\mathrm{o}}^{\mathrm{u}}(t)\end{aligned} \tag{5.36}$$

$$\begin{aligned}\frac{ds_{\mathrm{o}}^{\mathrm{d}}(t)}{dt} &= -\gamma v_{\mathrm{or}} n_{\mathrm{or}}(t) \left[\frac{s_{\mathrm{o}}^{\mathrm{d}}(t)}{K_{\mathrm{ro}} + s_{\mathrm{o}}^{\mathrm{d}}(t)}\right] \left[\frac{a(t)}{a(t) + K_{\mathrm{ac}}}\right] \left(1 - \frac{n_{\mathrm{or}}(t)}{n_{\mathrm{or,max}}}\right) \\ &- \gamma v_{\mathrm{oi}} n_{\mathrm{oi}}(t) \left[\frac{s_{\mathrm{o}}^{\mathrm{d}}(t)}{K_{\mathrm{oi}} + s_{\mathrm{o}}^{\mathrm{d}}(t)}\right] \left[\frac{a(t)}{a(t) + K_{\mathrm{ac}}}\right] \left(1 - \frac{n_{\mathrm{oi}}(t)}{n_{\mathrm{oi,max}}}\right) \\ &+ k s_{\mathrm{o}}^{\mathrm{u}}(t) - k s_{\mathrm{o}}^{\mathrm{d}}(t)\end{aligned} \tag{5.37}$$

$$\begin{aligned}\frac{ds_{\mathrm{r}}^{\mathrm{u}}(t)}{dt} &= -\gamma v_{\mathrm{ro}} n_{\mathrm{ro}}(t) \left[\frac{s_{\mathrm{r}}^{\mathrm{u}}(t)}{K_{\mathrm{ro}} + s_{\mathrm{r}}^{\mathrm{u}}(t)}\right] \left[\frac{o(t)}{o(t) + K_{\mathrm{ox}}}\right] \left(1 - \frac{n_{\mathrm{ro}}(t)}{n_{\mathrm{ro,max}}}\right) \\ &- \gamma v_{\mathrm{ri}} n_{\mathrm{ri}}(t) \left[\frac{s_{\mathrm{r}}^{\mathrm{u}}(t)}{K_{\mathrm{ri}} + s_{\mathrm{r}}^{\mathrm{u}}(t)}\right] \left[\frac{o(t)}{o(t) + K_{\mathrm{ox}}}\right] \left(1 - \frac{n_{\mathrm{ri}}(t)}{n_{\mathrm{ri,max}}}\right) \\ &+ k s_{\mathrm{r}}^{\mathrm{d}}(t) - k s_{\mathrm{r}}^{\mathrm{u}}(t)\end{aligned} \tag{5.38}$$

$$\begin{aligned}\frac{ds_{\mathrm{r}}^{\mathrm{d}}(t)}{dt} &= \gamma v_{\mathrm{or}} n_{\mathrm{or}}(t) \left[\frac{s_{\mathrm{r}}^{\mathrm{d}}(t)}{K_{\mathrm{or}} + s_{\mathrm{r}}^{\mathrm{d}}(t)}\right] \left[\frac{a(t)}{a(t) + K_{\mathrm{ac}}}\right] \left(1 - \frac{n_{\mathrm{or}}(t)}{n_{\mathrm{or,max}}}\right) \\ &+ \gamma v_{\mathrm{ir}} n_{\mathrm{ir}}(t) \left[\frac{s_{\mathrm{i}}^{\mathrm{d}}(t)}{K_{\mathrm{ir}} + s_{\mathrm{i}}^{\mathrm{d}}(t)}\right] \left[\frac{a(t)}{a(t) + K_{\mathrm{ac}}}\right] \left(1 - \frac{n_{\mathrm{ir}}(t)}{n_{\mathrm{ir,max}}}\right) \\ &+ k s_{\mathrm{r}}^{\mathrm{u}}(t) - k s_{\mathrm{r}}^{\mathrm{d}}(t)\end{aligned} \tag{5.39}$$

$$\begin{aligned}\frac{ds_{\mathrm{i}}^{\mathrm{u}}(t)}{dt} &= -\gamma v_{\mathrm{io}} n_{\mathrm{io}}(t) \left[\frac{s_{\mathrm{i}}^{\mathrm{u}}(t)}{K_{\mathrm{io}} + s_{\mathrm{i}}^{\mathrm{u}}(t)}\right] \left[\frac{o(t)}{o(t) + K_{\mathrm{ox}}}\right] \left(1 - \frac{n_{\mathrm{io}}(t)}{n_{\mathrm{io,max}}}\right) \\ &+ \gamma v_{\mathrm{ri}} \left[\frac{n_{\mathrm{ri}}(t) s_{\mathrm{r}}^{\mathrm{u}}(t)}{K_{\mathrm{ri}} + s_{\mathrm{r}}^{\mathrm{u}}(t)}\right] \left[\frac{o(t)}{o(t) + K_{\mathrm{ox}}}\right] \left(1 - \frac{n_{\mathrm{ri}}(t)}{n_{\mathrm{ri,max}}}\right) \\ &+ k s_{\mathrm{i}}^{\mathrm{d}}(t) - k s_{\mathrm{i}}^{\mathrm{u}}(t)\end{aligned} \tag{5.40}$$

$$\begin{aligned}\frac{ds_{\mathrm{i}}^{\mathrm{d}}(t)}{dt} &= -\gamma v_{\mathrm{ir}} n_{\mathrm{ir}}(t) \left[\frac{s_{\mathrm{i}}^{\mathrm{d}}(t)}{K_{\mathrm{ir}} + s_{\mathrm{i}}^{\mathrm{d}}(t)}\right] \left[\frac{a(t)}{a(t) + K_{\mathrm{ac}}}\right] \left(1 - \frac{n_{\mathrm{ir}}(t)}{n_{\mathrm{ir,max}}}\right) \\ &+ \gamma v_{\mathrm{oi}} n_{\mathrm{oi}}(t) \left[\frac{s_{\mathrm{o}}^{\mathrm{d}}(t)}{K_{\mathrm{oi}} + s_{\mathrm{o}}^{\mathrm{d}}(t)}\right] \left[\frac{a(t)}{a(t) + K_{\mathrm{ac}}}\right] \left(1 - \frac{n_{\mathrm{oi}}(t)}{n_{\mathrm{oi,max}}}\right) \\ &+ k s_{\mathrm{i}}^{\mathrm{u}}(t) - k s_{\mathrm{i}}^{\mathrm{d}}(t)\end{aligned} \tag{5.41}$$

Here, new parameters v_{oi}, v_{ir}, v_{ri} and v_{io} are defined, representing the maximal growth rates of the four new microbial populations, K_{oi}, K_{ir}, K_{ri} and K_{io} representing their half-saturation constants with respect to their redox chemical substrate, and $n_{\mathrm{oi,max}}$, $n_{\mathrm{ir,max}}$, $n_{\mathrm{ri,max}}$, $n_{\mathrm{io,max}}$ representing their maximal population densities. For simplicity, it is assumed that $v_{\mathrm{oi}} = v_{\mathrm{ir}} = v_{\mathrm{ri}} = v_{\mathrm{io}} = v_{\mathrm{or}} = v_{\mathrm{ro}}$, $K_{\mathrm{oi}} = K_{\mathrm{ir}} = K_{\mathrm{ri}} = K_{\mathrm{io}} = K_{\mathrm{or}} = K_{\mathrm{ro}}$ and $n_{\mathrm{oi,max}} = n_{\mathrm{ir,max}} = n_{\mathrm{ri,max}} = n_{\mathrm{io,max}} = n_{\mathrm{or,max}} = n_{\mathrm{ro,max}}$, i.e. that all populations have identical growth parameters. Also, it has been implicitly assumed in Eqs. 5.26-5.41 that all populations have equal yield parameter γ and equal half-saturation constants with respect to oxygen or acetate (K_{ox} and K_{ac}). Finally equal diffusion constants are assumed for all three chemical redox species.

The full parameter set used in numerical calculations is then: $v_{\mathrm{oi}} = v_{\mathrm{ir}} = v_{\mathrm{ri}} = v_{\mathrm{io}} = v_{\mathrm{or}} = v_{\mathrm{ro}} = 1\ \mathrm{h}^{-1}$, $K_{\mathrm{oi}} = K_{\mathrm{ir}} = K_{\mathrm{ri}} = K_{\mathrm{io}} = K_{\mathrm{or}} = K_{\mathrm{ro}} = 1\ \mu\mathrm{M}$, $n_{\mathrm{oi,max}} = n_{\mathrm{ir,max}} = n_{\mathrm{ri,max}} = n_{\mathrm{io,max}} = n_{\mathrm{or,max}} = n_{\mathrm{ro,max}} = 1 \times 10^9$ cells per litre, $k = 0.1\ \mathrm{h}^{-1}$, $d = 0.01\ \mathrm{h}^{-1}$, $\gamma = 3 \times 10^{-8}\ \mu$mol/cell, $s_{\mathrm{tot}} = 50$ mM, L=20 μEinstein $\mathrm{s}^{-1}\mathrm{m}^{-2}$, $K_{\mathrm{ox}} = 1\ \mu\mathrm{M}$, $K_{\mathrm{ac}} = 1\ \mu\mathrm{M}$, $\gamma_{\mathrm{ox}} = 3 \times 10^{-8}\ \mu$mol/cell, $\gamma_{\mathrm{ac}} = 3 \times 10^{-8}$

μmol/cell, $\beta_{ox} = \beta_{ox} = 0.5$

Fig. 5.6 shows the steady-state predictions of this model, obtained by numerical integration of Eqs. 5.26-5.41 by the Runge-Kutta method (see chapter 2). This model does indeed show a regime shift as the organic matter concentration is increased (thus increasing the availability of acetate).

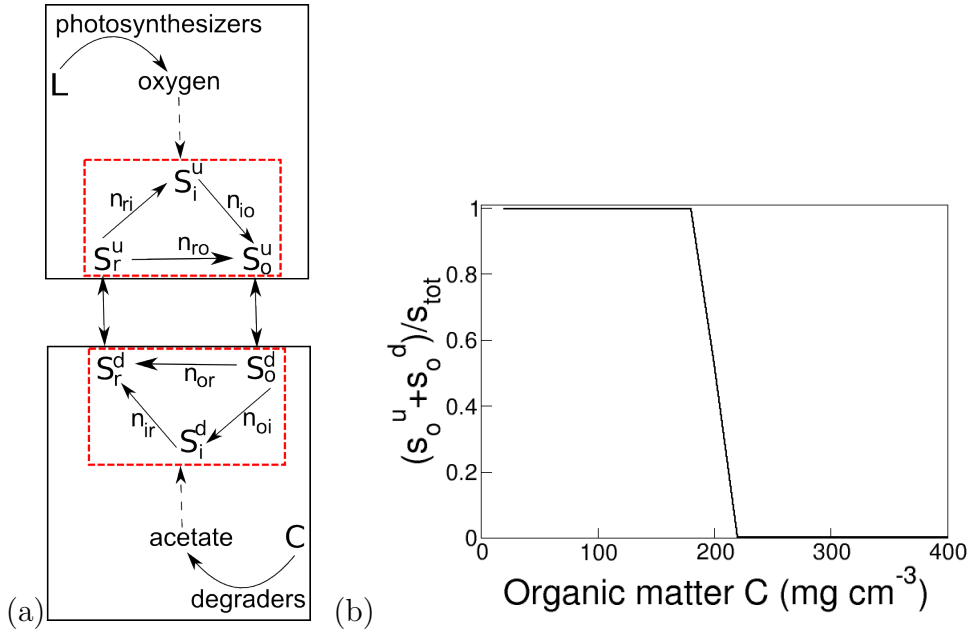

Figure 5.6 (a): A two-box microbial nutrient-cycling model with an intermediate chemical species $s_{\mathrm{i}}(t)$. An increase in oxygen availability stimulates all reactions within the upper red box, while an increase in acetate availability stimulates all reactions within the lower red box. (b): Redox regime shift in a model with an intermediate chemical redox state. These results were obtained by numerical solution using the Runge-Kutta method of Eqs. 5.26-5.41 for the steady state. The global redox state of the system $((s_{\mathrm{o}}^{\mathrm{u}} + s_{\mathrm{o}}^{\mathrm{d}})/s_{\mathrm{tot}})$ is plotted as a function of the concentration C of organic carbon.

5.4 Conclusions

Microbial populations are key mediators of the Earth's biogeochemical cycles [4]. The models presented in this chapter and the previous chapter show that microbial population dynamics can have important consequences for the response of microbially-mediated biogeochemical cycles to environmental changes. Under circumstances where microbial population density is limited by factors other than the concentration of the nutrient being cycled, these models predict that microbially-mediated redox-cycling systems can undergo regime shifts in their redox state in response to small changes in the availability of oxygen or acetate, which drive the oxidative and reductive redox-cycling reactions respectively. These regime shifts arise from the interplay between the nonlinearity of microbial population dynamics and the cyclic ecosystem topology. Diverse environmental perturbations are expected to affect the availability of oxygen, acetate (and other equivalent electron acceptors or donors), including temperature-mediated changes in oxygen solubility and changes in organic matter abundance due to eutrophication, suggesting that redox regime shifts may be a common occurrence in the natural environment. More generally, these models reveal that microbial population dynamics can lead to qualitative changes in the behaviour of biogeochemical cycles, with significant ecosystem-level consequences.

Regime shifts are a well-known phenomenon in many ecosystems [109], and have played an important role in the Earth's history [157]. This chapter has suggested a new mechanism by which regime shifts may occur in microbe-mediated geochemical cycles, and provides clear criteria for the conditions under which these shifts should be expected. These criteria are likely to be satisfied for the natural sulfur and nitrogen cycles. Furthermore, the fact that redox regime shifts were preserved even with all of the additional "layers" in the model that were added in chapter 5, suggests that redox regime shifts may be common in the natural environment. Indeed, the analogous behaviour of zero-

order ultransensivity in intracellular enzyme cycles is known to be widespread in nature (despite the fact that the intracellular environment contains a great deal of stochasticity [136]) because additional layers of complexity do not affect the core "motif" of saturated enzyme cycles producing an ultrasensitive response. Similarly, although biogeochemical cycles can contain more layers of complexity than we have included in any model here (for example, additional abiotic chemical processes) this does not invalidate our modelling prediction that redox regime shifts could occur in saturated microbially-mediated biogeochemical cycles, provided that the necessary conditions for ultrasensitive behaviour are not affected.

This phenomenon may also be relevant for iron cycling in the Archean or Proterozoic oceans, due to their much lower oxygen concentrations and potentially much higher concentrations of iron, than present-day oceans. Indeed, redox regime shifts may even help to explain changes in the Earth's biogeochemical cycles associated with mass extinction events, such as the rise in ocean sulfide levels during the end-Permian extinction event (251 My ago), which is believed to have poisoned the oceans and killed as much as 90% of all marine macroscopic species on Earth [20].

Chapter 6

Experimental Work: Changes to Microbial Community Structure and Function in Response to Environmental Perturbations

6.1 Introduction and Background

In this chapter we present a detailed experimental study of the response of a model microbial ecosystem to nutrient perturbations. A set of 144 freshwater sediment-water microcosms (known as "Winogradsky columns") were subjected to a range of nutrient perturbations. The effects of these chemical perturbations on the microbial community were examined using a combination of high-throughput sequencing and chemical analysis. Chemical data show that the nutrient perturbations applied caused the ecosystem to transition into a different global environmental state. Sequence data revealed that this transition imprints on the

microbial community, causing a strong decrease in α-diversity and compositional changes.

The microbial community was then divided into key "functional groups", each of which carries out a different metabolic process (for example, cellulose degrading micro-organisms represent one of these functional groups). Analysing our sequence data for each functional group separately revealed that different functional groups respond to the environmental perturbation in different ways. Some groups display a high degree of "functional redundancy", maintaining a stable overall relative abundance and diversity in response to the nutrient perturbations, because different taxa within these groups appear to be adapted to different environmental conditions and are able to substitute for each other when conditions change. Other functional groups undergo drastic changes in diversity and abundance in response to the chemical perturbations. This work reveals that the relationship between function and diversity in microbial ecology may not be a simple one, describable by theories previously formulated for macro-organisms, but rather is specific to the ecosystem process that a microbial functional group is responsible for.

6.1.1 The Relationship Between Diversity, Function and Response to Environmental Change

An important unanswered question in microbial ecology concerns how the diversity of a microbial community or population affects that communitys' "function" [158, 159]. The function of a microbial community or population refers to the fundamental ecosystem processes that a microbial community or population is responsible for, e.g. sulfate reducing micro-organisms often perform the "function" of oxidizing organic compounds and reducing sulfate. The impact of diversity on the function of a microbial ecosystem is important for industrial applications where functional control is required (e.g. in wastewater

treatment plants [160]) or to maintain microbial ecosystem function despite environmental change (e.g. in global biogeochemical cycles [4].) Many studies have attempted to understand the relationship between diversity and function in microbial ecosystems using experimental approaches [73, 161] or traditional ecological theory [158, 162]. The results of these studies are contradictory. Some work suggests that a high level of species diversity allows microbial ecosystems to maintain a stable function whilst undergoing drastic changes in community composition [163]. Alternatively, other experiments have found that diversity has no impact on the response of microbial communities to perturbations [164], or that a higher level of species diversity actually *decreases* stability by increasing the number of antagonistic interactions between taxa [30].

Environmental changes can drastically affect the overall function of a microbial community [165] by promoting or inhibiting different ecosystem processes. For example, the Deepwater Horizon oil spill dramatically increased the abundance of denitrification and hydrocarbon degradation pathways in the marine microbial community of the Gulf of Mexico [166].

Previous work has focused on the *overall* response of a microbial ecosystem to a perturbation [167–169], without investigating how the specific functional groups that make up the ecosystem are affected. In reality, the observed environmental function of a microbial community is the result of many different metabolic processes, each of which is performed by a particular functional group of micro-organisms; different functional groups may compete or cooperate with each other (e.g. sulfate reducers and methanogens can compete for hydrogen [128]). In this chapter, we use microcosm experiments to analyse the response of specific functional groups of micro-organisms to an environmental perturbation, and examine how changes within functional groups affect the structure and function of the community as a whole.

6.1.2 The Advantage of Microcosm Studies

This chapter focuses on the response of an experimental microbial ecosystem to environmental perturbations. As our experimental system, we selected the well-studied "Winogradsky column" [5]. Winogradsky columns are small closed ecosystems containing pond sediment and water in which microbial populations can proliferate, stimulated by the initial addition of nutrients (in this case a carbon source and a sulfur source). After incubation for several weeks a complex nutrient-cycling microbial ecosystem, driven by light energy, becomes established in these columns. The ecosystem that develops is stratified, with an oxygenated top layer in the water and upper-sediment, and anoxic sub-surface layers in the lower-sediment. Winogradsky columns have been known to be self-sustaining for many decades [170, 171].

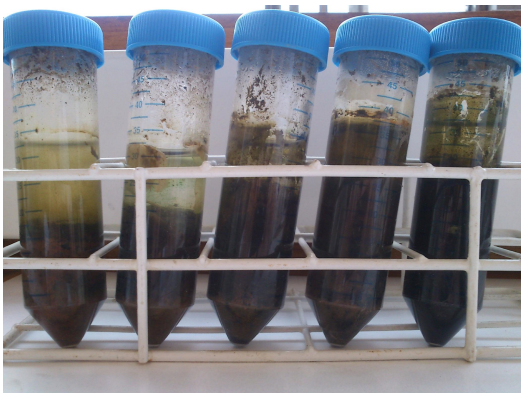

Figure 6.1 Picture of a range of Winogradsky columns 16 weeks after setup.

Experiments with microcosm communities such as Winogradsky columns have many advantages compared to conducting in-situ experiments in the natural environment. The Winogradsky column retains much of the species diversity and spatial structure of a natural nutrient-cycling microbial community. Its relative simplicity compared to full-scale natural ecosystems allows complex whole-system behaviour to be understood at the level of individual processes and components, in a way that "scales up" to the real environment. Moreover, the small sizes

and relatively short developmental timescales of microbial microcosms allow a degree of experimental control and replication that would be impossible in macro-ecological systems [172].

6.1.3 The Sulfur and Carbon Cycles in Our Microcosms

In this study, we apply controlled environmental perturbations to a set of microbial freshwater microcosms. Fig. 6.2 shows a simplified schematic diagram of the key microbial functional groups, metabolic transformations and abiotic chemical reactions which we expect to see in these microcosms. Central to this network is the coupling between the microbially-mediated carbon and sulfur cycles. The microbial carbon cycle in this system is driven by cellulose that we supply at the beginning of the experiment, and once the initial supply of cellulose has run out, by the organic matter generated by biomass growth, such as the growth of oxygenic phototrophs.

In the microbial sulfur cycle in our microcosms, sulfur is shuttled between its most oxidized state (SO_4^{2-}) and its most reduced state (H_2S) via a series of intermediate oxidation states (which are not shown in the diagram for simplicity) [6]. The reduction step in the sulfur cycle, which transforms sulfate to sulfide, is performed by sulfur reducing bacteria. This step requires an electron donor such as hydrogen or acetate. Sulfate reducing bacteria face strong competition for electron donors from many other functional groups of micro-organisms, such as methanogens [128] and aerobes [173]. Electron donors are in turn supplied by organic-matter degrading microbes, thus an increased supply of organic matter stimulates the production of sulfide by supplying an increased quantity of electron donors [4, 6]). This is one of the key mechanisms by which the sulfur and carbon cycles are coupled in our system.

Indeed, perturbations to the carbon cycle are known to have a particularly strong effect on sulfate reduction rates in the natural environment. For example,

seasonal variations in organic matter availability can cause drastic changes in sulfide concentrations in coastal sediments [174], and the microbial reduction of sulfate to hydrogen sulfide is responsible for as much as 50% of organic carbon usage in marine sediments [156].

The oxidation step of the sulfur cycle; i.e. the transformation of sulfide to sulfate, can be performed in several ways. Firstly, sulfur oxidizing bacteria can use oxygen to oxidize sulfide, the oxygen being supplied by oxygenic phototrophic micro-organisms (photosynthesizers). The oxidation of sulfide can also proceed abiotically, since oxygen reacts very rapidly with sulfide [175]. This abiotic reaction can have the consequence that rapid sulfide production can overwhelm oxygen recharge and cause anoxia. Importantly sulfide can also be oxidized anaerobically, by phototrophic microbes such as green sulfur bacteria (*Chlorobi*). Furthermore, sulfide reacts abiotically at different rates with various forms of iron, including aqueous Fe^{2+} and reactive iron oxides such as ferrihydrite [176], to form iron sulfides. This effectively represents a sulfide "sink", as sulfide which has reacted with iron is chemically inert, and is no longer available to oxidation by micro-organisms.

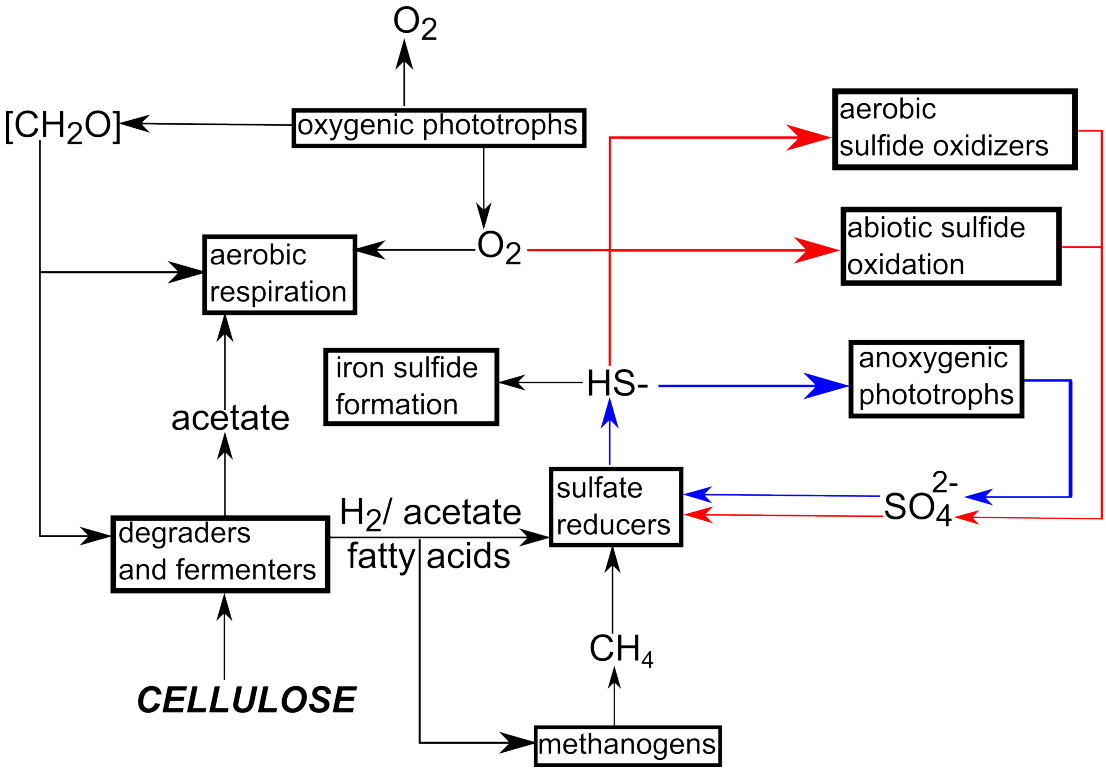

Figure 6.2 Schematic diagram of some of the key ecosystem process in our Winogradsky columns. For the sulfur cycling components, processes labelled with a red arrow require oxygen, and processes labelled with a blue arrow are anaerobic. Processes labelled with black arrows are not directly part of the sulfur cycle.

6.1.4 Experimental Strategy

In this section we briefly outline our broad experimental strategy before moving on to discuss our methods in more detail in the next section. The purpose of our microcosm study is to examine the effect of an environmental perturbation on a microbial ecosystem, both chemically and in terms of the composition and diversity of the microbial community. We apply a nutrient perturbation in the form of different amounts of cellulose and sulfate to each microcosm at the beginning of the experiment, and then leave the microcosms to incubate for 16 weeks. The idea is that varying the amounts of cellulose and sulfate which are added at the start of our experiments will cause changes in both the microbial

carbon and sulfur cycles in our microcosms, with corresponding changes in the microbial processes that drive the ecosystem. These changes can be measured after 16 weeks with a combination of chemical measurements and high-throughput sequencing of the microbial community.

Our chemical measurements consist of vertical depth profiles of sulfide and oxygen at the end of the experiment. Sulfide is measured using voltammetry (described in chapter 3) and oxygen is measured using a florescent probe (described in section 6.2.3 of this chapter). We expect to see a change in the final concentrations of sulfide and oxygen as a function of the initial cellulose and sulfate supplied to each microcosm, indicating a change in overall ecosystem function.

We then examine how changes in overall ecosystem function are driven by, and imprint on, the microbial community. We do this by sampling and sequencing the microbial community after 16 weeks. Dividing the microbial sequence data into functional groups then reveals how the *overall* changes in the microbial community result from changes within different functional populations of microorganisms.

6.2 Methods

In this section we outline the methods of our microcosm experiment in terms of sampling and setup, chemical measurements, and high-throughput sequencing. Fig. 6.3(a) displays a schematic workflow illustrating all of the stages of the experiment. The underlying principles of these methods are described in detail in chapter 3.

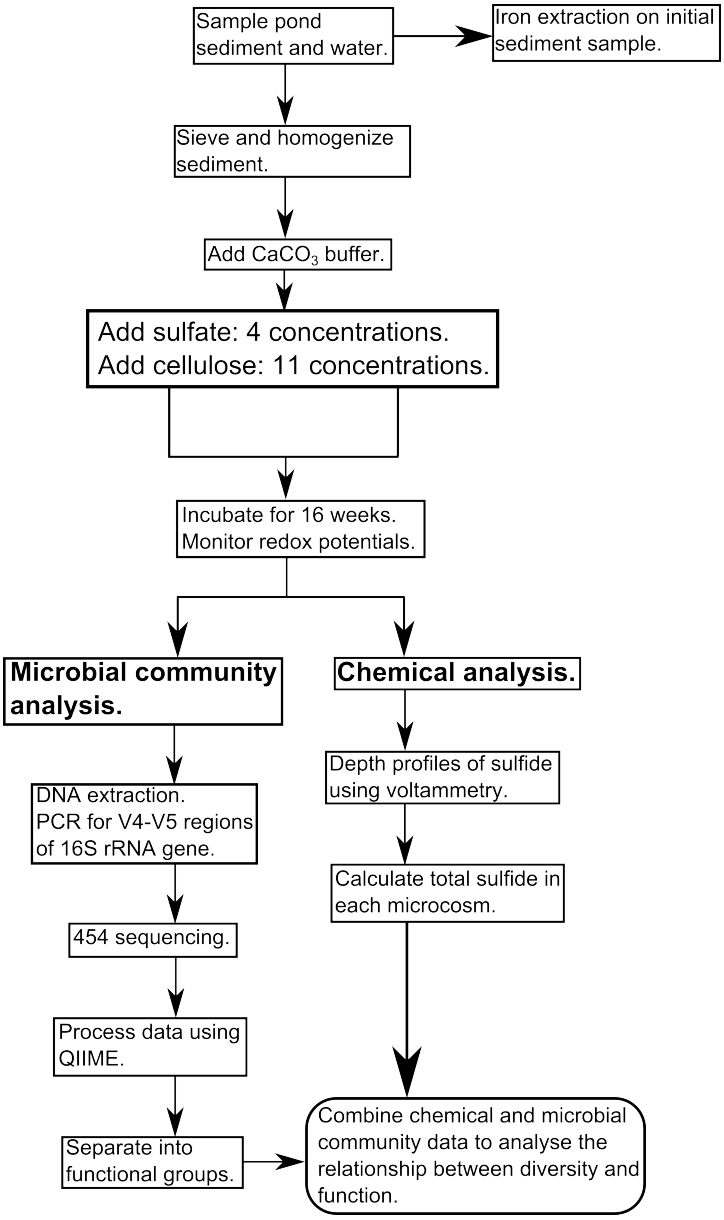

Figure 6.3 Schematic workflow illustrating the various stages of the experiment.

6.2.1 Sampling and Setup

We set up 144 Winogradsky column microcosms using sediment and water sampled from a local freshwater pond (Blackford Pond, 55.92° N, −3.19° W, mean depth=0.9 m, surface area=0.01km^2, mean pH=8.70). The sediment was sieved (1 mm pore size) to remove debris and the mixture was homogenized thoroughly

after sieving. 25 g of sediment was added to each microcosm. Organic matter was added in the form of cellulose, in the amounts of 0 g, 0.09 g, 0.19 g, 0.28 g, 0.38 g, 0.47 g, 0.56 g, 0.66 g, 0.75 g, 0.85 g and 0.94 g of added cellulose per microcosm. Sulfate was added in the form of $CaSO_4$ anhydrite to the final concentrations 0 μmol/g, 18 μmol/g, 73 μmol/g, and 146 μmol/g, (where the units refer to moles per g of sediment). Triplicate microcosms were set up for each combination of initial cellulose and sulfate. Additional microcosms were set up for redox potential monitoring, using the sulfate concentrations of 0 μmol/g and 146 μmol/g for the organic matter amounts of 0 g, 0.19 g, 0.38 g, 0.56 g, 0.75 g and 0.94 g. The 132 triplicate microcosms combined with the 12 additional redox potential microcosms brought the total number of microcosms to 144. Each sediment sample was again homogenized thoroughly after each chemical addition. 0.0625 g $CaCO_3$ per microcosm was added as a buffer. 25 g of sediment was then added to 50 ml falcon tubes and topped up with sampled water.

These microcosms were then incubated under a cycle of 16 hours light and 8 hours dark with a light intensity of 100 μmol $m^{-2}s^{-1}$ and a temperature of 22.5°C. As a convenient way to detect when the microcosms had reached a steady state, redox potentials of the microcosms were monitored weekly until it appeared the populations had stabilised and a steady state had been reached, which took approximately 16 weeks. Redox potentials were measured (by Fiona Strathdee) using a Pt electrode versus an Ag/AgCl reference at 3 heights in the microcosm, in the water, in the sediment and at the water-sediment interface, according to the method outlined in Pagaling et al (2014) [170]. Redox potentials were only measured on a subset of the microcosms, which were not ultimately sampled and sequenced. Redox potential is taken to be a rough measure of overall changes in microbial activity, and has been used for this purpose in other studies [177]. Figs 6.4-6.5 shows some of this redox potential data across a range of microcosms over the first 10 weeks of the experiment. After around 6 weeks the redox potential measurements begin to stabilise, indicating that microcosm chemical composition and community function is starting to approach a steady state.

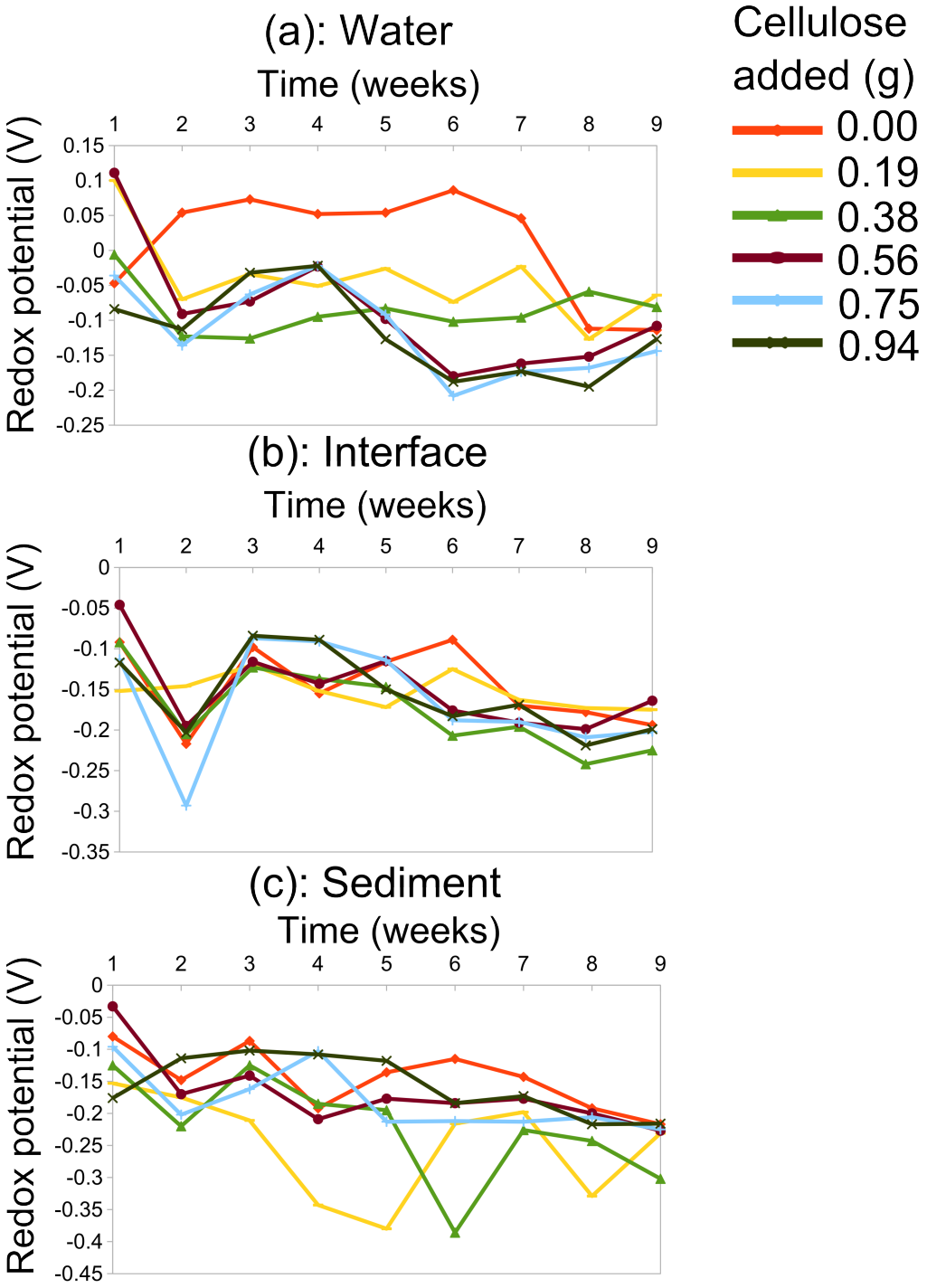

Figure 6.4 Redox potential measurements over the first 10 weeks of the experiment for a range of microcosms for initial sulfate of 0 μmol/g with different initial cellulose. (a): Redox measurements made in the water. (b) Redox measurements made at the sediment-water interface. (c) Redox measurements made in the sediment. All redox potential measurements were made by Fiona Strathdee.

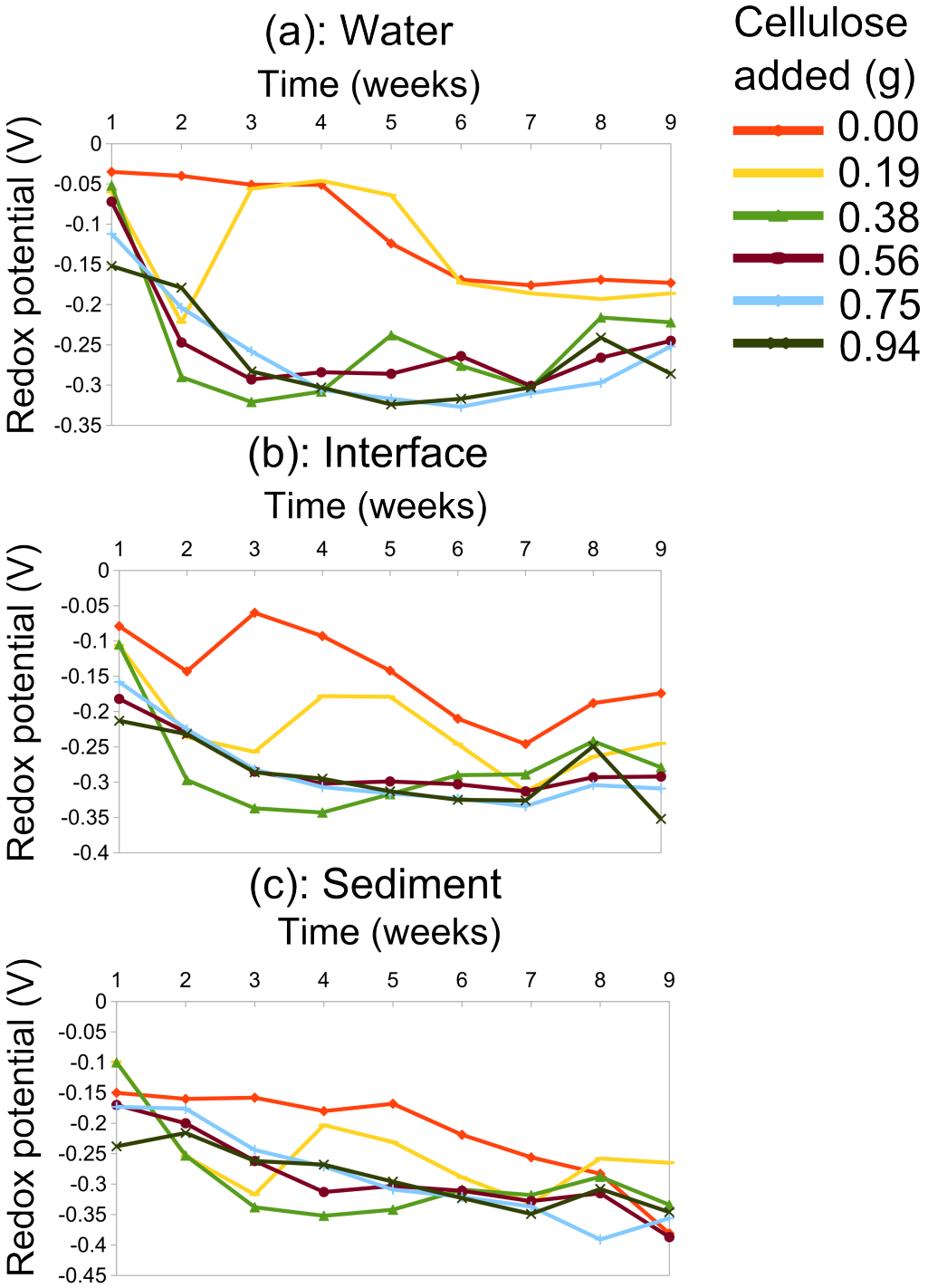

Figure 6.5 Redox potential measurements over the first 10 weeks of the experiment for a range of microcosms for initial sulfate of 146 μmol/g with different initial cellulose. (a): Redox measurements made in the water. (b) Redox measurements made at the sediment-water interface. (c) Redox measurements made in the sediment. All redox potential measurements were made by Fiona Strathdee.

6.2.2 High-throughput Sequencing

Crucial to our analysis is the measurement of species composition via 16S rRNA sequence analysis (see chapter 3). The cost of sequencing all 144 replicates would have been prohibitively high, and therefore we chose a representative range of initial conditions for sequencing. We sequenced one replicate for the initial nutrient concentrations of 0 g, 0.19 g, 0.28 g, 0.38 g, 0.47 g, 0.56 g, 0.75 g, 0.94 g added cellulose per microcosm, for the sulfate concentrations of 0 μmol/g, 73 μmol/g, and 146 μmol/g.

DNA extraction and PCR

To prepare samples for sequence analysis, microcosm samples were homogenized by vortexing the sediment and water together. Community DNA was then extracted from 1 g sediment/water mixture using an UltraClean Soil DNA Isolation Kit (MoBio). All PCR reactions were set up in a PCR6 Vertical Laminar Airflow Cabinet with UV sterilisation (Labcaire Systems Ltd.). Both reaction tubes and PCR mixtures were treated for 15 minutes with 15 W UV light (wavelength = 254 nm) to destroy contaminating DNA, prior to addition of dNTPs, Taq polymerase and template DNA [170].

The V4 and V5 regions of bacterial 16S rRNA genes were amplified using 515F (GAGTGNCAGCMGCCGCGGTAA) and 926R (CCGYCAATTYMTTTRAGTTT) primers in a two-round nested PCR procedure. To allow for simultaneous sequencing of many samples we used a barcoding strategy (see chapter 3). First round PCR products used unbarcoded primers and were used as templates (1 μl) for nested PCR amplification. Second round PCR then introduced barcoded primers. All PCR reactions contained 1 x Taq buffer plus additional $MgCl_2$ (to a final concentration of 3.0 mM), 0.2 mM of each dNTP, 0.2 mg/ml of BSA, 0.4 μM of each of the primers and 1.25 U of Taq DNA polymerase (Roche Applied Science), with the volume made up to 50 μl with PCR grade water

(Sigma).

PCR conditions were 95°C for 5 minutes followed by 20 cycles for the first round and 25 cycles for the second round of 95°C for 1 minute, 58 °C for 1 minute and 72°C for 1 minute with a final extension of 72°C for 10 minutes.

After amplification, PCR products for 454 sequencing were run on 1% TAE-agarose gels, gel purified using a Wizard SV Gel and PCR Clean-Up System (Promega), eluting in a final volume of 50 μl of nuclease-free water, and quantified spectrophotometrically. Prior to sequencing the samples were pooled in equimolar amounts. Pyrosequencing of samples was carried out on a 1/4 plate of a Roche 454 (Titanium) sequencer using both forward and reverse primers (Centre for Genomic Research, University of Liverpool), generating a dataset of approximately 260,000 raw sequencing reads.

Analysis of Sequence Data Using QIIME

The raw sequence data that the sequencer generates has to be processed before it can be interpreted and analysed. Sequences generated from pyrosequencing of bacterial 16S rRNA gene amplicons were processed using the Quantitative Insights Into Microbial Ecology (QIIME v1.8) [86] pipeline. QIIME analysis was carried out jointly by the author and Dr Andrew Free of the School of Biological Sciences. An explanation of the stages in QIIME analysis of 16S rRNA sequence data from a 454 sequencer is presented in chapter 3.

Sequences were denoised with the Denoiser algorithm [89]. Next, OTUs were clustered at 97% pairwise identity by uclust and taxonomy was assigned to representative sequences. These were then aligned to the Greengenes inputed core reference alignment using PyNAST. Sequences which failed to align were removed from the OTU table. Finally, chimeras detected by ChimeraSlayer were removed [90]

Broad community comparison was determined using the Bray-Curtis coefficient which accurately captures diversity differences in various types of model data

sets [98]. An index of 100 indicates identical samples, whereas an index of 0 indicates no common species [94] (as described in chapter 3). Nonmetric multi-dimensional scaling (NMDS) plots generated from the Bray-Curtis similarity matrices in Primer 6 were used to represent the distance between each sample in two-dimensional space [94]. Primer 6 was also used for additional statistical analysis. PERMANOVA and PERMDISP analyses were carried out using the PERMANOVA+ add-on to Primer 6 to test for significant differences in the distribution and dispersion, respectively, of sets of communities based on Bray-Curtis similarities [94].

Bray-Curtis similarities were calculated on a relative abundance dataset, where each value was normalised to the number of OTUs within that sample [91]. All other analyses were performed on data rarefied down to a depth of 1546 sequences per sample. The reason for this is that the overall number of sequences per sample can vary wildly, and this must be accounted for so that comparisons can be made (see chapter 3). α-diversity was determined using the Shannon index, as described in chapter 3.

6.2.3 Chemical Measurements

To assess the functional state of our microcosms we measured vertical profiles of sulfide and oxygen at the end of the experiment. Vertical profiles of sulfide were taken for all replicates. Vertical profiles of oxygen were taken on a representative subset of microcosms.

Voltammetry: Sulfide Measurements

Sulfide depth profiles were acquired using square wave voltammetry sweeping from 0 V to -1.7 V, with a scanning rate of 500 mV/s with a conditioning step of -0.8 V (see chapter 3). The purpose of the conditioning step is ensure there

is no sulfide attached to the electrode before the measurement is made. Each data point is an average over 3 replicate voltammagrams. The working electrode was attached to a micro-manipulator so that chemical depth profiles could be obtained. The counter and reference electrodes were positioned statically at the top of the microcosm. Fig. 6.6 shows a typical voltammagram with a peak at -0.8 V indicating the presence of sulfide. We then integrated the sulfide depth profiles to get measures of total sulfide content in each microcosm.

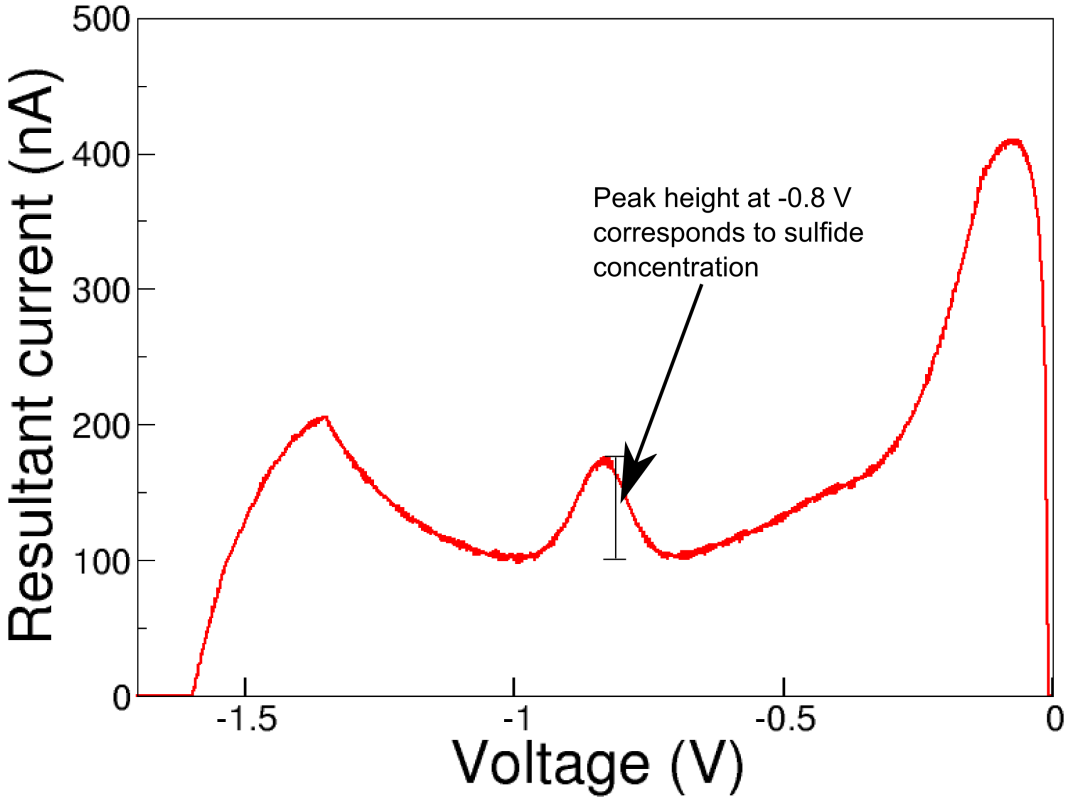

Figure 6.6 Typical voltammagram from a sulfidic microcosm. A peak at approximately -0.8 V indicates the presence of sulfide. The height of this peak in current corresponds to the sulfide concentration; the conversion between sulfide concentration and peak height in current is determined by the calibration curve presented in chapter 3.

Oxygen Measurements

Oxygen depth profiles were acquired using a Pyroscience Optical Oxygen Meter - FireStingO_2 system. This system has a 3 mm diameter florescent probe which measures dissolved oxygen concentrations. This probe can also be attached to a micro-manipulator so that depth profiles of oxygen can be obtained.

6.2.4 Reactive Iron Extraction

It is important to establish the concentration of the iron available to react with sulfide in our microcosms. The availability of iron or oxides could strongly affect the sulfide concentrations that we measure at the end of the experiment, because many iron oxides react rapidly with sulfide (see Fig. 6.2).
To determine the availability of so-called "reactive iron", a sequential extraction was carried out on the initial sediment (i.e. a sample of sediment from before the experiment started). This extraction consists of three steps of shaking and heating a sediment sample in different chemical solutions each of which liberates the free ions Fe^{2+} and Fe^{3+} from different iron compounds [178]. The concentrations of these free ions in each solution can then be quantified using spectroscopy (ICP-OES), which was performed by Dr Lorna Eades of the School of Chemistry. Different chemicals are used to target different types of iron compound. Sodium acetate targets iron carbonate phases such as siderite and ankerite. Sodium dithionite targets iron oxides that easily react with sulfide, such as hematite and goethite. Ammonium oxalate targets the less reactive iron oxide, magnetite. However, iron carbonates and magnetite are unreactive with sulfide over the timescale of our experiment, and are therefore not discussed further [176]. Full details of the iron extraction protocol are given in Poulton and Canfield (2005) [178].

6.3 Results: A Shift in Chemical Composition in Response to the Nutrient Perturbation

We now move on to discussing the results of the experiment. In this section, we briefly discuss the results from the chemical analysis, before moving on to discuss the microbial community analysis, which is the focus of this chapter.
The purpose of the experiment was to investigate how microbial ecosystem function and composition change with the chemical perturbations that we apply (the addition of varying amounts of cellulose and sulfate at the start of the experiment). The results of our chemical analysis (measurements of sulfide depth profiles) show that indeed there is a strong response of the functional state of the ecosystem to these chemical perturbations.

6.3.1 A Transition to a Sulfidic Ecosystem State

Depth Profiles of Sulfide and Oxygen and Their Integration to Measure Overall Ecosystem State

Fig. 6.7(a) shows depth profiles of sulfide and oxygen from a range of microcosms. In these depth profiles, we observe a clear transition point in the vertical direction between oxic and sulfidic regions. We expect to see oxygen at the top of the microcosm, due to oxygenic photosynthesis in the water. We expect to see sulfide at the bottom of the microcosm because sulfate reduction is known to occur deep in the anoxic zone of the sediment [179, 180]. In most microcosms we do not see overlapping zones of oxygen and sulfide: this is as expected because oxygen and sulphide react rapidly together [175]. We note that the depth profiles of sulfide and oxygen observed in our experiment are similar in shape to those obtained in studies of freshwater and marine sediments in the natural environment[181, 182].

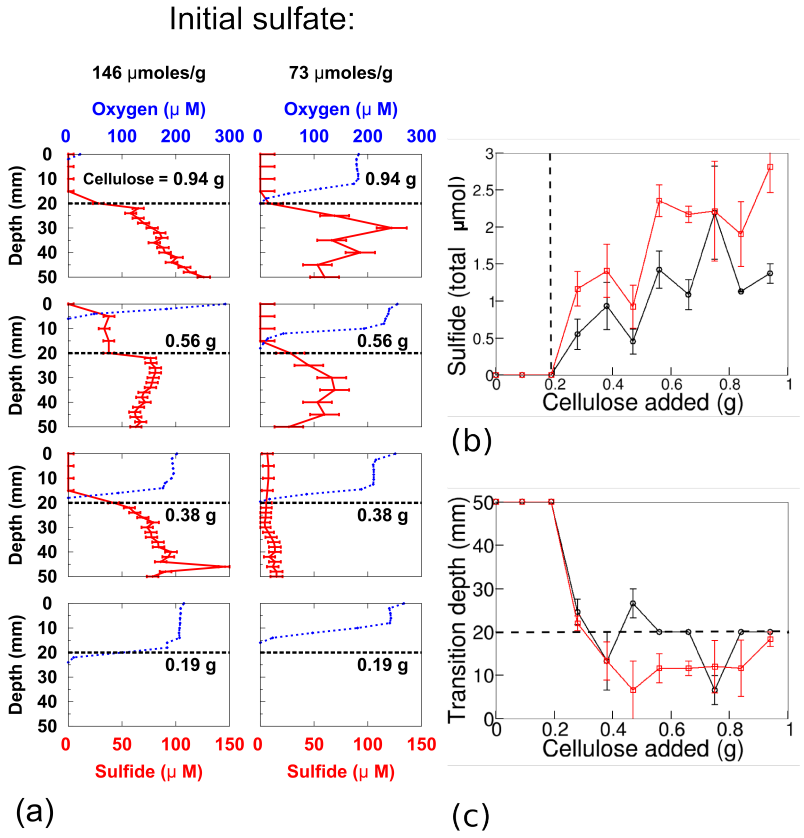

Figure 6.7 Set of plots displaying some of the chemical data from our microcosm experiment. On each plot shown the black dashed line marks the water-sediment boundary. (a) Depth profiles of sulfide (red lines) and oxygen (blue lines) plotted for microcosms with a range of concentrations of cellulose (increasing bottom to top) and for 2 different sulfate concentrations. Error bars generated by a combination of the error on the calibration and the error on the voltammetric measurement of current. The initial sulfate is displayed at the top of each column. The initial cellulose (g) supplied to the microcosm is displayed on each plot. (b): The total sulfide in each microcosm after 16 weeks as a function of the initial organic matter supply, averaged over replicate microcosms. Shown for the two initial sulfate concentrations of 73 μmol sulfate /g (black line) and 146 μmol sulfate /g (red line). At a threshold quantity of organic matter, a transition occurs to sulfidic state. (c) Depth of the transition point between oxic and sulfidic zones as a function of the initial organic matter supply. A depth of 50 mm means that no transition point occurred because no sulfide was ever measured (since the height of the microcosms is 50 mm). Shown for the two initial sulfate concentrations of 73 μmol sulfate /g (black line) and 146 μ mol sulfate /g (red line). For (b) and (c) errors come from averaging over measurements from triplicate microcosms.

To obtain a simple measure of the overall state of the ecosystem, sulfide depth profiles were numerically integrated and the result of this integration was multiplied by the cross sectional area of each microcosm to calculate the total amount of sulfide in each microcosm. These amounts were then averaged over triplicate microcosms with the same initial conditions to produce the results described in the next section.

A Shift in Ecosystem State with Initial Organic Matter Concentration

Plotting the total sulfide in each microcosm after 16 weeks as a function of the initial mass of cellulose supplied to the microcosm we obtain interestingresults. Fig. 6.7(b) shows that below a critical concentration of added cellulose (in this case between 0.2 g and 0.38 g per microcosm) no sulfide can be measured. Above this threshold concentration, the system transitions into a state where detectable sulfide is present at the start of the experiment. In the remainder of this chapter, we will refer to microcosms containing measurable sulfide (i.e. on the right of the transition in Fig. 6.7(b)) as "sulfidic" and microcosms containing no measurable sulfide (i.e. on the left of the transition in Fig. 6.7(b)) as "non-sulfidic".

The presence of this sulfidic transition is dependent on the concentration of sulfate that is present. While we observe a transition for the initial conditions of 73 μmol sulfate/g and 146 μmol sulfate/g , when we plot the equivalent data for 0 μmol sulfate/g and 18 μmol sulfate/g, no such transition is visible: for these lower concentrations of added sulphate, no measurable sulfide is present after 16 weeks. This suggests that an initial sulfate concentration between 18 and 73 μmol sulfate/g sediment is necessary in order for us to observe a transition to a sulfidic state as a function of the initial organic matter supplied.

A further interesting point is worth noting here. Fig. 6.7(c) plots the depth of the transition point between oxic and sulfidic zones as a function of the initial cellulose concentration (i.e. organic matter supply). After the dramatic transition

to a sulfidic state at approximately 0.2 g of initial cellulose, the transition depth remains approximately flat with organic matter loading. In our microcosms the depth of the transition point between the oxygenated zone at the top and the sulfidic zone at the bottom does not seem to be changed by the applied nutrient perturbations.

Clearly, the applied environmental perturbations of sulfate and cellulose have had a dramatic impact on the function of this freshwater microbial community. Having observed that there is an interesting transition an obvious question that arises is how this transition emerges from the biotic and abiotic reactions that we expect to be happening in our microcosms. We address this topic in much greater detail with a modelling analysis in chapter 7. However, in this chapter we only briefly discuss the *cause* of the transition. We thus address just one possible hypothesis here: the idea that the transition might be caused by an abiotic buffering effect, due to the reaction of sulfide with iron. Iron and iron oxide minerals (such as ferrihydrite) are known to react rapidly with sulfide, and thus can have a strong effect on observed sulfide concentrations [176]. This could produce a buffering effect, where at low concentrations of initial organic matter all of the sulfide that the micro-organisms produce reacts with iron in the sediment, and is thus not observed by our electrodes when we make chemical measurements after 16 weeks. To determine whether this buffering effect is possible, we needed to analyse the amount of iron present in the initial sediment.

Quantifying the Amount of Iron in the Initial Sediment

To test our hypothesis that the shift shown in Fig. 6.7(b) could be caused by the reaction of sulfide with iron or iron oxides we carried out a reactive iron extraction (as described in the Methods section) to determine whether the reactive iron pool was large enough to produce the sulfidic transition seen in Fig. 6.7(b). This showed that there are 100 μmol Fe^{2+}/g sediment available for sulfidation (reaction with sulfide) in each microcosm. This equates to approximately 2.5

mmoles of reactive iron per microcosm in total. This is larger than the quantity of sulfide measured in our microcosms (of the order of 1 μmoles), and this makes it possible that the transition seen in Fig. 6.7(b) is related to a buffering effect by the reactive iron pool. The size of the iron pool available for reaction with sulfide that we have determined comprises many different iron oxides such as goethite, hematite, and akaganeite, and free iron (Fe^{2+}) each of which reacts with sulfide on different timescales (from days to months, or even years)[183]. Thus, a full understanding of the relationship between sulfide and iron in our microcosms would require a detailed kinetic model.

However, the focus of this chapter is not the cause of the sulfidic transition, and thus we do not discuss this further here. Instead, in this chapter, we focus on the effect of the transition on the microbial community. For a more detailed discussion of the cause of the transition to a sulfidic state as a function of organic matter loading, see chapter 7.

6.4 The Microbial Community

Chemical analysis has demonstrated that increased organic matter availability causes a transition to a sulfidic environmental state. Since the sulfide in our system is microbially produced, this transition must be linked to the dynamics and structure of the microbial community (although abiotic reactions can also play a role, which we discuss in chapter 7). Furthermore, since sulfide is toxic to most micro-organisms, it is likely that this chemical transition will itself affect the microbial community. Our microcosms therefore represent an interesting case of an environmental perturbation causing an ecosystem change which then itself generates a different ecological state. In the ecological literature, this phenomenon is known as "niche construction" [184]. In this section we examine the changes in the microbial community, after 16 weeks incubation, as the initial amount of cellulose and sulfate is varied. We first carry out this analysis at the level of the

microbial community as a whole, then at the level of different functional groups of micro-organisms, and finally *within* these functional groups.

6.4.1 The Response of the Microbial Community as a Whole

Fig. 6.8 details "raw" results of our sequencing analysis, in terms of the phyla comprising the community for the range of microcosms sequenced. Some clear trends are immediately apparent. For example, the phylum *Chlorobi* is generally more abundant in microcosms with higher initial sulfate. This is not surprising since *Chlorobi* oxidize sulfide, and is therefore likely to be more abundant in microcosms with higher initial sulfate because they contain more sulfide.
However, to go further than broad qualitative statements about which phyla are more or less abundant in different conditions, we need to apply some of the multivariate statistical techniques that were discussed in chapter 3, and this is presented in the next subsection.

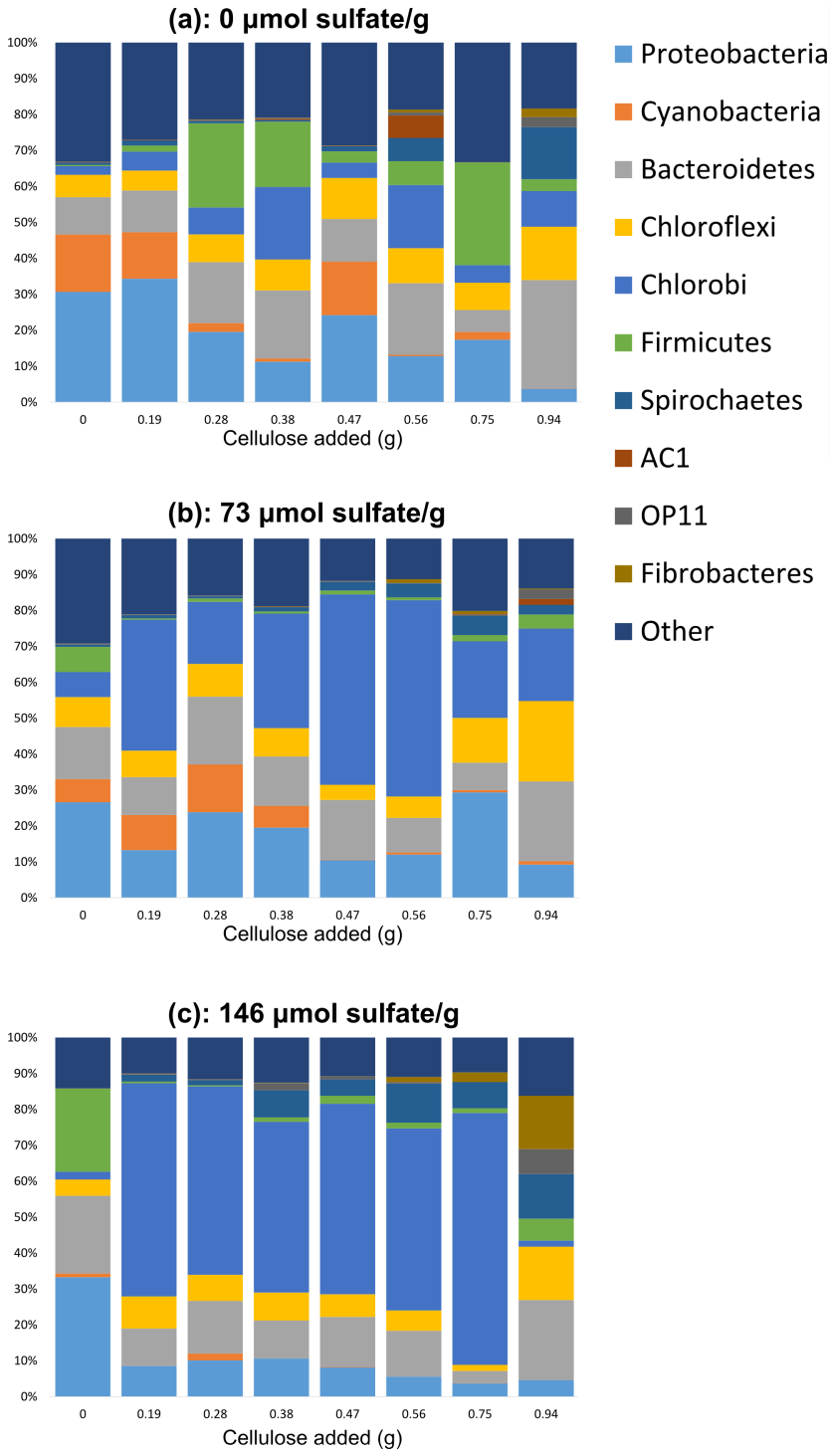

Figure 6.8 The microbial community composition (at the level of phylum) at the end of the experiment for the range of initial sulfate and cellulose concentrations sequenced. Any phylum comprising <5% of the community was grouped into "other". Initial sulfate conditions (a): 0 μ mol/g, (b): 73 μmol/g, and (c): 146 μmol/g. Initial cellulose added increases left to right across each plot.

The Effect of the Initial Chemical State on the Microbial Community

Fig. 6.9(a) shows an NMDS plot generated from the full set of sequence data at OTU (species) level. The theory behind NMDS plots is discussed in chapter 3. In simple terms, each datapoint on an NMDS plot represents the microbial community of one microcosm and datapoints are clustered closer together if the microbial communities are more similar. In Fig. 6.9(a), colours represent the initial cellulose concentration and shapes represent the initial sulfate concentration. We see that there is no obvious clustering of datapoints according to cellulose (colour). However, statistical analysis shows that initial cellulose does drive a somewhat statistically significant change in the community composition (PERMANOVA: P = 0.016, Pseudo-F = 1.3754).

However in Fig. 6.9(a) there does seem to be a clustering according to initial sulfate (shape), and this is borne out by statistical analysis which shows that initial sulfate concentration is a key driver of the overall composition of the community (PERMANOVA: P = 0.001, Pseudo-F = 2.5953). Furthemore PERMDISP tests showed no statistical significance for sulfate, indicating that sulfate produces no change in the variability *between* non-replicate microcosms (β-diversity).

Fig. 6.9(c) examines the change in α-diversity according to the Shannon index (as described in chapter 2). Because α-diversity was calculated using the Shannon index, it considers both richness (the number of OTUs) and the evenness of the abundance distribution of OTUs (see chapter 3). We see that the α-diversity is significantly lower for higher initial sulfate concentrations but not for higher initial cellulose concentrations. We can calculate a mean diversity for the 3 increasing sulfate conditions of 7.7 ± 0.4, 6.6 ± 0.5 and 4.7 ± 0.4 respectively. Again this is borne out by statistics, which shows that initial sulfate drives a significant change in diversity, but initial cellulose does not (Two-way ANOVA: Sulfate statistics: P = 1×10^{-5}; F = 23.5. Cellulose statistics: No significance).

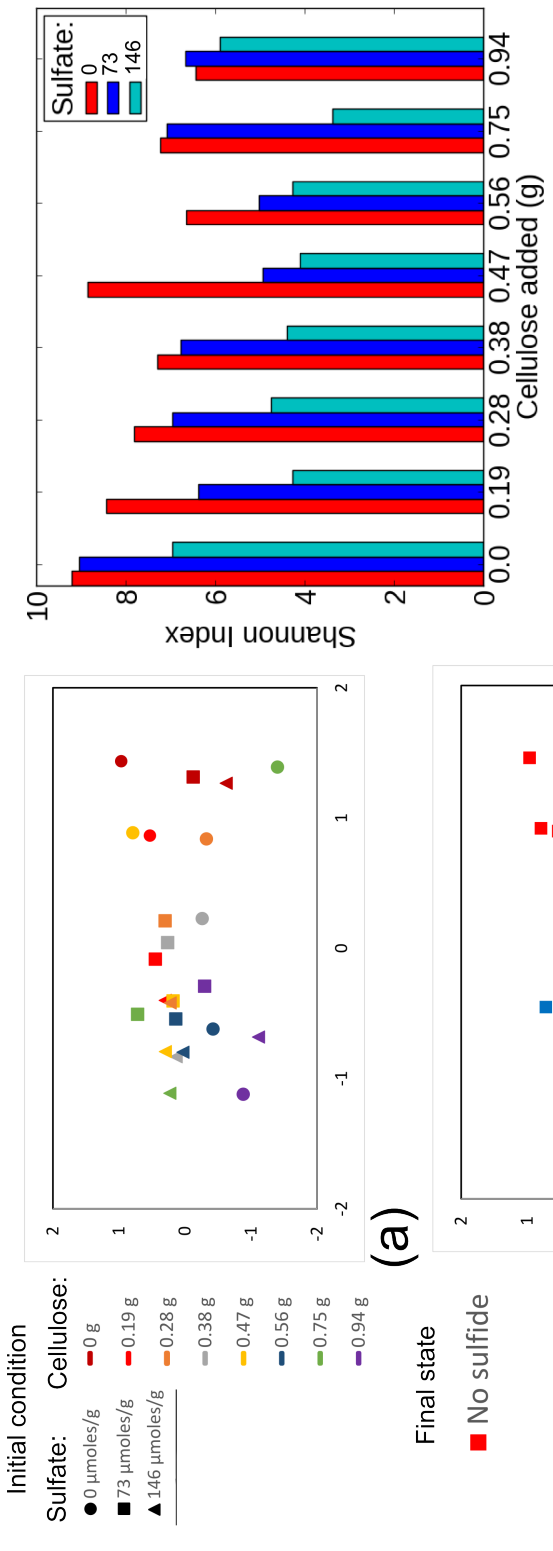

Figure 6.9 (a) and (b) are NMDS plots at OTU level performed on a dataset transformed to the relative abundance of each OTU. (a): Initial chemical condition is represented by colours and shapes as shown in the key. (b): Final chemical state (after 16 weeks) represented by colour. (c): Shannon diversity, calculated on a dataset rarefied to a depth of 1546 sequences per sample. Shown as a function of initial cellulose for three different sulfate concentrations (μmol/g).

The Effect of the Sulfidic Transition on the Microbial Community

Fig. 6.9(b) shows an NMDS plot generated from the same data as the NMDS plot shown in Fig. 6.9(a), i.e. the community composition of the entire community, at the OTU level. However, this time the datapoints are coloured based on whether the microcosm corresponding to that microbial community contained measurable sulfide after 16 weeks or not (i.e. what side of the transition seen in Fig. 6.7(b) the microcosm was on). Plotting the data in this way shows that the transition to the sulfidic state produces a drastic change in the composition of the microbial community. There is a clear difference between the microbial community of a sulfidic and a non-sulfidic microcosm, which again, is borne out by statistical analysis (PERMANOVA: P = 0.001, Pseudo-F = 2.9582). Furthermore we also observe greater variability in community composition among the non-sulfidic microcosms than among the sulfidic ones (PERMDISP: F = 13.154; P = 0.005, mean distances to centroid = 60.2 and 56.6 respectively), indicating that the environment being sulfidic or not *does* impact on the β-diversity.
The presence of sulfide also drives a statistically significant decrease in α-diversity (One-way ANOVA: P=0.001, F = 4.3). In a non-sulfidic microcosm mean diversity was 7.4 $\pm$ 0.4 whereas in a sulfidic microcosm mean diversity was 5.3 $\pm$ 0.4.

6.4.2 Assigning Functional Groups

Clearly, the transition to a sulfidic state causes a change in both the composition and the diversity of the microbial community. However, the detailed nature of the compositional change, and the reason for the decrease in diversity are not clear. To gain a deeper understanding of the effects of environmental perturbations on community composition in our microcosms we tried to probe our sequence data for information on functional changes to the community. To this end, the community

was divided into different functional groups, each of which is responsible for a different metabolic process, as shown in the schematic of Fig. 6.2. This is not a simple task, since 16S rRNA data does not automatically provide information on metabolic function. In this section we discuss how the community was divided into functional groups, before discussing the results of our community analysis at the level of each functional group in the next section.

Predicting the functional capabilities of microbial communities from 16S rRNA data is a central problem in microbial ecology, and many tools have been developed for this purpose. For example, PICRUSt (Phylogenetic Investigation of Communities by Reconstruction of Unobserved States) is a tool that uses 16S rRNA sequence data to predict a distribution of functional genes [185]. However, tools such as PICRUSt were optimised for studying the human microbiome, and as such are poorly suited to analysing environmental data likes ours.

Consequently, we impose our own functional classification scheme on our sequence data. Our classification is able to assign between approximately 40% and 90% of the microbial community with known metabolic "functions" (depending on the sample). Functional groups were assigned according to the following list, using code written by Catherine Mills.

1. **Anoxygenic phototrophs**: This group anaerobically oxidize sulfide using anoxygenic photosynthesis [137]. In doing so, they compete with oxygenic phototrophs for CO_2. We define this group as the green sulfur bacteria phylum *Chlorobi*, green non-sulfur bacteria class *Chloroflexi*, purple sulfur bacteria order *Chromatiales*, and purple non-sulfur bacteria family *Rhodospirillaceae* [186].

2. **Oxygenic phototrophs (photosynthesizers)**: This group generate oxygen which performs the important ecosystem function of abiotically oxidizing sulfide, as well as providing an electron acceptor for aerobic metabolism. We define this group as the phylum *Cyanobacteria* which also includes chloroplasts sequenced from *Eukarya*. This is a peculiarity

of the sequencing, because of the close evolutionary relatedness between chloroplasts and *Cyanobacteria*; chloroplasts were once free bacteria, that were swallowed up by other bacteria and became so-called "endosymbionts" [187]. Although these chloroplasts are not bacteria, they are included as they contribute to oxygen production and thus can be considered part of the same functional group.

3. **Degraders**: This group are responsible for degrading cellulose and other long chain organics, which then supplies electron donors such as acetate and hydrogen for other groups (such as the sulfate reducers) to use. We define this group as the phyla *Bacteroidetes*, *Firmicutes*, *Planctomycetes*, *Fibrobacteres* and *Spirochaetae*. *Bacteroidetes* and *Firmicutes* are biodegraders of long chain organic molecules such as cellulose in many environments [188]. *Fibrobacteres* are known as a cellulose degrading phylum [189]. *Spirochaetae* are known for degrading some organics [190–192], and although not all members of this phylum are able to degrade cellulose specifically they are known to contribute to rates of cellulose degradation by contributing to fermentation [190, 193]. *Planctomycetes* are known degrades of various heteropolysaccharides [194–196].

4. **Sulfate reducers**: This group produce sulfide by coupling the reduction of sulfate to the oxidation of electron donors that are generated by the degradation of the organic matter (mainly cellulose) by the degrader population. All currently known sulfate reducers can be grouped into seven phylogenetic lineages [137]. In our sequence data, we mainly observe sulfate reducers within the class *Deltaproteobacteria* in orders such as *Desulfarculales*,*Desulfobacterales*,*Desulfovibrionales*,*Desulfomonadales* [137]. We also observe the family *Thermodesulfovibrionaceae* within the phylum *Nitrospirae* as well as the two sulfate reducing genera *Desulfosporosinus* and *Desulfotomaculum* from the phylum *Firmicutes* [137] (obviously these two genera were not also included within the group "degraders", which

includes all other taxa within *Firmicutes*).

The procedure described here for classifying into functional groups is necessarily somewhat arbitrary and involves various assumptions. All taxa within the level of taxonomy specified are assumed to perform the associated ecosystem process or function, for example, all taxonomic levels within the phylum *Chlorobi* are assumed to be performing anoxygenic photosynthesis. Moreover, the list above does not necessarily include *all* known bacteria able to carry out these reactions, rather, it only includes the ones that we found in our microcosms. To analyse a different dataset, we would need to add more groups in each class, to account for taxa that might be found in that dataset. Furthermore, some metabolic groups are very hard to classify in this way. For example, in our dataset, aerobic organic matter oxidizers were not assigned due to the difficulty of pinpointing exactly which taxa are responsible for this process, because so many organisms possess the capability to perform aerobic metabolism.

Functional Groups That Are Not Included

Here, we briefly note that some of the functional groups shown in Fig. 6.2 are not included, in our analysis, for various reasons. These groups were as follows:

1. **Aerobic sulfide oxidizers**: This group aerobically oxidize sulfide produced by the sulfate reducers. However, surprisingly, no common aerobic sulfide oxidizing bacteria such as *Beggiatoa* or *Thiothrix*, were found in any of our microcosm datasets, and therefore they do not feature in our analysis [197].

2. **Methanogens**: This group compete with sulfate reducers for electron donors. Since all methanogens are Archaea [198], our primers (which were designed for bacteria) were unable to detect them, and they are not discussed further in this chapter.

6.4.3 Functional Group Abundances Change with Ecosystem State

We first assess how the overall functional composition of the microcosm communities changes as we vary the amounts of added cellulose and sulfate. To this end, we plot the total relative abundance of each functional group (i.e. its fraction of the whole community), as well as the α-diversity (calculated using the Shannon index) of each functional group, as a function of the amount of added cellulose, for the various concentrations of added sulfate. These data are shown in Fig 6.10. We note that by relative abundance here we refer to abundance relative to the entire set of sequences for each sample (as before), and not abundance relative to just those sequences that were assigned into functional groups. We do not know absolute abundances (because the number of sequences recovered from a given sample is not a measure of how much DNA was in it) but only relative abundances.

It is immediately apparent from this data that the response to the nutrient perturbation in terms of relative abundance and diversity is unique to each functional group. The relative abundance and diversity of some functional groups is not affected by the nutrient perturbations. Other groups undergo strong changes in relative abundance and/or diversity in response to the nutrient perturbations we apply.

Degraders and sulfate reducers (panels (c) and (d) in Fig. 6.10) both maintain a stable abundance and diversity in response to an increase in the availability of sulfate and cellulose.

On the other hand, both groups of phototrophs (panels (a) and (b) in Fig. 6.10) respond strongly to changes in initial sulfate and cellulose, but in very different ways. Both oxygenic and anoxygenic phototrophs show a collapse in diversity as nutrient availability increases. The only difference is that anoxygenic phototrophs are stimulated by sulfide, and oxygenic phototrophs are poisoned

by sulfide, meaning that increasing sulfide in the microcosm causes the relative abundance of the oxygenic phototrophs to decrease, and the abundance of the anoxygenic phototrophs to increase.

However, the increase in relative abundance of the anoxygenic phototrophs is coupled to a drastic decrease in α-diversity (the diversity of taxa *within* this group). Conversely, the collapse in the diversity and abundance of the oxygenic phototrophs with initial sulfate and cellulose is probably related to sulfide toxicity, as sulfide is toxic to most oxygenic phototrophs in high concentrations, and can inhibit oxygenic photosynthesis even in low concentrations [199, 200].

To summarize, we see that different functional groups show different changes in abundance and diversity with ecosystem perturbations. To understand in more detail how community composition is changing with these perturbations, we also investigate community changes at the level of individual taxa within functional groups. In the next section, we analyse the changes in the *composition* of each functional group.

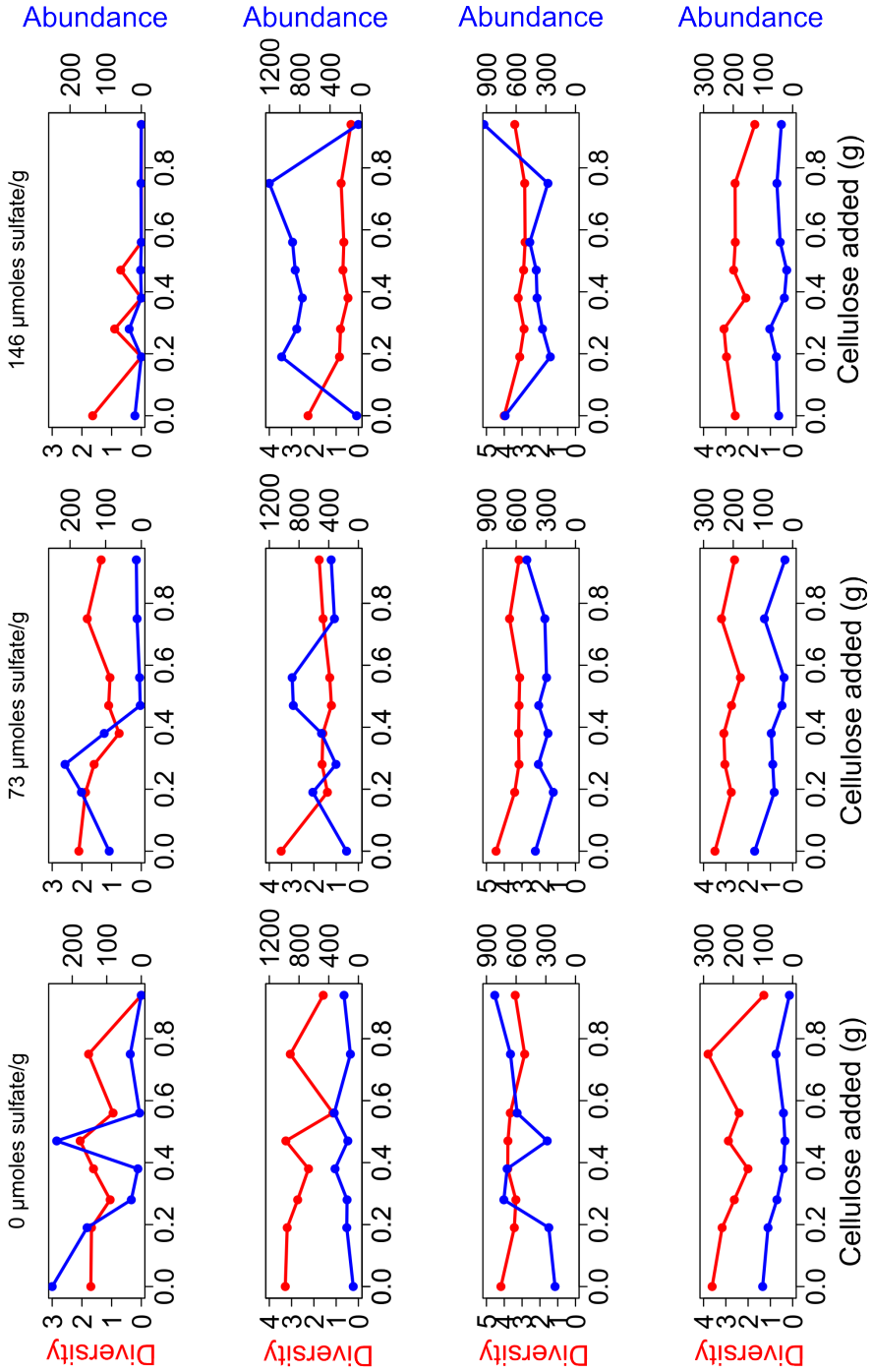

Figure 6.10 Changes in Shannon diversity (red) and abundance (blue) of each functional group. Rows display functional groups, columns display initial sulfate concentrations, and the x axis of each graph displays initial cellulose. Data generated using code supplied by Catherine Mills.

6.4.4 Compositional Changes Within Microbial Functional Groups

We have seen that nutrient perturbations cause the relative abundance and diversity of some functional groups to change, but how are these changes manifested *within* these functional groups? Furthermore, what is the explanation for why other functional groups do not undergo changes in abundance and diversity? To try to answer these questions we now "zoom in" to unravel changes occurring at a deeper taxonomic level by analysing changes in the relative abundance of individual taxa within each functional group, and changes in the overall composition of each functional group.

Multivariate Statistical Analysis of Functional Groups

To investigate how the taxon composition within each functional group changes in our experiments, we first make NMDS plots, in which each point represents the taxonomic composition of a given sample, taking into account only taxa within a specific functional group. These plots are generated using Bray-Curtis similarity at OTU level, for each functional group.

We note here that the multivariate statistics and NMDS plots for the oxygenic phototrophs are not included. This is because many of the high nutrient microcosms contain no oxygenic phototrophs at all and a Bray-Curtis comparison between two samples, both containing no oxygenic phototrophs produces no output in PRIMER. As a result, PRIMER is not able to generate NMDS plots or statistical analysis for this functional group.

To look for effects of environmental perturbations, we first represent datapoints in colour and shape by the initial chemical state of the system (sulfate and cellulose) in Fig. 6.11. We then colour the datapoints by the presence of the sulfidic transition in Fig. 6.12. The statistical analyses on both these plots is

shown in Fig. 6.13 which presents PERMANOVA and PERMDISP statistics analysing whether a statistically significant compositional change occurs within each functional group, in response to the sulfate and cellulose perturbations, and the sulfidic transition.

There is no obvious clustering by cellulose (colour), but there is some observable clustering by sulfate (shape) in Fig. 6.11. However, PERMANOVA analysis (see Fig. 6.13) shows that sulfate drives a compositional change in all functional groups, and cellulose drives a compositional change in both the degraders and sulfate reducers. This is interesting, because the analysis presented in the previous section (see Fig. 6.10) showed that both the sulfate reducers and cellulose degraders undergo no changes in abundance and diversity in response to nutrient perturbations. Taken together, our analysis shows that the degraders and sulfate reducers are highly functionally redundant; these groups maintain a stable abundance and diversity in response to nutrient perturbations, while undergoing strong compositional changes.

In Fig 6.10 we instead colour code according to the sulfidic transition. Once again, clustering of the datapoints is much clearer in this representation (as in Fig. 6.7(b)). It is clear from Fig. 6.12 that the sulfidic transition drives a change in the composition of all functional groups, and this is also borne out by the PERMANOVA analysis presented in Fig. 6.13. Again, this supports the hypothesis that the degraders and sulfate reducers are functionally redundant, because although this analysis shows that both of these groups undergo compositional changes over the sulfidic transition, neither group changed in overall diversity or abundance over the sulfidic transition (see Fig. 6.10).

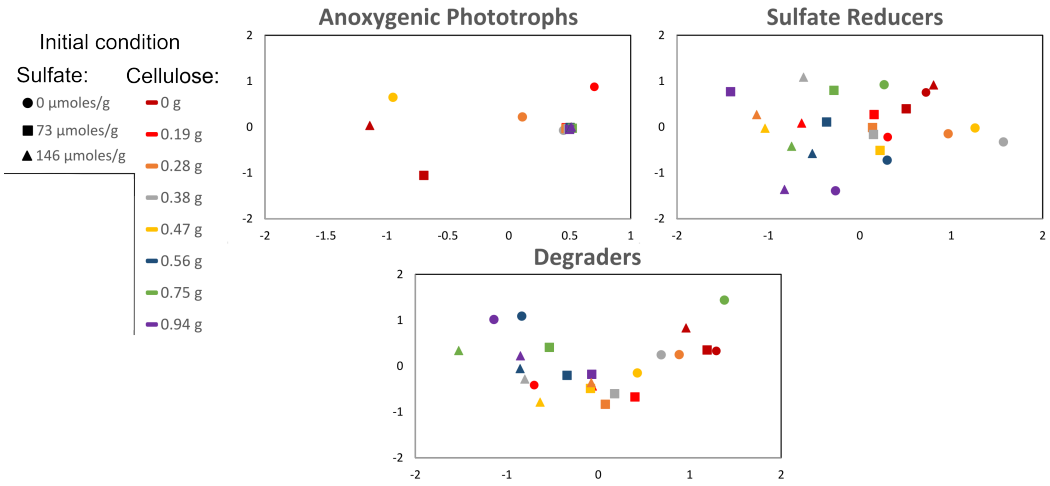

Figure 6.11 NMDS plot at OTU level for each functional group where colours represent initial cellulose and shapes represent initial sulfate. Statistical analysis on these data is presented in Fig. 6.13.

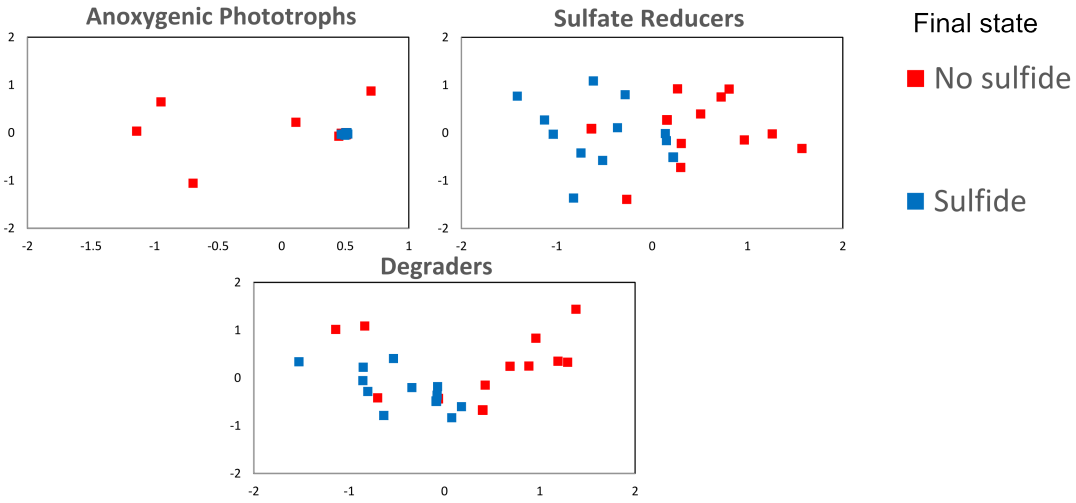

Figure 6.12 NMDS plot at OTU level for each functional group where colour represents whether the microcosm contained measurable sulfide or not after 16 weeks. For all functional groups there is a clear division. Statistical analysis on these data is presented in Fig. 6.13.

(a): PERMANOVA

Functional group	Sulfate	Cellulose	Sulfidic transition
Anoxygenic phototrophs	p = 0.004, F = 2.8	p = 0.1, F = 1.4	p = 0.001, F = 5.6
Degraders	p = 0.011, F = 1.3	p = 0.045, F = 1.3	p = 0.001, F = 2.9
Sulfate reducers	p = 0.002, F = 1.7	p = 0.028, F = 1.19	p = 0.008, F = 1.6

(b): PERMDISP

Functional group	Sulfate	Cellulose	Sulfidic transition
Anoxygenic phototrophs	p = 0.03, F = 8.5	p = 0.3, F = 4.5	p = 0.001, F = 78.2
Degraders	p = 0.17, F = 2.5	p = 0.27, F = 2.82	p = 0.018, F = 8.8
Sulfate reducers	p = 0.525, F = 0.8	p = 0.81, F = 0.9	p = 0.67, F = 0.19

Figure 6.13 Statistical analysis for individual functional groups at OTU level. Effects with a P value <0.01 are coloured blue. Effects with 0.01 <P value< 0.05 are coloured orange. (a): PERMNANOVA statistics. (b): PERMDISP statistics.

6.4.5 Combined Analysis of Functional Groups

To understand in more detail which individual taxa are causing the changes in community composition shown in Fig. 6.11 and Fig. 6.12 and 6.10 we analyse this data at an even deeper level. Fig. 6.14 shows how the relative abundance of individual species within each functional group changes with initial sulfate and cellulose.

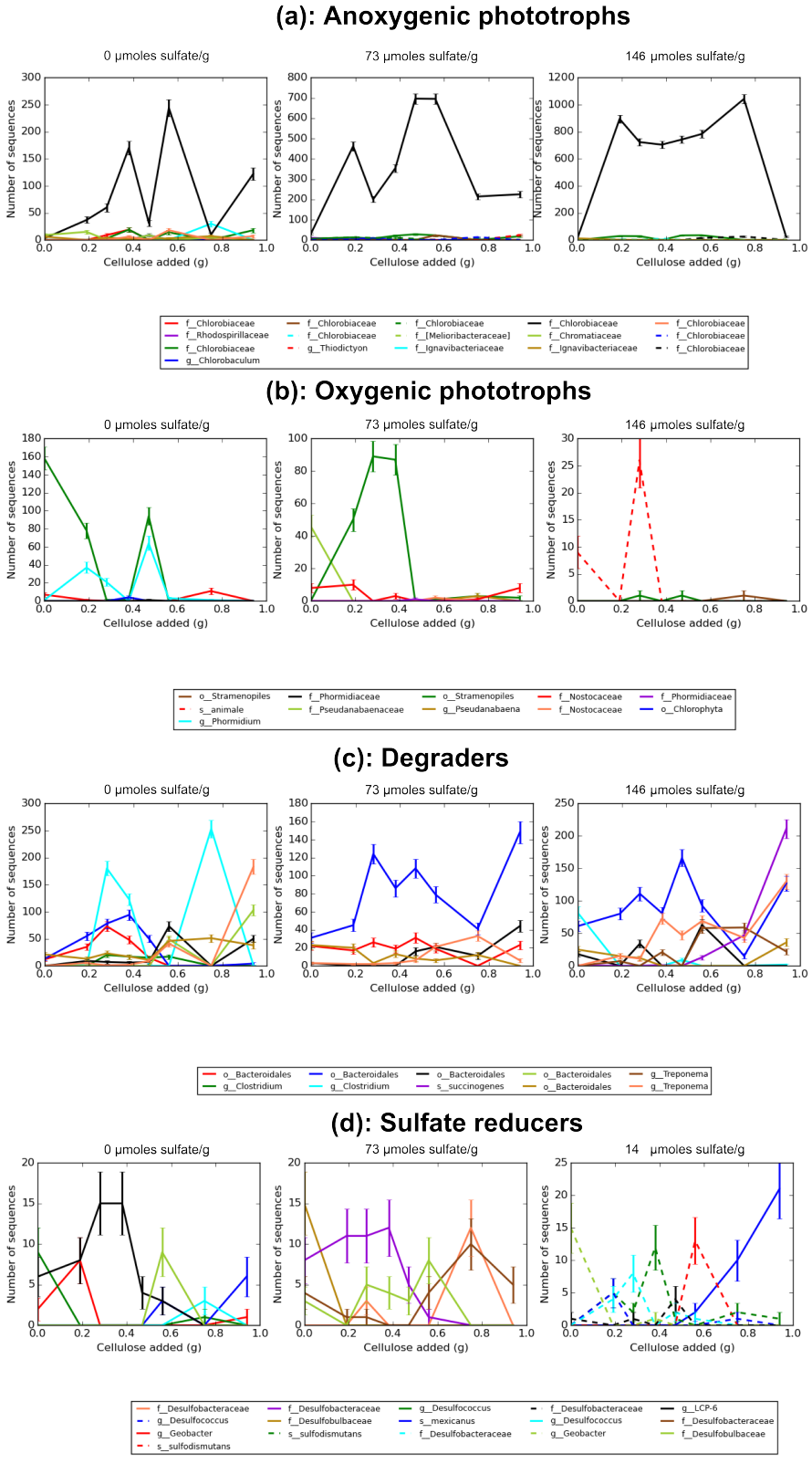

Figure 6.14 Individual OTUs within each functional group. An OTU is included in this analysis if it represents one of the top two most abundant OTUs in at least one microcosm. Plot generated by Catherine Mills.

We now discuss the results of Fig. 6.14 within the context of all of our other analysis for each functional group. Taken together, our analysis clearly shows that the nutrient perturbations have different effects on different functional groups.

1. **Anoxygenic phototrophs:** Increasing initial sulfate caused the abundance of anoxygenic phototrophs to increase dramatically (Fig. 6.10). However, this increase in the abundance of anoxygenic phototrophs is (perhaps surprisingly) combined with a decrease in α-diversity. Fig. 6.14 reveals the reason for this. The increasing sulfide concentration selects for a particular species of green sulfur bacteria; a genus of *Chlorobi* within the family *Chlorobiaceae*. Furthermore, this species is also the most abundant taxon in the low sulfate condition. This is also the explanation for the changes in community composition of the anoxygenic phototrophs as a function of both initial sulfate and the sulfidic transition (Figs. 6.11 and 6.12).

   It is interesting to speculate on the possible reasons for these trends. In the natural environment, different bacteria of the family *Chlorobiaceae* are adapted to exploit different light intensities at different depths [201]. It is possible that in our microcosms this diverse range of light intensities is not available, removing many of the ecological niches that some *Chlorobiaceae* are adapted to. Furthermore, anoxygenic phototrophs do not have a versatile metabolism, for instance, they cannot use multiple alternative electron donors like sulfate reducers can. Potentially, in our microcosms, all anoxygenic phototrophs are competing for carbon dioxide and sulfide at the same light intensity (i.e. in the same ecological niche) and thus we hypothesize that increasing nutrient availability selects for the fittest species of sulfide oxidizing anoxygenic phototroph, causing a collapse in α-diversity. Another explanation is that the increase in sulfide availability caused the anoxygenic phototrophs to follow a predicted ecological relationship between diversity and nutrient availability; many ecological studies have

found that the diversity of a microbial functional group is low at low nutrient availability, peaks at intermediate availability and is low at high nutrient availability [202, 203](a so-called "unimodal" relationship). It is possible that the increasing sulfide availability pushed the diversity of anoxygenic phototrophs past an intermediate diversity peak, and into a region of predictable low diversity.

2. **Oxygenic phototrophs:** Our data show that, increasing sulfate causes a decrease in the diversity and abundance of oxygenic phototrophs (Fig. 6.10). We speculate that this happens because a threshold of sulfide toxicity has been crossed. It is known that in high ly sulfidic environments (such as hot springs) oxygenic photosynthesis can be completely replaced by anoxygenic, sulfide-dependant photosynthesis [199]. Furthermore, even relatively low concentration s of sulfide (10 μM or less) are known to *inhibit* oxygenic photosynthesis in many cyanobacterial strains [200]. It is likely that the presence of sulfide selects for those few oxygenic phototrophs that are able to either resist sulfide toxicity, or switch to an anoxygenic metabolism.

   The analysis of the species present within the oxygenic phototrophs presented in Fig. 6.14 supports this suggestion. For example, for the 73 μmol sulfate/g condition *Pseudanabaena* became established; this taxon is known to show some sulfide tolerance [204]. Furthermore in the 146 μmol sulfate/g condition all of the most abundant oxygenic phototrophs were part of the genus *Phormidium* which is known to be able to carry out oxygenic photosynthesis in the presence of sulfide [199, 205].

   However, we do note that that many microcosms did not contain sulfide extending up into the water column (as Fig 6.7 shows). It is possible that there was sulfide in the water earlier in the experiment that had been re-oxidized by the time measurements were made. However, it is also possible that there was never any sulfide in the water layer meaning that in theory,

many cyanobacteria could have been able to avoid toxic concentrations of sulfide. Consequently, we also note an alternative explanation for the decrease in abundance and diversity of oxygenic phototrophs that was observed in high sulfide microcosms. Potentially, the bloom of anoxygenic phototrophs in high nutrient microcosms caused a depletion of other essential nutrients, such as nitrogen and phosphorus, meaning that these microcosms were not nutrient-rich enough to also support a population of cyanobacteria. In essence, this would mean that high levels of sulfide stimulate anoxygenic phototrophic bacteria to such an extent that they dramatically outcompete oxygenic phototrophs for essential nutrients (as opposed to direcly poisioning the cyanobacteria).

3. **Degraders:** In our data, the abundance and diversity of the degraders (Fig. 6.10) does not change in response to changes in initial sulfate or cellulose, or the presence of the sulfidic transition. We speculate that this arises due to a high degree of functional redundancy. Looking in more detail (Fig. 6.14) we see that this may be related to the fact that there are many different species of degrader present in our microcosms, which apparently coexist. We hypothesize that different members of this coexisting community may prefer different environmental conditions. However, Figs. 6.11-6.13 show that the sulfidic transition causes a change in the composition of this functional group and Fig. 6.14 shows that different species become abundant at almost every condition of sulfate and cellulose. For example, in medium and high sulfate microcosms the most abundant degrader was a member of the phylum *Bacteroidetes*, whereas at zero sulfate the most abundant species was of the genus *Clostridium* which is a member of the *Firmicutes* phylum. This indicates suggests that different taxa within the degrader community are adapted to different concentrations of sulfate and organic matter.

   It is possible that this apparent functional redundancy of the degrader

population is related to the fact that there are many different metabolic strategies for degrading cellulose. At very high sulfate and cellulose the most abundant cellulose degrader is *Fibrobacteres succinogenes* which is known to have a unique method of cellulose degradation that does not rely on cellulase enzymes like most cellulolytic bacteria [206]. At low cellulose and sulfate concentrations the most abundant degrader was *Clostridium*. A previous study reported that *Clostridium* degrades cellulose more effectively when concentrations are low due to the accumulation of intracellular inhibitory compounds [207]. Furthermore *Clostridium* does use cellulase enzymes. We speculate the difference in the cellulose-degrading mechanisms between *Fibrobacteres succinogenes* and *Clostridium* may be what makes them best adapted to high and low cellulose conditions respectively. Interestingly, *Treponema* is thought to degrade cellulose in a consortium with classic cellulose degraders (it is known to do this with *Fibrobacteres succinogenes* in particular [208]) and is abundant across almost all cellulose and sulfate conditions. This potentially indicates that *Treponema* is able to form a consortium with many different cellulose degraders, regardless of the mechanism being used.

4. **Sulfate reducers:** Sulfate reducers, like the degrading population, maintain a stable relative abundance and diversity across environmental gradients, indicating functional redundancy. Fig 6.13 shows that different taxa proliferate at different concentrations of sulfate and organic matter.
   In our microcosms most sulfate reducers were in the class *Deltaproteobacteria*, with the most abundant orders being *Desulfobacterales*, *Desulfovibrionales*, *Desulfuromonadales*, *Desulfarculales* (in order of most to least abundant). Fig. 6.14 shows that different initial sulfate conditions produce a very different species composition for the sulfate reducers. For example, at high cellulose and sulfate *Desulfovibrio mexicanus* became dominant. *Desulfovibrionaceae* and *Desulfovibrionales* were associated

with the highest sulfate concentration, and *Desulfobulbaceae* was associated with a lower sulfate concentration. The lowest sulfate concentration (zero added) was associated with *Thermodesulfovibrionaceae* from the phylum *Nitrospirae*.

Again, similarly to the degrading population, this functional redundancy may be related to the diversity of metabolic strategies for reducing sulfate. Sulfate reducers are able to utilise a wide variety of electron donors such as lacate, acetate or hydrogen, creating a variety of exploitable environmental niches, and making them able to adapt to variations in the abundance of these electron donors as a functional group [137]. It is also likely that sulfate reducers have adapted to various depth-defined micro-niches in terms of factors such as pH or redox potential [16].

6.5 Discussion and Conclusions

6.5.1 The Relationship Between Function and Diversity is Unique to Each Functional Group

We carried out a detailed microcosm study of the microbial freshwater sulfur cycle and found that organic matter induces a transition to a sulfidic state above a threshold value of 18 μmol sulfate/g sediment. The transition to a sulfidic state occurs at a threshold cellulose concentration of 0.2 g added cellulose per microcosm. We note here that the exact threshold point in both cellulose and sulfate could be anywhere between 18 μmol sulfate/g sediment and 73 μmol sulfate /g sediment, and between and 0.2 g and 0.38 g added celullose per microcosm.

We suspect that when the organic matter concentration is low, any sulfide produced by sulfate reduction is re-oxidized quickly. Indeed, it is known that, in

marine environments, the system often quickly re-oxidizes any sulfide produced [209]. In our system sulfide is likely to be re-oxidized by abiotic reaction with iron and with oxygen, and by biotic oxidation by micro-organisms. The biotic oxidation of sulfide by micro-organisms appears to be carried out by anoxygenic phototrophs (which are abundant in our microcosms) and not by aerobic sulfide oxidizers (which we do not observe in our microcosms). When the organic matter concentration exceeds a critical threshold however, the sulfide production rate exceeds the capacity of the system to re-oxidize sulfide. The ecosystem then transitions into a sulfidic state.

We then show how this chemical transition imprints on the microbial community. High-throughput sequencing analysis revealed that the chemical changes in our microcosms were accompanied by a transition in the composition of the microbial community. Increasing sulfate concentrations and the presence of sulfide at steady state are both associated with a drastic decrease in α-diversity when measured across the whole community.

We then divided the community into functional groups of microbes, each of which is thought to be responsible for different metabolic processes. The effect of the sulfate and cellulose perturbations on these functional groups was non-trivial. Some groups undergo drastic changes in relative abundance and diversity, causing the chemical pathways that characterise the ecosystem to change fundamentally. Other microbial groups display a high degree of "functional redundancy", with different taxa being adapted to take advantage of changing chemical conditions while maintaining a stable group-level abundance.

We suggest that whether a functional group is stable or unstable in response to an environmental perturbation may be related to the diversity of metabolic strategies that can potentially carry out that ecosystem process. Both the organic matter degrading and sulfate reducing communities seem well adapted to take advantage of fluctuating nutrient availability, and both of these processes are characterized by a diverse suite of microbial metabolic strategies to carry them out (sulfate reducers can use many different electron donors, and degraders can use

externally secreted cellulase enzymes, an internal cellulosome, or degrade cellulose in symbiotic consortia). Both the phototrophic communities show a decrease in diversity as nutrient availability increases, and for both of these processes there is only one metabolic strategy that can be used to carry them out.

In particular, these results show that it is difficult to establish general laws about the relationship between diversity and function in microbial ecology. For example, increasing nutrient availability (sulfide) caused a drastic increase in abundance and a drastic decrease in the diversity of the anoxygenic phototrophs, while an analagous increase in nutrient availability (sulfate) for sulfate reducers causes no such change. Our work suggest that an understanding of the specifics of the ecosystem processes and geochemistry of individual environments is necessary to understanding the effects of environmental perturbations on microbial ecosystems.

6.5.2 Sharp Transitions in Microbial Communities

This work also represents a novel contribution to the study of transitions between ecosystem states in microbial communities. Although the existence of sharp transitions in response to perturbations has previously been a high-profile topic in systems ecology (with many examples, such as changes in the microbial community in response to organic matter loading in the leaves of carniverous pitcher plants [107]), the study of such "regime shifts" in microbial ecosystems has been largely neglected [165, 210]. As such, microcosm communities represent the ideal model system for understanding the response of microbial nutrient-cycling communities to environmental perturbations, since they have the advantage of retaining many of the features of the real ecosystem (such as moderate microbial diversity, spatial structure, and abiotic interactions) while allowing the controlled manipulation of environmental perturbations.

Some previous work has suggested that microbial ecosystems may be highly

resistant to perturbations due to micro-organisms' ability to modify their own growth rate, and change their respiratory mechanism [165]. For example, one study suggested that the soil microbial community is largely composed of facultative anaerobes, allowing the community to remain stable in response to rapid changes between oxic and anoxic conditions [211]. However, a few observations of the existence of sharp transitions in microbial communities in response to environmental perturbations seem to contradict this picture, with 3 examples being: 1) a shift between iron reducing and sulfate reducing states in a sediment ecosystem in response to changes in overlying groundwater flow rate [212], 2) a nitrogen-cycling batch reactor undergoing abrupt transitions in microbial community composition in response to chemical changes [161], 3) a shift in the resident microbial community of a coral in response to transient temperature changes [213]. Despite these key examples, very few studies have focused on the stability of solely microbial ecosystems in response to environmental perturbations [210].

6.5.3 Is the Experimental Sulfidic Transition A Redox Regime Shift?

The models presented in chapters 4 and 5 predicted that a gradual increase in the availability of organic matter should produce a "redox regime shift" in biogeochemical cycles where the concentration of the substrate being cycled is very high (saturating the kinetics of microbial growth). These models also predicted that the microbial sulfur cycle might be particularly likely to produce such a redox regime shift. Given we observed a similar sulfidic transition in the experiment (see Fig 6.7b), it is interesting to speculate as to whether the experiment has truly reproduced the model prediction.

Unfortunately, we are unable to state that Fig 6.7b proves our model prediction,

because there are many processes that could give rise to similar behavior, in particular, abiotic buffering of sulfide by reaction with iron and oxygen is likely to produce such a shift. In the next chapter, we attempt to construct a model of our microcosm experiment that includes these buffering reactions, to see if we can show that the sulfidic transition seen in Fig 6.7b is produced by abiotic buffering effects instead of being a true "redox regime shift". In order to conclusively demonstrate that a redox regime shift has been observed in this experiment, a detailed chemical analysis of all of the possible oxidation states of the sulfur cycle as well as other relevant chemicals such as iron and iron oxides, compared to a model that accounts for these abiotic chemical reactions, would be required.

6.5.4 The Environmental Relevance of this Experiment

Environmental perturbations similar to the ones that we applied have a profound impact on the modern day climate. In coastal regions, increased marine deposition of organic matter has led to the proliferation of large "oxygen minimum zones", these are anoxic "dead zones" in the ocean which are completely devoid of complex marine life [139]. Furthermore global warming is thought to be causing the expansion of these oxygen minimum zones by driving a decrease in oceanic O_2 solubility [214].

However, despite the fact that this is a key environmental issue, the response of microbial communities to environmental change remains poorly understood [215]. For example, increases in global mean temperature are likely to increase the rate of the microbial decomposition of soil carbon, but predictions of the strength of this effect vary wildly (as discussed in chapter 2) [48]. The effects of anthropogenic perturbations on microbial ecosystems are particularly important; for example, up to one third of the world's oceans are estimated to be under medium to high impact from ecological stresses created by human activities [216]. As another example, nitrogen inflow from agricultural waste is

fundamentally altering ecosystems and microbial communities in coastal regions; often generating large anoxic "dead zones" [139]. This work raises the possibility that an understanding of ecosystems processes in experimental model ecosystems (such as Winogradsky columns) may ultimately allow these consequences to be managed in natural ecosystems.

Chapter 7

Including Realistic Chemistry in Models of Microbial Ecosystems

7.1 Introduction

The experimental results presented in chapter 6 showed that stimulating a microbial freshwater sulfur-cycling ecosystem with organic matter can cause a shift, or transition, to a sulfidic state. Furthermore, the effect of this transition on the microbial community was examined in detail. However, the *cause* of the transition to a sulfidic state has not been fully explained.

The models presented in chapters 4 and 5 suggest that such transitions between oxic and anoxic states in nutrient-cycling ecosystems may result from nonlinearities in the underlying microbial population dynamics. However, it is also entirely possible that effects arising from abiotic chemical reactions could cause a shift to a sulfidic state. For example, as discussed in chapter 6, the abiotic reaction of sulfide with iron can affect environmental sulfide concentrations [176]. Fully deciphering the cause of the transition to the sulfidic state that we see in our experiments thus requires an understanding of the abiotic chemical reactions in

the system, as well as the reactions mediated by microbial life. In this chapter we discuss computational models for our experimental microcosms that incorporate realistic abiotic chemistry. These models also include microbial dynamics for some of the functional groups of microbes that were identified in the previous chapter; sulfate reducers, methanogens and organic matter degraders.

The models described in this chapter reveal two processes that can give rise to transition to a sulfidic state in this system: 1) a buffering effect arising from the abiotic reaction of sulfide with oxygen and iron and 2) effects arising from the thermodynamic limitation of microbial respiration.

7.2 Background: The Geochemist's Workbench

7.2.1 Introduction to The Geochemist's Workbench

Previous models (chapters 4 and 5), were implemented using custom-written software. In this chapter, however, a software package called "The Geochemist's Workbench" will be used for all mathematical modelling [217]. The Geochemist's Workbench is a numerical solver for thermodynamic and kinetic chemical equations which is widely used by engineers, geologists and environmental chemists. It has been used to model arsenic rich landfill sites [218], acid mine waste [219], nuclear waste [220] and the chemistry of ancient oceans [221]. The Geochemist's Workbench has also been applied to modelling microbial processes. For example, to model the bacterial reduction of uranium [14], bacterial sulfate reduction [222] and many other microbially-mediated processes [223, 224].

Implementing a model using The Geochemist's Workbench has many advantages compared to using custom-written software. The Geochemist's Workbench comes already equipped with detailed thermodynamic datasets defining many environmentally important chemical reactions, and it uses these databases to calculate the equilibrium state of very chemically complex systems. Since the

number of relevant reactions may be in the tens or hundreds this is much easier than implementing them all from scratch in a custom-written code. Furthermore it is possible to easily enable or disable reactions at will, and thus determine the effect of each individual reaction on the system.

The basic principles underlying the way The Geochemist's Workbench works are as follows. Consider a generic reversible reaction in which chemical components A and B react to form the products C and D.

$$a\mathrm{A} + b\mathrm{B} \rightleftharpoons c\mathrm{C} + d\mathrm{D} \tag{7.1}$$

This reaction has an associated equilibrium constant (K_{eq}) defined in Eq. 7.2.

$$\log\left(K_{\mathrm{eq}}\right) = \log\left(\frac{[\mathrm{C}]^c[\mathrm{D}]^d}{[\mathrm{A}]^a[\mathrm{B}]^b}\right) \tag{7.2}$$

In Eq. 7.2, K_{eq} is defined is defined in terms of the chemical concentrations at equilibrium (when free energy is minimised). This is essentially a mass-balance equation, meaning that, for example, if the concentrations of chemicals B, C and D were known, Eq. 7.2 could be used to predict the concentration of chemical A at equilibrium. The Geochemist's Workbench uses the Newton-Raphson method to solve a set of mass balance equations like Eq. 7.2 for all of the abiotic reactions in the system [217].

The Geochemist's Workbench contains several different "modules" that are designed for modelling different types of processes. The modules that are used to model microbial processes are React, X1t and X2t. X1t and X2t are designed to model spatially heterogeneous systems in 1-D and 2-D respectively, whereas the React module assumes spatial homogeneity. In this chapter the React module of The Geochemist's Workbench will be used. Fig. 7.1 shows a schematic diagram detailing the "workflow" of The Geochemist's Workbench for a model implemented in the React module.

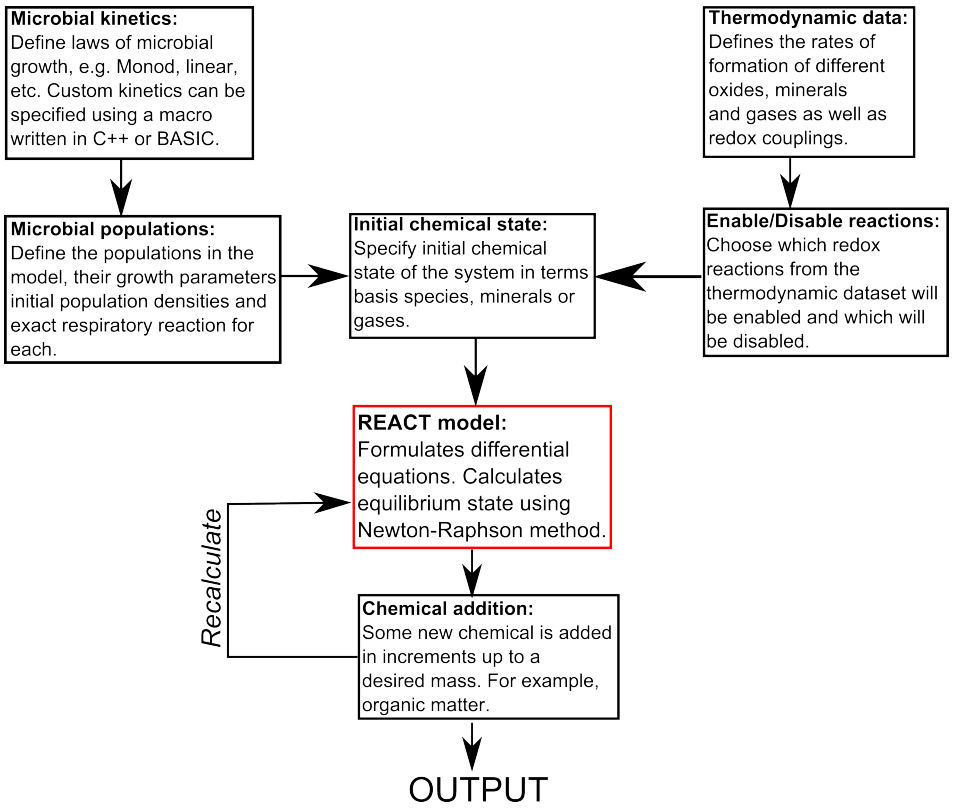

Figure 7.1 Schematic diagram indicating the components of the React module in The Geochemist's Workbench package.

The basic principle of the React module is to calculate the effect of kinetic processes on the system, assuming chemical equilibrium for the associated abiotic geochemical reactions. For example, the effect of gradually titrating a chemical into to system at some rate, or the effect of processes such as microbial respiration. In the React module, a set of differential equations describing the kinetic processes is iterated numerically, while at the same time the abiotic equilibrium solution for the entire chemical system is still calculated separately using a Newton-Raphson method. More specifically, the implementation of a model in React consists of three parts:

1. **The thermodynamic dataset:** An in-built thermodynamic dataset which contains information on many abiotic chemical reactions. All work in this chapter uses the Lawrence Livermore National Laboratory (LLNL)

Thermodynamic Database as the thermodynamic dataset [225].

Within this thermodynamic dataset all chemicals are classified within one of several groups, such as a mineral, a redox species or a "basis species". The set of basis species defines the set of chemicals that are the building blocks for every other chemical in the thermodynamic dataset. Furthermore, all basis species are linearly independent, meaning no basis species can be defined in terms of any other basis species. Examples of basis species are H^+, Cl^- and Na^+ [217].

Every mineral, redox species or aqueous species must be defined by some chemical reaction of formation, like the generic reaction described in Eq. 7.1. Equilibrium constants (see Eq. 7.2) defining the propensity for the reaction to occur are defined at different temperatures (up to 500°C). If, at some temperature, the reaction tends strongly towards the left hand side, then the concentration of the reactants will be higher than the concentrations of the products at equilibrium, making $\log(K_{\text{eq}})$ positive because $\left(\frac{[C][D]}{[A][B]}\right) < 1$.

For example, sodium phosphate ($NaHPO_4^-$) is defined as an aqueous species that forms out of one sodium ion (Na^+, a basis species) and one phosphate ion (HPO_4^-, a basis species). At all temperatures (up to 500°C) the $\log(K_{\text{eq}})$ for this reaction is negative. This means that sodium and phosphate ions tend to to react together and form a sodium phosphate precipitate (i.e. come out of solution). As a counter example, sodium chloride is defined as an aqueous species that forms out of one sodium ion and one chloride ion, but in this case, at all temperatures the $\log(K_{\text{eq}})$ for this reaction is *positive*. This means that the sodium chloride molecule is highly soluble.

2. **The initial system:** A requirement of the React module in The Geochemist's Workbench is that the initial state of the system has to be specified. This is specified in terms of properties such as the mass of solvent water, the temperature and the quantities of any minerals or the

concentrations of any dissolved chemicals.

Furthermore, a "charge balance" chemical must be specified. In The Geochemist's Workbench, a charge neutrality condition must be always be fulfilled. This condition could be broken immediately if the set of specified chemicals in the initial system does not achieve charge neutrality (which is likely). To maintain charge neutrality, the system adjusts the concentration of a a "dummy" ion specified by the user. For obvious reasons, this component will be an ion that does not participate in the chemical reactions of interest for the system; typically this is Na^+ or Cl^-. In this chapter, Na^+ is adjusted to maintain electroneutrality, because this ion has little effect on the microbial sulfur cycle, which is the subject of this chapter.

3. **User-defined kinetic processes:** A set of user-defined processes of interest that alter the chemical state of the system. These could be microbial population growth or metabolism or the removal or addition of chemicals from the system. Including microbial populations requires the user to define the required kinetic equation to describe microbial metabolism and the corresponding set of growth parameters; no microbial growth parameters are included within The Geochemist's Workbench dataset per se. Modelling microbial populations within The Geochemist's Workbench is described in more detail in the next subsection.

7.2.2 Modelling Microbial Growth With the Inclusion of Thermodynamic Terms

In this chapter, we have chosen to model microbial growth using slightly different kinetic equations to those used in chapters 4 and 5. Here, the kinetic equations used will include a term that explicitly accounts for the thermodynamics of the metabolic reaction being performed, as discussed in chapter 2. This is important, because Monod kinetics alone would predict that a microbe will continue to

metabolize substrate until none remains, but in reality microbes can only grow if there is enough energy available in the environment for them to respire [66, 67]. In microbial respiration an electron is removed from some electron donor D and added to some electron acceptor A (as described in chapter 2); the free energy released in this reaction is then used to synthesize ATP, which is used for growth. A generic microbial respiratory reaction is defined in Eq. 7.3, where mATP molecules are synthesized and D^+ and A^- are the oxidized and reduced forms of the electron donor and acceptor respectively.

$$\mathrm{D} + \mathrm{A} + m\mathrm{ADP} + m\mathrm{PO}_4^{3-} \rightarrow \mathrm{D}^+ + \mathrm{A}^- + m\mathrm{ATP} \tag{7.3}$$

The standard method for describing microbial kinetics within The Geochemist's Workbench is as follows. The rate of change of the microbial population density is defined according to Eq. 7.4, where n defines a biomass density (mg biomass/kg water), Y defines a growth yield (mg biomass/mol), r defines a nutrient consumption rate (mol/s) and D defines a death rate (s^{-1}). n_{w} (kg) is the mass of water in the system.

$$\frac{dn}{dt} = \frac{Yr}{n_{\mathrm{w}}} - Dn \tag{7.4}$$

The nutrient consumption rate r is given by Eq. 7.5

$$r = n_{\mathrm{w}} v n \left(\frac{[\mathrm{D}]}{K_{\mathrm{D}} + [\mathrm{D}]}\right)\left(\frac{[\mathrm{A}]}{K_{\mathrm{A}} + [\mathrm{A}]}\right) \times \mathrm{F_T} \tag{7.5}$$

where the terms in brackets are Monod terms describing saturating dependence on the concentrations of electron donor and acceptor respectively. K_{D} and K_{A} are the half saturation constants associated with the electron donor and the electron acceptor respectively. v is a specific nutrient consumption rate per unit biomass in mol/(mg biomass)$^{-1}$s^{-1}.

In Eq. 7.5, F_T is the thermodynamic limitation function for microbial growth, that we introduced in chapter 2. This imposes the limitation that microbes are not able to grow if conditions are such that their respiratory reaction fails to provide enough free energy to synthesize ATP. Specifically, following Jin et al [67] we use:

$$F_{\mathrm{T}} = \begin{cases} 1 - \exp\left(\dfrac{\Delta G + m\Delta G_{\mathrm{ATP}}}{\chi RT}\right), & \text{if } \Delta G + m\Delta G_{\mathrm{P}} \leq 0 \quad (7.6a) \\ 0, & \text{if } \Delta G + m\Delta G_{\mathrm{P}} \geq 0 \quad (7.6b) \end{cases}$$

For simplicity, for all microbial populations discussed in this chapter, we set $m = 1$, assuming 1 ATP molecule is synthesized per electron transferred through the electron transport chain. χ defines the number of protons translocated across the membrane per reaction (see chapter 2). For example, for microbial sulfate reduction with acetate $\chi = 5$ because 5 protons are pumped per cycle of the electron transport chain [37].

As Fig. 7.1 shows, custom kinetics for microbial processes can also be defined to replace the standard kinetic equations described in Eqs. 7.4-7.6. Later in this chapter, we describe how to define custom rate laws for a population of cellulose degraders for which the thermodynamic limitation term (Eq. 7.6) is not appropriate.

7.2.3 Implementation of The Geochemist's Workbench in this Chapter

Once the initial chemical state of the system, physical parameters, and microbial kinetics are specified, the React module can then proceed to perform numerical solutions of the relevant kinetic and chemical thermodynamic equations. In this chapter, we set up models, implemented in React, designed to mimic the chemical and physical conditions of our microcosm experiments (described in chapter 6).

All models simulate a 50 ml system and are run for 16 weeks to simulate the length of time the microcosm experiment was run for. For all models in this chapter, dissolved chlorine and sodium concentrations are both set initially to 3 mM, this initial concentration is chosen to allow easy variation to achieve charge neutrality. Where direct attempts are made to reproduce experimental data chemical concentrations for oxygen, iron, sulfate and cellulose are set to experimentally measured values for our microcosm experiments.

7.3 Results: Models of Important Abiotic Processes

Before introducing the microbial population dynamics in the next section, in this section, we briefly discuss abiotic reactions that will be particularly important for the system modelled in this chapter.

7.3.1 The Abiotic Oxidation of Sulfide

In the previous chapter, we tested the hypothesis that our experimentally-observed transition to a sulfidic state could have been caused by the buffering of sulfide by reactive iron. By experimentally measuring the concentration of reactive iron, we found that the concentration was large enough (100 μmol/g) to allow the reaction of iron with sulfide to generate the switchlike behaviour through a buffering effect.

However, the reaction of sulfide with abiotic iron is not the only abiotic reaction that could potentially buffer the sulfide concentration in our experiments, and thus cause a sudden transition in the observed sulfide concentration. The abiotic oxidation of sulfide, shown in Eq. 7.7, is also an important redox reaction in this

system [175].

$$HS^- + 2O_2(aq) \rightleftharpoons SO_4^{2-} + H^+ \tag{7.7}$$

To examine the potential effect of this redox reaction in our experiments, we first simulate a very simple model containing no microbial populations. Fig. 7.2 shows the effect of titrating sulfide into a box containing a fixed amount of dissolved oxygen (in water) into which sulfide is added. In these simulations, sulfate and oxygen concentrations are set to environmentally representative concentrations ($O_2(aq) = 100$ μM, $SO_4^{2-} = 1$ mM [115]). The results are markedly different depending on whether the abiotic oxidation of sulfide (Eq. 7.7) is included in the model (solid lines) or is disabled completely (dashed lines). When the oxidation of sulfide is included in the model then any sulfide titrated into the box reacts very quickly with oxygen. This decreases the dissolved oxygen concentration until only trace concentrations remain once enough sulfide has been added, and the system is anoxic. At this point the addition of further sulfide causes the system to abruptly transition into a sulfidic state. In contrast, when the abiotic oxidation of sulfide is disabled, the observed sulfide concentration gradually increases as sulfide is titrated into the system.

Clearly the simple abiotic oxidation of sulfide can produce a sharp transition between oxic and sulfidic system states upon addition of sulfide. This transition happens when the amount of sulfide added to the system exceeds the capacity of the oxygen present to react with it. In our microcosms, sulfide is produced by sulfate reducers in response to organic matter decomposition; thus it makes sense that the more organic matter we add, the faster sulfide will be produced in the microcosms. Thus it seems plausible that the transition to a sulfidic state which we see in our microcosm experiments might be related to the abiotic oxidation of sulfide.

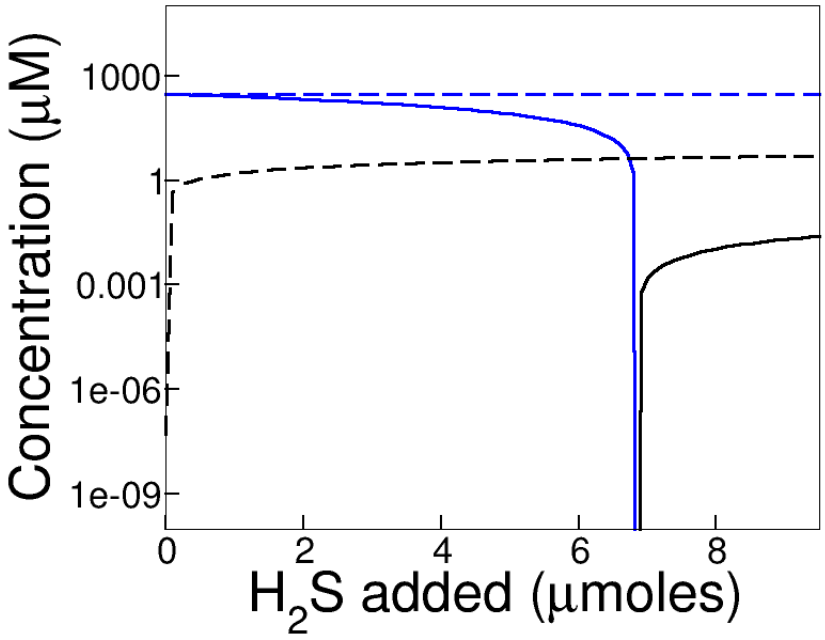

Figure 7.2 Graph showing the effect of titrating sulfide into a homogenous oxygenated system. Dissolved HS^- (black lines) and O_2 (blue lines) are plotted as a function of the quantity of sulfide added to the system. A sharp transition between oxic and sulfidic states occurs in the case where the redox reaction of sulfide with oxygen (shown in Eq. 7.4) is turned *on* (solid lines) but not when this redox reaction is turned *off* (dashed lines). Initial conditions: $SO_4^{2-} = 1\text{mM}$, $Na^+ = 3000\mu\text{M}$, $Cl^+ = 3000\mu\text{M}$, $O_2(\text{aq}) = 100\mu\text{M}$.

7.3.2 The Abiotic Oxidation of Acetate

Acetate (CH_3COO^-) is likely to be an important chemical species in our microcosms because it is used as an electron donor by sulfate reducers and methanogens. In our microcosms, acetate it is produced by decomposition of cellulose. When acetate comes into contact with oxygen, it can react according to Eq. 7.8.

$$CH_3COO^- + 2O_2 \rightleftharpoons 2HCO_3^- + H^+ \tag{7.8}$$

In principle, the reaction shown in Eq. 7.8 could also be included in our models,

like the abiotic oxidation of sulfide. In our microcosms, however, acetate is unlikely to come into contact with oxygen because acetate production via the degradation of cellulose occurs deep in the anoxic zone of sediment (deeper than the zone where sulfate reduction occurs) [179, 180]. In this chapter, we thus disable the reaction corresponding to Eq. 7.8. Furthermore, we note that this reaction is unlikely to be significant even if enabled, as the spontaneous oxidation of acetate proceeds very slowly at normal temperatures.

7.4 Results: Including Microbial Populations to Replicate our Microcosm Experiment

7.4.1 Introduction

In this section, we develop a model, implemented in the React module, which includes microbial populations representing some of the key functional groups of microbes discussed in chapter 6. The key advantage of using a Geochemist's Workbench model is that it allows us to account for all possible abiotic reactions that may affect the system, as well as account for the kinetics and thermodynamics of microbial growth. To examine the effect of each population we gradually add these populations one by one to the model, building up to the most detailed model containing all of the populations at the end of the section. We first include sulfate reducers, followed by methanogens, before moving on to including cellulose degraders. We then move on to attempting to reproduce the experimental switch to a sulfidic state, by examining how the final chemical state of the microcosm (after 16 weeks) responds to increasing organic matter availability. The models presented in this chapter are simulated for 4 months (16 weeks), to reproduce the length of time that the microcosms were incubated. We note that, although we assumed that the microcosm experiment presented

in chapter 6 had reached steady state when we made chemical measurements and took samples after 16 weeks (based on redox potential data) this is not a necessary assumption of our model (although our model simulations do seem to reach a steady state after 16 weeks).

The Geochemist's Workbench solves microbial kinetics numerically, finding an equilibrium solution for all abiotic reactions at the end of each timestep. This means the kinetics of the microbial populations may not have reached steady state by the end of the run (although all abiotic reactions will be at equilibrium). In all these simulations a homogeneous 50 ml volume is assumed, to reproduce the volume of each microcosm from the experimental work. The full set of kinetic parameters for the microbial populations included in this chapter are as shown in Table 7.1. We note here a specific limitation of the fact that this model is spatially homogeneous. In reality, the growth of anaerobes such as sulfate reducers and methanogens, is inhibited by the presence of oxygen. (This was also a limitation of the spatially homogeneous model presented in chapter 4). By not explicitly including the inhibition of these populations by oxygen in this spatially homogeneous model, we are assuming that in reality, these populations would be growing in sediment zones where they are spatially separated from oxygen.

7.4.2 Simulating the Dynamics of a Single Microcosm

In our experiments, electron donors (such as acetate) generated by cellulose degradation are used by sulfate reducers to reduce sulfate to sulfide. Increasing the initial supply of cellulose to the microcosm produces a transition to a sulfidic state because increased cellulose increases the production of electron donors which in turn increases sulfide production rates. We first simplify the model by replacing cellulose degradation by a constant supply of acetate over the entire 16 weeks, whose rate is assumed to increase with the amount of added cellulose. To mimic changing the cellulose concentration, we examine the effect of varying this acetate

Table 7.1 Microbial growth parameters used in the React model within The Geochemist's Workbench. Cellulose degraders have no ΔG_P or χ because the thermodynamic limitation function F_T is not used to model this population. Methanogens have no half saturation constant for an electron donor K_D because for acetoclastic methanogenesis, acetate functions as both electron donor and an electron acceptor (it is a disproportionation reaction, where one carbon atom is oxidized and one carbon atom is reduced). ΔG_P is the amount of energy conserved in the synthesis of ATP and is estimated to be -45 kJ(mol)$^{-1}$ for all populations in this chapter. The initial biomass density was estimated based on literature values of the biomass density of sulfate reducers for similar lake systems [226].

Parameter	Sulfate reducers	Methanogens	Cellulose degraders
v (mol$mg^{-1}s^{-1}$)	1×10^{-9} [119]	1×10^{-9} [148]	1×10^{-9} [227]
K_A (molal)	5×10^{-6} [119]	1×10^{-3} [148]	$\approx$ 1mM [228]
K_D (molal)	7.0×10^{-5} [37, 126]	NA	NA
χ	5 [37, 173]	2 [37, 173]	NA
ΔG_P (kJ/mol)	-45 [120]	-45 [120]	NA
Initial Biomass (mg/kg)	1.0×10^{-3} [226]	1.0×10^{-3} [226]	1.0×10^{-3} [226]
Y (mg/mol)	1.0×10^{3} [119]	1.0×10^{3} [148]	3.6×10^{4} [229]

supply rate across a range of microcosms. Finally, towards the end of the chapter, we include explicitly a population of cellulose degrading micro-organisms.

Including Sulfate Reducers

We first include a population of sulfate reducing bacteria in the model. Because these produce the sulfide that we measure in the microcosm experiment, even the simplest possible model must include a population of sulfate reducers.
The sulfate reducers respire according to the reaction shown in Eq. 7.9.

$$CH_3COO^- + SO_4^{2-} + H^+ \rightleftharpoons 2HCO_3^- + H_2S(aq) \tag{7.9}$$

Eq. 7.9 describes the respiratory reaction of a population of micro-organisms that couple the reduction of sulfate (the electron acceptor) to the oxidation of acetate (the electron donor). This is a very common sulfate reduction pathway in nature, although hydrogen, pyruvate, lactate, and many other compounds can also be used as electron donors [137]. Some of the taxa found in our sequencing analysis of our microcosm experiments are known to use acetate, such as *Desulfobacteraceae* [137, 230].
In our model, the microbial growth parameters associated with microbial sulfate reduction are chosen as follows. The half saturation constant with respect to the electron acceptor (K_A) has been measured to be 4.8μM and 7.3μM for sulfate reducing genera that were present in the microcosms (*Desulfovibrio*) [126] . Furthermore K_A has been measured to a similar order of magnitude for *Thermodesulfovibrio* [231], another genus that was present in the microcosms. In this chapter we take $K_A = 5.0\mu$M, following these experimental results, as well as other modelling approaches [37, 173].
The half saturation constant with respect to the electron donor (K_D) has been measured experimentally to be in the range $10 - 70$ μM [119]. We set $K_D = 70$

μM. The growth yield Y is set to 1×10^3mg biomass/mol [119, 120]. The specific growth rate $v = 1 \times 10^{-9}$ mol/(mg biomass)$^{-1}$ s^{-1} [119, 232]. For microbial sulfate reduction with acetate $\chi = 5$, because 5 protons are pumped per cycle of the electron transport chain [37].

The Response of Sulfate Reducers to Acetate Influx in the Absence of Abiotic Buffering

We have already seen that the abiotic reaction of sulfide with either iron or oxygen can generate a switch to a sulfidic state via a buffering effect. To understand the effect of the underlying microbial dynamics in this model, we first simulate a model without these abiotic buffering effects. A simple schematic of this model is shown in Fig. 7.3

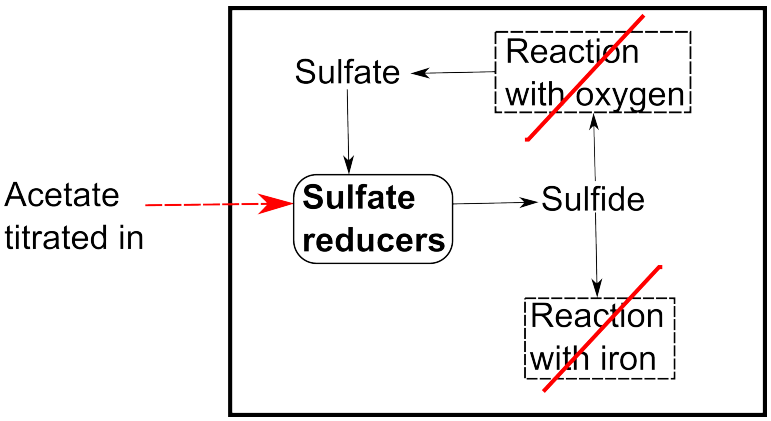

Figure 7.3 Schematic diagram indicating the key processes in the simple homogeneous React model containing only sulfate reducers. Red lines indicate disabled abiotic processes.

Fig. 7.4 shows the change in chemical state of our model as acetate is titrated into the system at a constant rate over 16 weeks. This models the supply of electron donors via cellulose degradation over time in our experiment. The model consists of sulfate reducers in a homogeneous system with initial chemical conditions

simulating a sulfidic and anoxic sediment ($HS^- = 0.1$mM, $O_2(aq) = 0$). 10 g of acetate are supplied in total over 16 weeks, meaning there is an acetate inflow rate of $\approx 2 \times 10^{-8}$mol/s.

Fig. 7.4(a) shows that a transition to a sulfidic state as acetate is added over time. It is important to note that, in this model the abiotic oxidation of sulfide as described in Eq. 7.4 is disabled, and thus cannot have been the cause of the transition (unlike the transition seen in Fig. 7.2, which *was* caused by this reaction). Furthermore, there is no iron present, and so the transition cannot have been generated by a buffering reaction with reactive iron. Instead, this transition is related to thermodynamic limitation of the microbes respiratory reaction by the thermodynamic limitation function F_T, as Fig. 7.4(b) shows.

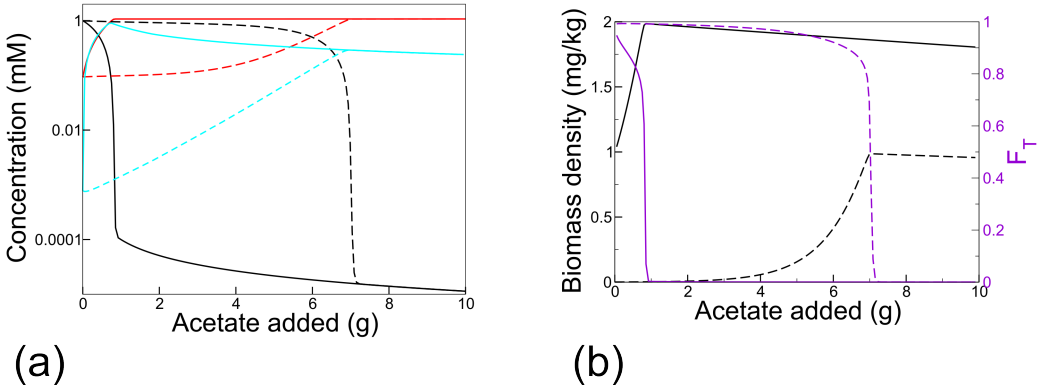

Figure 7.4 Time-course graphs showing the impact of gradual acetate input on sulfate reducers over 16 weeks. All abiotic redox reactions are disabled. Solid lines are for initial biomass = 1 mg/kg, dashed lines are for initial biomass = 0.001 mg/kg. Initial conditions: pH = 8.1, $SO_4^{2-} = 1$mM, $Na^+ = 3000\mu$M, $Cl^+ = 3000\mu$M, $CH_3COO^- = 0.1$nM, $HCO_3^- = 0.8\mu$M, $HS^- = 0.1$mM. (a) Chemical concentrations: Sulfide = Red. Sulfate = Black. Bicarbonate = Turquoise. (b) F_T and the biomass density of the sulfate reducers. Once the sulfate availability collapses, and the carbonate builds up, the population switches to becoming thermodynamically limited.

We note that the transition to a sulfidic state seen in Fig. 7.4 is not the same type of transition as the redox regime shifts discussed in chapters 4/5; Fig. 7.4

displays a transition to a sulfidic state *over time* in a model containing only sulfate reducers, whereas chapters 4/5 discuss how transitions at steady state arise from the dynamics of a full microbial nutrient cycle (i.e. in models with both sulfate reducers and sulfide oxidizers). In general, the models presented in this chapter will discuss transitions to a sulfidic state as a result of abiotic buffering effects or the thermodynamics of microbial growth, whereas the models presented in chapter 4/5 discussed regime shifts arising from the saturating growth kinetics of microbial populations. We can understand why we see a transition to a sulfidic state in this new model, using the following reasoning. At low acetate concentrations the respiration of the sulfate reducers is not thermodynamically limited ($F_T = 1$) because the high availability of sulfate generates enough free energy in their respiratory reaction to synthesize ATP. The respiration rate (and therefore the sulfide production rate) is instead limited by the availability of acetate. Increasing acetate availability then increases the sulfate reduction rate and causes the sulfide concentration to increase. However, as the sulfate reducers grow they produce carbonate as a waste product (see Eq. 7.9). This carbonate builds up in the system, contributing to the thermodynamic limitation of the population, since the thermodynamic limitation function F_T decreases with increasing carbonate (see Eq. 7.6)

Furthermore, in this particular model we have assumed that sulfate (which is consumed by conversion to sulfide) is not replaced (i.e. there is no "inflow" of sulfate). Thus, at some critical total mass of added acetate the sulfate concentration drops low enough relative to the concentration of carbonate that the thermodynamics of sulfate reduction become limiting (in the growth equation, $F_T = 0$), meaning that the population is no longer able to produce sulfide, and the sulfide concentration abruptly "flattens out". From Fig. 7.4 we see that this flattening out happens quite abruptly. This is because F_T imposes a strict cutoff on microbial respiration; as soon as the population is not able to synthesize ATP its respiration stops completely.

Fig. 7.4 also shows that nature of the transition to a sulfidic state in this model

is dependent on the initial biomass density. The solid lines show the modelling results if the initial biomass density is high (1.0 mg/kg) and the dashed lines show the results if the initial biomass density is low (0.001 mg/kg). If the initial biomass density is low, the system remains in a non-sulfidic state for longer. This is because with low initial biomass density, the population first has to grow to a large enough density to produce noticeable quantities of sulfide. If the initial biomass density is much higher, then the population is already able to produce large quantities of sulfide and so the transition to a sulfide state occurs sooner (i.e. at a lower concentration of added acetate, and sooner in time).

Including Both Abiotic and Biotic Sulfide Oxidation in the Model Can Lead to a Double Transition as Acetate is Added

The simple models presented so far have revealed two mechanisms that can cause a transition to a sulfidic state in our microcosms.

1. **Abiotic buffering effects:** Sulfide reacts very rapidly with oxygen [175]. In our first model (Fig. 7.2) we saw that for a purely abiotic system, increasing the concentration of exogeneously added sulfide could lead to a switch-like transition in the steady-state sulfide concentration, because the fixed quantity of oxygen in the system is only able to buffer a threshold quantity of sulfide. Below this threshold the system is oxic because any sulfide produced would react with oxygen; above the threshold measurable sulfide was present. In the natural environment, or in our microcosm experiments, such a transition could occur due to a shift in the balance between the oxygen production rate from photosynthetic bacteria and the sulfide production rate from sulfate reducers. Furthermore, iron or iron oxides can also buffer sulfide, potentially producing a similar effect [176].

2. **Thermodynamic limitation:** Our second simple model, Fig. 7.4, showed that the biotic reduction of sulfate could also lead to transition from a

system where oxygen dominates to a system where sulfide dominates. It is important to note that this transition is driven by the thermodynamic term (Eq. 7.6) in the growth reaction (Eq. 7.5). Specifically the strict condition that the microbes cannot grow if they cannot obtain enough energy from their respiratory reaction to synthesize ATP can cause a transition. If there were no thermodynamic limitation term (F_T), then the sulfide concentration would continue to increase indefinitely as more electron donors (acetate) are supplied to the system (although Monod kinetics would cause the respiration rate to slow down gradually as sulfate becomes less available).

However, so far, these effects have been observed in separate models; in the first model we neglected microbial population dynamics while in the second we neglected the abiotic buffering of sulfide by reaction with oxygen and iron. We now simulating a model including both of these effects, as well as a population of methanogens.

Including Methanogens

In the environment, methanogens compete with sulfate reducers for electron donors such as acetate [128]. Since both our experiments and models have shown that acetate is limiting for sulfate reduction, it possible that the presence of methanogens in the model would affect acetate availability and thereby affect the concentrations of sulfide produced. In this subsection, we discuss the inclusion of methanogens.

The primary methanogenic pathways in the natural environment use either acetate or hydrogen as an electron donor [233]. In this chapter we consider acetate as the electron donor (acetoclastic methanogenesis); i.e. we model methanogenesis according to the reaction of Eq. 7.10.

$$CH_3COO^- + H_2O \rightleftharpoons CH_4(aq) + 2HCO_3^- \tag{7.10}$$

Importantly, in reaction 7.10 acetate functions as both an electron donor and acceptor; i.e. reaction 7.10 is a disproportionation reaction, where one carbon atom of the acetate is oxidized and one carbon atom is reduced. Thus only one saturation constant, for acetete, is needed, and this is estimated in the literature to be 1 mM [148]. For simplicity in this model we set the maximal growth rate and the yield to be the same as for the population of sulfate reducers, but experimental studies also suggest that this is a reasonable assumption [148]. It has been estimated that $\chi = 2$ for methanogenesis, meaning that 2 protons are translocated per respiratory reaction [37, 173].

Fig. 7.5 shows a schematic diagram of this two population model, also illustrating key abiotic processes.

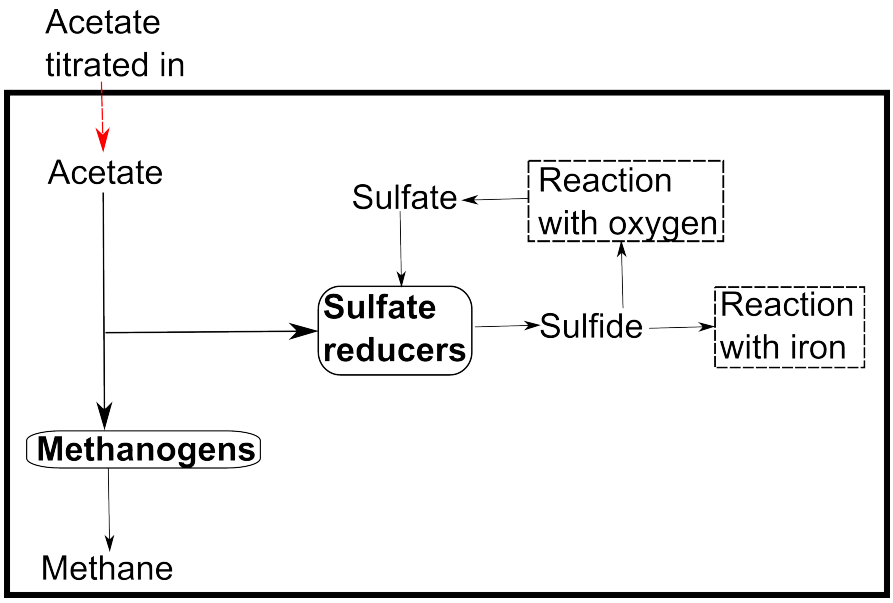

Figure 7.5 Schematic diagram indicating the key processes in the two population homogeneous React model containing sulfate reducers and methanogens.

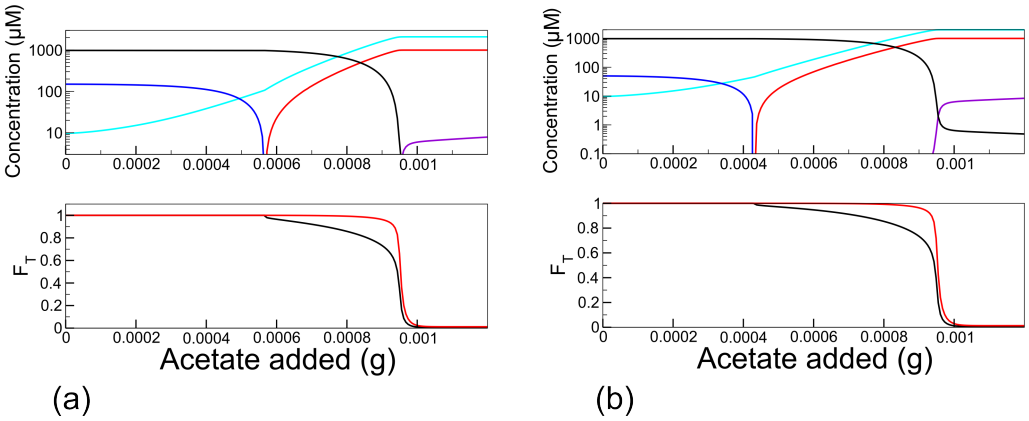

Figure 7.6 Time-course graphs showing the impact of gradual acetate input on sulfate reducers and methanogens over 16 weeks. Acetate inflow rate of 1×10^{-5}g/day. (a) Initial $O_2(aq) = 150$ μM. (b) Initial $O_2(aq) = 50$ μM. Top: Chemical concentrations: Red = Sulfide, Blue = Oxygen, Purple = Methane, Turquoise = Carbonate, Black = Sulfate. Bottom: Thermodynamic limitation function F_T: Black = Sulfate reducers, Red = Methanogens. Initial conditions: pH = 8.1, $SO_4^{2-} = 1$ mM, $Na^+ = 3000$ μM, $Cl^+ = 3000$ μM, $CH_3COO^- = 0.1$ nM, $O_2(aq) = 150$ μM, $HCO_3^- = 10.0$ μM, $HS^- = 0.1$ mM, $CH_4(aq) = 0.1$ μ M. A "cascading transition" occurs, where first sulfate reducers become limited, followed by methanogens.

Fig. 7.6 shows the effect of gradually adding acetate (at a rate of 1×10^{-5}g/day) in a model containing sulfate reducers, methanogens and the abiotic buffering of sulfide by oxygen and iron.

The transitions we see in this model are driven by both abiotic buffering effects and the thermodynamic limitation of microbial growth. Because both sulfide and methane react with oxygen the transition point is controlled by the initial oxygen concentration, as the comparison between Fig. 7.6(a) and Fig. 7.6(b) shows. Once there is no oxygen remaining, we see two transitions; first a transition to a sulfidic state and later a transition to a state in which both sulfide and methane are at high concentration. The reason the sulfidic transition occurs first (at a lower quantity of added acetate) is that sulfate reducers out-compete methanogens for acetate when acetate concentrations are low, because the half saturation constant for acetate is 1000 times smaller for the sulfate reducers. Indeed, it is known that

in the natural environment, sulfate reducers generally out-compete methanogens for electron donors for this reason [234]. The behaviour of this model can be thought of as a "cascading series of transitions", in which a shift in the sulfide concentration is followed by a shift in the methane concentration.

This "cascading regime shift" can also be seen in the thermodynamic limitation functions of each population (F_T) shown in the right panel of Fig. 7.6. At low amounts of added acetate neither population is thermodynamically limited. Increasing the amount of added acetate causes the sulfate reducers to start becoming limited once carbonate builds up and sulfate becomes depleted, at some threshold quantity of added acetate. Once this happens, the methanogens start to respire faster, before they in turn become thermodynamically limited as carbonate builds up even more. Eventually, both populations become thermodynamically limited.

7.4.3 Reproducing the Experimental Transition in a Two Population Model

Thus far (Figs. 7.4 and 7.6), we have investigated what happens as acetate is gradually titrated into a model of a single microcosm over time, to mimic a steady supply of electron donors from the degradation of cellulose by a microbial population. We have seen that once the total amount of acetate added reaches a critical threshold, the model can undergo a transition to a sulfidic state. However, the experimental transition discussed in chapter 6 was a transition after 16 weeks, for a series of microcosms with a range of initial organic matter concentrations. To reproduce this, in our simulations, we need to run a series of simulations with varying acetate inflow rates. This mimics supplying an increased amount of cellulose to the microcosms initially (assuming that a higher initial cellulose concentration would stimulate the cellulose degrading population and result in a higher acetate supply rate). We then record the total amount of sulfide in the

microcosm after 16 weeks.

Fig. 7.7 shows the effect of varying the acetate inflow rate on the final chemical state of the system for the model shown in Fig. 7.5. A transition to a sulfidic state occurs at a critical value of the acetate inflow rate, mimicking the experimental transition as a function of added celllulose seen in chapter 6. Furthermore, Fig. 7.7 shows that the presence of methanogens actually has very little effect on the final chemical state of the system. The circular symbols show the result of simulating a model containing only sulfate reducers, the lines show the result of simulating a model containing both sulfate reducers and methanogens. This shows that methanogens actually have very little effect on the final system state.

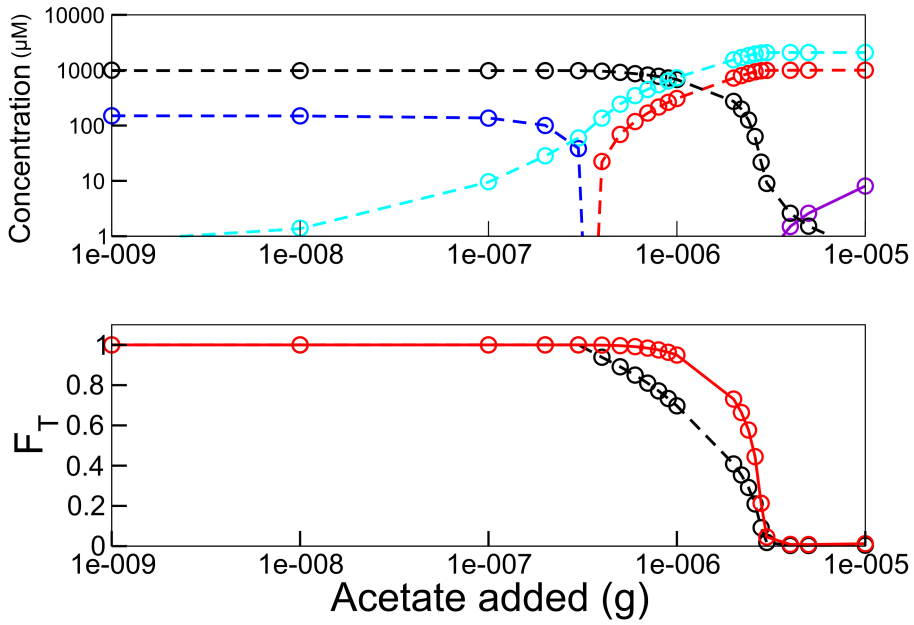

Figure 7.7 Graph showing the effect of varying the acetate inflow rate on the chemical state of the system after 16 weeks. Symbols = Model without methanogens Lines = Model with methanogens. Initial conditions: pH = 8.1, $SO_4^{2-} = 1$mM, $Na^+ = 3000\mu$M, $Cl^+ = 3000\mu$M, $CH_3COO^- = 0.1\mu$M, $O_2(aq) = 150\mu$M, $HCO_3^- = 0.8\mu$M, $CH_4(aq) = 0.1\mu$M. $Fe^{++} = 0.1$mmoles/g to reproduce the quantity of iron available for reaction with sulfide that was determined in the reactive iron extraction (as discussed in chapter 6). (a) Final chemical state of the system: Oxygen = Blue. Sulfide = Red. Sulfate = Black. Methane = Violet. Bicarbonate = Turquoise. (b) Thermodynamic limitation function. Black = Sulfate reducers. Red = Methanogens.

However, although this model appears to qualitatively reproduce the transition to a sulfidic state seen in the microcosm experiment, there is a complication. So far, we have assumed a constant acetate supply rate, proportional to the initial cellulose concentration. In reality though, cellulose may not be degraded at a rate that is constant in time throughout the 16 week experiment. To account for this we need to actually include a population of cellulose degraders in the model and vary the quantity of initial cellulose supplied to the system.

7.5 Including Cellulose Degraders

Thus far, for simplicity, we have mimicked the degradation of organic matter in our experiments by a constant external supply of acetate. We mimicked the experimental variation of the initial quantity of cellulose supplied to the microcosm by increasing this acetate supply rate, and found that doing so does drive a transition to a sulfidic state when measured after 16 weeks. However, in our experiments the microcosms were not directly supplied with acetate. Instead they were supplied with cellulose which was then degraded and fermented by microbes to produce electron donors such as acetate and hydrogen. A more realistic model of this system should include the kinetics of cellulose-degrading microbes, which we discuss in this section.

In this chapter we assume that all cellulose degradation is anaerobic, because the cellulose was mixed into the anaerobic sediment in our experiments. In fact, cellulose can be degraded either aerobically or anaerobically [235].

Accurately modelling the process of microbial organic matter degradation can be difficult. There are two main reasons for this difficulty.

1. Cellulose degradation is an ecologically complex process. Cellulose degradation in anaerobic environments is typically undertaken by symbiotic consortia of cellulolytic microbes that directly degrade the cellulose macropolymer via hydrolysis to produce cellobiose and glucose, and fermentative microbes that convert these products into lactate, acetate, ethanol, CO_2 and H_2 [235]. This makes cellulose degradation much harder to model than processes that can be more easily attributed to one functional group, such as sulfate reduction.

2. The biochemical mechanisms involved in the degradation of the cellulose molecule are complex and diverse. Some bacteria excrete enzymes that perform extracellular cellulose degradation (cellulases). Others have a

cellulosome, a membrane bound multicomponent system that mediates the attachment of the bacterium to cellulose fibres [235]. This biochemical complexity means that assigning a thermodynamic limitation term (Eq. 7.6a) based on the free energy of the microbe's respiratory reaction (as we have done for the other microbial populations in this chapter) is not feasible. Thus we are forced to reply on simpler assumptions for the microbial growth kinetics.

7.5.1 The Kinetics of Cellulose Degradation

Because of the difficulty in representing accurately the thermodynamics of cellulose degradation, we choose to model the growth kinetics of the cellulose degraders in our model via a simple Monod term multiplied by a logistic population size limitation as in chapters 4 and 5. Eq. 7.11 describes the dynamics of a cellulose degrading population as represented in our model.

$$\frac{\mathrm{d}n}{\mathrm{d}t} = \frac{Yr}{n_w} - Dn \tag{7.11}$$

For the cellulose degrading population the nutrient consumption rate r is defined by Eq. where [C] represents the cellulose concentration, K_C represents the half saturation constant with respect to cellulose, and all other terms are defined as before.

$$r = n_w v n \left(\frac{[\mathrm{C}]}{K_C + [\mathrm{C}]}\right)\left(1 - \frac{n}{n_{\max}}\right) \tag{7.12}$$

This consists of Monod growth kinetics and a logistic population size limitation term (of the same form as the populations modelled in chapters 4 and 5). Eqs. 7.11-7.12 can then be solved numerically along with the other equations that define the model.

Most studies on the growth kinetics of cellulolytic bacteria have focused on the gut microbiome of ruminant animals so we take our parameter values from this literature. The important parameters are the half saturation constant K_C, the maximal growth rate v and the growth yield Y. A specific nutrient consumption rate per unit biomass of $v = 1 \times 10^{-9}$mol(cellulose)mg^{-1}(biomass)hr^{-1} has been experimentally determined [227]. The yield is estimated to be 3.6×10^4 mg(biomass)/mol(cellulose)[229]. The half saturation constant of the cellulase enzyme is roughly 1mM [228], although this value can be subject to temperature dependence [25]. We set the maximal population density of the cellulose degraders to be $n_{\max}$ =10.0 mg (biomass)/kg [236].

7.5.2 Reproduction of the Experimental Transition in a Model with Cellulose Degraders

Having included a population of cellulose degraders in the model we now ask whether our model can quantitatively reproduce the experimental transition to a sulfidic state as a function of the initial cellulose supplied to the microcosm (seen in chapter 6). Fig. 7.8 shows a schematic diagram of this model.

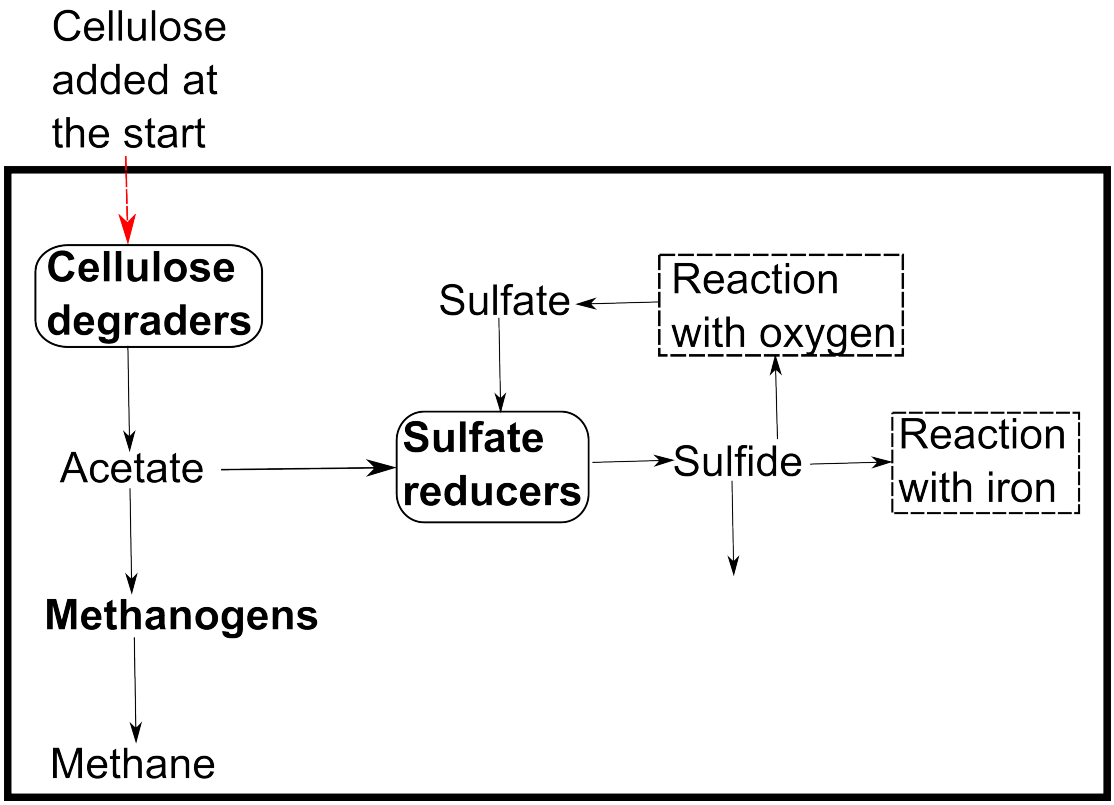

Figure 7.8 Full schematic of the model containing cellulose degraders, sulfate reducers and methanogens. Also illustrates some of the key abiotic processes in the system.

Fig. 7.9 shows the result of varying the initial quantity of cellulose supplied to this model. A transition to a sulfidic state does occur, and this transition is caused both by an abiotic buffering with oxygen and iron, and the thermodynamic limitation of the population of sulfate reducers by the build-up of carbonate. Abiotic buffering with oxygen causes the sudden appearance of observable sulfide after 16 weeks once the organic matter availability is high enough to stimulate the production of enough sulfide to remove all of the oxygen from the system.

Comparing Figs. 7.9(a) and (b) shows that the initial oxygen concentration controls the quantity of organic matter at which a sulfidic transition occurs; if the initial oxygen concentration is lower, the transition occurs at a lower threshold concentration of organic matter, because less sulfide needs to be produced to remove all of the oxygen. Eventually, at some organic matter loading, enough carbonate is produced to cause the respiration of the sulfate reducers to become thermodynamically limiting. At this point F_T transitions to zero and the concentration of sulfide produced after 16 weeks abruptly flattens outs.

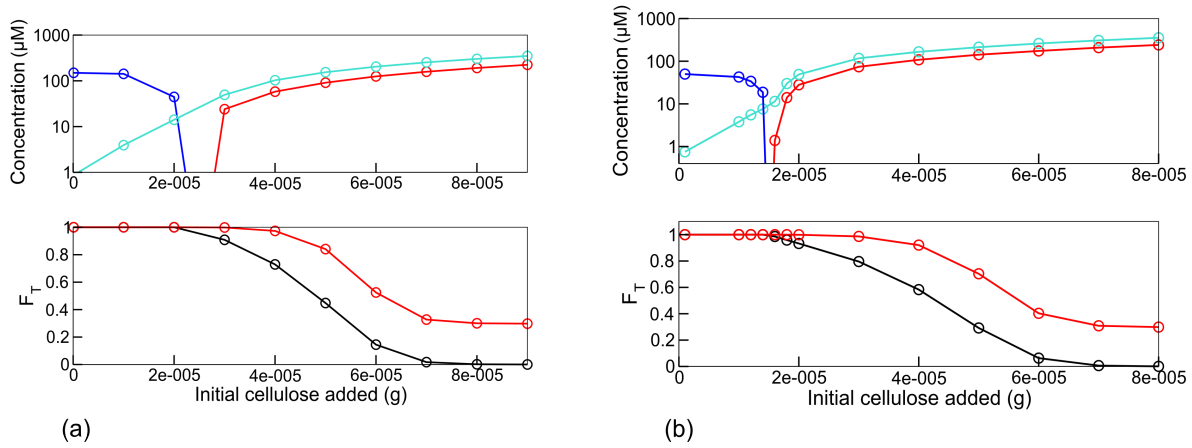

Figure 7.9 Graph showing the effect of varying the initial cellulose supply on the chemical state of the system after 16 weeks. Sulfate is not shown because it is so high as to be unaffected across the simulation. (a) Initial $O_2(aq) = 150\mu M$. (b) Initial $O_2(aq) = 50\mu M$. Other initial conditions: pH = 8.1, $SO_4^{2-} = 73mM$ to represent the middle sulfate condition in our microcosm experiment, $Na^+ = 3000\mu M$, $Cl^+ = 3000\mu M$, $CH_3COO^- = 0.1\mu M$, $HCO_3^- = 0.8\mu M$, $CH_4(aq) = 0.1\mu M$. $Fe^{++} = 0.1$mmoles/g to reproduce the quantity of iron available for reaction with sulfide that was determined in the reactive iron extraction (as discussed in chapter 6). (a) Final chemical state of the system: Oxygen = Blue. Sulfide = Red. Sulfate = Black. Bicarbonate = Turquoise. (b) Thermodynamic limitation function. Black = Sulfate reducers. Red = Methanogens.

However, the model does not accurately reproduce the *quantity* of added cellulose that induces a transition. In the experiment, a transition to a sulfidic state

occurred at approximately 0.2 g of added cellulose per microcosm. Fig. 7.9 shows that this model predicts a sulfidic transition at a *much* lower quantity of added cellulose (between 20 and 40 μg). This discrepancy could be explained by some feature not currently included in the model, such as spatial resolution. Further work extending this model to include proper spatial resolution could allow it to reproduce this more accurately. It is known that the separation of microbial processes into biogeochemical "zones" at different depths is an important factor controlling the dynamics of microbial sediment-water ecosystems in the natural environment. For example, the production of sulfide by sulfate reduction occurs in an anoxic zone, below the zone of nitrate reduction but above the zones of methanogenesis and fermentation [179]. This "zoning" causes the rates of microbial processes to be strongly affected by the spatial dynamics of system, for example, if oxygen begins to penetrate deeper into the sediment, it can inhibit sulfate reduction. Including spatial resolution in our model will be necessary to capture these effects.

7.6 Discussion and Conclusion

The models presented in this chapter have revealed new processes that can give rise to oxic-anoxic transitions in systems like those of our experiments. First, the abiotic reaction of sulfide with oxygen causes a buffering effect that can give rise to a transition to a sulfidic state. The abiotic reaction of sulfide with iron can also cause a similar buffering reaction. Combined, iron and oxygen produce an overall buffering effect on sulfide concentrations, in a way that can result in a transition to a sulfidic state.

Second, the thermodynamic limitation of microbial respiration causes respiration rates to transition to zero once some chemical threshold is crossed. This threshold is defined by there being enough free energy available for the microbe's respiratory

reaction to allow the synthesis of ATP ($\Delta G_P = -45$ kJ/mol). Once the environment does not provide enough energy for ATP to be synthesized, growth stops completely.

The model succeeds at qualitatively reproducing our experimental results, by reproducing a transition to a sulfidic state as a function of the initial cellulose supplied, in a model system with realistic abiotic chemistry mimicking the chemistry of our microcosms. The quantitative result, i.e. the amount of cellulose that needs to be added to cause the transition is not reproduced however.

The methanogens and sulfate reducers in this model become thermodynamically limited because of a build up of carbonate. In the environment, there can be other populations of micro-organisms called homoacetogens that consume this carbonate [137]. Consequtently, these homoacetogens could potentially prevent the sulfate reducing and methanogenic populations from becoming thermodynamically limited. It would be very interesting to simulate a version of this model containing homoacetogens to see how they affects the thermodynamic limitation of the other populations.

However, the fact that this model qualitatively succeeds at reproducing a sulfidic transition as a function of added cellulose, raises the intriguing possibility that, if improved, similar models could be used to make predictions about the levels of organic matter loading that could cause a sulfidic transition in the environment, a key environmental issue. Organic matter loading is known to lead to the proliferation of so-called sulfidic "dead zones" in coastal oceans [139], however, these remain highly unpredictable, and a model that can reliably predict how much nutrient loading will lead to a transition to an anoxic system state could be valuable.

Chapter 8

Conclusions

In this thesis we have examined the effect of environmental changes on microbial ecosystems using a combination of experimental and modelling approaches. This has relevance to both understanding specific microbial ecosystems, such as microbial freshwater ecosystems, and also to understanding microbially-mediated biogeochemical cycles on a global scale. Overall, the work presented in this thesis has revealed that a wide variety of effects can cause transitions between environmental states in response to environmental changes in microbial nutrient-cycling ecosystems.

Inspired by the lack of microbial population dynamics in current models for global microbially-mediated biogeochemical cycles, we first developed generic microbial nutrient-cycling models. We found that the inherent nonlinearity of microbial growth can lead to abrupt regime shifts between redox states ("redox regime shifts") in response to changes in the availability of electron donors and acceptors, or in response to changes in environmental parameters that drive the production of electron donors and acceptors. This model makes specific predictions about the environments where we would expect to observe redox regime shifts. In particular, we predict that microbial growth must be saturated with respect to the chemical

element being cycled, must be sensitive to changes in the availability of electron donors and acceptors, and the microbial population density must be limited by some factor other than the concentration of the element being cycled (such as carbon availability). These conditions lead to the prediction that redox regime shifts are likely in the microbial nitrogen and sulfur cycles, and also potentially the microbial iron cycle in the ancient oceans.

There are many potential avenues for further work with this model. The "redox regime shifts" that we observe in biogeochemical cycles are mathematically analogous to the well-known phenomenon of zero-order ultrasensitive switching in intracellular enzyme kinetics because the dynamics of both are driven by a directly analogous saturating function (called Michaelis-Menten kinetics in intracellular enzymatic systems, and Monod kinetics in microbial ecosystems). It would be interesting to extend the mathematical analogy between these systems, to see if some of the well-established understanding of ultrasensitivity in enzymatic cycles applies to microbially-mediated biogeochemical cycles. For example, intracellular enzymatic cycles are coupled such that a shift in one enzymatic cycle can generate a cascading series of transitions throughout the entire system [237]. Microbially-mediated biogeochemical cycles are coupled together in a similar way, for example, it is known that the oceanic sulfur and nitrogen cycles are closely related via a coupling between microbial sulfide oxidation and nitrate reduction [238]. It would be interesting to predict similar cascading transitions between global redox states of biogeochemical cycles in a more detailed model containing many coupled nutrient cycles.

We then examined the effect of a nutrient perturbation on an experimental microbial ecosystem containing closely coupled microbial sulfur and carbon cycles. We found that a threshold quantity of initial organic matter drives a transition in the final sulfide concentration of these microcosms after 16 weeks of incubation. This transition to a sulfidic state is driven by, and imprints on, the microbial community, meaning that these microcosms represent an interesting case of a system generating its own environmental state, that it then responds to (this is

known as "niche construction" in the ecological literature [184]).

Analysing the microbial community at the level of populations responsible for specific ecosystem processes ("functional groups") revealed that each functional group of microbes responds to the perturbation in a distinct way. Some groups are highly functionally redundant and maintain a stable relative abundance and diversity across the environmental gradient (sulfate reducers and organic matter degraders). For the oxygenic phototrophs, relative abundance and diversity appear to be strongly coupled, and both dramatically decrease in response to the environmental change. For anoxygenic phototrophs, relative abundance and diversity were decoupled, and the abundance of the group increased while the diversity decreased.

Further experimental work could attempt to construct a "synthetic ecosystem" formed from known and culturable species to test the relationship between the abundance and diversity of different functional groups, and the environmental role of different functional groups. For example, we could attempt to establish a synthetic ecosystem in sterile sediment with certain functional groups missing, or with certain functional groups being more or less diverse than normal. However, this could be very challenging. A potentially easier way of doing something similar would be to take the microcosms from the end of an experiment and innoculate them with consortia of micro-organisms in an attempt to re-establish an earlier community composition. For example, the diversity of the anoxygenic phototrophs completely collapsed in the high initial sulfate microcosms, because this condition selected for one particular taxon, which became highly abundant. We could re-inoculate this microcosm with a diversity of anoxygenic phototrophs, to observe if a diverse community of anoxygenic phototrophs could become re-established.

We then constructed a model incorporating realistic abiotic chemical interactions in an attempt to understand the cause of the sulfidic transition in the experiment. To do this we used the software package "The Geochemist's Workbench" which is able to calculate the equilibrium state of complex chemical systems. An

important feature of the microbial kinetics which we used in these models is a thermodynamic limitation function that limits microbial growth by the amount of free energy that is available in their respiratory redox reaction; imposing the strict limitation that the micro-organisms are not able to grow if they are not able to obtain enough free energy to synthesize ATP. This thermodynamic limitation of the microbial growth kinetics was able to generate a transition between chemical states. Furthermore, this model revealed that abiotic buffering reactions of sulfide with both oxygen and iron are also able to generate a transition to a sulfidic state. Including cellulose degraders in this model allowed us to qualitatively reproduce our experimental observation of a transition to a sulfidic state as function of initial added cellulose, after 16 weeks incubation. However, the model predicted a transition at a lower concentration of added cellulose than was observed in the experiment.

Further work will need to extend this model to establish the cause of the transition to a sulfidic state in the microcosm experiment and account for this discrepancy between the model and the experiment. It is very likely that spatial effects will be important to solving these problems. Biogeochemical zoning is known to be an important factor driving the evolution of similar microbial ecosystems in nature [37, 179, 180]. Therefore, extending "The Geochemist's Workbench" model to include spatial dynamics will be essential to understanding whether the sulfidic transition in our experiments is really driven by saturation of the microbial population dynamics (as in chapters 4 and 5) or whether it is instead generated by either abiotic buffering reactions or the thermodynamic limitation of the microbial population (as the models in chapter 7 predict).

Another potentially interesting angle would be to include oxygenic phototrophs in The Geochemist's Workbench model, and include a term that represents the poisoning of oxygenic phototrophs by sulfide. Sulfide begins to inhibit oxygenic photosynthesis even at low concentrations [200]. Thus, the production of sulfide generates a negative feedback loop, where sulfide removes oxygen by abiotic buffering, and then destroys the capacity of the system to produce new oxygen by

oxygenic phototsynthesis. Including this process in our models might be expected to produce interesting effects, like hysteresis.

A very ambitious idea for further work would be to combine all of the results presented in this thesis into one model. This model would incorporate realistic abiotic chemistry, microbial dynamics and a diversity of microbial functional groups (such as sulfate reducers). Such a model could allow us to reproduce and explain both the transition in the microcosm experiment *and* the effect of this transition on the abundance and diversity of different functional groups. Furthermore, such a model, if successful, could potentially be used to predict and manage the consequences of environmental catastrophes in microbial ecosystems in the environment.

Overall, the work presented in this thesis has revealed the advantages of constructing simple models to unravel the dynamics of microbial ecosystems. However, such models need to be informed by experimental work to be useful. The link between computational models and experimental model systems such as microcosms is potentially a very fruitful one, because the degree of experimental control afforded by a microcosm experiment can allow model predictions to be directly tested.

Appendix A

Constructing Voltammetric Electrodes

Using the methods described by Luther et al. [105] a 100 micron gold-amalgam working electrode (PEEK-Epoxy body) was constructed. A 100 μm diameter gold (Au) wire was soldered to the conductor wire of BNC cable within a body of 0.125-diameter PEEK (polyethyletherketone) tubing. Epoxy is injected into the tip of the tubing which contained the gold wire that was previously soldered to the conductor wire of the BNC cable (this stage of the process was performed by Dr Ian Butler from the School of Geosciences).

Once constructed the electrode surface was sanded with 400 grit paper, and then polished with four diamond polishes of successively smaller size (15; 6; 1; and 0.25 m) using a small electrical polisher. Then the electrode was plated with mercury (Hg) by reducing Hg(II) from a solution of 0.1 M mercury dissolved in 0.05 M nitric acid (0.1 M Hg/0.05 M HNO_3 solution) for 4 min at a potential of 0.1 V, while purging with nitrogen (N_2) to remove any oxygen. The mercury/gold amalgam interface was conditioned for 90 seconds at 9 V in a 1 M sodium hydroxide (NaOH) solution, with the electrode on the negative terminal and platinum wire on the positive terminal. This was to ensure that the mercury interface was strongly attached to the electrode surface. The electrode was then ready for calibration.

Appendix B

Including Cellulose in the Thermodynamic Dataset

Including cellulose degradation in a model to be solved by the React module of The Geochemist's Workbench also presents a technical challenge. The Geochemist's Workbench requires all chemicals to be defined in terms of equilibrium constants across the temperature range of the thermodynamic dataset, but cellulose is not present in the database and needs to be added by the user. Thus a reaction describing cellulose within a Geochemist's Workbench model needs to be defined and added to the database. However, this presents the problem that cellulose could degrade abiotically into these chemical components in the model. Including cellulose therefore requires the definition of a "fictive redox species" as follows.

Eq. B.1 describes the formation of a redox species $Cellulose_{aq}$ out of chemical components that are already within the thermodynamic dataset. It is termed a "fictive redox species" because the system is set up such that $Cellulose_{aq}$ should never be present in the model. Eq. B.2 then describes the formation of the desired chemical (cellulose) in terms of the fictive redox chemical $Cellulose_{aq}$.

$$Cellulose_{aq} \rightleftharpoons 3CH_3C00^- + 3H^+ \tag{B.1}$$

$$\text{Cellulose} \rightleftharpoons \text{Cellulose}_{\text{aq}} \tag{B.2}$$

The equilibrium constants are set up such that Eq. B.2 predominates strongly towards the formation of cellulose and Eq. B.1 predominates strongly towards the formation of acetate. Furthermore the reaction in Eq. B.1 is decoupled, to prevent acetate from precipitating out as the fictional compound $\text{Cellulose}_{\text{aq}}$.

Appendix C

List of Publications

[1] - Bush, T. Butler, I. B., Free, A. and Allen, R. J. Redox regime shifts in microbially-mediated biogeochemical cycles. *Biogeosciences*, 12:3713-3724, 2015. doi: 10.5194/bg-12-3713-2015

Biogeosciences, 12, 3713–3724, 2015
www.biogeosciences.net/12/3713/2015/
doi:10.5194/bg-12-3713-2015

Biogeosciences Open Access

Redox regime shifts in microbially mediated biogeochemical cycles

T. Bush[1], **I. B. Butler**[2], **A. Free**[3], **and R. J. Allen**[1]

[1]SUPA, School of Physics and Astronomy, University of Edinburgh, King's Buildings, Edinburgh EH9 3FD, UK
[2]School of Geosciences, University of Edinburgh, King's Buildings, Edinburgh EH9 3FE, UK
[3]Institute of Cell Biology, School of Biological Sciences, University of Edinburgh, King's Buildings, Edinburgh EH9 3BF, UK

Correspondence to: T. Bush (t.bush@sms.ed.ac.uk)

Received: 30 January 2015 – Published in Biogeosciences Discuss.: 17 February 2015
Revised: 27 May 2015 – Accepted: 1 June 2015 – Published: 17 June 2015

Abstract. Understanding how the Earth's biogeochemical cycles respond to environmental change is a prerequisite for the prediction and mitigation of the effects of anthropogenic perturbations. Microbial populations mediate key steps in these cycles, yet they are often crudely represented in biogeochemical models. Here, we show that microbial population dynamics can qualitatively affect the response of biogeochemical cycles to environmental change. Using simple and generic mathematical models, we find that nutrient limitations on microbial population growth can lead to regime shifts, in which the redox state of a biogeochemical cycle changes dramatically as the availability of a redox-controlling species, such as oxygen or acetate, crosses a threshold (a "tipping point"). These redox regime shifts occur in parameter ranges that are relevant to the present-day sulfur cycle in the natural environment and the present-day nitrogen cycle in eutrophic terrestrial environments. These shifts may also have relevance to iron cycling in the iron-containing Proterozoic and Archean oceans. We show that redox regime shifts also occur in models with physically realistic modifications, such as additional terms, chemical states, or microbial populations. Our work reveals a possible new mechanism by which regime shifts can occur in nutrient-cycling ecosystems and biogeochemical cycles, and highlights the importance of considering microbial population dynamics in models of biogeochemical cycles.

1 Introduction

Metabolic conversions mediated by microorganisms play a key role in the Earth's biogeochemical cycles (Falkowski et al., 2008; Madigan et al., 2009; Fenchel et al., 1998). For example, microbial nitrogen fixation contributes an estimated 100–200 Tg of nitrogen to the world's oceans annually (Karl et al., 2002), while the microbial decomposition of soil carbon exceeds the anthropogenic contribution of carbon dioxide to the atmosphere by an order of magnitude (Aguilos et al., 2013). Predicting the response of these cycles to environmental changes, including climate change, is a central current challenge in Earth system science (IPPC, 2013). However, mathematical models for global geochemical cycles often represent microbially mediated transformations as crude "black boxes" (Allison and Martiny, 2008): for example, microbial decomposition in soil is often represented as a first-order decay process (Todd-Brown et al., 2012; Westrich and Berner, 1984). Indeed, many of the models cited in the most recent IPCC report use linear representations of microbially mediated processes (IPPC, 2013). This simplified picture contrasts strongly with the wealth of data on microbial community diversity and functional complexity which is being generated by recent advances in high-throughput sequencing technology (Nikolaki and Tsiamis, 2013). There is thus an urgent need to re-evaluate the role of microbial population dynamics in biogeochemical models (Todd-Brown et al., 2012; Allison et al., 2010).

Here, we use simple mathematical models to show that microbial population dynamics can have important qualitative effects on the response of microbially mediated biogeochemical cycles to environmental change. Specifically, nu-

Published by Copernicus Publications on behalf of the European Geosciences Union.

trient limitations on microbial population growth can lead to abrupt changes in redox state in response to a gradual change in an environmental parameter. Sharp transitions, often described as regime shifts, are known to occur in diverse systems in response to diverse stimuli; examples range from aquatic ecosystems in the leaves of carnivorous pitcher plants (Sirota et al., 2013) to large-scale shifts in terrestrial vegetation cover (Higgins and Scheiter, 2012). These shifts are usually attributed to specific features of the system structure (or "topology"; Scheffer et al., 2009). Our work suggests that, for biogeochemical cycles, nonlinear effects arising from microbial population dynamics can lead to sharp transitions between broadly oxidized and reduced system states, even for systems with simple topologies. We term this a "redox regime shift", i.e., a nonlinear transition in the predominant redox state of a biogeochemical cycle in response to a gradual change in an environmental stimulus. In some other studies, the term "regime shift" has been associated with bistability. Here, we use the term simply to describe a sharp response, without any implied bistability.

In a biogeochemical cycle, a chemical element is shuttled between its oxidized and reduced forms in a series of steps that may be biotically or abiotically mediated (Falkowski et al., 2008). Figure 1 illustrates simplified topologies of the iron, sulfur, carbon, and nitrogen cycles (Fig. 1a–d) (Falkowski et al., 2008; Fenchel et al., 1998; Galloway et al., 2004; Canfield et al., 2005). To encapsulate the basic topology of these cycles, we begin by considering a simplified two-state model (Fig. 1e), in which an oxidized form of a chemical element (here denoted s_o) is converted via microbial metabolism to a reduced form (s_r), which is recycled back to the oxidized form either by a second microbial metabolism or by an abiotic reaction. Although this model is topologically very simple, it reveals an important and nontrivial regime shifting behavior. Later in this paper we show that this behavior is preserved in more realistic models that include features such as spatial heterogeneity, multiple redox states, and explicit coupling to the environment.

A redox reaction in a biogeochemical cycle couples the oxidation/reduction of the element being cycled to the reduction/oxidation of another chemical species. For example, in the sulfur cycle, the microbial reduction of sulfate can be coupled to the oxidation of acetate (Rickard, 2012), while in the nitrogen cycle, the oxidation of ammonia can be coupled to the reduction of molecular oxygen (Fenchel et al., 1998). In this paper, in order to avoid confusion, we refer to the latter chemical species (in these examples acetate or oxygen) as the "auxiliary electron donor/acceptor". The auxiliary electron donor/acceptor may be supplied from some external source (e.g., oxygen from the atmosphere) or may be generated by another biogeochemical process (e.g., microbial decomposition producing acetate). Many different chemical species can act as auxiliary electron donors or acceptors; for example, acetate or hydrogen can function as the electron donor for reductive reactions, while nitrate or oxygen can function as the electron acceptor for oxidative reactions. The redox-shifting behavior which arises in our models is generic, independent of which chemical species performs the role of auxiliary electron donor/acceptor.

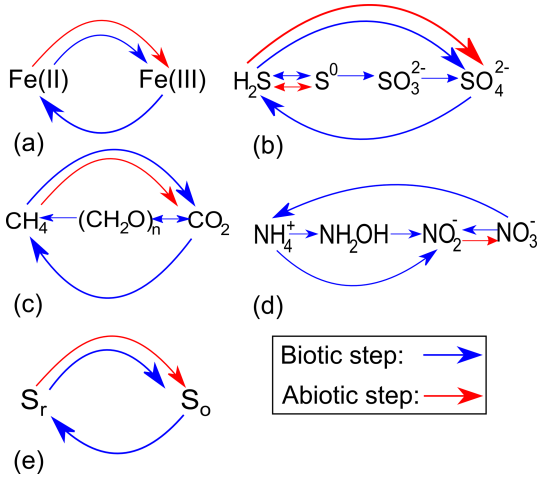

Figure 1. Schematic view of the biogeochemical redox cycles involving iron, sulfur, carbon, and nitrogen **(a–d)** (Falkowski et al., 2008; Fenchel et al., 1998; Galloway et al., 2004; Canfield et al., 2005), together with the model investigated in the first part of this work **(e)**. In all panels, oxidation reactions proceed to the right, and reduction reactions proceed to the left. Biologically catalyzed (metabolic) reactions are shown in blue, and abiotic reactions are shown in red. We note that abiotic reduction reactions are not shown, as these are minor reactions in the natural environment (but can be included in our model; see Sect. S1). We also note that many intermediate chemical states are not shown (particularly for the nitrogen and sulfur cycles) but inclusion of extra states does not affect our conclusions; see Supplement. In panel **(e)**, s_r and s_o represent the reduced and oxidized forms of the chemical element being cycled.

Crucially, if the auxiliary electron acceptor/donor is in short supply then its availability can control the rate of the redox reaction, and hence the flux of the biogeochemical cycle. Moreover, in natural environments, the availability of electron acceptors and donors is strongly dependent on the environmental conditions. For example, in aquatic ecosystems, the supply of oxygen depends on its solubility, which is temperature-dependent (Shaffer et al., 2009), and on the rate of photosynthesis (López-Urrutia et al., 2006), while the supply of acetate depends on the rate of microbial decomposition of organic matter, which can be drastically affected by factors like sewage effluent or phosphorus inflow from agricultural runoff (Conant et al., 2011).

Here, we show that changes in the supply of auxiliary electron acceptors or donors (such as oxygen or acetate) caused by environmental perturbations can have drastic effects on microbially mediated biogeochemical cycles. We first show that these perturbations can cause regime shifts in redox state for simple, spatially homogenous models. We then demon-

194

Table 1. Description of the notation used in the text.

Notation	Meaning
s_o	Concentration of the oxidized form of the chemical species being cycled
s_r	Concentration of the reduced form of the chemical species being cycled
n_{ro}	Population density of the oxidizing microbial population
n_{or}	Population density of the reducing microbial population

strate that the same phenomena can also occur in more realistic models which include features such as explicit supply of auxiliary electron acceptors or donors via microbial metabolism, intermediate redox states, and spatial heterogeneity (such that the nutrient supply is limited by transport processes). These regime shifts do not depend sensitively on the detailed structure of our equations or model, but instead result from the interplay between cyclic system topology and nonlinear microbial population growth requiring multiple nutrients. These redox regime shifts are predicted to occur in parameter ranges relevant to the natural sulfur and nitrogen cycles, and may also be relevant to iron cycling in the iron-containing ancient oceans.

2 Mathematical models for redox-cycling dynamics

Our aim is to predict the response of microbially mediated biogeochemical cycles to changes in the availability of auxiliary electron acceptors and donors, such as oxygen and acetate. We begin with a simple and generic "two-state" representation of a biogeochemical cycle; later we show that the same phenomena also occur in more complex models. In our two-state model (Fig. 1e), a chemical element is cycled between its oxidized and reduced forms, whose concentrations are denoted by s_o and s_r, respectively. The reduction step $s_o \rightarrow s_r$ (blue right-to-left arrow in Fig. 1e) is assumed to be biotic, i.e., mediated by microbial metabolism. This step requires an auxiliary electron donor, such as acetate. The oxidation step $s_r \rightarrow s_o$ may occur biotically or abiotically (indicated by the blue and red left-to-right arrows in Fig. 1e), and requires an auxiliary electron acceptor, such as oxygen. We have not included the possibility of an abiotic reduction reaction in our model because these are typically minor reactions at ambient temperatures in the natural environment (with the notable exception of the reaction of Fe(III) with sulfide; e.g., Canfield, 1989); further work could extend this model to include such reactions. It is important to note that, in reality, a given biogeochemical function may be performed by many coexisting microbial species (taxa); for example many different genetically distinct taxa can use acetate to reduce sulfate (Madigan et al., 2009). In our models, we group together all these "metabolically equivalent" taxa into a single effective population.

2.1 Fully biotic redox cycles

If both the oxidative and reductive steps in the redox cycle are mediated by microorganisms, the dynamics of our two-state model can be represented by the following set of differential equations (in which the dot represents a time rate of change):

$$\dot{n}_{or} = n_{or} G_{or}(s_o, n_{or}) - d n_{or}, \quad (1)$$

$$\dot{n}_{ro} = n_{ro} G_{ro}(s_r, n_{ro}) - d n_{ro}, \quad (2)$$

$$\dot{s}_r = \gamma \left[n_{or} G_{or} - n_{ro} G_{ro} \right] = -\dot{s_o}. \quad (3)$$

The variables in this dynamical system are n_{ro} and n_{or}, the population densities of the oxidizing and reducing microbial populations, respectively, and the concentrations s_o and s_r of the oxidized and reduced forms of the chemical species being cycled (Table 1 presents a key for this terminology). Equations (1) and (2) describe the microbial population dynamics; the reducing and oxidizing populations have growth rates $G_{or}(s_o, n_{or})$ and $G_{ro}(s_r, n_{ro})$, respectively, which depend not only explicitly on s_o and s_r but also implicitly on the concentrations of the auxiliary electron donor and acceptor, respectively. Both populations are assumed to be removed from the system at a constant rate d (e.g., due to viral predation and/or washout). Equation (3) describes changes in the substrate dynamics due to microbial consumption and production; here γ is a yield coefficient, which is assumed for simplicity to be the same for both reactions.

The growth rate functions G_{or} and G_{ro} play a crucial role in the model. The microbial growth rate on a limiting nutrient is often described by a Monod function $vs/(K+s)$, where s is the nutrient concentration, v is the maximal growth rate, and K is the nutrient concentration at which the growth rate is half-maximal (Ingraham et al., 1983). While other, more complicated growth rate functions have been proposed (Button, 1985), the Monod form encapsulates the key fact that the growth rate is nutrient-dependent at low nutrient concentration but becomes saturated at high nutrient concentration. For a microbial population performing a redox reaction, the "nutrient" s is likely to be the chemical species being cycled, while the concentration of the auxiliary electron acceptor/donor can be implicitly included in the value of the maximal growth rate v.

Importantly, however, in the natural environment, the rate of microbial growth may be limited by other factors such as the availability of carbon or micronutrients, toxin or waste product formation at high densities, or simply competition for space (Hibbing et al., 2010). To account for this in a generic way, we multiply the Monod term by a population density-limitation factor $(1 - n/n_{max})$, where the parameter n_{max} sets a maximal population density. This type of logistic population density limitation is a convenient and commonly used way to encapsulate growth limitation by factors not explicitly included in the model (Marino et al., 2013; Jones and Lennon, 2010; Berry and Widder, 2014). To check the validity of this approach, we also simulated a model in which

195

population growth is instead explicitly limited by availability of an additional nutrient (e.g., carbon). These simulations gave qualitatively similar results to those presented here; see Supplement.

These considerations lead to simple forms for the microbial growth rates in our "two-state" model:

$$G_{\mathrm{or}} = \left[\frac{v_{\mathrm{or}} s_{\mathrm{o}}}{K_{\mathrm{or}} + s_{\mathrm{o}}}\right] \times \left[1 - \frac{n_{\mathrm{or}}}{n_{\mathrm{or,\,max}}}\right], \quad (4)$$

$$G_{\mathrm{ro}} = \left[\frac{v_{\mathrm{ro}} s_{\mathrm{r}}}{K_{\mathrm{ro}} + s_{\mathrm{r}}}\right] \times \left[1 - \frac{n_{\mathrm{ro}}}{n_{\mathrm{ro,\,max}}}\right], \quad (5)$$

in which the parameters are v_{or} and v_{ro}, the maximal growth rates for the reducing and oxidizing microorganisms, respectively; K_{or} and K_{ro}, the concentrations of the chemical species $\mathrm{s_o}$ or $\mathrm{s_r}$ at which the growth rate is half-maximal; and $n_{\mathrm{or,\,max}}$ and $n_{\mathrm{ro,\,max}}$, the maximal densities of the two populations. Importantly, the concentrations of the auxiliary electron donors and acceptors (e.g., acetate and oxygen) are implicit in the maximal growth rate parameters v_{or} and v_{ro}: we expect v_{or} to increase with the availability of the auxiliary electron donor, while v_{ro} will increase with the availability of the auxiliary electron acceptor. By including the auxiliary electron acceptor/donor concentrations as parameters controlling the maximal growth rates, we neglect the possibility that they may be depleted by utilization. This is, however, included in the more realistic versions of the model presented later in the paper.

2.2 Biotic–abiotic redox cycles

If the oxidation step in the redox cycle is instead abiotic, the model has only three variables: the population density of the reducing microbial population n_{or} and the concentrations of the oxidized and reduced forms of the chemical species being cycled, s_{o} and s_{r}. In this case, the dynamics of the microbial population n_{or} are still described by Eq. (1), but the chemical dynamics obey

$$\dot{s_{\mathrm{r}}} = -F(s_{\mathrm{r}}) + \gamma n_{\mathrm{or}} G_{\mathrm{or}} = -\dot{s_{\mathrm{o}}}. \quad (6)$$

Here, the abiotic oxidation rate is described by the function $F(s_{\mathrm{r}})$. Abiotic oxidation reactions can occur spontaneously (e.g., the abiotic oxidation of hydrogen sulfide; Goldhaber, 2003), or they can be catalyzed (e.g., some electron transfer processes on mineral surfaces; Schoonen and Strongin, 2005) or limited by transport processes (Roden, 2004). To account for these factors in a generic way, we assume a Michaelis–Menten form for $F(s_{\mathrm{r}})$ (Naidja and Huang, 2002):

$$F = \frac{v_{\mathrm{a}} s_{\mathrm{r}}}{K_{\mathrm{a}} + s_{\mathrm{r}}}, \quad (7)$$

where v_{a} is the maximal abiotic rate constant (which may implicitly depend on a catalyst concentration) and K_{a} is the concentration s_{r} at which the abiotic reaction rate is half-maximal. If K_{a} is large such that $K_{\mathrm{a}} \gg s_{\mathrm{r}}$, the reaction rate becomes linear in s_{r}, describing a spontaneous process.

2.3 Steady-state solutions

Analytical predictions for the steady-state population densities and the concentrations of the oxidized and reduced forms of the chemical species being cycled (s_{o} and s_{r}) can be obtained for both the fully biotic model (Eqs. 1–3) and the biotic–abiotic model (Eqs. 1 and 6). These are given in the Supplement, Sects. S1 and S2.

3 Regime shifts caused by population-density limitation

Our models allow us to investigate system-level responses to environmental change. We focus on environmental changes that affect the availability of auxiliary electron acceptors or donors, such as temperature-related changes in oxygen solubility (Shaffer et al., 2009), changes in photosynthesis rate, or changes in the abundance or rate of decomposition of organic matter (Conant et al., 2011). For the fully biotic cycle, the parameters v_{or} and v_{ro} are proxies for the availability of auxiliary electron donors and acceptors, respectively. For the biotic–abiotic cycle, the equivalent parameters are v_{or} and v_{a}. We quantify the response of the ecosystem to changes in auxiliary electron donor or acceptor abundance via the steady-state fraction of the oxidized chemical species, $s_{\mathrm{o}}/s_{\mathrm{tot}}$, which acts as a proxy for the global redox state of the system.

Our main result is that, for both the fully biotic and the biotic–abiotic models, our model can undergo regime shifts: sharp changes in the predominant redox state of the system as the availability of auxiliary electron acceptors or electron donors (such as oxygen or acetate) crosses a critical threshold (Fig. 2). These regime shifts happen under circumstances where the total concentration of the chemical element being cycled ($s_{\mathrm{tot}} = s_{\mathrm{o}} + s_{\mathrm{r}}$) is high, such that $s_{\mathrm{tot}} \gg K_{\mathrm{or}}, K_{\mathrm{ro}}, K_{\mathrm{a}}$, implying that the microbial population density is limited by factors other than the availability of s_{o} or s_{r}. In contrast, for lower concentrations of the chemical element being cycled, $s_{\mathrm{tot}} < K_{\mathrm{or}}, K_{\mathrm{ro}}, K_{\mathrm{a}}$, the model predicts a more gradual change in system state as the availability of the auxiliary electron acceptor or donor varies.

Figure 2a and c show results for the fully biotic cycle model; in Fig. 2a, we vary the maximal reducer growth rate v_{or}, mimicking a change in auxiliary electron acceptor abundance, while in Fig. 2c we vary the maximal oxidizer growth rate v_{ro}, mimicking a change in auxiliary electron donor abundance. As expected, these perturbations lead to profound changes in the system's global redox state (as measured by the fraction of the oxidized chemical species s_{o}), from oxidized to reduced (Fig. 2a) or vice versa (Fig. 2c). Crucially, the sharpness of this transition increases as we increase the total abundance of the chemical species being cycled, s_{tot}. When s_{tot} is large enough to saturate the growth rates of the relevant microbial populations ($s_{\mathrm{tot}} \gg K_{\mathrm{or}}, K_{\mathrm{ro}}$), we obtain a "switch-like" response, which we term a redox regime shift.

196

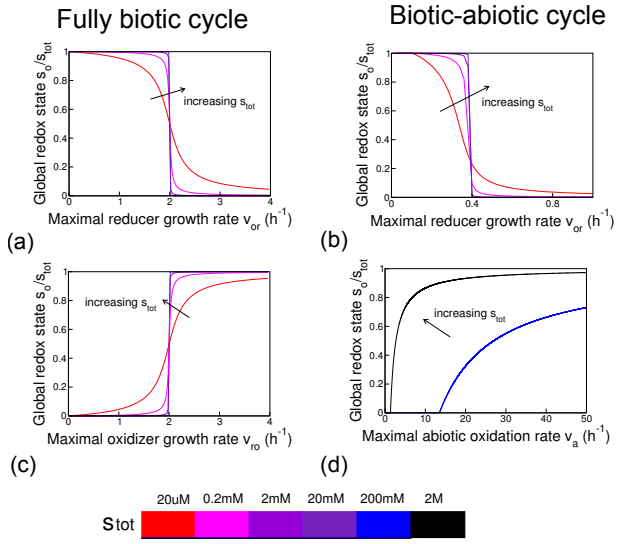

Figure 2. Redox regime shifts in model nutrient cycles. The global redox state, as measured by the oxidized fraction s_o/s_{tot}, predicted by the steady-state solution of the model equations for the fully biotic cycle (**a** and **c**, Eqs. 1–3) or the biotic–abiotic cycle (**b** and **d**, Eqs. 1, 2, and 6) is plotted as a function of parameters that form proxies for the degree of reductive or oxidative driving. v_{or} is taken as a proxy for electron donor (acetate) availability, and v_{ro} is taken as a proxy for electron acceptor (oxygen) availability. These parameters are, for reductive driving, the maximal growth rate of the reductive population, v_{or} (**a** and **b**, keeping v_{or} fixed at $2\,h^{-1}$ or $v_a = 0.2\,\mu M\,h^{-1}$), and, for oxidative driving, either the maximal growth rate of the oxidative population v_{ro} (**c**, keeping v_{ro} fixed at $2\,h^{-1}$) or the maximal abiotic oxidation rate v_a (**d**, also with $v_{ro} = 2\,h^{-1}$). The results show a shift between oxidized and reduced ecosystem states as a threshold in reductive or oxidative driving is crossed; the sharpness of this transition increases with the concentration of the chemical species being cycled, s_{tot} (shown in the color bar). The other parameters are $K_{or} = K_{ro} = K_a = 1\,\mu M$ (Ingvorsen et al., 1984), $n_{or,\,max} = n_{or,\,max} = 9 \times 10^7$ cells L^{-1}, $d = 0.1\,h^{-1}$, and $\gamma = 3 \times 10^{-8}$ µmoles cell^{-1} (Jin et al., 2013). The analytic forms for the steady-state solutions are given in Sect. S1.

For the fully biotic cycle, the model prediction is symmetric with respect to changes in v_{or} and v_{ro} (electron donor and acceptor; compare Fig. 2a and c). Consequently, it is the *ratio* of $v_{or}\,/\,v_{ro}$ (mimicking a change in the ratio of auxiliary electron donor/acceptor abundance) that drives the behavior of the model.

Figure 2b and d show equivalent results for the biotic–abiotic cycle model. In this case also, the model predicts regime shifts in response to both increasing auxiliary electron donor or acceptor availability (Fig. 2b and d, respectively), for large concentrations of the chemical species being cycled ($s_{tot} \gg K_{or}, K_{ro}, K_a$). However, in contrast to the situation for the fully biotic cycle, here the responses to changes in auxiliary electron acceptor and donor are qualitatively different in shape (compare Fig. 2b and d). This is because the biotic and abiotic reaction rates (the two terms in Eq. 6) have different functional dependences on s.

Importantly, the behavior of our model does not depend strongly on its other parameters. In particular, the total microbial population density is not important for the results of Fig. 2, as we show analytically in Sect. S3. For the fully biotic cycle, the steady-state solution of the model depends only on the ratio of the maximal population density parameters ($n_{ro,\,max}/n_{or,\,max}$) and not on the absolute values of the maximal population density $n_{ro,\,max}$ and $n_{or,\,max}$. Moreover the ratio $n_{ro,\,max}/n_{or,\,max}$ affects only the threshold point at which the regime shift happens, not the qualitative switching behavior (see Sect. S3 for more details). Thus we expect to see redox regime shifts across environments with very different microbial population densities, even for systems with very large microbial populations, and for those where the sizes of the oxidizing and reducing populations are different, as long as the microbial population density is ultimately limited by a factor other than the concentration of the chemical element being cycled. It is important to note, however, that the *timescale* over which the system responds to environmental change does depend on the population density; for large populations, the system responds more slowly. For the biotic–abiotic cycle, the mathematical results are slightly more complicated but the conclusions are broadly similar (see Sect. S3).

3.1 Regime shifts also occur in models with spatial heterogeneity and chemical sinks

The oxidation and reduction steps in natural microbial nutrient cycles are usually spatially separated (Fenchel et al., 1998). Extending our model, we find that our prediction of redox regime shifting behavior is robust to the inclusion of spatial separation between reductive and oxidative zones; indeed, the resulting transport limitation of chemical species s_o and s_r actually enhances the switching phenomenon (see Sect. S5).

In the natural environment, coupling between the different redox cycles shown in Fig. 1 may also be important. For example, sulfide reacts with iron ultimately to form pyrite, which represents a stable sink for iron and sulfide (Raiswell and Canfield, 2012). We find that our model still produces redox regime shifts when we include extra terms to simulate these sink effects (see Sect. S6).

3.2 Origin of the regime shifts

The redox regime shifts which we observe in our model arise from the interplay between nonlinear population growth, which can be limited by factors other than the chemical species being cycled, and the topology of the biogeochemical cycle. In our model, the global redox state is controlled by the balance between oxidative and reductive chemical fluxes. An increase in the availability of the auxiliary electron ac-

ceptor stimulates the oxidation reaction, resulting in an increase in concentration of the oxidized chemical species, s_o. If there were no other growth-limiting factor, this increase in s_o would stimulate the growth of the reducing microbial population, which consumes s_o; thus the global redox state would respond only gradually to changes in electron acceptor availability (and likewise for changes in the electron donor availability), as shown in Fig. 2 for small values of s_{tot} (red lines). However, the situation is different if the microbial population density is limited by other factors (such as carbon availability). In this case an increase in auxiliary electron acceptor availability increases s_o, but the reducer population cannot respond to this increase in s_o because it is already close to its maximal population density. Once the auxiliary electron acceptor supply crosses a critical threshold, the production rate of s_o exceeds the maximal consumption capacity of the reducer population and the system undergoes a regime shift to an oxidized state, as in Fig. 2 for large values of s_{tot} (blue lines). The same scenario holds in reverse for changes in the availability of the auxiliary electron donor; here, as electron donor availability increases, a redox regime shift from an oxidized to a reduced system state occurs.

4 Mapping to enzyme kinetics

Interestingly, the system-scale regime shifts that we observe in our biogeochemical models can be mapped directly onto a well-known molecular-scale phenomenon in intracellular biochemical signaling networks. In biological cells, responses to environmental signals are often mediated by phosphorylation–dephosphorylation cycles, in which a target enzyme is activated by addition of a phosphate group, and deactivated by removal of the phosphate group; the kinase and phosphatase enzymes mediating these reactions act in opposition to each other (Alberts et al., 2002). Phosphorylation–dephosphorylation cycles can exhibit "zero-order ultrasensitivity", in which they respond extremely sensitively to changes in the level of signal, because the enzymes have become saturated, decoupling the enzymatic conversion rates from the concentration of substrate (Goldbeter and Koshland, 1981). Although they act on very different length and timescales, biogeochemical cycles are topologically similar to phosphorylation–dephosphorylation cycles. In fact, one can show mathematically that our models, in the steady state, map exactly onto the classic Goldbeter–Koshland model for phosphorylation–dephosphorylation cycles (Goldbeter and Koshland, 1981), and that the regime shifts observed in our models are equivalent to the ultrasensitive signal responses predicted by this model (see Sect. S7). This raises the interesting possibility of mapping molecular-level dynamic phenomena onto biogeochemical models more generally – a direction that may prove fruitful in future work.

5 Redox regime shifts in a more realistic model

Thus far our investigation has focused on a rather simplified model for microbially mediated biogeochemical cycles. In this simple model, varying v_{ro} and v_{or} was assumed to be analogous to varying the availability of auxiliary electron acceptors (such as oxygen or nitrate) and electron donors (such as acetate or hydrogen), respectively. In reality, however, auxiliary electron acceptors or donors may be supplied, or utilized by, other biotic or abiotic processes, and thus we expect their concentrations to vary with the system dynamics. We now introduce a more ecologically realistic model in which the concentrations of the auxiliary electron acceptor/donor are explicitly represented, and allowed to vary. For this model, we find the same redox regime-shifting behavior as in the simple model described previously.

Specifically, we focus on an example in which acetate is the auxiliary electron donor and oxygen is the auxiliary electron acceptor. We suppose that acetate is produced by microbial decomposition of organic matter (long-chain organics such as lignin or cellulose; Rickard, 2012); we represent explicitly in the model not only the concentration of acetate but also the population density of the decomposer population. Likewise, we suppose that oxygen is generated by photosynthetic microorganisms; the model includes explicitly the dynamics of the photosynthesizer population as well as the oxygen concentration. External environmental inputs control the population dynamics of the decomposers and the photosynthesizers; these inputs are the organic matter concentration and the light intensity, respectively. Our model is shown schematically in Fig. 3a; we assume that oxidative and reductive processes occur in different spatial zones, represented by boxes and coupled by chemical transport of s_o and s_r. For simplicity, we consider transport only of the chemical species being cycled (s_o and s_r); allowing transport of oxygen/acetate would cause spatial shifting of the redox zones, which, although interesting, would be better investigated in a model with more detailed spatial resolution. In the model, the growth rate of the oxidizing microbial population (n_{ro}) is assumed to depend on the concentrations of both s_r and the auxiliary electron acceptor (i.e., oxygen), via a multiplicative Monod term, with explicit population density limitation, and the equivalent scenario holds for the reducer population. Multiplicative Monod kinetics is the most widely used method of modeling microbial growth limitation by multiple substrates (Moore et al., 2002; Jin and Bethke, 2005). However we note that Liebig's law of the minimum provides an alternative (Saito et al., 2008), which would not affect our qualitative results. Our model also includes a linear loss term for the auxiliary electron acceptors or donors, which represents competitive consumption by other populations. Full details and dynamical equations for this model are presented in Sect. S8.

Our simulations show that this model indeed undergoes redox regime shifts (Fig. 3b). In particular, the system re-

198

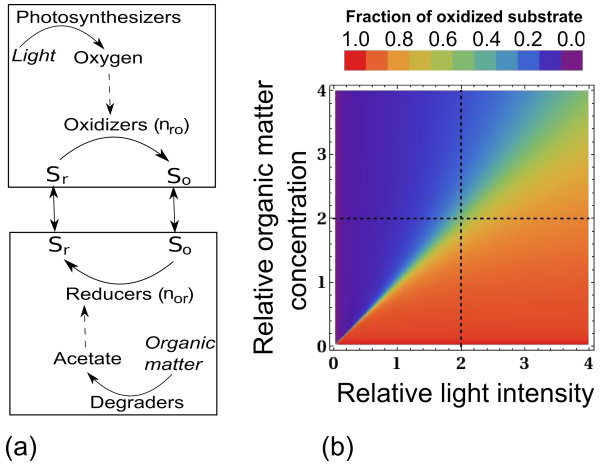

Figure 3. Redox regime shifts in a "complete ecosystem" model. **(a)** Illustration of the model. Oxidative and reductive processes take place in separate spatial zones, linked by chemical diffusion. The model explicitly represents the population dynamics of microbial photosynthesizers, decomposers, reducers, and oxidizers, and the chemical dynamics of oxygen, s_o, s_r, and acetate. Light intensity and organic matter availability are treated as control parameters. The dynamical equations corresponding to the model are presented in Sect. S8, Eqs. (S45)–(S54); these are integrated numerically to find the steady-state solution. Parameter values are also listed in the Supplement. **(b)** Steady-state solution of the model illustrated in **(a)**, obtained numerically, plotted as a function of the control parameters, light intensity (relative to the typical value 10 µE $s^{-1}\,m^{-2}$; Huisman et al., 2006) and organic matter concentration (relative to the typical value 100 mg cm^{-3}; Allison et al., 2010). The color represents the global redox state (see color key). The model shows redox regime shifts as the organic matter concentration is varied at fixed light intensity (vertical dashed line) or as the light intensity is varied at fixed organic matter concentration (horizontal dashed line).

dox state, as measured by the ratio s_o/s_{tot} (shown by color in Fig. 3b), changes sharply in response to changes in either organic matter availability (which stimulates the decomposer population and hence the reducer population), or to changes in light intensity (which stimulates the photosynthesizers and hence the oxidizer population). As organic matter availability increases at fixed light intensity (vertical dashed line in Fig. 3b), the redox state of the system changes sharply from oxidized to reduced (red to purple). Likewise, as the light intensity increases for fixed organic matter concentration (horizontal dashed line in Fig. 3b), the redox state also undergoes a regime shift, in this case from reduced (purple) to oxidized (red). We observe similar regime-shifting behavior in equivalent models where the oxidation step is abiotic (see Sect. S8). We have also shown that the qualitative behavior of the model is not dependent on the strength of the loss term representing competition for auxiliary electron acceptors/donors (see Sect. S10).

Since many natural redox cycles involve intermediate steps between the most oxidized and most reduced states (e.g., the nitrogen and sulfur cycles in Fig. 1), we have also simulated a version of the model which includes a redox state intermediate between s_o and s_r. This model also shows regime shifts between predominantly oxidized and predominantly reduced system states (see Sect. S9).

6 Conditions for redox regime shifts

Our analysis provides a clear set of criteria that need to be satisfied for redox regime shifts to occur. These are as follows:

1. The density of the redox-cycling microbial populations must ultimately be limited by a factor other than the concentration of the chemical element being cycled. This factor could be the concentration of another nutrient (see Sect. S4), or space limitation. It is important to note, however, that the population density need not be small; large populations are also predicted to show regime shifts, albeit with longer response times.

2. The total concentration of the element being cycled must be high enough to saturate the growth rates of the microbial reducers and oxidizers (or the abiotic oxidation reaction): $s_{tot} \gg K_{or}$, K_{ro}, K_a. This ensures that the growth of the redox-cycling populations will become saturated with respect to s, causing a switch-like response to changes in auxiliary electron acceptor or donor availability (as in Fig. 2).

3. The growth rates of the redox-cycling populations must be unsaturated with respect to the concentrations of the auxiliary electron acceptor and/or donor, so that the system responds to changes in auxiliary electron acceptor or donor availability.

7 Are redox regime shifts likely in the natural environment?

Thus far we have established our model, demonstrated that the predicted redox regime shift is robust as complications are introduced, and defined the conditions required for redox regime shifts to occur. We now assess whether these conditions are likely to be prevalent in the natural environment.

7.1 Condition 1: a factor exists that ultimately limits population density

In the natural environment, there are many possible limiting factors for microbial population density. Microbial growth requires sources not only of energy but also of carbon, nitrogen, phosphorus, sulfur, and other, trace biomass components (Madigan et al., 2009; Ingraham et al., 1983).

199

For redox-cycling microbial populations, the redox reaction provides an energy source, but cannot satisfy all the requirements for formation of biomass. It is thus almost inevitable that growth is ultimately limited by the availability of biomass components rather than the redox species. Indeed, carbon limitation is common in microbial soil/sediment communities (Demoling et al., 2007), while in ocean communities nitrogen or phosphorus is often growth-limiting (Mills et al., 2008).

7.2 Condition 2: high concentration of the chemical element being cycled

Our second condition states that $s_{tot} \gg K_{or}, K_{ro}$ (i.e., the oxidizer/reducer growth rate must be saturated with respect to s_r or s_o). To assess whether this condition is fulfilled in the natural environment, we surveyed measured values of the half-saturation constants K_{or} or K_{ro} for redox-cycling microorganisms reported in the literature, and compared these values with typical concentrations of the chemical species being cycled, in various environmental settings. The results of this survey are shown in Table 2. For sulfur-cycling organisms, these data suggest that the concentration of the chemical species being cycled can exceed the half-saturation constant of the relevant microbial populations, $s_{tot} \gg K_{or}, K_{ro}$. For example, marine sulfate reducers are generally not limited by sulfate, because sulfate is highly abundant (indeed it is the second most abundant anion in the oceans; Goldhaber, 2003). For nitrogen-cycling organisms these data suggest that redox regime shifts are unlikely to occur in "typical" nitrogen-cycling environments, such as the open ocean. However, there are many examples where anthropogenic influences such as agricultural runoff can lead to very high concentrations of nitrate such as lakes or groundwater aquifers. For example, groundwater sources often contain in excess of 400 µM nitrate. Data on the proportion of groundwater bodies across the EU in 2003 with a mean nitrate concentration in excess of 400 µM reported 80 % in Spain, 50 % in the UK, 36 % in Germany, 34 % in France, and 32 % in Italy (Rivett et al., 2008). Such high nitrate levels exceed the relevant half-saturation constant of 10 µM, and for this reason, we would expect redox regime shifts in the nitrogen cycle to occur in eutrophic terrestrial ecosystems.

In contrast, our data survey suggests that redox regime shifts are unlikely to be associated with carbon cycles, because the typical half-saturation constant for methanogenesis is large relative to typical environmental concentrations of acetate.

For the iron cycle, our survey suggests that redox regime shifts are unlikely in modern-day environments, but may have occurred in the past. While modern oceanic concentrations of dissolved Fe^{2+} ions are low, the ancient oceans may have contained high concentrations of Fe^{2+} (≈ 1 mM), suggesting that redox regime shifts could have occurred in the comparatively iron-rich Archean or Proterozoic iron cycles (Canfield, 1998).

7.3 Condition 3: low auxiliary electron acceptor or donor availability

Condition 3 states that, for biotic redox reactions, the concentration of the auxiliary electron donor or acceptor must be low enough that changes in their availability affect the growth rate of the microbial reducers/oxidizers (i.e., the oxidative and reductive microbial metabolic reactions must be unsaturated with respect to the auxiliary electron acceptor/donor).

Biotic reduction processes often take place in the presence of strong competition for auxiliary electron donor, for example, sulfate-reducing microorganisms typically compete with methanogens for acetate (Muyzer and Stams, 2008). The concentration of acetate in freshwater sediments is typically about 1 µM (Roden and Wetzel, 2003) but can be as high as 100 µM (Burdige, 2002). This compares to approximate half-saturation constants for growth with respect to acetate of 70 µM for sulfate reduction and 12 µM for methanogenesis (Roden and Wetzel, 2003; Ingvorsen et al., 1984), suggesting that indeed these reactions are very likely to be unsaturated with respect to acetate.

For oxidative processes, oxygen is the most widely used auxiliary electron acceptor. The supply of oxygen is expected to be rate-limiting for growth in oxygen-poor environments (which are becoming more common in the coastal oceans; Diaz and Rosenberg, 2008). The half-saturation constant with respect to oxygen for bacterial sulfide oxidation is 1–20 µM (Klok et al., 2012; González-Sánchez and Revah, 2007), and while the concentration of oxygen in oxygen-saturated (i.e., fully aerated) water is 0.3 mM (Kamyshny et al., 2011), significant competition for oxygen means that the concentration is much lower in many environments (Shaffer et al., 2009). It is interesting to note that oxygen concentrations were also low in the Proterozoic and Archean oceans (Canfield, 1998).

Taken together, this analysis suggests that the redox regime shifts predicted by our model are likely to be relevant in the present-day natural environment, with respect to the sulfur and nitrogen cycles, and may also have played a role in iron cycling in the iron-containing Proterozoic and Archean oceans.

7.4 What perturbations might cause redox regime shifts?

How likely are the changes in auxiliary electron acceptor/donor concentrations that could trigger redox regime shifts in biogeochemical cycles? Focusing on oxygen as the most significant natural auxiliary electron acceptor, oxygen concentrations in oceans or inland water bodies can be affected by temperature changes (for example, a 4.8 °C global

200

Table 2. Typical values for the half saturation constants K_{or} or K_{ro} for microbial growth, for various nutrient-cycling organisms, compared to typical values for the concentrations of the relevant nutrients in marine environments. All values are given rounded to an order of magnitude.

Nutrient cycle	Reaction	Organism	K_{or} or K_{ro}	Concentration range
Sulfur	$H_2S \rightarrow SO_4^{2-}$	*Thiothrix* or *Thiobacillus*	1 µM (Canfield et al., 2005)	$0.1\,\mu M \leq [H_2S] \leq 100\,\mu M$ (Goldhaber, 2003)
	$SO_4^{2-} \rightarrow H_2S$	*Desulfovibrio*	1 µM (Ingvorsen and Jorgensen, 1984; Tarpgaard et al., 2011)	$0.1\,\mu M \leq [SO_4^{2-}] \leq 10\,mM$ (Goldhaber, 2003)
Iron	$Fe^{2+} \rightarrow Fe^{3+}$	*Thiobacillus ferrooxidans*	1 mM (Wichlacz and Unz, 1985)	$1\,pM \leq [Fe^{2+}] \leq 100\,\mu M$ (Landing and Bruland, 1987; Canfield et al., 1993)
	Fe(III) oxide $\rightarrow Fe^{2+}$	*Shewanella putrefaciens*	1 mM (Bonneville et al., 2004)	$0.1\,\mu M \leq$ [Fe(III) oxide] $\leq 10\,mM$ (Thamdrup and Canfield, 1996; Canfield et al., 1993)
Carbon	$CH_4 \rightarrow CO_2$	*Methylocystis*	0.1 µM (Baani and Liesack, 2008)	$1\,nM \leq [CH_4] \leq 100\,\mu M$ (Reeburgh, 2007)
	$CH_3CO_2^- \rightarrow CH_4$	*Methanosarcina*	1 mM (Dale et al., 2006)	$0.1\,\mu M \leq [CH_3CO_2^-] \leq 100\,\mu M$ (Burdige, 2002)
Nitrogen	$NH_4^+ \rightarrow NO_3^-$	*Nitrosomonas*	1 µM (Koper et al., 2010)	$0.01\,\mu M < [NH_4^+] \leq 100\,\mu M$ (Rees et al., 2006; Blackburn et al., 1993)
	$NO_3^- \rightarrow NO_2^-$	*Flavobacterium*	10 µM (Betlach and Tiedje, 1981)	$0.01\,\mu M < [NO_3^-] \leq 10\,\mu M$ (Rees et al., 2006; Blackburn et al., 1993)

temperature increase has been predicted to cause a 68 % reduction in the mean oceanic oxygen concentration; Shaffer et al., 2009) and by perturbations which affect the balance between photosynthesis and oxygenic respiration, such as eutrophication (which can lead to drastic increases of biomass, generating "oxygen minimum zones"; Diaz and Rosenberg, 2008). Furthermore, over Phanerozoic time, pO_2 varied between 15 and 37 %, which represents a variation large enough to generate redox regime shifts (Berner, 1999). Further work could parameterize our model to investigate whether a redox regime shift is possible within the range of published values for atmospheric oxygen and oceanic iron and sulfate on the early Earth, taking into account the evidence for the progressive changes in these parameters through geologic time from the Paleoproterozoic to the Phanerozoic.

The availability of auxiliary electron donors (such as acetate, lactate, or hydrogen) is expected to be altered by changes in the rate of organic matter degradation, which has been predicted to increase with temperature (Conant et al., 2011), and is also sensitive to changes in the abundance of organic matter due to sewage or phosphorus influx (Todd-Brown et al., 2012). Changes in electron donor availability could also arise due to competition effects, such as reductive degradation of pollutants (Beaudet et al., 1998), or perturbations in other biogeochemical cycles. This raises the interesting possibility that a redox regime shift in one biogeochemical cycle could trigger shifts in others, due to changes in the level of competition for auxiliary electron donors.

Furthermore, it is possible that redox regime shifts could occur in response to changes in the inflow rates of auxiliary electron donors and acceptors, instead of changes in the growth rates of the microbial populations within the environment that supply them. It is highly likely that such a system would produce redox regime shifts in response to variation in these fixed input rates. For example, future models could look at whether seasonal temperature-induced mixing effects can generate redox regime shifts.

8 Discussion

Microbial populations are key mediators of the Earth's biogeochemical cycles (Falkowski et al., 2008). Our work shows that microbial population dynamics can have important consequences for the response of biogeochemical cycles to environmental changes. Under circumstances where the microbial population density is limited by factors other than the concentration of the chemical being cycled (e.g., by the concentration of another limiting nutrient), our models predict that redox-cycling systems can undergo regime shifts in their predominant redox state in response to small changes in the availability of auxiliary electron acceptors or donors (such as oxygen and acetate), which drive the oxidative and reductive redox-cycling reactions, respectively. These regime

201

shifts arise from the interplay between the nonlinearity of microbial population dynamics, multiple nutrient limitation, and the cyclic system topology. Diverse environmental perturbations are expected to affect the availability of auxiliary electron acceptors and donors, including temperature-mediated changes in oxygen solubility and changes in organic matter abundance due to eutrophication, suggesting that these redox regime shifts may be common in the natural environment.

Regime shifts are a well-known phenomenon in many ecosystems (Scheffer et al., 2009), including microbial ecosystems (Bürgmann et al., 2011). They are known to occur in biogeochemical cycles (Blodau and Knorr, 2006) and have played an important role in the Earth's history – a notable example being the transition to an oxic atmosphere around 2.3 Ga (Lenton and Watson, 2011). Our work suggests a new mechanism by which regime shifts may occur in microbially mediated biogeochemical cycles. This mechanism is identified here in a very simple and generic model but also shown to exist in more realistic models. Further work could extend our models to include detailed spatial or temporal dynamics and/or additional environmental variables such as temperature or pH.

Our analysis also predicts clear criteria for the conditions under which redox regime shifts should be expected. By analyzing parameter values for a range of natural environments, we show that these criteria are likely to be satisfied for the natural sulfur and nitrogen cycles. This phenomenon may also be relevant for iron cycling in the Archean or Proterozoic oceans, due to their much lower oxygen concentrations and potentially much higher concentrations of iron than present-day oceans. Indeed, redox regime shifts may even help to explain changes in the Earth's biogeochemical cycles associated with mass extinction events, such as the rise in ocean sulfide levels during the end-Permian extinction event (251 Ma), which is believed to have poisoned the oceans and killed as much as 90 % of all macroscopic species on Earth (Benton and Twitchett, 2003). More generally, our work reveals that microbial population dynamics can lead to qualitative changes in the behavior of biogeochemical cycles, with significant system-level consequences. Better understanding of microbial population dynamics is vital for accurate prediction of the effects of anthropogenic changes on the Earth's systems, both on small and large scales.

The Supplement related to this article is available online at doi:10.5194/bg-12-3713-2015-supplement.

Author contributions. T. Bush performed the calculations, data analysis, and computer simulations. All authors contributed to the project design, data interpretation, and writing of the manuscript.

Acknowledgements. We thank Charles Cockell, Jan Haeberle, Casey Bryce, Sophie Nixon, Patrick Warren, and Justin Whitehouse for discussions. T. Bush is supported by an EPSRC DTA studentship and R. J. Allen by a Royal Society University Research Fellowship. This work was supported by the US Army Research Office under grant number 64052-MA.

Edited by: J. Middelburg

References

Aguilos, M., Takagi, K., Liang, N., Watanabe, Y., Teramoto, M., Goto, S., Takahashi, Y., Mukai, H., and Sasa, K.: Sustained large stimulation of soil heterotrophic respiration rate and its temperature sensitivity by soil warming in a cool-temperate forested peatland, Tellus B, 65, 20792, 2013.

Alberts, B., Johnson, A., Lewis, J., Raff, M., Roberts, K., and Walter, P.: Molecular Biology of the Cell, 4 edn., New York, Garland Science, 183–208, 2002.

Allison, S. D. and Martiny, J. B. H.: Resistance, resilience, and redundancy in microbial communities, P. Natl. Acad. Sci. USA, 105, 11512–11519, 2008.

Allison, S. D., Wallenstein, M. D., and Bradford, M. A.: Soil-carbon response to warming dependent on microbial physiology, Nat. Geosci., 3, 336–340, 2010.

Baani, M. and Liesack, W.: Two isozymes of particulate methane monooxygenase with different methane oxidation kinetics are found in Methylocystis sp. strain SC2., P. Natl. Acad. Sci. USA, 105, 10203–10208, 2008.

Beaudet, R., Lévesque, M. J., Villemur, R., Lanthier, M., Chénier, M., Lépine, F., and Bisaillon, J. G.: Anaerobic biodegradation of pentachlorophenol in a contaminated soil inoculated with a methanogenic consortium or with Desulfitobacterium frappieri strain PCP-1., Appl. Microbiol. Biot., 50, 135–141, 1998.

Benton, M. J. and Twitchett, R. J.: How to kill (almost) all life: the end-Permian extinction event, Trends Ecol. Evol., 8, 358–365, 2003.

Berner, R. A.: Atmospheric oxygen over Phanerozoic time., P. Natl. Acad. Sci. USA, 96, 10955–10957, 1999.

Berry, D. and Widder, S.: Deciphering microbial interactions and detecting keystone species with co-occurrence networks, Front. Microbiol., 5, 219, doi:10.3389/fmicb.2014.00219, 2014.

Betlach, M. R. and Tiedje, J. M.: Kinetic explanation for accumulation of nitrite, nitric oxide, and nitrous oxide during bacterial denitrification, Appl. Environ. Microb., 42, 1074–1084, 1981.

Blackburn, T. H., Blackburn, N., Mortimer, R., Coleman, M., and Lovley, D. R.: Rates of microbial processes in sediments, Philos. T. R. Soc. Lond. A, 344, 49–58, 1993.

Blodau, C. and Knorr, K.-H.: Experimental inflow of groundwater induces a "biogeochemical regime shift" in iron-rich and acidic sediments, J. Geophys. Res., 111, G02026, doi:10.1029/2006JG000165, 2006.

Bonneville, S., Van Cappellen, P., and Behrends, T.: Microbial reduction of iron(III) oxyhydroxides: effects of mineral solubility and availability, Chem. Geol., 212, 255–268, 2004.

Burdige, D.: Sediment pore waters, in: Biogeochemistry of Marine Dissolved Organic Matter, edited by: Hansell, D. and Carlson, C., Academic Press, Massachusetts, 611–663, 2002.

Bürgmann, H., Jenni, S., Vazquez, F., and Udert, K. M.: Regime shift and microbial dynamics in a sequencing batch reactor for nitrification and anammox treatment of urine, Appl. Environ. Microb., 77, 5897–907, doi:10.1128/AEM.02986-10, 2011.

Button, D. K.: Kinetics of nutrient-limited transport and microbial growth, Microbiol. Rev., 49, 270–297, 1985.

Canfield, D. E.: Reactive iron in marine sediments, Geochim. Cosomochim. Ac., 53, 619–632, 1989.

Canfield, D. E.: A new model for Proterozoic ocean chemistry, Nature, 396, 450–453, 1998.

Canfield, D. E., Thamdrup, B., and Hansen, J.: The anaerobic degradation of organic matter in Danish coastal sediments: iron reduction, manganese reduction and sulfate reduction, Geochim. Cosomochim. Ac., 57, 3867–3883, 1993.

Canfield, D. E., Thamdrup, B., and Kristensen, E.: Aquatic geomicrobiology, Adv. Mar. Biol., 48, 347–357, 2005.

Conant, R. T., Ryan, M. G., Ågren, G. I., Birge, H. E., Davidson, E. A., Eliasson, P. E., Evans, S. E., Frey, S. D., Giardina, C. P., Hopkins, F. M., Hyvönen, R., Kirschbaum, M. U. F., Lavallee, J. M., Leifeld, J., Parton, W. J., Megan Steinweg, J., Wallenstein, M. D., Martin Wetterstedt, J. A., and Bradford, M. A.: Temperature and soil organic matter decomposition rates – synthesis of current knowledge and a way forward, Glob. Change Biol., 17, 3392–3404, doi:10.1111/j.1365-2486.2011.02496.x, 2011.

Dale, A. W., Regnier, P., and Van Cappellen, P.: Bioenergetic controls on anaerobic oxidation of methane (AOM) in coastal marine sediments: a theoretical analysis, Am. J. Sci., 306, 246–294, 2006.

Demoling, F., Figueroa, D., and Baath, E.: Comparison of factors limiting bacterial growth in different soils, Soil Biol. Biochem., 39, 2485–2495, 2007.

Diaz, R. J. and Rosenberg, R.: Spreading dead zones and consequences for marine ecosystems, Science, 321, 926–929, 2008.

Falkowski, P. G., Fenchel, T., and Delong, E. F.: The microbial engines that drive Earth's biogeochemical cycles, Science, 320, 1034–1039, doi:10.1126/science.1153213, 2008.

Fenchel, T., King, G., and Blackburn. T. H.: Bacterial Biogeochemistry: The Ecophysiology of Mineral Cycling, Elsevier, San Diego, 1–34, 1998.

Galloway, J. N., Dentener, F. J., Capone, D. G., Boyer, E. W., Howarth, R. W., Seitzinger, G. P., Cleveland, C. C., Green, P. A., Holland, E. A., K arl, D. M., Michaels, A. F., Porter, J. H., Townsend, A. R., and Vorosmarty, C. J.: Nitrogen cycles: past, present and future, Biogeochemistry, 70, 153–226, 2004.

Goldbeter, A. and Koshland, D. E.: An amplified sensitivity arising from covalent modification in biological systems, P. Natl. Acad. Sci. USA, 78, 6840–6844, 1981.

Goldhaber, M.: Sulfur-rich sediments, in: Treatise on Geochemistry, Vol. 7, edited by: Mackenzie, F., Holland, H., and Turekian, K., Elsevier, Amsterdam, 257–288, 2003.

González-Sánchez, A., and Revah, S.: The effect of chemical oxidation on the biological sulfide oxidation by an alkaliphilic sulfoxidizing bacterial consortium, Enzyme. Microb. Tech., 40, 292–298, 2007.

Hibbing, M. E., Fuqua, C., Parsek, M. R., and Peterson, S. B.: Bacterial competition: surviving and thriving in the microbial jungle, Nat. Rev. Microbiol., 8, 15–25, 2010.

Higgins, S. I. and Scheiter, S.: Atmospheric CO_2 forces abrupt vegetation shifts locally, but not globally, Nature, 488, 209–212, 2012.

Huisman, J., Pham Thi, N., Karl, D. M., and Sommeijer, B.: Reduced mixing generates oscillations and chaos in the oceanic deep chlorophyll maximum, Nature, 439, 322–325, 2006.

Ingraham, J. L., Maaloe, O., and Neidhardt, F. C.: Growth of the Bacterial Cell, Sinauer Associates, Sunderland, Mass, 227–265, 1983.

Ingvorsen, K. and Jorgensen, B. B.: Kinetics of sulfate uptake by freshwater and marine species of Desulfovibrio, Arch. Microbiol, 139, 61–66, 1984.

Ingvorsen, K., Zehnder, A. J. B., and Jorgensen, B. B.: Kinetics of sulfate and acetate uptake by Desulfobacter postgatei, Appl. Environ. Microb., 47, 403–408, 1984.

IPPC: Carbon and other biogeochemical cycles, in: Climate Change 2013: The Physical Science Basis, 465–570, 2013.

Jin, Q. and Bethke, C. M.: Predicting the rate of microbial respiration in geochemical environments, Geochim. Cosmochim. Ac., 69, 1133–1143, 2005.

Jin, Q., Roden, E. E., and Giska, J. R.: Geomicrobial kinetics: extrapolating laboratory studies to natural environments, Geomicrobiol. J., 30, 173–185, 2013.

Jones, S. E. and Lennon, J. T.: Dormancy contributes to the maintenance of microbial diversity, P. Natl. Acad. Sci. USA, 107, 5881–5886, 2010.

Kamyshny, A., Zerkle, A. L., Mansaray, Z. F., Ciglenečki, I., Bura-Nakić, E., Farquhar, J., and Ferdelman, T. G.: Biogeochemical sulfur cycling in the water column of a shallow stratified sea-water lake: Speciation and quadruple sulfur isotope composition, Mar. Chem., 127, 144–154, doi:10.1016/j.marchem.2011.09.001, 2011.

Karl, D., Michaels, A., Bergman, B., and Capone, D.: Dinitrogen fixation in the world's oceans, Biogeochemistry, 57, 47–98, 2002.

Klok, J. B. M., Graaff, M. D., Bosch, P. L. F. V. D., Boelee, N. C., Keesman, K. J., and Janssen, A. J. H.: A physiologically based kinetic model for bacterial sulfide oxidation, Water Res., 47, 483–492, 2012.

Koper, T. E., Stark, J. M., Habteselassie, M. Y., and Norton, J. M.: Nitrification exhibits Haldane kinetics in an agricultural soil treated with ammonium sulfate or dairy-waste compost, FEMS Microbiol. Ecol., 74, 316–322, 2010.

Landing, W. and Bruland, K.: The contrasting biogeochemistry of iron and manganese in the Pacific Ocean, Geochim. Cosomochim. Ac., 51, 29–43, 1987.

Lenton, T. M. and Watson, A.: Revolutions that Made the Earth, Oxford, Oxford University Press, 845–852, 2011.

López-Urrutia, A., San Martin, E., Harris, R. P., and Irigoien, X.: Scaling the metabolic balance of the oceans, P. Natl. Acad. Sci. USA, 103, 8739–8744, 2006.

Madigan, M. T., Martinko, J. M., Dunlap, P. V., and Clark, D. P.: Brock Biology of Microorganisms, 12th edn., Pearson Education Inc., San Francisco, 673–703, 2009.

Marino, S., Baxter, N. T., Huffnagle, G. B., Petrosino, J. F., and Schloss, P. D.: Mathematical modeling of primary succession of

murine intestinal microbiota, P. Natl. Acad. Sci. USA, 111, 1–6, 2013.

Mills, M. M., Moore, C. M., Langlois, R., Milne, A., Achterberg, A., Nachtigall, K., and Lochte, K.: Nitrogen and phosphorus co-limitation of bacterial productivity and growth in the oligotrophic subtropical North Atlantic, Limnol. Oceanogr., 53, 824–834, 2008.

Moore, J. K., Doney, S. C., Kleypas, J. A., Glover, D. M., and Fung, I. Y.: An intermediate complexity marine ecosystem model for the global domain, Deep-Sea Res. Pt. II, 49, 403–462, 2002.

Muyzer, G. and Stams, A. J. M.: The ecology and biotechnology of sulphate-reducing bacteria, Nat. Rev. Microbiol., 6, 441–454, 2008.

Naidja, A. and Huang, P. M.: Significance of the Henri–Michaelis–Menten theory in abiotic catalysis: catechol oxidation by δ-MnO2, Surf. Sci., 506, L243–L249, 2002.

Nikolaki, S. and Tsiamis, G.: Microbial diversity in the era of omic technologies, BioMed Research International, 2013, 958719, 2013.

Raiswell, R. and Canfield, D. E.: The iron biogeochemical cycle past present and future, Geochemical Perspectives, 1, 1–220, 2012.

Reeburgh, W.: Oceanic methane biogeochemistry, Chem. Rev., 107, 486–513, 2007.

Rees, A. P., Woodward, E. M. S., and Joint, I.: Concentrations and uptake of nitrate and ammonium in the Atlantic Ocean between 60° N and 50° S, Deep-Sea. Res. Pt. II., 53, 1649–1665, 2006.

Rickard, D.: Sulfidic Sediments and Sedimentary Rocks, Elsevier, Amsterdam, 319–343, 2012.

Rivett, M. O., Buss, S. R., Morgan, P., Smith, J. W. N., and Bemmett, C. D.: Nitrate attenuation in groundwater: A review of biogeochemical controlling processes, Water. Res., 42, 4215–4232, doi:10.1016/j.watres.2008.07.020, 2008.

Roden, E. E.: Analysis of long-term bacterial vs. chemical Fe(III) oxide reduction kinetics, Geochim. Cosomochim. Ac., 68, 3205–3216, doi:10.1016/j.gca.2004.03.028, 2004.

Roden, E. E. and Wetzel, R. G.: Competition between Fe(III)-reducing and methanogenic bacteria for acetate in iron-rich freshwater sediments., Microb. Ecol., 45, 252–258, 2003.

Saito, M., Goepfert, T. J., and Ritt, J.: Some thoughts on the concept of colimitation: three definitions and the importance of bioavailability, Limnol. Oceanogr., 53, 276–290, 2008.

Scheffer, M., Bascompte, J., Brock, W. A., Brovkin, V., Carpenter, S. R., Dakos, V., Held, H., van Nes, E. H., Rietkerk, M., and Sugihara, G.: Early-warning signals for critical transitions, Nature, 461, 53–59, 2009.

Schoonen, M. and Strongin, D.: Catalysis of electron transfer reactions at mineral surfaces, in: Environmental Catalysis, edited by: Grassian, V., CRC Press, Boca Raton, 37–60, 2005.

Shaffer, G., Olsen, S. M., and Pedersen, J. O. P.: Long-term ocean oxygen depletion in response to carbon dioxide emissions from fossil fuels, Nat. Geosci., 2, 105–109, 2009.

Sirota, J., Baiser, B., Gotelli, N. J., and Ellison, A. M.: Organic-matter loading determines regime shifts and alternative states in an aquatic ecosystem, P. Natl Acad. Sci. USA, 110, 7742–7747, 2013.

Tarpgaard, I. H., Roy, H., and Jorgensen, B. B.: Concurrent low- and high-affinity sulfate reduction kinetics in marine sediment, Geochim. Cosomochim. Ac., 75, 2997–3010, 2011.

Thamdrup, B. and Canfield, D. E.: Pathways of carbon oxidation in continental margin sediments off central Chile, Limnol. Oceanogr., 41, 1629–1650, 1996.

Todd-Brown, K. E. O., Hopkins, F. M., Kivlin, S. N., Talbot, J. M., and Allison, S. D.: A framework for representing microbial decomposition in coupled climate models, Biogeochemistry, 109, 19–33, 2012.

Westrich, J. T. and Berner, R. A.: The role of sedimentary organic matter in bacterial sulfate reduction: the G model tested, Limnol. Oceanogr., 29, 236–249, 1984.

Wichlacz, P. L. and Unz, R. F.: Growth kinetics of attached iron-oxidizing bacteria., Appl. Environ. Microb., 50, 460–467, 1985.

Bibliography

[1] Bush, T., Butler, I. B., Free, A., and Allen, R. J. Redox regime shifts in microbially-mediated biogeochemical cycles. *Biogeosciences*, 12:3713–3724, 2015. doi: 10.5194/bg-12-3713-2015.

[2] Bluth, G. J. S., Schnetzler, C. C., Krueger, A. J., and Walter, L. S. The contribution of explosive volcanism to global atmospheric sulphur dioxide concentrations. *Nature*, 366:327–329, 1993. doi: 10.1038/366327a0.

[3] Liu, Z. and Zhou, J. Contribution of carbonate rock weathering to the atmospheric CO2 sink. *Environ. Geol.*, 39(9):1053–1058, 2000. doi: 10.1007/s002549900072.

[4] Falkowski, P. G., Fenchel, T., and Delong, E. F. The microbial engines that drive Earth's biogeochemical cycles. *Science*, 320(5879):1034–1039, May 2008. doi: 10.1126/science.1153213.

[5] Madigan, M. T., Martinko, J. M., Dunlap, P. V., and Clark, D. P. *Brock Biology of Microorganisms*. Pearson Education Inc, San Francisco, 12th edition, 2009.

[6] Fenchel, T., King, G. M., and Blackburn, T. H. *Bacterial Biogeochemistry: The Ecophysiology of Mineral Cycling*. Elsevier, San Diego, 1998.

[7] Karl, D., Michaels, A., Bergman, B., and Capone, D. Dinitrogen fixation in the worlds oceans. *Biogeochemistry*, 57:47–98, 2002. doi: 10.1007/978-94-017-3405-9_2.

[8] Aguilos, M., Takagi, K., Liang, N., Watanabe, Y., Teramoto, M., Goto, S., Takahashi, Y., Mukai, H., and Sasa, K. Sustained large stimulation of soil heterotrophic respiration rate and its temperature sensitivity by soil warming in a cool-temperate forested peatland. *Tellus. B. Chem. Phys. Meteorol.*, 65, 2013. doi: 10.3402/tellusb.v65i0.20792.

[9] Pikuta, E. V., Hoover, R. B., and Tang, J. Microbial extremophiles at the limits of life. *Crit. Rev. Microbiol.*, 33(3):183–209, 2007. doi: 10.1080/10408410701451948.

[10] Parkes, R. J., Cragg, B. A., Bale, S. J., Getlifff, J. M., Goodman, K., Rochelle, P. A., Fry, J. C., Weightman, A. J., and Harvey, S. M. Deep bacterial biosphere in Pacific Ocean sediments. *Nature*, 371(6496):410—-413, 1994. doi: 10.1038/371410a0.

[11] Wadham, J. L., Arndt, S., Tulaczyk, S., Stibal, M., Tranter, M., Telling, J., Lis, G. P., Lawson, E., Ridgwell, A., Dubnick, A., Sharp, M. J., Anesio, A. M., and Butler, C. E. H. Potential methane reservoirs beneath Antarctica. *Nature*, 488(7413):633–637, 2012. doi: 10.1038/nature11374.

[12] Harmsen, H. J. M., Prieur, D., and Jeanthon, C. Distribution of microorganisms in deep-sea hydrothermal vent chimneys investigated by whole-cell hybridization and enrichment culture of thermophilic subpopulations. *Appl. Environ. Microbiol.*, 63(7):2876–2883, 1997.

[13] O'Malley, M. A. 'Everything is everywhere: but the environment selects': ubiquitous distribution and ecological determinism in microbial biogeography. *Stud. Hist. Philos. Biol. Biomed. Sci.*, 39(3):314–25, 2008. doi: 10.1016/j.shpsc.2008.06.005.

[14] Brooks, S. C., Fredrickson, J. K., Carroll, S. L., Kennedy, D. W., Zachara, J. M., Plymale, A. E., Kelly, S. D., Kemner, K. M., and Fendorf, S. Inhibition of bacterial U(VI) reduction by calcium. *Environ. Sci .Technol.*, 37(9):1850–1858, 2003. doi: 10.1021/es0210042.

[15] Hu, H., Lin, H., Zheng, W., Tomanicek, S. J., Johs, A., Feng, X., Elias, D. A., Liang, L., and Gu, B. Oxidation and methylation of dissolved elemental mercury by anaerobic bacteria. *Nat. Geosci.*, 6(9):751–754, 2013. doi: 10.1038/ngeo1894.

[16] Dar, S. A., Stams, A. J. M., Kuenen, J. G., and Muyzer, G. Co-existence of physiologically similar sulfate-reducing bacteria in a full-scale sulfidogenic bioreactor fed with a single organic electron donor. *Appl. Microbiol. Biotechnol.*, 75(6):1463–72, 2007. doi: 10.1007/s00253-007-0968-y.

[17] Rothman, D. H. and Al, E. Methanogenic burst in the end-Permian carbon cycle. *Proc. Natl. Acad. Sci. USA.*, 111(15):5462–7, 2014. doi: 10.1073/pnas.1318106111.

[18] Canfield, D. E., Ngombi-Pemba, L., Hammarlund, E. U., Bengtson, S., Chaussidon, M., Gauthier-Lafaye, F., Meunier, A., Riboulleau, A., Rollion-Bard, C., Rouxel, O., Asael, D., Pierson-Wickmann, A. C., and El Albani, A. Oxygen dynamics in the aftermath of the Great Oxidation of Earth's atmosphere. *Proc. Natl. Acad. Sci. USA.*, 110(42):16736–16741, October 2013. ISSN 1091-6490. doi: 10.1073/pnas.1315570110.

[19] Rosing, M. T., Bird, D. K., Sleep, N. H., Glassley, W., and Albarede, F. The rise of continentsAn essay on the geologic consequences of photosynthesis. *Palaeogeogr. Palaeoclimatol. Palaeoecol.*, 232(2-4):99–113, March 2006. ISSN 00310182. doi: 10.1016/j.palaeo.2006.01.007.

[20] Benton, M. J. and Twitchett, R. J. How to kill (almost) all life: the end-Permian extinction event. *Trends. Ecol. Evol.*, 8(7):358,365, 2003. doi: 10.1016/s0169-5347(03)00093-4.

[21] Petsch, S. T. *The Global Oxygen Cycle*, volume 8. Elsevier, 2003.

[22] Shaffer, G., Olsen, S. M., and Pedersen, J. O. P. Long-term ocean oxygen depletion in response to carbon dioxide emissions from fossil fuels. *Nat. Geosci.*, 2(2):105–109, 2009. doi: 10.1038/ngeo420.

[23] Allison, S. D., Wallenstein, M. D., and Bradford, M. A. Soil-carbon response to warming dependent on microbial physiology. *Nat. Geosci.*, 3:336–340, 2010. doi: 10.1038/ngeo846.

[24] IPPC. Climate change 2013: The physical science basis. Chapter 6: Carbon and other biogeochemical cycles. pages 465–570, 2013.

[25] Todd-Brown, K. E. O., Hopkins, F. M., Kivlin, S. N., Talbot, J. M., and Allison, S. D. A framework for representing microbial decomposition in coupled climate models. *Biogeochemistry*, 109:19–33, 2012. doi: 10.1007/s10533-011-9635-6.

[26] Westrich, J. T. and Berner, R. A. The role of sedimentary organic matter in bacterial sulfate reduction: The G model tested. *Limnol. Oceanogr.*, 29 (2):236–249, 1984. doi: 10.4319/lo.1984.29.2.0236.

[27] Editorial article, A golden age for microbiol ecology. *Nat. Rev. Microbiol.*, 6, 2008.

[28] McCann, K. S. The diversity-stability debate. *Nature*, 405(6783), 2000. doi: 10.1038/35012234.

[29] Naeem, S. and Li, S. Biodiversity enhances ecosystem reliability. *Nature*, 390:507–509, 1997.

[30] Becker, J., Eisenhauer, N., Scheu, S., and Jousset, A. Increasing antagonistic interactions cause bacterial communities to collapse at high diversity. *Ecol. Lett.*, 15:468–474, 2012. doi: 10.1111/j.1461-0248.2012.01759.x.

[31] Goldblatt, C., Lenton, T. M., and Watson, A. J. Bistability of atmospheric oxygen and the Great Oxidation. *Nature*, 443:683–686, 2006. doi: 10.1038/nature05169.

[32] Kump, L. R., Pavlov, A., and Arthur, M. A. Massive release of hydrogen sulphide to the surface ocean and atmosphere during intervals of ocean anoxia. *Geology*, 33(5):397–400, 2005. doi: 10.1130/g21295.1.

[33] Bergman, N. M., Lenton, T. M., and Watson, A. J. COPSE: A new model of biogeochemical cycling over Phanerozoic time. *Am. J. Sci.*, 304(5):397–437, 2004. doi: 10.2475/ajs.304.5.397.

[34] Berner, R. A. and Kothavala, Z. GEOCARB III: A revised model of atmospheric CO2 over phanerozoic time. *Am. J. Sci.*, 301(2):182–204, 2001. doi: 10.2475/ajs.301.2.182.

[35] Cox, P. M., Betts, R. A., and et al. Jones, C. D. Acceleration of global warming due to carbon-cycle feedbacks in a coupled climate model. *Nature*, 408(6809):184–187, 2000.

[36] Bodirsky, B. L., Popp, A., Weindl, I., Dietrich, J. P., Rolinski, S., Scheiffele, L., Schmitz, C., and Lotze-Campen, H. N2O emissions from the global agricultural nitrogen cycle - current state and future scenarios. *Biogeosciences*, 9(10):4169–4197, 2012. doi: 10.5194/bg-9-4169-2012.

[37] Bethke, C. M., Ding, D., Jin, Q., and Sanford, R. A. Origin of microbiological zoning in groundwater flows. *Geology*, 36(9):739–742, 2008. doi: 10.1130/G24859A.1.

[38] Canfield, D. E. Models of oxic respiration, denitrification and sulfate reduction in zones of coastal upwelling. *Geochim. Cosmochim. Acta.*, 70 (23):5753–5765, 2006. doi: 10.1016/j.gca.2006.07.023.

[39] Marinov, I. and Sarmiento, J. L. The role of the oceans in the global carbon cycle: An overview. In Follows, M. and Oguz, T., editors, *Ocean Carbon Cycle and Climate*, pages 251–295. Kluwer academic publishers, Norwell, Massachusetts, 2004.

[40] Broecker, W. S. and Peng, T. H. Glacial to interglacial changes in the operation of the global carbon-cycle. *Radiocarbon*, 28(2A):309–327, 1986.

[41] Galloway, e. a., J. N. The Nitrogen Cascade. *Bioscience*, 53(4):341–356, 2003.

[42] Monod, J. The growth of bacterial cultures. *Ann. Rev. Microbiol*, 3, 1949.

[43] Moore, J. K., Doney, S. C., Kleypas, J. A., Glover, D. M., and Fung, I. Y. An intermediate complexity marine ecosystem model for the global domain. *Deep Sea Res. Part 2 Top. Stud. Oceanogr.*, 49(1-3):403–462, 2002. doi: 10.1016/s0967-0645(01)00108-4.

[44] Knorr, W. Annual and interannual CO2 exchanges of the terrestrial biosphere: process-based simulations and uncertainties. *Global Ecol. Biogeogr.*, 9(3):225–252, 2000. doi: 10.1046/j.1365-2699.2000.00159.x.

[45] Todd-Brown, K. E. O., Randerson, J. T., Post, W. M., Hoffman, F. M., Tarnocai, C., Schuur, E. A. G., and Allison, S. D. Causes of variation in soil carbon simulations from CMIP5 Earth system models and comparison with observations. *Biogeosciences*, 10(3):1717–1736, 2013. doi: 10.5194/bg-10-1717-2013.

[46] Friedlingstein, P., Cox, A. P., Betts, B. R., Bopp, C. L., Von Bloh, A. W., Brovkin, D. V., Cadule, D. P., Doney, E. S., Eby, F. M., Fung, G. I., Bala, H. G., John, I. J., Jones, H. C., Joos, C. F., Kato, J. T., Kawamiya, K. M., Knorr, K. W., Lindsay, L. K., Matthews, M. H. D., Raddatz, G. N. T., Rayner, O. P., Reick, A. C., Roeckner, O. E., Schnitzler, P. K. G., Schnur, P. R., Strassmann, P. K., Weaver, J. A. J., Yoshikawa, G. C., and Zengq, N. Climate-carbon cycle feedback analysis: Results from the (CMIP)-M-4 model intercomparison. *J. Clim.*, 19(4):3337–3353, 2006. doi: 10.1175/jcli3800.1.

[47] Schimel, J. Soil carbon: Microbes and global carbon. *Nat. Clim. Chang.*, 3(10):867–868, 2013. doi: 10.1038/nclimate2015.

[48] William, R. W., Bonan, G. B., and Allison, S. D. Global soil carbon projections are improved by modelling microbial processes. *Nat. Clim. Chang.*, 3(10):909 –912, 2013. doi: 10.1038/nclimate1951.

[49] Lawrence, C. R., Neff, J. C., and Schimel, J. P. Does adding microbial mechanisms of decomposition improve soil organic matter models? A comparison of four models using data from a pulsed rewetting experiment. *Soil Biol. Biochem.*, 41:1923–1934, 2009. doi: 10.1016/j.soilbio.2009.06.016.

[50] Huisman, J., Pham Thi, N., Karl, D. M., and Sommeijer, B. Reduced mixing generates oscillations and chaos in the oceanic deep chlorophyll maximum. *Nature*, 439(7074):322–5, 2006. doi: 10.1038/nature04245.

[51] Treseder, K. K., Balser, T. C., Bradford, M. A., Brodie, E. L., Dubinsky, E. A., Eviner, V. T., Hofmockel, K. S., Lennon, J. T., Levine, U. Y., MacGregor, B. J., Pett-Ridge, J., and Waldrop, M. P. Integrating microbial ecology into ecosystem models: challenges and priorities. *Biogeochemistry*, 109(1-3):7–18, 2011. doi: 10.1007/s10533-011-9636-5.

[52] Herbert, D., Elsworth, R., and Telling, R. C. The Continuous Culture of Bacteria; a Theoretical and Experimental Study. *J. Gen. Microbiol.*, 14(3): 601–622, 1956. doi: 10.1099/00221287-14-3-601.

[53] Contois, D. E. Kinetics of bacterial growth: relationship between population density and specific growth rate of continuous cultures. *J. Gen. Microbiol.*, 21:40–50, 1959. doi: 10.1099/00221287-21-1-40.

[54] Ingraham, J. L., Maaloe, O., and Neidhardt, F. C. *Growth of the Bacterial Cell*. Sinauer Associates, Sunderland, Mass, 1983.

[55] Mills, C. M., M. M. and. Moore, Langlois, R., Milne, A., Achterberg, E., Nachtigall, K., Lochte, K., Geider, R. J., and LaRoche, J. Nitrogen and phosphorus co-limitation of bacterial productivity and growth in the oligotrophic subtropical North Atlantic. *Limnol. Oceanogr.*, 53(2):824–834, 2008. doi: 10.4319/lo.2008.53.2.0824.

[56] Megee, R. D., Drake, J. F., Frederick, A. G., and Tsuchiya, H. M. Studies in intermicrobial symbiosis Saccharomyces cerevisiae and Lactobacillus casei. *Can. J. Microbiol.*, 18(11):1733–1742, 1972. doi: 10.1139/m72-269.

[57] Jin, Q. and Bethke, C. M. Predicting the rate of microbial respiration in geochemical environments. *Geochim. Cosmochim. Acta.*, 69(5):1133–1143, 2005.

[58] Droop, M. R. The nutrient status of algal cells in continuous culture. *J. Mar. Biol. Assoc. U.K.*, 54(4):825–855, 1974. doi: 10.1017/s002531540005760x.

[59] Rhee, G. Y. Effects of N:P atomic ratios and nitrate limitation on algal growth, cell composition, and nitrate uptake. *Limnol. Oceanogr.*, 23(1): 10–25, 1978. doi: 10.4319/lo.1978.23.1.0010.

[60] Klausmeier, C. A., Litchman, E., and A., L. S. Phytoplankton growth and stoichiometry under multiple nutrient limitation. *Limnol. Oceanogr.*, 49(4): 1463–1470, 2004. doi: 10.4319/lo.2004.49.4_part_2.1463.

[61] Saito, M., Goepfert, T. J., and Ritt, J. Some thoughts on the concept of colimitation: Three definitions and the importance of bioavailability. *Limnol. Oceanogr.*, 53(1):276–290, 2008. doi: 10.4319/lo.2008.53.1.0276.

[62] Hibbing, M. E., Fuqua, C., Parsek, M. R., and Peterson, S. B. Bacterial competition: surviving and thriving in the microbial jungle. *Nat. Rev. Microbiol.*, 8(1):15–25, 2010. doi: 10.1038/nrmicro2259.

[63] Marino, S., Baxter, N. T., Huffnagle, G. B., Petrosino, J. F., and Schloss, P. D. Mathematical modeling of primary succession of murine intestinal microbiota. *Proc. Natl. Acad. Sci. USA.*, 111:1–6, 2013. ISSN 1091-6490. doi: 10.1073/pnas.1311322111.

[64] Jones, S. E. and Lennon, J. T. Dormancy contributes to the maintenance of microbial diversity. *Proc. Natl. Acad. Sci. USA.*, 107(13):5881–6, March 2010. ISSN 1091-6490.

[65] Berry, D. and Widder, S. Deciphering microbial interactions and detecting keystone species with co-occurrence networks. *Front. Microbiol.*, 5(May): 219, January 2014. ISSN 1664-302X. doi: 10.3389/fmicb.2014.00219.

[66] Jin, Q. and Bethke, C. M. The thermodynamics and kinetics of microbial metabolism. *Am. J. Sci.*, 307(4):643–677, 2007. doi: 10.2475/04.2007.01.

[67] Jin, Q. and Bethke, C. M. A new rate law describing microbial respiration. *Appl. Environ. Microbiol.*, 69(4):2340–2348, 2003. doi: 10.1128/AEM.69.4.2340-2348.2003.

[68] Alberts, B., Johnson, A., Lewis, J., Raff, M., Roberts, K., and Walter, P. *Molecular Biology of the Cell*. Garland Science, New York, 5 edition, 2008.

[69] Boudart, M. Consistency between kinetics and thermodynamics. *J. Phys. Chem.*, 80(26):2869–2870, 1976. ISSN 00092509. doi: 10.1016/0009-2509(67)80056-3.

[70] Strogatz, S. H. *Nonlinear Dynamics and Chaos*. Westview Press, Cambridge MA, 2000.

[71] Press, W. H., Teukolsky, S. A., Vetterling, W. T., and Flannery, B. P. *Numerical Recipes: The Art of Scientific Computing*. Cambridge University Press, 3 edition, 1983.

[72] Shendure, J. and Lieberman Aiden, E. The expanding scope of DNA sequencing. *Nat. Biotechnol.*, 30(11):1084–94, 2012. ISSN 1546-1696. doi: 10.1038/nbt.2421.

[73] Nielsen, U. N., Ayres, E., Wall, D. H., and Bardgett, R. D. Soil biodiversity and carbon cycling: a review and synthesis of studies examining diversity-function relationships. *Eur. J. Soil Sci.*, 62(1):105–116, 2011. doi: 10.1111/j.1365-2389.2010.01314.x.

[74] Pace, N. R. A molecular view of microbial diversity and the biosphere. *Science*, 276(5313):734 –40, 1997. doi: 10.1126/science.276.5313.734.

[75] Tan, S. C. and Yiap, B. C. DNA, RNA, and protein extraction: The past and the present. *J. Biomed. Biotechnol.*, 2009, 2009. doi: 10.1155/2009/574398.

[76] Raes, J., Korbel, J. O., Lercher, M. J., and Von Mering, P., C.and Bork. Prediction of effective genome size in metagenomic samples. *Genome Biol.*, 8(1):R10, 2007. doi: 10.1186/gb-2007-8-1-r10.

[77] Loman, N. J., Misra, R. V., Dallman, T. J., Constantinidou, C., Gharbia, S. E., Wain, J., and Pallen, M. J. Performance comparison of benchtop high-throughput sequencing platforms. *Nat. Biotechnol.*, 30(5), 2012. doi: 10.1038/nbt.2198.

[78] Venter, J. C., Remington, K., Heidelberg, J. F., Halpern, A. L., Rusch, D., Eisen, J. A., Wu, D., Paulsen, I., Nelseon, K. E., Nelson, W., Fouts, D. E., Levy, S., Knap, A. H., Lomas, M. W., Nelson, K., White, O., Peterson, J., Hoffman, J., Parsons, R., Baden-Tillson, H., Pfannkoch, C., Rogers, Y. H., and Smith, H. O. Environmental genome shotgun sequencing of the Sargasso Sea. *Science*, 304(5667):66–74, 2004. doi: 10.1126/science.1093857.

[79] Tringe, S. G. and Hugenholtz, P. A renaissance for the pioneering 16S rRNA gene. *Curr. Opin. Microbiol.*, 11(5):442–446, 2008. doi: 10.1016/j.mib.2008.09.011.

[80] Huse, S. M., Dethlefsen, L., Huber, J. A., Welch, D. M., Relman, D. A., and Sogin, M. L. Exploring microbial diversity and taxonomy using SSU rRNA hypervariable tag sequencing. *PLoS Genet.*, 4(11), 2008. doi: 10.1371/journal.pgen.1000255.

[81] Balch, W. E., Magrum, L. J., Fox, G. E., Wolfe, R. S., and Woese, C. R. An ancient divergence among the bacteria. *J. Mol. Evol.*, 9:305–311, 1977. doi: 10.1007/BF01796092.

[82] Woese, C. R. Bacterial Evolution. *Microbiology.*, 51(2):221–271, 1987. doi: 10.1139/m88-093.

[83] Bartlett, J. M. S. and Stirling, D. A short history of the polymerase chain reaction. In Bartlett, J. M. S. and Stirling, D., editors, *PCR Protocols*, volume 226. Humana Press Inc., Totowa. New Jersey, 2 edition, 2003. ISBN 0896036421.

[84] Schematic drawing of the PCR cycle., 2015. URL `http://commons.wikimedia.org/wiki/File:Polymerase_chain_reaction.svg`.

[85] Wang, G. C. Y. and Wang, Y. Frequency of formation of chimeric molecules as a consequence of PCR coamplification of 16S rRNA genes from mixed bacterial genomes. *Appl. Environ. Microbiol.*, 63(12):4645–4650, 1997. doi: 10.1099/13500872-142-5-1107.

[86] Caporaso, J. G., Kuczynski, J., Stombaugh, J., Bittinger, K., Bushman, F. D., Costello, E. K., Fierer, N., Peña, A. G., Goodrich, J. K., Gordon, J. I., Huttley, G. A., Kelley, S. T., Knights, D., Koenig, J. E., Ley, R. E., Lozupone, C. A., Mcdonald, D., Muegge, B. D., Pirrung, M., Reeder, J., Sevinsky, J. R., Turnbaugh, P. J., Walters, W. A., Widmann, J., Yatsunenko, T., Zaneveld, J., and Knight, R. QIIME allows analysis of high-throughput community sequencing data. *Nat. Methods*, 7(5):335–336, 2010. ISSN 1548-7091. doi: 10.1038/nmeth0510-335.

[87] Navas-Molina, J. A., Peralta-Sánchez, J. M., González, A., McMurdie, P. J., Vázquez-Baeza, Y., Xu, Z., Ursell, L. K., Lauber, C., Zhou, H., Song, S. J., Huntley, J., Ackermann, G. L., Berg-Lyons, D., Holmes, S., Caporaso, J. G., and Knight, R. Advancing our understanding of the human microbiome using QIIME. *Methods in Enzymology*, 531:371–444, 2013. doi: 10.1016/B978-0-12-407863-5.00019-8.

[88] Balzer, S., Malde, K., and Jonassen, I. Systematic exploration of error sources in pyrosequencing flowgram data. *Bioinformatics*, 27:304–309, 2011. doi: 10.1093/bioinformatics/btr251.

[89] Quince, C., Lanzen, A., Davenport, R. J., and Turnbaugh, P. J. Removing noise from pyrosequenced amplicons. *BMC bioinformatics.*, 12(1):38, 2011. doi: 10.1186/1471-2105-12-38.

[90] Haas, B. J., Gevers, D., Earl, A. M., Feldgarden, M., Ward, D. V., Giannoukos, G., Ciulla, D., Tabbaa, D., Highlander, S. K., Sodergren, E., Methé, B., DeSantis, T. Z., Petrosino, J. F., Knight, R., and Birren, B. W. Chimeric 16S rRNA sequence formation and detection in Sanger and 454-pyrosequenced PCR amplicons. *Genome Res.*, 21:494–504, 2011. doi: 10.1101/gr.112730.110.

[91] McMurdie, P. J. and Holmes, S. Waste Not, Want Not: Why Rarefying Microbiome Data Is Inadmissible. *PLoS Comput. Biol.*, 10(4), 2014. doi: 10.1371/journal.pcbi.1003531.

[92] Pedrós-Alió, C. Marine microbial diversity: can it be determined? *Trends Microbiol.*, 14(6):257–263, 2006. doi: 10.1016/j.tim.2006.04.007.

[93] Whittaker, R. J., Willis, K. J., and Field, R. Scale and species richness : towards a general, hierarchical theory of species diversity. *Diversity.*, 28: 453–470, 2001. doi: 10.1046/j.1365-2699.2001.00563.x.

[94] Clarke, K. R. and Warwick, R. M. *Change in Marine Communities: An Approach to Statistical Analysis.* Plymouth, UK, 2nd edition, 2001.

[95] Hill, T. C. J., Walsh, K. A., Harris, J. A., and Moffett, B. F. Using ecological diversity measures with bacterial communities. *FEMS. Microbiol. Ecol.*, 43: 1–11, 2003. doi: 10.1016/s0168-6496(02)00449-x.

[96] Stevens, H. and Ulloa, O. Bacterial diversity in the oxygen minimum zone of the eastern tropical South Pacific. *Environ. Microbiol.*, 10(5):1244–1259, May 2008. doi: 10.1111/j.1462-2920.2007.01539.x.

[97] Mikucki, J. A. and Priscu, J. C. Bacterial Diversity Associated with Blood Falls , a Subglacial Outflow from the Taylor Glacier , Antarctica. *Appl. Environ. Microbiol.*, 73(12):4029–4039, 2007. doi: 10.1128/AEM.01396-06.

[98] Kuczynski, J., Liu, Z., Lozupone, C., McDonald, D., Fierer, N., and Knight, R. Microbial community resemblance methods differ in their ability to detect biologically relevant patterns. *Nat. Methods*, 7(10):813–U67, 2010. doi: 10.1038/nmeth.1499.

[99] Anderson, M. J.

[100] Hanson, T. E., Luther, G. W., Findlay, A. J., MacDonald, D. J., and Hess, D. Phototrophic sulfide oxidation: environmental insights and a method for kinetic analysis. *Front. Microbiol.*, 4(382), 2013. doi: 10.3389/fmicb.2013.00382.

[101] Luther, G. W., Rozan, T. F., Taillefert, M., Nuzzio, D. B., Di Meo, C., Shank, T. M., Lutz, R. A., and Cary, S. C. Chemical speciation drives hydrothermal vent ecology. *Nature*, 410:813–816, 2001. doi: 10.1038/35071069.

[102] Gundersen, J. K., Jorgensen, B. B., Larsen, E., and Jannasch, H. W. Mats of giant sulphur bacteria on deep-sea sediments due to fluctuating hydrothermal flow. *Nature*, 360(6403):454–456, 1992. doi: 10.1038/360454a0.

[103] Brendel, P. J. and Luther, G. W. Determination of metal (bi)sulfide stability constants of Mn2+, Fe2+, Co2+, Ni2+, Cu2+ and Zn2+ by voltammetric methods. *Environ. Sci. Technol.*, 30:671–679, 1996. doi: 10.1021/es950417i.

[104] Luther, G. W., Brendel, P. J., Lewis, B. L., Sundby, B., Lefrançois, L., Silverberg, N., and Nuzzio, D. B. Simultaneous measurement of O2, Mn, Fe, I-, and S(-II) in marine pore waters with a solid-state voltammetric microelectrode. *Limnol. Oceanogr.*, 43:325–333, 1998. doi: 10.4319/lo.1998.43.2.0325.

[105] Luther, G. W., Glazer, B. T., Ma, S., Trouwborst, R. E., Moore, T. S., Metzger, E., Kraiya, C., Waite, T. J., Druschel, G., Sundby, B., Taillefert, M., Nuzzio, D. B., Shank, T. M., Lewis, B. L., and Brendel, P. J. Use of voltammetric solid-state (micro)electrodes for studying biogeochemical processes: Laboratory measurements to real time measurements with an in situ electrochemical analyzer (ISEA). *Mar. Chem.*, 108(3-4):221–235, January 2008. doi: 10.1016/j.marchem.2007.03.002.

[106] Brendel, P. J. and Luther, G. W. Development of a gold amalgam voltammetric microelectrode for the determination of dissolved Fe, Mn, O2 and S(-II) in porewaters of marine and freshwater sediments. *Environ. Sci. Technol.*, 29:751–761, 1995. doi: 10.1021/es00003a024.

[107] Sirota, J., Baiser, B., Gotelli, N. J., and Ellison, A. M. Organic-matter loading determines regime shifts and alternative states in an aquatic ecosystem. *Proc. Natl Acad. Sci. USA.*, 110:7742–7747, April 2013. ISSN 1091-6490.

[108] Higgins, S. I. and Scheiter, S. Atmospheric CO2 forces abrupt vegetation shifts locally, but not globally. *Nature*, 488(7410):209–12, August 2012. ISSN 1476-4687.

[109] Scheffer, M., Bascompte, J., Brock, W. A., Brovkin, V., Carpenter, S. R., Dakos, V., Held, H., Van Nes, E. H., Rietkerk, M., and Sugihara, G. Early-warning signals for critical transitions. *Nature*, 461:53–59, 2009. doi: 10.1038/nature08227.

[110] Galloway, J. N., Dentener, F. J., Capone, D. G., Boyer, E. W., Howarth, R. W., Seitzinger, S. P., Asner, G. P., Cleveland, C. C., Green, P. A., Holland, E. A., Karl, D. M., Michaels, A. F., Porter, J. H., Townsend, A. R., and Vorosmarty, C. J. Nitrogen Cycles: Past, Present and Future. *Biogeochemistry*, 70(2):153–226, 2004. doi: 10.1007/s10533-004-0370-0.

[111] Canfield, D. E., Thamdrup, B., and Kristensen, E. Aquatic Geomicrobiology. *Adv. Mar. Biol.*, 48:347–357, 2005.

[112] López-Urrutia, A., San Martin, E., Harris, R. P., and Irigoien, X. Scaling the metabolic balance of the oceans. *Proc. Natl. Acad. Sci. USA.*, 103(23): 8739–8744, June 2006. ISSN 0027-8424.

[113] Conant, R. T., Ryan, M. G., A., G. I., Birge, H. E., Davidson, E. A., Eliasson, P. E., Evans, S. E., Frey, S. D., Giardina, C. P., Hopkins, F. M., Hyvönen, R., Kirschbaum, M. U. F., Lavallee, J. M., Leifeld, J., Parton, W. J., Megan Steinweg, J., Wallenstein, M. D., Martin Wetterstedt, J. A., and Bradford, M. A. Temperature and soil organic matter decomposition rates - synthesis of current knowledge and a way forward. *Glob. Chang. Biol.*, 17(11):3392–3404, 2011. doi: 10.1111/j.1365-2486.2011.02496.x.

[114] Canfield, D. E. Reactive iron in marine sediments. *Geochim. Cosomochim. Ac.*, 53:619–632, 1989. doi: 10.1016/0016-7037(89)90005-7.

[115] Goldhaber, M. B. Sulfur-rich sediments. In Mackenzie, F. T., Holland, H. D., and Turekian, K. K., editors, *Treatise on Geochemistry Volume 7*, pages 257–288. Elsevier, Amsterdam, 2003.

[116] Schoonen, M. A. A. and Strongin, D. R. Catalysis of electron transfer reactions at mineral surfaces. In Grassian, V., editor, *Environmental Catalysis*, pages 37–60. CRC Press, Boca Raton, 2005.

[117] Roden, E. E. Analysis of long-term bacterial vs. chemical Fe(III) oxide reduction kinetics. *Geochim. Cosomochim. Ac.*, 68(15):3205–3216, 2004. doi: 10.1016/j.gca.2004.03.028.

[118] Naidja, A. and Huang, P. M. Significance of the HenriMichaelisMenten theory in abiotic catalysis: catechol oxidation by δ-MnO2. *Surf. Sci.*, 506 (1-2):L243–L249, 2002. doi: 10.1016/s0039-6028(02)01375-4.

[119] Ingvorsen, K., Zehnder, A. J. B., and Jorgensen, B. B. Kinetics of Sulfate and Acetate Uptake by Desulfobacter postgatei. *Appl. Environ. Microbiol.*, 47(2):403–8, February 1984. doi: 10.1007/bf00692713.

[120] Jin, Q., Roden, E. E., and Giska, J. R. Geomicrobial Kinetics: Extrapolating Laboratory Studies to Natural Environments. *Geomicrobiol. J.*, 30(2):173–185, 2013. doi: 10.1080/01490451.2011.653084.

[121] Goldbeter, A. and Koshland, D. E. Sensitivity amplification in biochemical systems. *Q. Rev. Biophys*, 15:555–591, 1982.

[122] Alberghina, L., Höfer, T., and Vanoni, M. Molecular networks and system-level properties. *J. Biotechnol.*, 144(3):224–33, 2009. doi: 10.1016/j.jbiotec.2009.07.009.

[123] Goldbeter, A. and Koshland, D. E. An amplified sensitivity arising from covalent modification in biological systems. *Proc. Natl Acad. Sci. USA*, 78: 6840–6844, 1981. doi: 10.1073/pnas.78.11.6840.

[124] Klok, J. B. M., De Graaff, M., Van Den Bosch, P. L. F., Boelee, N. C., Keesman, K. J., and Janssen, A. J. H. A physiologically based kinetic model for bacterial sulfide oxidation. *Water Res.*, 47(2):483–492, 2012. doi: 10.1016/j.watres.2012.09.021.

[125] González-Sánchez, A. and Revah, S. The effect of chemical oxidation on the biological sulfide oxidation by an alkaliphilic sulfoxidizing bacterial consortium. *Enzyme. Microb. Tech.*, 40(2):292–298, 2007. doi: 10.1016/j.enzmictec.2006.04.017.

[126] Ingvorsen, K. and Jorgensen, B. B. Kinetics of sulfate uptake by freshwater and marine species of Desulfovibrio. *Arch. Microbiol.*, 139:61–66, 1984. doi: 10.1007/bf00692713.

[127] Kristjansson, J. K., Schonheit, P., and Thauer, R. Different Ks values for hydrogen of methanogenic bacteria and sulfate reducing bacteria: An explanation for the apparent inhibition of methanogenesis by sulfate. *Arch. Microbiol.*, 131:278–282, 1982. doi: 10.1007/bf00405893.

[128] Lovely, D. R., Dwyer, D. F., and Klug, M. J. Kinetic analysis of competition between sulfate reducers and methanogens for hydrogen in sediments. *Appl. Environ. Microbiol.*, 43:1373–1379, 1982.

[129] Aiba, S. Growth kinetics of photosyntheic microorganisms. *Adv. Biochem. Eng.*, 23:85–156, 1982. doi: 10.1007/3540116982_3.

[130] Schou, C., Rasmussen, G., Kaltoft, M. B., Henrissat, B., and Schulein, M. Stereochemistry, specificity and kinetics of the hydrolysis of reduced cellodextrins by nine cellulases. *Eur. J. Biochem.*, 217:947–953, 1993. doi: 10.1111/j.1432-1033.1993.tb18325.x.

[131] Amore, A., Pepe, O., Ventorino, V., Birolo, L., Giangrande, C., and Faraco, V. Cloning and recombinant expression of a cellulase from the cellulolytic strain Streptomyces sp G12 isolated from compost. *Microb. Cell. Fact.*, 111 (164), 2012. doi: 10.1186/1475-2859-11-164.

[132] Osborne, B. A. and Geider, R. J. The minimum photon requirement for photosynthesis. *New Phytol.*, 106:631–645, 1987.

[133] Hu, Z. H., Wang, G., and Yu, H. Q. Anaerobic degradation of cellulose by rumen microorganisms at various pH values. *Biochem. Eng. J.*, 21(1): 59–62, 2004. doi: 10.1016/j.bej.2004.05.004.

[134] Demoling, F., Figueroa, D., and Baath, E. Comparison of factors limiting bacterial growth in different soils. *Soil. Biol. Biochem.*, 39(10):2485–2495, 2007. doi: 10.1016/j.soilbio.2007.05.002.

[135] Canfield, D. E. A new model for Proterozoic ocean chemistry. *Nature*, 396: 450–453, 1998.

[136] O. G. Berg, J. P. . M. E. Fluctuations and Quality of Control in Biological Cells: Zero-Order Ultrasensitivity Reinvestigated. *Biophysical Journal*, 79: 1228–1236, 2000.

[137] Muyzer, G. and Stams, A. J. M. The ecology and biotechnology of sulphate-reducing bacteria. *Nat. Rev. Microbiol.*, 6:441–454, 2008. doi: 10.1038/nrmicro1892.

[138] Roden, E. E. and Wetzel, R. G. Competition between Fe(III)-reducing and methanogenic bacteria for acetate in iron-rich freshwater sediments. *Microb. Ecol.*, 45(3):252–8, 2003. doi: 10.1007/s00248-002-1037-9.

[139] Diaz, R. J. and Rosenberg, R. Spreading dead zones and consequences for marine ecosystems. *Science*, 321(5891):926–9, 2008. doi: 10.1126/science.1156401.

[140] Kamyshny, A., Zerkle, A. L., Mansaray, Z. F., Ciglenečki, I., Bura-Nakić, E., Farquhar, J., and Ferdelman, T. G. Biogeochemical sulfur cycling in the water column of a shallow stratified sea-water lake: Speciation and quadruple sulfur isotope composition. *Mar. Chem.*, 127(1-4):144–154, 2011. ISSN 03044203. doi: 10.1016/j.marchem.2011.09.001.

[141] Wichlacz, P. L. and Unz, R. F. Growth kinetics of attached iron-oxidizing bacteria. *Appl. Environ. Microbiol.*, 50(2):460–467, 1985.

[142] Landing, W. M. and Bruland, K. W. The contrasting biogeochemistry of iron and manganese in the Pacific Ocean. *Geochim. Cosomochim. Ac.*, 51 (1):29–43, 1987. doi: 10.1016/0016-7037(87)90004-4.

[143] Canfield, D. E., Thamdrup, B., and Hansen, J. W. The anaerobic degradation of organic matter in Danish coastal sediments: Iron reduction, manganese reduction and sulfate reduction. *Geochim. Cosomochim. Ac.*, 57(16):3867–3883, 1993. doi: 10.1016/0016-7037(93)90340-3.

[144] Bonneville, S., Van Cappellen, P., and Behrends, T. Chapter II. *Chem. Geol.*, 212(Iii):255–268, 2004.

[145] Thamdrup, B. and Canfield, D. E. Pathways of carbon oxidation in continental margin sediments off central Chile. *Limnol. Oceanogr.*, 41(8): 1629–50, December 1996. ISSN 0024-3590.

[146] Baani, M. and Liesack, W. Two isozymes of particulate methane monooxygenase with different methane oxidation kinetics are found in Methylocystis sp. strain SC2. *Proc. Natl Acad. Sci. USA.*, 105(29):10203–10208, 2008. doi: 10.1073/pnas.0702643105.

[147] Reeburgh, W. S. Oceanic methane biogeochemistry. *Chem. Rev.*, 107(2): 486–513, 2007. doi: 10.1002/chin.200720267.

[148] Dale, A. W., Regnier, P., and Van Cappellen, P. Bioenergetic controls on anaerobic oxidation of methane (AOM) in coastal marine sediments : A theoretical analysis. *Am. J. Sci.*, 306:246–294, 2006. doi: 10.2475/ajs.306.4.246.

[149] Burdige, D. J. *Sediment pore waters.* Academic Press, Massachusetts, 2002.

[150] Koper, T. E., Stark, J. M., Habteselassie, M. Y., and Norton, J. M. Nitrification exhibits Haldane kinetics in an agricultural soil treated with ammonium sulfate or dairy-waste compost. *FEMS. Microbiol. Ecol.*, 74(2): 316–22, November 2010. ISSN 1574-6941.

[151] Rees, A. P., Woodward, E. M. S., and Joint, I. Concentrations and uptake of nitrate and ammonium in the Atlantic Ocean between 60N and 50S. *Deep. Sea. Res. Pt II.*, 53(14-16):1649–1665, July 2006. ISSN 09670645.

[152] Blackburn, T. H., Blackburn, N. D., Mortimer, R. T. G., Coleman, M. L., and Lovley, D. R. Rates of microbial processes in sediments. *Phil. Trans. R. Soc. Lond. A.*, 344(1670):49–58, 1993. doi: 10.1098/rsta.1993.0074.

[153] Betlach, M. R. and Tiedje, J. M. Kinetic explanation for accumulation of nitrite, nitric oxide, and nitrous oxide during bacterial denitrification. *Appl. Environ. Microbiol.*, 42(6):1074–84, 1981.

[154] Berner, R. A. Atmospheric oxygen over Phanerozoic time. *Proc. Natl Acad. Sci. USA.*, 96(20):10955–10957, 1999. doi: 10.1073/pnas.96.20.10955.

[155] Beaudet, R., Lévesque, M. J., Villemur, R., Lanthier, M., Chénier, M., Lépine, F., and Bisaillon, J. G. Anaerobic biodegradation of pentachlorophenol in a contaminated soil inoculated with a methanogenic consortium or with Desulfitobacterium frappieri strain PCP-1. *Appl. Microbiol. Biotechnol.*, 50(1):135–41, 1998. doi: 10.1007/s002530051268.

[156] Jorgensen, B. B. Mineralization of organic matter in the sea bed - the role of sulphate reduction. *Nature*, 296, 1982. doi: 10.1038/296643a0.

[157] Lenton, T. M. and Watson, A. *Revolutions that made the earth.* Oxford University Press, Oxford, 2011.

[158] Crawford, J. W., Harris, J. A., Ritz, K., and Young, I. M. Towards an evolutionary ecology of life in soil. *Trends Ecol. Evol.*, 20(2):81–7, 2005. doi: 10.1016/j.tree.2004.11.014.

[159] Torsvik, V. and Ovreas, L. Microbial diversity and function in soil: from genes to ecosystems. *Curr. Opin. Microbiol.*, 5(3):240–245, June 2002. doi: 10.1016/S1369-5274(02)00324-7.

[160] Daims, H., Taylor, M. W., and Wagner, M. Wastewater treatment: a model system for microbial ecology. *Trends Biotechnol.*, 24(11):483–489, 2006. doi: 10.1016/j.tibtech.2006.09.002.

[161] Bürgmann, H., Jenni, S., Vazquez, F., and Udert, K. M. Regime shift and microbial dynamics in a sequencing batch reactor for nitrification and anammox treatment of urine. *Appl. Environ. Microbiol.*, 77(17):5897–907, 2011. doi: 10.1128/AEM.02986-10.

[162] Horner-Devine, M. C., Carney, K. M., and Bohannan, B. J. M. An ecological perspective on bacterial biodiversity. *P. Roy. Soc. B-Biol. Sci.*, 271:113–122, 2004. doi: 10.1098/rspb.2003.2549.

[163] Fernandez, A. S., Hashsham, S. A., Dollhopf, S. L., Raskin, L., Glagoleva, O., Dazzo, F. B., Hickey, R. F., Criddle, C. S., and Tiedje, J. M. Flexible community structure correlates with stable community function in methanogenic bioreactor communities perturbed by glucose. *Appl. Environ. Microbiol.*, 66(9):4058–4067, 2000. doi: 10.1128/AEM.66.9.4058-4067.2000.

[164] Wertz, S., Degrange, V., Prosser, J. I., Poly, F., Commeaux, C., Guillaumaud, N., and Le Roux, X. Decline of soil microbial diversity does

not influence the resistance and resilience of key soil microbial functional groups following a model disturbance. *Environ. Microbiol.*, 9:2211–2219, 2007. doi: 10.1111/j.1462-2920.2007.01335.x.

[165] Allison, S. D. and Martiny, J. B. H. Resistance , resilience , and redundancy in microbial communities. *Proc. Natl. Acad. Sci. USA.*, 105:11512–11519, 2008.

[166] Mason, O. U., Scott, N. M., Gonzalez, A., Robbins-Pianka, A., Bæ lum, J., Kimbrel, J., Bouskill, N. J., Prestat, E., Borglin, S., Joyner, D. C., Fortney, J. L., Jurelevicius, D., Stringfellow, W. T., Alvarez-Cohen, L., Hazen, T. C., Knight, R., Gilbert, J. A., and Jansson, J. K. Metagenomics reveals sediment microbial community response to Deepwater Horizon oil spill. *ISME J.*, 8(7):1464–75, 2014. doi: 10.1038/ismej.2013.254.

[167] Keiser, A. D., Strickland, M. S., Fierer, N., and Bradford, M. A. The effect of resource history on the functioning of soil microbial communities is maintained across time. *Biogeosciences*, 8:1477–1486, 2011. doi: 10.5194/bg-8-1477-2011.

[168] Castro, H. F., Classen, A. T., Austin, E. E., Norby, R. J., and Schadt, C. W. Soil microbial community responses to multiple experimental climate change drivers. *Appl. Environ. Microbiol.*, 76(4):999–1007, 2010. doi: 10.1128/AEM.02874-09.

[169] Waldrop, M. P., Zak, D. R., and Sinsabaugh, R. L. Microbial community response to nitrogen deposition in northern forest ecosystems. *Soil Biol. Biochem.*, 36:1443–1451, 2004. doi: 10.1016/j.soilbio.2004.04.023.

[170] Pagaling, E., Strathdee, F., Spears, B. M., Cates, M. E., Allen, R. J., and Free, A. Community history affects the predictability of microbial ecosystem development. *ISME J.*, pages 1–12, August 2014. doi: 10.1038/ismej.2013.150.

[171] Dyer, B. D. *A Field Guide to Bacteria*. Cornell University Press, 2003.

[172] Jessup, C. M., Kassen, R., Forde, S. E., Kerr, B., Buckling, A., Rainey, P. B., and Bohannan, B. J. M. Big questions, small worlds: Microbial model systems in ecology. *Trends Ecol. Evol.*, 19(4):189–197, 2004. doi: 10.1016/j.tree.2004.01.008.

[173] Jin, Q. and Bethke, C. M. Cellular energy conservation and the rate of microbial sulfate reduction. *Geology*, 37(11):1027–1030, 2009. doi: 10.1130/G30185A.1.

[174] Crill, P. M. and Martens, C. S. Biogeochemical cycling in an organic-rich coastal marine basin. 6. Temporal and spatial variations in sulfate

reduction rates. *Geochim. Cosmochim. Acta.*, 51(5):1175–1186, 1987. doi: 10.1016/0016-7037(87)90210-9.

[175] Luther, G. W., Findlay, A. J., Macdonald, D. J., Owings, S. M., Hanson, T. E., Beinart, R. A., and Girguis, P. R. Thermodynamics and kinetics of sulfide oxidation by oxygen: a look at inorganically controlled reactions and biologically mediated processes in the environment. *Front. Microbiol.*, 2:62, 2011. doi: 10.3389/fmicb.2011.00062.

[176] Raiswell, R. and Canfield, D. E. The Iron Biogeochemical Cycle Past and Present. *Geochemical Perspectives*, 1(1), 2012.

[177] Rabaey, K., Rodríguez, J., Blackall, L. L., Keller, J., Gross, P., Batstone, D., Verstraete, W., and Nealson, K. H. Microbial ecology meets electrochemistry: electricity-driven and driving communities. *ISME J.*, 1: 9–18, 2007. doi: 10.1038/ismej.2007.4.

[178] Poulton, S. W. and Canfield, D. E. Development of a sequential extraction procedure for iron: implications for iron partitioning in continentally derived particulates. *Chem. Geol.*, 214(3-4):209–221, January 2005. doi: 10.1016/j.chemgeo.2004.09.003.

[179] Jorgensen, B. B. Bacteria and Marine Biogeochemistry. In Schulz, H. D. and Zabel, M., editors, *Marine Geochemistry*, chapter 5, pages 173–207. Springer-Verlag, Berlin, 1 edition, 2000.

[180] Middelburg, J. J. and Levin, L. A. Coastal hypoxia and sediment biogeochemistry. *Biogeosciences Discussions*, 6:3655–3706, 2009. doi: 10.5194/bgd-6-3655-2009.

[181] Visscher, P. T., Beukema, J., and Van Gemerden, H. In situ characterization of sediments: Measurements of oxygen and sulfide profiles with a novel combined needle electrode. *Limnol. Oceanogr.*, 36:1476–1480, 1991. doi: 10.4319/lo.1991.36.7.1476.

[182] Jø rgensen, B. B., Revsbech, N. P., Blackburn, T. H., and Cohen, Y. Diurnal cycle of oxygen and sulfide microgradients and microbial photosynthesis in a cyanobacterial mat sediment. *Appl. Environ. Microbiol.*, 38(1):46–58, 1979. ISSN 0099-2240.

[183] Raiswell, R. and Canfield, D. E. The iron biogeochemical cycle past present and future. *Geochemical Perspectives*, 1(1):1–220, 2012. doi: 10.7185/geochempersp.1.1.

[184] Laland, K. N., Odling-Smee, F. J., and Feldman, M. W. Evolutionary consequences of niche construction and their implications for ecology. *Proc. Natl. Acad. Sci. USA.*, 96(August):10242–10247, 1999. doi: 10.1073/pnas.96.18.10242.

[185] Langille, M. G. I., Zaneveld, J., Caporaso, J. G., McDonald, D., Knights, D., Reyes, J. A., Clemente, J. C., Burkepile, D. E., Vega Thurber, R. L., Knight, R., Beiko, R. G., and Huttenhower, C. Predictive functional profiling of microbial communities using 16S rRNA marker gene sequences. *Nat. Biotechnol.*, (9):814–21, 2013. doi: 10.1038/nbt.2676.

[186] Kondratieva, E. N., Pfenning, N., and Truper, H. G. The Phototrophic Prokaryotes. In Balows, A., Truper, H. G., Dworkin, M., Harder, W., and Schleifer, K. H., editors, *The Prokaryoates: A Handbook on the Biology of Bacteria: Ecophysiology, Isolation, Identification, Applications*, chapter 13, pages 312–330. Springer Verlag, New York, 2 edition, 1992.

[187] Ochoa de Alda, J. A. G., Esteban, R., Diago, M. L., and Houmard, J. The plastid ancestor originated among one of the major cyanobacterial lineages. *Nat. Commun.*, 5:4937, 2014. doi: 10.1038/ncomms5937.

[188] Dedysh, S. N., Pankratov, T. A., Belova, S. E., Kulichevskaya, I. S., and Liesack, W. Phylogenetic Analysis and In Situ Identification of Bacteria Community Composition in an Acidic Sphagnum Peat Bog. *Appl. Environ. Microbiol.*, 72(3):2110–2117, 2006. doi: 10.1128/AEM.72.3.2110.

[189] Ransom-Jones, E., Jones, D. L., McCarthy, A. J., and McDonald, J. E. The Fibrobacteres: an Important Phylum of Cellulose-Degrading Bacteria. *Microb. Ecol.*, 63(2):267–281, 2012. doi: 10.1007/s00248-011-9998-1.

[190] Leschine, S. B. Cellulose degradation in anaerobic environments. *Annu. Rev. Microbiol.*, 49:399–426, 1995. doi: 10.1146/annurev.micro.49.1.399.

[191] Caro-Quintero, A., Ritalahti, K. M., Cusick, K. D., Löffler, F. E., and Konstantinidis, K. T. The Chimeric Genome of Sphaerochaeta : Nonspiral Spirochetes That Break with the Prevalent Dogma in Spirochete Biology. *MBio*, 3(3):1–9, 2012. doi: 10.1128/mBio.00025-12.Editor.

[192] Brune, A. Symbiotic digestion of lignocellulose in termite guts. *Nat. Rev. Microbiol.*, 12(3):168–80, 2014. doi: 10.1038/nrmicro3182.

[193] Abt, B., Göker, M., Scheuner, C., Han, C., Lu, M., Misra, M., Lapidus, A., Nolan, M., Lucas, S., Hammon, N., Deshpande, S., Cheng, J., Tapia, R., Goodwin, L. A., Pitluck, S., Liolios, K., Pagani, I., Ivanova, N., Mavromatis, K., Mikhailova, N., Huntemann, M., Pati, A., Chen, A., Palaniappan, K., Land, M., Hauser, L., Jeffries, C. D., Rohde, M., Spring, S., Gronow, S., Detter, J. C., Bristow, J., Eisen, J. A., Markowitz, V., Hugenholtz, P., Kyrpides, N. C., Woyke, T., and Klenk, H. Genome sequence of the thermophilic fresh-water bacterium Spirochaeta caldaria type strain (H1(T)), reclassification of Spirochaeta caldaria, Spirochaeta stenostrepta, and Spirochaeta zuelzerae in the genus Treponema as Treponema caldaria comb. nov., Trep. *Stand. Genomic Sci.*, 8(1):88–105, 2013. doi: 10.4056/sigs.3096473.

[194] Chipman, L., Podgorski, D., Green, S., Kostka, J., and Cooper, W. Decomposition of plankton-derived dissolved organic matter in permeable coastal sediments. *Limnol. Oceanogr.*, 55(2):857–871, 2010. doi: 10.4319/lo.2009.55.2.0857.

[195] Moore, E. K., Hopmans, E. C., Rijpstra, W. I. C., Villanueva, L., Dedysh, S. N., Kulichevskaya, I. S., Wienk, H., Schoutsen, F., and Sinninghe Damsté, J. S. Novel mono-, di-, and trimethylornithine membrane lipids in northern wetland planctomycetes. *Appl. Environ. Microbiol.*, 79(22):6874–84, 2013. doi: 10.1128/AEM.02169-13.

[196] Ivanova, A. O. and Dedysh, S. N. Abundance, diversity, and depth distribution of planctomycetes in acidic northern wetlands. *Front. Microbiol.*, 3:5, 2012. doi: 10.3389/fmicb.2012.00005.

[197] Friedrich, C. G., Rother, D., Bardischewsky, F., and Quentmeier, A. Oxidation of Reduced Inorganic Sulfur Compounds by Bacteria : Emergence of a Common Mechanism? *Appl. Environ. Microbiol.*, 67(7):2873–2882, 2001. doi: 10.1128/AEM.67.7.2873.

[198] Garcia, J. L., Patel, B. K., and Ollivier, B. Taxonomic, phylogenetic, and ecological diversity of methanogenic Archaea. *Anaerobe*, 6:205–226, 2000. doi: 10.1006/anae.2000.0345.

[199] Cohen, Y., Jorgensen, B. B., Revsbech, N. P., and Poplawski, R. Adaptation to Hydrogen Sulfide of Oxygenic and Anoxygenic Photosynthesis among Cyanobacteria. *Appl. Environ. Microbiol.*, 51(2):398–407, 1986.

[200] Miller, S. R. and Bebout, B. M. Variation in sulfide tolerance of photosystem II in phylogenetically fiverse Cyanobacteria from sulfidic habitats variation in sulfide tolerance of photosystem II in phylogenetically diverse Cyanobacteria from sulfidic habitats. *Appl. Environ. Microbiol.*, 70(2):736–744, 2004. doi: 10.1128/AEM.70.2.736.

[201] Montesinos, E., Guerrero, R., Abella, C., and Esteve, I. Ecology and physiology of the competition for light between Chlorobium limicola and Chlorobium phaeobacteroides in natural habitats. *Appl. Environ. Microbiol.*, 46(5):1007–1016, 1983.

[202] Vallina, S. M., Follows, M. J., Dutkiewicz, S., Montoya, J. M., Cermeno, P., and Loreau, M. Global relationship between phytoplankton diversity and productivity in the ocean. *Nat. Commun.*, 5:4299, 2014. doi: 10.1038/ncomms5299.

[203] Smith, V. H. Microbial diversity-productivity relationships in aquatic ecosystems. *FEMS. Microbiol. Ecol*, 62:181–186, 2007. doi: 10.1111/j.1574-6941.2007.00381.x.

[204] Myers, J. L. and Richardson, L. L. Adaptation of cyanobacteria to the sulfide-rich microenvironment of black band disease of coral. *FEMS Microbiol. Ecol.*, 67(2):242–51, 2009. doi: 10.1111/j.1574-6941.2008.00619.x.

[205] Myers, J. L., Sekar, R., and Richardson, L. L. Molecular detection and ecological significance of the cyanobacterial genera Geitlerinema and Leptolyngbya in black band disease of corals. *Appl. Environ. Microbiol.*, 73 (16):5173–82, 2007. doi: 10.1128/AEM.00900-07.

[206] Suen, G., Weimer, P. J., Stevenson, D. M., Aylward, F. O., Boyum, J., Deneke, J., Drinkwater, C., Ivanova, N. N., Mikhailova, N., Chertkov, O., Goodwin, L. A., Currie, C. R., Mead, D., and Brumm, P. J. The complete genome sequence of Fibrobacter succinogenes S85 reveals a cellulolytic and metabolic specialist. *PloS One*, 6(4):e18814, 2011. doi: 10.1371/journal.pone.0018814.

[207] Desvaux, L., Guedon, E., Petitdemange, H., Scientifique, D., Grignard, V., and Poincare, H. Cellulose catabolism by Clostridium cellulolyticum growing in batch culture on defined medium. *Appl. Environ. Microbiol.*, 66 (6):2461–2470, 2000. doi: 10.1128/aem.66.6.2461-2470.2000.

[208] Kudo, H., Cheng, K. J., and Costerton, J. W. Interactions between Treponema bryantii and cellulolytic bacteria in the in vitro degradation of straw cellulose. *Can. J. Microbiol.*, 33(3):244–8, 1987. doi: 10.1139/m87-041.

[209] Brüchert, V., Jorgensen, B. B., Neumann, K., Riechmann, D., Schlösser, M., and Schulz, H. Regulation of bacterial sulfate reduction and hydrogen sulfide fluxes in the central namibian coastal upwelling zone. *Geochim. Cosmochim. Acta.*, 67(23):4505–4518, 2003. doi: 10.1016/S0016-7037(03)00275-8.

[210] Botton, S., Van Heusden, M., Parsons, J. R., Smidt, H., and Van Straalen, N. Resilience of microbial systems towards disturbances. *Crit. Rev. Microbiol.*, 32(2):101–12, 2006. doi: 10.1080/10408410600709933.

[211] DeAngelis, K. M., Silver, W. L., Thompson, A. W., and Firestone, M. K. Microbial communities acclimate to recurring changes in soil redox potential status. *Environ. Microbiol.*, 12(12):3137–3149, 2010. doi: 10.1111/j.1462-2920.2010.02286.x.

[212] Blodau, C. and Knorr, K. H. Experimental inflow of groundwater induces a biogeochemical regime shift in iron-rich and acidic sediments. *J. Geophys. Res.*, 111(G2):G02026, 2006. doi: 10.1029/2006JG000165.

[213] Mao-Jones, J., Ritchie, K. B., Jones, L. E., and Ellner, S. P. How microbial community composition regulates coral disease development. *PLoS Biol.*, 8 (3):e1000345, 2010. doi: 10.1371/journal.pbio.1000345.

[214] Keeling, R. F., Koertzinger, A., and Gruber, N. Ocean Deoxygenation in a Warming World. *Ann. Rev. Mar. Sci.*, 2:199–229, 2010. doi: 10.1146/annurev.marine.010908.163855.

[215] Shade, A., Peter, H., Allison, S. D., Baho, D. L., Berga, M., Bürgmann, H., Huber, D. H., Langenheder, S., Lennon, J. T., Martiny, J. B. H., Matulich, K. L., Schmidt, T. M., and Handelsman, J. Fundamentals of microbial community resistance and resilience. *Front. Microbiol.*, 3:417, 2012. doi: 10.3389/fmicb.2012.00417.

[216] Halpern, B. S., Walbridge, S., Selkoe, K. A., Kappel, C. V., Micheli, F., D'Agrosa, C., Bruno, J. F., Casey, C., K. S.and Ebert, Fox, H. E., Fujita, R., Heinemann, D., Lenihan, H. S., Madin, E. M. P., Perry, M. T., Selig, E. R., Spalding, M., Steneck, R., and Watson, R. A global map of human impact on marine ecosystems. *Science*, 319(5865):948–952, 2008. doi: 10.1126/science.1149345.

[217] Bethke, C. M. *Geochemical and Biogeochemical Reaction Modelling.* Cambridge University Press, 2010.

[218] Keimowitz, A. R., Mailloux, B. J., Cole, P., Stute, M., Simpson, H. J., and Chillrud, S. N. Laboratory investigations of enhanced sulfate reduction as a groundwater arsenic remediation strategy. *Environ. Sci. Technol.*, 41(19): 6718 –24, 2007. doi: 10.1016/j.biotechadv.2011.08.021.Secreted.

[219] Berger, A. C., Bethke, C. M., and Krumhansl, J. L. A process model of natural attenuation in drainage from a historic mining district. *Appl. Geochem.*, 15:655–666, 2000. doi: 10.1016/S0883-2927(99)00074-8.

[220] Kaszuba, J. P. and Runde, W. H. The aqueous geochemistry of neptunium: Dynamic control of soluble concentrations with applications to nuclear waste disposal. *Environ. Sci. Technol.*, 33(505):4427–4433, 1999. doi: 10.1021/es990470x.

[221] Posth, N. R., Hegler, F., Konhauser, K. O., and Kappler, A. Alternating Si and Fe deposition caused by temperature fluctuations in Precambrian oceans. *Nat. Geosci.*, 1(10):703–708, 2008. doi: 10.1038/ngeo306.

[222] Davidson, M. M., Bisher, M. E., Pratt, L. M., Fong, J., Southam, G., Pfiffner, S. M., Reches, Z., and Onstott, T. C. Sulfur isotope enrichment during maintenance metabolism in the thermophilic sulfate-reducing bacterium Desulfotomaculum putei. *Appl. Environ. Microbiol.*, 75(17):5621–5630, 2009. doi: 10.1128/AEM.02948-08.

[223] Bethke, C. M., Sanford, R. A., Kirk, M. F., Jin, Q., and Flynn, T. M. The thermodynamic ladder in geomicrobiology. *Am. J. Sci.*, 311:183–210, 2011. doi: 10.2475/03.2011.01.

[224] Labrenz, M., Druschel, G. K., Thomsen-Ebert, T., Gilbert, B., Welch, S. A., Kemner, K. M., Logan, G. A., Summons, R. E., De Stasio, G., Bond, P. L., Lai, B., Kelly, S. D., and Banfield, J. F. Formation of sphalerite (ZnS) deposits in natural biofilms of sulfate-reducing bacteria. *Science*, 290:1744–1747, 2000. doi: 10.1126/science.290.5497.1744.

[225] Delaney, J. M. and Lundeen, S. R. The LLNL Thermodynamical Database: Lawrence Livermore National Laboratory Report. *UCRL-21658*, page 150, 1990.

[226] Foti, M., Sorokin, D. Y., Lomans, B., Mussman, M., Zacharova, E. E., Pimenov, N. V., Kuenen, J. G., and Muyzer, G. Diversity, activity, and abundance of sulfate-reducing bacteria in saline and hypersaline soda lakes. *Appl. Environ. Microbiol.*, 73(7):2093–2100, 2007. ISSN 00992240. doi: 10.1128/AEM.02622-06.

[227] Russell, J. B., Muck, R. E., and Weimer, P. J. Quantitative analysis of cellulose degradation and growth of cellulolytic bacteria in the rumen. *FEMS Microbiol. Ecol.*, 67(2):183–197, 2009. doi: 10.1111/j.1574-6941.2008.00633.x.

[228] Andrić, P., Meyer, A. S., Jensen, P. A., and Dam-Johansen, K. Effect and modeling of glucose inhibition and in situ glucose removal during enzymatic hydrolysis of pretreated wheat straw. *Appl. Biochem. Biotechnol.*, 160(1):280–97, 2010. doi: 10.1007/s12010-008-8512-9.

[229] Weimer, P. J. Effects of dilution rate and pH on the ruminal cellulolytic bacterium Fibrobacter succinogenes S85 in cellulose-fed continuous culture. *Arch. Microbiol.*, 160(4):288–294, 1993. doi: 10.1007/bf00292079.

[230] Miletto, M., Williams, K. H., N'Guessan, A. L., and Lovley, D. R. Molecular analysis of the metabolic rates of discrete subsurface populations of sulfate reducers. *Appl. Environ. Microbiol.*, 77(18):6502–6509, 2011. doi: 10.1128/AEM.00576-11.

[231] Sonne-hansen, J. and Westermann, P. Kinetics of sulfate and hydrogen uptake by the yhermophilic sulfate-reducing bacteria Thermodesulfobacterium sp. strain. *Appl. Environ. Microbiol.*, 65(3):1304–1307, 1999.

[232] Oude Elferink, S. J. W. H., Luppens, S. B. I., Marcelis, C. L. M., and Stams, A. J. M. Kinetics of acetate oxidation by two sulfate reducers isolated from anaerobic granular sludge. *Appl. Environ. Microbiol.*, 64(6):2301–2303, 1998. doi: 10.1080/01490459809378058.

[233] Kotsyurbenko, O. R., Chin, K. J., Glagolev, M. V., Stubner, S., Simankova, M. V., Nozhevnikova, A. N., and Conrad, R. Acetoclastic and hydrogenotrophic methane production and methanogenic populations in an acidic West-Siberian peat bog. *Environ. Microbiol.*, 6:1159–1173, 2004. doi: 10.1111/j.1462-2920.2004.00634.x.

[234] Lovley, D. R. and Klug, M. J. Sulfate reducers can outcompete methanogens at freshwater sulfate concentrations. *Appl. Environ. Microbiol.*, 45(1):187–192, 1983.

[235] Coughlan, M. P. and Mayer, F. The Cellulose-Decomposing Bacteria and Their Enzyme Systems. In Ballows, A., Truper, H. G., Dworkin, M., Harder, W., and Shleifer, K., editors, *The Prokaryoates: A Handbook on the Biology of Bacteria: Ecophysiology, Isolation, Identification, Applications*, chapter 20, pages 460–517. Springer Verlag, New York, 2 edition, 1991.

[236] Van Duyl, F. and Kop, A. J. Seasonal patterns of bacterialproduction and biomass in intertidal sediments of the western Dutch Wadden Sea. *Mar. Ecol. Prog. Ser.*, 59(3):249–261, 1990. doi: 10.3354/meps059249.

[237] Thattai, M. and Van Oudenaarden, A. Attenuation of noise in ultrasensitive signaling cascades. *Biophys. J.*, 82:2943–2950, 2002. doi: 10.1016/S0006-3495(02)75635-X.

[238] Canfield, D. E., Stewart, F. J., Thamdrup, B., De Brabandere, L., Dalsgaard, T., Delong, E. F., Revsbech, N. P., and Ulloa, O. A cryptic sulfur cycle in oxygen-minimum-zone-waters off the Chilean coast. *Science*, 330:1375–1378, 2010. doi: 10.1126/science.1196889.